
SIGILLVM · MAGISTRI · ET · SCHOLARIVM
STUDII · LIPSIENSIS

NON-EQUILIBRIUM TRANSPORT IN QUANTUM HALL EDGE STATES

Von der Fakultät für Physik und Geowissenschaften
der Universität Leipzig
genehmigte

DISSERTATION

zur Erlangung des akademischen Grades

Doctor rerum naturalium

Dr.rer.nat.

vorgelegt

von M.Sc. Mirco Milletarí
geboren am 21/05/1980 in Rom (Italien)

Gutachter: Prof. Dr. Bernd Rosenow
Prof. Dr. Walter Metzner

Tag der Verleihung: 16 September 2013

PREFACE

Dimensionality plays a central role in modern physics. With Einstein's theory of relativity we have got used to think about a four dimensional world. Since then, two opposite trends developed: on the high energy side, physicists looked at theories with increasingly higher dimension in order to accommodate all the known forces of nature. Here, the dimension of the physical space is dictated by a request of consistency of those theories[1]. On the other side of the energy spectrum, low dimensionality initially attracted physicists due to the possibility of an exact treatment of many problems[2]. This initial, purely academic interest in low dimensional systems, turned into a field of its own with the possibility of realizing such systems in a laboratory. It was soon understood that a deep connection between low dimensionality and interactions exists. On an intuitive level, we can understand this connection by realizing that low dimensionality is achieved by reducing the degrees of freedom of a system. The reduced number of degrees of freedom increases the probability of interaction between different particles. A "conspiracy" of low dimensionality, low temperatures and interactions with external fields gives rise to many different states of matter. At the classical level, different states of matter are classified within Landau's theory in terms of their symmetries. One of the most striking results of modern condensed matter physics is the emergence of a new paradigm in the classification of different states of matter, namely topological classification [2]. A topological state is characterized at low temperature by an energy gap separating the ground-state from the lowest excited state. In a topological phase, the observables of the system do not depend on the specific geometrical aspects of the space the system lives in [3]. The most famous example of a topological state is probably the quantum Hall effect (QHE), taking place in a two dimensional electron gas (2DEG) at high magnetic fields. The conductance of samples exhibiting the QHE is exactly quantized in multiples of a quantity, the filling fraction ν, that can be related to the topological properties of the system. The filling fraction also characterizes different kinds of quantum Hall (QH) states. We can in general distinguish the integer (IQH) from the fractional (FQH) quantum Hall states, according to the allowed values of ν. In particular, the FQHE represents a strongly correlated state of matter and it cannot be described within the framework of Fermi liquid theory. It has been shown that the edges of a system exhibiting the QHE support one dimensional gapless excitations moving only in one definite direction. In the case of the edges of a FQH state, those gapless states are strongly interacting, one dimensional systems described within the Luttinger liquid (LuL) universality class.

1 For example, a consistent (i.e. anomaly free) superstring theory necessitates 11 space-time dimensions [1].
2 One of the most famous example in statistical mechanics is probably the Ising model.

This thesis deals with the study of transport properties of integer and fractional QH edge states and it is based on the work I performed during my Ph.D. studies. The focus of this thesis is on LuL far from equilibrium and their relaxation dynamics. Since Boltzmann, a fundamental aspect of statistical mechanics has been the understanding of the emergence of an equilibrium state. Interactions play a crucial role in the thermalization process that drives a system through states described by the Gibbs equilibrium ensemble. Therefore seems counterintuitive that a strongly interacting system, such as the LuL, should not present any relaxation dynamics. This peculiar fact is due to the integrability of the Luttinger model, i.e. the existence of an infinite number of conserved quantities that precludes the equilibration process. However, in the past few years it has become clear that integrable systems can present some kind of relaxation, even though not towards the Gibbs equilibrium ensemble [4, 5]. Remarkably, the necessity of correctly taking into account some particular non-equilibrium configurations, also revealed the necessity of modifying bosonization, a technique widely used to study strongly interacting systems in one dimension [6–9]. In this work we focus on three different cases:

- Relaxation of high energy electrons injected in a $\nu = 1/3$ chiral LuL and in a standard LuL.
- Heating and the emergence of effective temperatures in a QH system at $\nu = 2/3$ partitioned by a QPC.
- Effect of relaxation on shot-noise measurement of the quasi-particle charge in a $\nu = 2$ QH state.

This thesis is organized as follows:

- In chapter one, I give an overview on the theory of the integer and fractional QHE. Even though the QH effect is a complex phenomenon involving many subtleties, I try to give an overview of its main characteristics: the quantized conductance, fractional charges and fractional statistics. Here, I also introduce the edge states through an intuitively simple argument. The chapter is supplemented by an appendix on the Landau-Ginsburg formulation of the QHE. I decided to add this appendix in order to clarify the origin and the structure of things like the hierarchical edge action used throughout this thesis. The content of this appendix results from an expansion of two talks I gave on the subject during these years.
- In chapter two, I introduce the central tool used in this thesis: bosonization. Bosonization makes possible to map a system of strongly interacting, one dimensional fermions, into a system of non interacting bosons. In this way it is possible to exactly solve the many-body quantum problem. The chapter is far from being a complete account on bosonization, but I hope it can help the reader throughout the thesis. In this chapter I also introduce the recently developed non-equilibrium bosonization technique. Building on the standard bosonization approach, I try to highlight the necessity for this

technique through examples and explicit calculations. In this section we also introduce the concept of full counting statistics (FCS), that turns out to be intimately related to non-equilibrium bosonization. The chapter is supplemented by an appendix where we show some details on bosonization. In this appendix we also give a proof of the Levitov-Lesovik formula of FCS.

- In chapter three I present the first work done during my Ph.D. studies. This chapter is based on the work published in [10]. Here we investigate energy relaxation through the injection of high energy electrons in the edge of a FQH system at filling $\nu = 1/3$ and in a non-chiral LuL. The proposed experimental setup consists of two quantum dots (QD) coupled to a one dimensional system. We find that, due to many body effects, high energy electrons do relax in the one dimensional system. However, the details of relaxation depend on wether the one dimensional system is a chiral or non-chiral LuL. For the non-chiral case we perform a finite temperature analysis of the tunneling current. For the non-chiral LuL, we study the tunneling current at zero temperature as a function of the continuous interaction parameter. In the latter case, we provide a perturbative analysis to highlight the origin of relaxation. Additional details are given in the related appendix.

- In chapter four we present a study on heating and energy transport in QH line junctions (LJ) between different filling fractions. This situation often appears in experimental situations where a QH bar is pinched by a quantum point contact (QPC). The aim of the QPC is to induce tunneling between the two counter-propagating edge states, by bringing them spatially close to each other. However, this process also changes the local filling fraction in the constriction, and generates a new interface in which counter-propagating edge modes appear. We investigate the relaxation between those different edge states in the presence of impurities using both an hydrodynamical and a mesoscopic scattering approach. We also study the emergence of local temperatures and energy transport through the system.

- In chapter five we consider a QH bar at filling fraction $\nu = 2$ [11]. The edges of this system consists of two co-propagating edge modes. In order to study the relaxation dynamics of this system, we consider a setup in which the two edge modes are selectively driven out of equilibrium with respect to each other by the action of two QPCs. The first QPC selectively drives out of equilibrium the outer edge mode, which then interacts with the unbiased inner one through a density-density interaction over the distance between the two QPCs. We describe the edge modes by two coupled chiral LuLs, and employ the method of non-equilibrium bosonization to study the relaxation dynamics of the inner one. We find that even asymptotically the edge distribution function does not thermalize, but instead depends in a sensitive way on the interaction strength between the two edge modes. The strong interaction between the two edge modes gives rise to charge fractionalization. In order to determine the value of the

fractional charge, we compute the shot noise and the Fano factor from the asymptotic distribution function of the inner edge mode at the second QPC. From comparison with a reference model of fractionalized excitations we find that the Fano factor can be close to the value of the fractionalized charge. Additional details can be found in the related appendix. The work of this chapter can be found in [11] and it has been submitted to PRL.

PUBLICATIONS

- S. Takei, M. Milletarí, and B. Rosenow. "Nonequilibrium electron spectroscopy of Luttinger liquids". In: *Phys. Rev. B (R)* 82 (2010), p. 041306

- M. Milletarí and B. Rosenow. "Shot Noise Signatures of Charge Fractionalization in the $\nu = 2$ Quantum Hall edge". In: *eprint arXiv:1207.1719* (7/2012)

Francis Line lived in lineland, and he liked it there. There was little that he didn't like about lineland, it was simple, but complex all the same. He was often in the same place for years at a time because of a people jam, where two peoples next to each other argued in the same place until they got along. Nobody ever died in lineland, they just slowly disintegrated until everybody forgot they had ever existed. They reproduced to the right and moved to the left and only reproduced once in their lives, so everybody to the right was younger. [...] They all traveled along the great line. Some thought that the line wasn't really a line at all, but a circle, because sometimes before their last bits disintegrated, people would claim to see children up ahead of them, but only the really old people talked about this.
— stillyellow[12]

ACKNOWLEDGEMENTS

Moving through the one dimensional realm has not been easy, and I would never have reached the other endpoint without the help and knowledge of my supervisor, Bernd Rosenow. During these years I also had the opportunity of discussing and collaborating with different people; each of them helped me understanding this complex, beautiful world of physics. Especially, I am in debt with So Takei, with whom I have started this adventure in the one dimensional realm and for being a true friend. My colleagues Mats Horsdal, Tony Wright and Timo Hyart, for the long discussions on physics, life and everything (if you ask me, I am not sure we even agreed that the answer is 42). I would also like to thank Walter Metzner for his support during the time spent at the Max Planck institute in Stuttgart. My M.Sc. supervisor in Rome, Roberto Raimondi, because he is the reason why I am still in physics. A special mention also goes to Alexander Schneider, for having carefully read a part of this thesis and found many of the typos.

Life, apparently, is more a sequence of curves than a straight line. Sometimes these curves take us away from our goal. I am glad my family always kept me on the right path, even when things got messy. In this German parenthesis of my life I met so many wonderful people, I thank all of them for having shared their time with me. Melissa, Valentina, Simona, Cristobal, Elisa, Sasha, Nadima, Andreas Schnyder, Gabi, Carina and Sandra in Stuttgart. In Leipzig, I am glad my world line crossed the one of Rosa, Aristide, Luisa, Janet, Selva, Lorenzo, Christian, Kuba and many others. To all of them I would like to dedicate this work.

This work is especially dedicated to the memory of my mother, who would have loved to see me getting here.

This thesis has been written in LaTeX, using the ArsClassica style [13].

Leipzig, february 8, 2013 Mirco Milletarí

CONTENTS

LIST OF FIGURES

LIST OF TABLES

1 THE QUANTUM HALL EFFECT

CONTENTS

The importance of Hall physics in our understanding of nature is far reaching, connecting together different branches of Physics, Mathematics and more recently computer science. The classical Hall effect, discovered by Edwin Hall in 1879 [14] gave us a deeper understanding of the conduction mechanism revealing the sign of the charge carriers. The experimental apparatus consisted of a metal immersed in a perpendicular magnetic field; when applying a current in the "x" direction a potential drop in the longitudinal and transverse "y" direction is measured. The Hall (transverse) and the longitudinal Resistance were then measured :

$$R_H \equiv \frac{V_y}{I_x} \quad , \quad R_L \equiv \frac{V_x}{I_x}. \tag{1.0.1}$$

With advances in electronics and low temperature physics, in 1980 von Klitzing, Dorda and Pepper discovered the quantum version of the Hall effect [15]. Experimentally, the Quantum Hall effect (QHE) is observed in a high mobility electron gas confined to a two dimensional region Ω (2DEG) of a semiconductor heterojunction at low temperatures ($T \simeq 4K$) and subject to a strong, uniform magnetic field perpendicular to Ω. In Fig. (1) a "Quantum Hall bar" is sketched together with a real sample; a current I_x from source to drain results as a consequence of a chemical potential imbalance. The four contacts allow for a measurement of R_H and R_L. One finds that R_H exhibits a universal behavior independent of the current I_x, and plateaus appear at some special values of the magnetic field where R_L becomes identically zero. Theoretically it was soon understood that the physics was described in terms of the previously introduced Landau energy levels (LL), and the plateau in the Hall resistance appear whenever one of those levels is completely filled, accounting for the observed macroscopic quantization. In 1985, Niu, Thouless and Wu explained the robustness of the IQHE

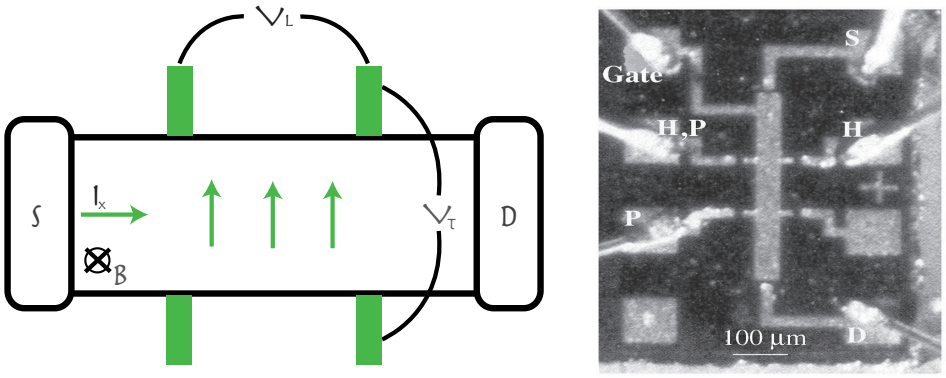

Figure 1: Quantum Hall bar. (Left) a sketch of the four terminal quantum Hall bar. (Right) the experimental silicon MOSFET device [16]

using topological arguments[1], relating the filling fraction to a topological invariant known as the Chern number [17], opening the way to the study of the so called topological states of matter. Two years after the discovery of the IQHE, Tsui, Stormer and Gossard [18] discovered that plateaus in the Hall resistance of a 2DEG can also appear when a LL is not completely filled, giving rise to a fractional Quantum Hall resistance. The Fractional Quantum Hall Effect (FQHE) turned out to be an optimal playground to understand strongly interacting systems, introducing concepts such as fractional charges and fractional statistics. Since then, many other states have been experimentally discovered, some of them having even stranger properties such as non-Abelian fractional statistics. Recently, a new Quantum Computation scheme has been proposed using non-Abelian quantum Hall states that goes under the name of Topological Quantum Computing [3]. In this chapter we will give an overview of Quantum Hall physics that will be essential in order to introduce tools and concepts that will be extensively used throughout this thesis. Due to the vast literature on the topic, the present overview can only scratch the surface of this fascinating subject. We refer to references [2, 19–23] for details.

1.1 PRELIMINARY CLASSICAL CONSIDERATIONS

Consider a two dimensional system of electrons in the presence of a magnetic field $\mathbf{B} = B\hat{z}$ and an electric field $\mathbf{E} = E_x\hat{x} + E_y\hat{y}$. In CGS Gaussian units the classical equations of motions for a charge carrier moving in the $x-y$ plane are:

$$\begin{aligned} \dot{p}_x &= qE_x + \frac{q}{c}u_y B - p_x/\tau \\ \dot{p}_y &= qE_y - \frac{q}{c}u_x B - p_y/\tau, \end{aligned} \tag{1.1.1}$$

1 The issue of disorder effects in the QHE is quite subtle. We briefly discuss this issue in section (1.2.1), where we mention another approach based on a non-linear sigma model.

where "q" is the charge of the carriers, u_i the velocity along direction i, c the speed of light and τ a relaxation time determined by collisions with impurities. We look for a stationary solution, i.e. $\dot{p}_x = \dot{p}_y = 0$ and use the definition of the current density $\mathbf{j} = n_e q\mathbf{u}$, n_e being the electron density. When the magnetic field is zero, we obtain the familiar Drude expression for the conductivity $\sigma_D = n_e q^2\tau/m$. However, as a result of the magnetic field, the conductivity is no longer a scalar but a tensor quantity. Solving Eq. (1.1.1), the components of the conductivity tensor are easily found to be:

$$\begin{aligned} \sigma_{xx} &= \frac{\sigma_D}{1+\omega_c^2\tau^2} \\ \sigma_{xy} &= \frac{\sigma_D\omega_c\tau}{1+\omega_c^2\tau^2}, \end{aligned} \tag{1.1.2}$$

and $\sigma_{yy} = \sigma_{xx}$, $\sigma_{yx} = -\sigma_{xy}$. Note that this last relation between components of the conductivity tensor is due to the isotropy of the system. From now on we will refer to the transverse component of the conductivity tensor as the Hall conductivity σ_H. Since what is measured in Hall bar experiments is the resistivity, we can invert the conductivity tensor, obtaining in this way

$$\begin{aligned} \rho_{xx} &= \frac{\sigma_{xx}}{\sigma_{xx}^2+\sigma_H^2} = \sigma_D^{-}1 \\ \rho_H &= \frac{\sigma_H}{\sigma_{xx}^2+\sigma_H^2} = \frac{B}{n_e c q}. \end{aligned} \tag{1.1.3}$$

Eq. (1.1.3) shows that it is indeed possible from a measurement of the Hall resistivity, to find the sign of the charge carriers.

In the dissipative limit $\omega_c\tau \ll 1$ we get back the Drude expression of the longitudinal conductivity, while for the transverse conductivity we find that $\sigma_{xy} \simeq \sigma_D\omega_c\tau$ (which goes to zero for strong disorder). In the opposite limit $\omega_c\tau \gg 1$ of high magnetic field, both ρ_{xx} and σ_{xx} vanish, while the transverse conductivity does not depend anymore on the disorder strength, and we find $\sigma_H = \rho_H^{-1}$. It is interesting to note that in two space dimensions, the conductivity (σ) and the conductance (G) have the same dimension, being related by a geometrical factor $G = \sigma L^{d-2}$ (L is the linear dimension of the system); this suggests that the measured quantities do not depend on the linear dimension of the sample. However, conductivity does depend on the aspect ratio of the system. Even though we derived the above results from purely classical arguments, it is instructive to multiply and divide σ_H by Planck's constant in order to form the dimensionless quantity

$$\nu = N_e\frac{\Phi_0}{\Phi(B)}, \tag{1.1.4}$$

called the filling fraction. Here N_e is the number of electrons in the 2DEG while the ratio between the total magnetic flux and the flux quantum $\Phi(B)/\Phi_0$ gives the number of flux quanta piercing the system[2]. In terms of the filling fraction, the Hall conductance can be

2 In CGS Gaussian units the flux quantum $\Phi_0 = hc/e = 4.135\times10^{-7}$ gauss cm^2, while in SI units $\Phi_0 = h/e = 4.136\times10^{-15}$Wb.

expressed as $\sigma_H = \nu e^2/h$, i.e. as a multiple of the quantum of conductance. In this way quantum mechanics enters the expression for σ_H only through the quantum of conductance. Obviously this semiclassical expression does not explain why σ_H should be quantized at all, neither it does explain the accuracy of the experimentally observed effect. We will show this in the next sections.

1.2 A QUICK REVIEW OF INTEGER QUANTUM HALL PHYSICS

From a microscopic point of view, the starting point is the non-relativistic limit of the gauged Dirac equation[3]. Interaction of particles with the electromagnetic field is introduced in the Hamiltonian via the $U(1)$ gauge field $\mathbf{A}$, through the spatial component of the covariant derivative:

$$\nabla \to \nabla - \imath \frac{(-e)}{\hbar c}\mathbf{A}. \tag{1.2.1}$$

The gauge field $\mathbf{A}$ is related to the magnetic field by the usual relation $\mathbf{B} = \nabla \wedge \mathbf{A}$, $-e$ is the electron's charge and c the speed of light. For the 2DEG in a strong perpendicular magnetic field we can generally distinguish different terms appearing in the Hamiltonian density:

$$\mathscr{H} = \mathscr{H}_k + \mathscr{H}_r + \mathscr{H}_c + \mathscr{H}_d. \tag{1.2.2}$$

Hereby we will consider the background magnetic field as not fluctuating and hence ignore the dynamical Maxwell term. Above, $\mathscr{H}_k$ is the kinetic term, $\mathscr{H}_r$ contains terms coming from the low energy expansion of the Dirac equation, namely the Zeeman term describing the interaction between the external magnetic field and the particle's spin, the Darwin term that brings correction to the energy of the state with total angular momentum $l = 0$ and the spin-orbit term. $\mathscr{H}_c$ contains the Coulomb interaction and $\mathscr{H}_d$ contains potential terms such as disorder and a confinement field.

In $2+1$ dimensions[4], a strong magnetic field suppresses the kinetic term in (1.2.2), making it smaller with respect to the interaction terms. We start by considering the IQH effect (we assume $\mathscr{H}_c$ to be small) in the case of fully polarized electrons, which means the cyclotron energy $\hbar\omega_c$ is bigger than the Zeeman splitting term (in the 2DEG). The Darwin and the spin-orbit term are also neglected in the following discussion. For the moment we also neglect $\mathscr{H}_d$.

The first important point to note is that in $2+1$ dimensions the magnetic field is a two component scalar, since the (completely antisymmetric) Levi-Civita tensor has only two indices [5] $(i, j = 1, 2 \equiv x, y)$:

$$B = \epsilon^{ij}\partial_i A_j. \tag{1.2.3}$$

3 Basically the Dirac equation is expanded for energies smaller than mc^2 in powers of v/c up to order $(v/c)^2$. See e.g. [24, 25].

4 Here we follow the terminology of non-relativistic field theory, and work with two spatial and a time dimension.

5 In the following discussion we make use of Einstein's convention of summation over contracted indices even though we are working in the non-relativistic regime.

In order to highlight the symmetry of the problem and make a smooth transition to the FQH case, we choose to work in the symmetric gauge $A^i = \frac{B}{2}\epsilon^{ij}x_j$ and introduce complex coordinates $z = x + \imath y$ and $\bar{z} = x - \imath y$ [2, 19]. The resulting Hamiltonian is given by :

$$\mathscr{H} = -\frac{1}{m^*}\left(\partial_z - \frac{\bar{z}}{4l_0^2}\right)\partial_{\bar{z}} - \frac{\omega_c}{2}, \tag{1.2.4}$$

where $l_0 = \sqrt{\Phi_0/2\pi B}$ is the magnetic length and m^* the effective mass. If not otherwise stated, we now work in natural units $\hbar = c = e = 1$. We can recognize Eq. (1.2.4) as the occupation number representation of the Hamiltonian of a quantum harmonic oscillator where $a = \partial_{\bar{z}}$ is the annihilation operator and $a^\dagger = \partial_z - \bar{z}/4l_0^2$ is the creation operator. As a result of interactions with the external magnetic field, the electrons have energy eigenvalues $\epsilon_n = \omega_c(n + 1/2)$, with an energy gap proportional to the cyclotron energy; these are the well known Landau levels (LL). Since the system is invariant with respect to rotations, the angular momentum m is a good quantum number and we can express the wave function of the system in this basis. The $n = 0$, single-particle wave functions are then given by:

$$\psi_{0,m}(z) = z^m e^{-\frac{|z|^2}{4l_0^2}}. \tag{1.2.5}$$

The above wave function describes anannulus of maximum radius $r_m = \sqrt{2ml_0^2}$. The area enclosed by the annulus is readily found by taking the expectation value with respect to the energy and angular momentum eigenstates $|0, m\rangle$(that is a linear combination of many cyclotron orbits with radius l_0 centered on a circle of radius r_m):

$$\langle 0, m|A_m|0, m\rangle = 2\pi(m + 1)l_0^2. \tag{1.2.6}$$

For a system of area $S = \pi R^2$, this means we should not consider states at distance $2ml_0^2 > R^2$. Using the definition of the magnetic length, we find in this way the maximum allowed eigenvalue of angular momentum $m_{max} + 1 \simeq \Phi(B)/\Phi_0 = N_\Phi$, that gives the number of flux quanta "piercing" the system. In the thermodynamic limit there are N_Φ single particle degenerate states in the lowest Landau level (LLL). Using definition (1.1.4) of the filling fraction, we then find :

$$\nu = \frac{N_e}{m_{max} + 1}. \tag{1.2.7}$$

So, when $\nu = 1$ every state $|0, m\rangle$ is filled with one electron, or equivalently we can say that there is a flux quantum for every electron in the system. The many-body wave function for the $\nu = 1$ QH state can be built by taking the Slater determinant of the single particle wave functions (1.2.5) :

$$\Psi(z_1, ..., z_N) = \prod_{i<j}^{N}(z_i - z_j)e^{-\sum_i \frac{|z_i|^2}{4l_0^2}}. \tag{1.2.8}$$

Finally, we can think about filling p higher LL as taking p copies of the lowest LL. Using the semiclassical expression for the Hall conductance we finally find:

$$\sigma_H = p\frac{e^2}{h}. \tag{1.2.9}$$

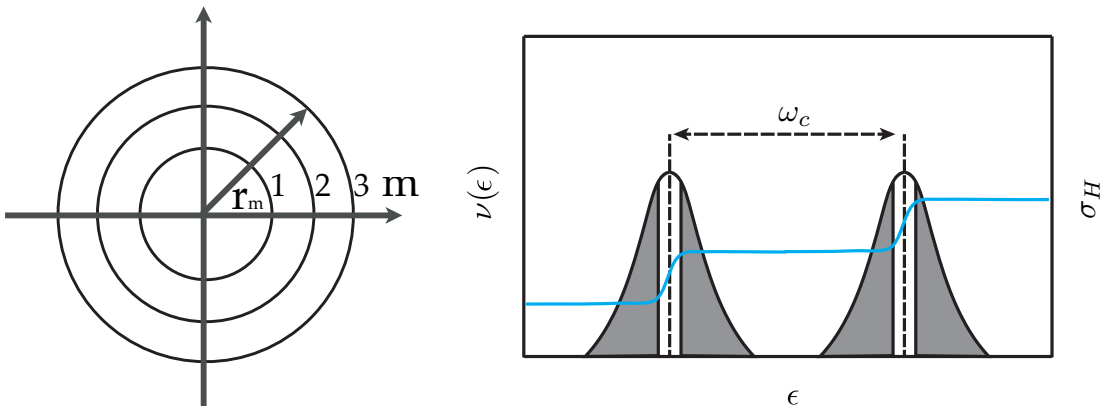

Figure 2: (Left) **The Quantum Hall droplet and its angular momentum eigenstates**. (Right) **Broadening of the LL due to impurities** : the shaded area represents the localized states while the white one around the center of the level represents delocalized states. Here $\nu(\epsilon)$ is the density of states. The blue curve is the QH conductance σ_H.

Suppose we fix the chemical potential in the system and then vary the external magnetic field. This operation will shift the LLs with respect to the chemical potential. As long as the chemical potential lies between two LLs, an integer number of levels will be filled and the quantized Hall conductance is expected to be measured. However, as we have previously pointed out, the single-particle states are highly degenerate, and it is not clear solely from the above derivation how the LL can actually be experimentally observed.

1.2.1 Dealing with disorder

From the above argument it is clear that something is missing in the description of the IQHE. As we have previously said, the Fermi level seems to jump from one LL to the other as the levels get filled up. In order to get the observed step-like behavior, we would need to lift the degeneracy of the single-particle states and also need additional states in the energy gap to be filled that do not contribute to the Hall conductance. It turns out that the addition of a random disorder potential fulfills both of these criteria. In the absence of a magnetic field it was shown that the random potential due to many impurities localizes the electronic states of a 2DEG [26]. In the presence of a magnetic field things become more complicated; however, it turns out that disorder broadens the LL into narrow conduction bands (see Fig. 2), and also provides the needed localized states between two LL. The amazing feature of the QHE is that disorder, although being an essential ingredient needed to observe the effect, does not destroy the precise value of the Quantum Hall conductance. This is in agreement with the high field limit of Eq. (1.1.2) derived from classical arguments. However, a fully quantum microscopic approach turns out to be quite complicated and far beyond the purpose of this section. One approach consists in mapping the disordered 2DEG in a large magnetic field onto a non-

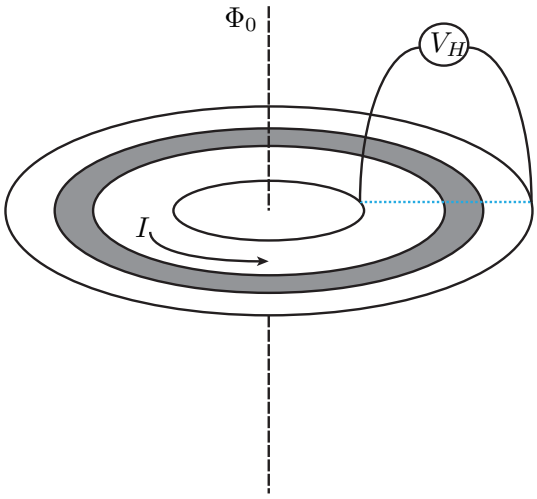

Figure 3: Laughlin's argument: A quantum Hall bar can be ideally bended into a Corbino disk geometry (the light blue dashed line represent the ideal cut). The shaded area represents localized states due to impurities. An additional flux quantum Φ_0 is adiabatically added to the system and a Hall voltage is measured with an external device. We consider the resistance of the measuring device to be much bigger than the quantum of resistance, such that charge on the two sides of the voltmeter is quantized in units of e.

linear sigma model [23, 27]. The surprising result of this approach is the appearance of a topological term in the effective action that elucidates the origin of the robustness of the effect. From a qualitative point of view Laughlin [28], and then Halperin [29] proposed an intriguing simple argument based on gauge invariance and the notion of a mobility gap. Consider the setup depicted in Fig. (3), where a QH bar is shaped into a Corbino disk geometry. We can ideally think that impurities only occupy the shaded region of the disk, and a Hall potential connects the two edges of the system. We consider the resistance of the measuring device to be much bigger than the quantum of resistance, such that charge on the two sides of the voltmeter is quantized in units of e. Due to the Hall potential, a current "I" circulates in the system. In addition to the uniform magnetic field, we now have a magnetic flux through the hole of the disk entering the Hamiltonian through the vector potential[6]

$$\mathbf{A}_\Phi(\mathbf{r}) = \frac{\Phi}{2\pi r}\mathbf{e}_\theta. \tag{1.2.10}$$

We may now think to add an extra integer number of flux quanta to the system; due to Faraday's law, this will cause an extra current in the system. From a quantum mechanical point of view, as long as the variation in the number of flux quanta $\Delta\Phi = q\Phi_0$ is an integer multiple of the flux quantum, we can gauge it away from the Hamiltonian. This leaves the spectrum of the Hamiltonian unchanged, but this does not imply that the energy of the state

6 here $\mathbf{e}_\theta = (-\sin\theta, \cos\theta, 0)$ is the unit vector in polar coordinates.

is left unchanged, since an original eigenstate of the Hamiltonian can evolve into another one having a different energy. Moreover the eigenfunctions acquire an Aronov-Bohm phase

$$\psi_n \to e^{\imath \frac{eq\Phi_0}{2\pi}\theta}\psi_n. \tag{1.2.11}$$

As a consequence of the flux insertion procedure, electrons should move from one side of the sample to the other; however the localized states in the middle of the disk prevent this process. Nevertheless, states at the border of the sample are gapless and electrons can pass from one side to the other of the sample through the external circuit. Since the circuit is not in a QH state, only an integer number p of electrons can go through it resulting in an energy variation $\Delta E = -peV_H$. Using the definition of the current as the derivative of the Hamiltonian with respect to the gauge field (1.2.10), and making use of the Hellmann-Feynman theorem, we can express the current in terms of the energy and flux variation[7]:

$$I = -c\frac{\Delta E}{\Delta \Phi} = \frac{p}{q}\frac{e^2}{h}V_H. \tag{1.2.12}$$

Even though the above expression does not tell us anything about the allowed values of p and q, it directly explains the QH effect solely on the basis of gauge invariance and shows how disorder, even though essential in the derivation, does not explicitly appear in the final expression. We can draw two other important conclusions from the above result : first of all the role of the edges as the gapless modes of the system, and second the possibility of having more than one flux quantum for every electron. In the next chapters we will elucidate the role of the edge states as chiral (i.e. propagating only in one direction) current carrying states, and show how the latter coclusion describes a strongly correlated state of matter known as the fractional QHE.

1.3 THE FRACTIONAL QUANTUM HALL EFFECT

We have seen that in the regime in which disorder is relevant, the IQHE is observed. At stronger magnetic fields, plateaus in the conductance are observed at rational values of the filling fraction. However, the single particle Hilbert space is now restricted to the lowest LL (LLL), so the observed plateaus cannot be solely explained in terms of the cyclotron gap as in the integer case. It turns out that Coulomb interaction dominates this phase of the 2DEG and it is responsible for lifting the LL degeneracy; however, Coulomb interaction effects turns out to be non-perturbative and therefore difficult to account for. In order to explain the FQHE Laughlin introduced a "trial" wave function based on the following observations:

- As showed in Eq. (1.2.8), the wave function can be built as a linear combination of the single-body states

$$\Psi(z_1, ..., z_N) = f(z_1, ...z_N)e^{-\sum_i \frac{|z_i|^2}{4l_0^2}}. \tag{1.3.1}$$

7 The Hellmann–Feynman theorem relates the variation of the total energy with respect to a parameter, to the expectation value of the variation of the Hamiltonian with respect to that same parameter.

where $f(z_1, ..., z_N)$ is a polynomial of particle positions.

- By assumption, the only relevant interaction in the system is the Coulomb one; this shows a strong repulsive part at short distance that tends to separate the electrons i.e. the wave function should become smaller when two electrons approach each other. Since the total angular momentum $M = \sum_i m_i$ is a conserved quantity, the wave function must be a function of the electron separation only :

$$f(z_1, ...z_N) \simeq \prod_{i<j}^{N} g(z_i - z_j) \tag{1.3.2}$$

- Since the total angular momentum M commutes with the Hamiltonian of the system, we can work in the total angular momentum basis. Basically, this means we need to choose $g(z_i - z_j)$ as an homogeneous polynomial in M

$$\Psi_q(z_1, ..., z_N) = \prod_{i<j}^{N} (z_i - z_j)^q e^{-\sum_i \frac{|z_i|^2}{4l_0^2}}, \tag{1.3.3}$$

where q labels states of different total angular momentum.

- Since we are working with fermions, Eq. (1.3.3) must be a totally antisymmetric function of its arguments. This means q must be an odd integer.

Eq. (1.3.3) is the celebrated Laughlin wave function, that nicely overlaps with the exact ground-state wave function computed from numerics [30]. At this point we can proceed as we did for the integer case and define the filling fraction. The maximum power of M, once one of the electron's coordinate has been fixed, is $M_{max} = (n_e - 1)q$. The maximum enclosed area is given by : $\langle A_M \rangle = \pi(M_{max} + 1)l_0^2$. The filling fraction is readily found to be:

$$\nu = \frac{N_e}{M_{max} + 1} = \frac{N_e}{(N_e - 1)q + 1} \sim \frac{1}{q}, \tag{1.3.4}$$

where the last expression on the r.h.s. is valid in the thermodynamic limit. Since q must be an odd integer, we will often use the expression $q = 2k + 1$, with k an integer. Consider for example the $\nu = 1/3$ quantum Hall state, then Eq. (1.3.3) posseses three zeros for every electron (or equivalently, three flux quanta are attached to one electron). By taking the square modulus of the wave function $|\Psi|^2 \sim r^6$ (r here is the inter-particle distance), we see that the probability that two electrons approach each other is very small, and the system is therefore incompressible. Physically, the zeros of the wave function are vortices, configurations where the density goes to zero at the vortex core, but a phase change is observed when performing a loop around them. The properties of the FQH state can be derived using the plasma analogy [2, 30]; however, in this chapter we will present some arguments based on a low-energy field theory description. Before looking at the transport properties, we briefly consider the construction of FQH states other than the ones in the Laughlin sequence.

1.3.1 Excitations

The Laughlin wave function describes a bound state of electrons with an odd number of flux quanta. If we change the number of flux quanta, we create quasi-particle excitations over the ground-state of the system. For example, we can think about introducing an additional quantum of flux by threading the system with a thin solenoid that can be successively eliminated via a gauge transformation, see Fig. (4). As a result of this operation, we will observe a change in the electron density at the point ξ where the solenoid has been inserted. Due to the incompressibility of the system, after the insertion of the solenoid electron will move towards the edge of the sample leaving behind a quasi-hole (qh). Formally this amounts to introducing an extra polynomial factor in Eq. (1.3.3)

$$\Psi_{qh}(z_1, ..., z_N; \xi) = \sqrt{N} \prod_i (z_i - \xi)^q \Psi_q(z_1, ..., z_N), \tag{1.3.5}$$

that corresponds to the insertion of q qhs. Here $\sqrt{N}$ is a normalization factor. As we will show later, these excitations have fractional charge $e^* = e/q$ and obey fractional statistics.

1.3.2 Hierarchical states

Since the quasi-particles introduced in the previous section are themselves charged particles moving in a perpendicular magnetic field, we may wonder if they can condense to form a new QH state. The problem consists then in finding the right values of the quasi-particle density for which a new state can emerge. Since the excitations over the ground-state have fractional statistics, they should be thought of as Anyons, i.e. particles having intermediate statistics with respect to fermions and bosons [31]. However we can treat them as fermions or bosons with attached flux quanta; this leads to three equivalent constructions of the hierarchical states : Haldane [32] derived a construction based on the bosonic approach, Jain [33] on the fermionic one and Halperin [34] on the anyonic. We start here by showing the main points of Haldane's construction, then we will describe Jain's idea of composite fermions and in (A.3) we will point out their equivalence.

As we have seen, Eq. (1.3.5) describes the quasi-holes in the system; to find the filling fraction we proceed as in the previous cases and consider the total angular momentum M. If we fix the coordinate of the qh, we are left with $N_e + 1$ possible states [8]. Since qhs are treated as bosons in this approach, a Laughlin state will form at $q = 2p$ ($p \in \mathbb{Z}$). The number of qhs needed to form a new QH state is given by the ratio between the total available quasi-particle states and the "critical area":

$$N_{qh} = \frac{N_e + 1}{2p}, \tag{1.3.6}$$

8 Remember that $\Psi_{qh}(z_1, ..., z_N; \xi)$ describes N_e possible states plus one coming from the additional hole.

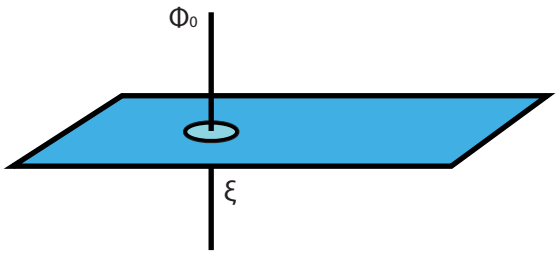

Figure 4: Creation of a quasi-hole at position ξ (light blue) by insertion of an additional flux quantum in the QH liquid (blue).

that also corresponds to the number of additional fluxes in the system. The total number of fluxes in the system is found by summing the fluxes of the original parent state and the additional ones: $N_{\phi,tot} = N_{\phi,par} + N_{\phi,qh}$. The filling fraction reads

$$\nu = \frac{N_e}{N_{\phi,tot}} = \frac{N_e}{(N_e - 1)q + 1 + \frac{N_e+1}{2p}} \sim \frac{1}{q + \frac{1}{2p}} \tag{1.3.7}$$

in the thermodynamic limit. We can use the same procedure to find an equivalent expression for the quasi-electrons, or note that there is simply a sign difference due to the opposite charge. Moreover, once the first hierarchical level has been formed, nothing stop us from re-iterating the same procedure using the former hierarchical state as the new parent state. In this way we obtain a continuous fraction expression for the filling fraction :

$$\nu = \frac{1}{2k + 1 \pm \frac{1}{2p_1 \pm \frac{1}{2p_2 \pm \frac{1}{2p_3 \pm \dots}}}}. \tag{1.3.8}$$

In principle we can observe any values of ν, however not all of these fractions are seen in experiments. As we descend in the hierarchy, the energy gap of the QH state becomes smaller and smaller, and so more easily destroyed by disorder and thermal fluctuations.

An alternative way to construct the hierarchical states consists in treating the quasi-particles as fermions. In his 1989 paper [33], Jain realized that the Laughlin wave function allows for an interesting alternative interpretation. The quasi-hole has been constructed by piercing the QH fluid with a solenoid carrying an additional flux quantum. For $q = 2k+1$ we can rewrite Eq. (1.3.3) as :

$$\Psi_{2k+1}(z_1, ..., z_N) = \prod_{i<j} (z_i - z_j)^{2k} \Psi_1(z_1, ..., z_N). \tag{1.3.9}$$

Now we can interpret $\Psi_1(z_1, ..., z_N)$ as the wave function of a completely filled LLL and the first polynomial term on the right hand side as the insertion of $2k$ additional fluxes in the system. Note that since $2k$ is even, this operation does not change the total parity of the wave function. Unlike the quasi-hole, where the coordinate of the inserted solenoid is fixed, here the solenoids are physically attached to the electrons filling up the LLL. The FQHE can then be understood in terms of an integer effect of so called "composite fermions"; Let us

ν	Haldane	Jain
2/3	$\frac{1}{1+\frac{1}{2}}$	$\frac{2}{-1+4}$
2/5	$\frac{1}{3-1/2}$	$\frac{2}{1+4}$
3/7	$\frac{1}{3-\frac{1}{2-1/2}}$	$\frac{3}{6+1}$

Table 1: Hierarchical construction. Comparison between filling fractions in the Haldane's and Jain's hierarchical constructions.

call p the effective integer filling, then following the scheme of the previous sections, we can express it as the ratio between the number of particles and the number of un-attached fluxes. Using the fact that the composite Fermion number $n_{c.F.} = \phi_0 N_e$, we find :

$$p = \frac{N_{c.f.}}{N_\phi - 2kN_{c.f}} = \frac{\nu}{1-2k\nu}. \tag{1.3.10}$$

The electronic filling factor ν is then found by inverting the above relation :

$$\nu = \frac{p}{\pm 1 + 2kp}, \tag{1.3.11}$$

where we have generalized the expression for the filling fraction to the construction of the quasi-hole. Note that in the above expression, the case $p = 1$ corresponds to the original Laughlin series. In table (1) we compare Haldane's and Jain's constructions for a few values of the electronic filling fraction; from the comparison it appears that the same experimentally observed state is originating from two different physical pictures, however in Appendix (A.3) we will point out that the two constructions are indeed equivalent.

1.4 EFFECTIVE FIELD THEORY

While it is possible to understand many properties of the integer and fractional QHE from the wave function approach, a low-energy field theory provides an easier way to derive its macroscopic properties. Transport quantities are in fact most easily computed in the field theory approach, together with properties such as fractional charges and statistics; moreover the field theory highlights the topological nature of the QHE and generalizes the derivation of the edge-state action to the hierarchical case. However, the validity of the effective theory can only be checked by comparing it to the numerical results of the microscopic theory.

In this section we will present a mean field analysis and draw some conclusions on the macroscopic observables of the system. Even though the mean field analysis highlights many features of the Chern-Simons action, it does not take into account the role of the Coulomb interaction and therefore it cannot be correct. For this reason, in appendix (A) we present a detailed derivation of the so called Ginzburg-Landau theory of the QHE [35], followed by the derivation of the generalized edge-state action.

1.4.1 Chern-Simons term

The flux attachment procedure proposed by Jain shows that it is indeed possible to create bound states of electrons and fluxes, and that these "new" particles show rather interesting properties such as fractional statistics. Wilczek showed that the anyonic statistics can emerge in a $2+1$ dimensional field theory of electrons dynamically coupled to a Chern-Simons[9] (CS) gauge field a_μ, whose strength is expressed by the following Lagrangian density:

$$\mathscr{L}_{CS} = \frac{\gamma}{4\pi}\epsilon^{\mu\nu\rho}a_\mu\partial_\nu a_\rho, \tag{1.4.1}$$

where γ is a coupling constant to be specified. Contrary to our experience where field's indices are contracted with the metric tensor, here all the indices are contracted with the Levi-Civita tensor. This apparently small difference actually makes a huge difference in the behavior of the CS term. Under a local coordinate transformation $x \to x'$, the vector field changes as $a_\mu(x) = \partial x'_\nu/\partial x_\mu a_\nu(x')$. However, this transformation leaves the action of the system invariant. The CS term is a topological term, i.e. its action does not depend on the metric, but only on the topology of the space. Since the energy of the system can be derived by varying the action with respect to the metric tensor, it follows that a topological field theory has only the trivial zero energy ground-state. From the above consideration it also follows that $\mathscr{H}_{CS} = 0$, meaning that the CS term is a pure gauge and precaution must be made when quantizing it[10]. Even though the CS field is a gauge field, its action is gauge invariant only for a system without boundaries. Upon a gauge transformation $a'_\mu = a_\mu + \partial_\mu\Lambda$, the CS action transforms as:

$$S' = S + \frac{\gamma}{4\pi}\int_\Omega \epsilon^{\mu\nu\rho}\partial_\mu(a_\nu\partial_\rho\Lambda). \tag{1.4.2}$$

The additional term is zero when evaluated over the hyper surface at infinity (i.e. in the bulk of the system), however for a theory with boundaries this term is not necessarily zero, leading to a gauge anomaly. In (A.4) we show that in order to have a properly gauge invariant theory, this term must be canceled by a counter-term coming from the edge; in the effective field theory the edge states naturally appears by demanding the gauge invariance of the CS Lagrangian !

1.4.2 Mean Field Analysis

The Lagrangian density for a system of spinless interacting electrons coupled to an external electromagnetic vector field A_μ, and a CS gauge field a_μ is given by:

$$\mathscr{L} = \imath\psi^\dagger D_0\psi - \frac{1}{2m}(D_i\psi)^2 - \lambda(\psi^\dagger\psi - \bar{\rho})^2 + \frac{\gamma}{4\pi}\epsilon^{\mu\nu\rho}a_\mu\partial_\nu a_\rho, \tag{1.4.3}$$

9 For a nice derivation of the Chern-Simons term from the Chern classification of topological field theories see for example [36].

10 This is a common problem of gauge theories, and the right procedure for quantizing them is to introduce constraints. This can be done using Dirac's canonical constrained quantization procedure[37] or the Fadeev-Popov Path integral approach [22].

where $i = (1,2) \equiv (x,y)$ are spatial coordinates and "$0 = t$" is the time one. The covariant derivative $D_\mu = \partial_\mu - \imath(A_\mu + a_\mu)$ takes care of the interaction between the matter and the gauge fields. Here, $\lambda = \lambda(x - x')$ is the Coulomb interaction strength and $\bar{\rho}$ is the average background density that constitutes the vacuum state of the theory. Finally, note that we are again omitting the Maxwell term since we are taking it as non-fluctuating. As we explain below, if γ is an even number, the CS term does not change the statistics of the fermions in Eq. (1.4.3). A mean field analysis gives us some interesting information on the behavior of the CS term. The saddle point solution for the gauge field a_μ gives :

$$\langle j^\mu \rangle = \frac{\gamma}{2\pi} \epsilon^{\mu\nu\rho} \partial_\nu a_\rho \tag{1.4.4}$$

where $j^\mu = (\rho, j^i)$ is the standard current operator. We immediately see that, contrary to the Maxwell term, the CS term does not have independent dynamics. Most interestingly, the resulting current is automatically conserved[11] due to Bianchi's identity $\epsilon^{\mu\nu\rho}\partial_\mu\partial_\nu a_\rho = 0$. To better understand the physics of Eq. (1.4.4) it is convenient to write it down in components:

$$\begin{aligned} \nabla \wedge \mathbf{a} &= \gamma^{-1}\Phi_0\langle\rho\rangle \\ \epsilon^{ji}\partial_0 a_j &= \gamma^{-1}\Phi_0\langle j^i\rangle. \end{aligned} \tag{1.4.5}$$

The first equation tells us that the effect of the effective CS magnetic field is to attach γ^{-1} flux quanta[12] to every electron in the system while the second tells us that these fluxes move together with the electron, i.e. they form a bound state that we can treat as a new composite particle. As one of the composite particles is exchanged with another, it acquires an Aharonov-Bohm phase of $(-1)^{1/\gamma}$. This means that if we treat the composite particles as fermions, as in Eq. (1.4.3), we need to choose $\gamma = 1/2p$. In this case, the value of γ can be chosen such as to partially cancel the external magnetic field[13]. On the other hand we can write a different theory in which the composite particles are considered as bosons by choosing $\gamma = 1/(2k+1)$. Choosing this second option, the fermionic fields in Eq. (1.4.3) can be exchanged with a complex scalar bosonic field Φ. In this way we obtain the Ginzburg-Landau theory in the presence of a CS field. In (A.1) we give a detailed account of this theory, however here we can draw some preliminary conclusions based on our knowledge of Ginzburg-Landau theories. We know that long-range order in a gauged Φ^4 theory will result in the Meissner effect $\mathbf{a} + \mathbf{A} = 0$; taking the curl of this last expression and using Eq. (1.4.5) gives $B = \Phi_0(2k+1)\langle\rho\rangle$, therefore we can identify the filling fraction $\nu = 1/(2k+1)$. Excitations above this mean field solution are gapped due to the Meissner effect and are vortex-like: $\Phi(r,\theta) = |\Phi(r)|e^{\imath\theta}$. By construction, these are the quasi-particles of the Laughlin. By varying the action with respect to A_0 we obtain the electromagnetic charge density, whose integral gives the charge of the particles in the system. We can find in this way that the quasi-particle charge is $e^* = e/(2k+1)$.

11 Conservation laws are usually derived from Noether's theorem that connects them to the space-time symmetries of the theory. However, in this case the conservation law does not involve the existence of any space-time symmetry but it follows from Bianchi's identity, that is related instead to the topology of space.

12 In natural units $\Phi_0 = 2\pi$.

13 Note that in the case of $\nu = 1/2$ this cancelation is exact.

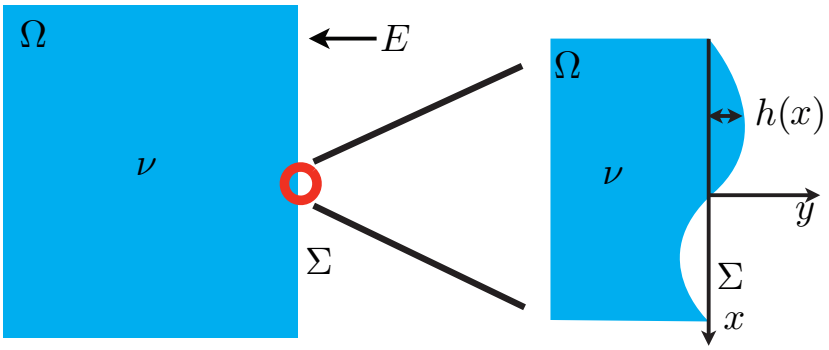

Figure 5: Edge states. (Left) a two dimensional region Ω filled with a QH fluid at filling fraction ν. At the boundary $\Sigma = \partial\Omega$ a field E confines the system in the y direction. (Right) Detail of the surface wave dynamics at the edge of the sample.

1.5 EDGE STATES FROM THE HYDRODYNAMICAL APPROACH: AN HEURISTIC DERIVATION

In section (1.2.1) we discussed Laughling's argument for the quantization of the Hall conductance. In Laughling's gedanken experiment we learned that, due to the request of gauge invariance, charge accumulates at the edges of the sample. Halperin [29] has been the first to suggest that gapless states exist at the border of an IQH sample and can be described in terms of one dimensional chiral Fermi Liquids. Later on, Wen suggested that in the case of the FQH effect, the edge states can be described in terms of a chiral Luttinger Liquid (LuL) [38–42], that is a strongly interacting, one dimensional chiral system (see chapter 2).

There is a simple way to understand why edge states should exist by making use of the results of the previous section[14]. We showed that Eq. (1.4.4) has a topological nature, i.e. current conservation follows directly from Bianchi's identity. However, consider the physical case of a sample with boundaries; the bulk of the system is in a QH state and is characterized by a constant $\sigma_H \neq 0$. The boundary separates the QH phase from a normal phase where $\sigma_H = 0$. This means that at the boundary σ_H is discontinuous. The continuity equation then gives

$$\partial_\mu j^\mu(x) = [\partial_\mu \sigma_H(x)]\epsilon^{\mu\nu\rho}\partial_\nu a_\rho(x) + \partial_\mu j^\mu_{bulk}(x); \tag{1.5.1}$$

the fermionic current is not anymore conserved. However, Eq. (1.5.1) cannot be the total current flowing in the system, that is instead given by $j^\mu_{total} = j^\mu_{bulk} + j^\mu_{edge}$. The edge currents exactly cancel the additional contribution coming from the term proportional to $\nabla \cdot \sigma_H(x)$ and gauge invariance is restored. In high energy physics, this lack of conservation of edge currents is generally known as the "gauge anomaly"[15]. In appendix (A.4) we show how the Chern-Simons effective field theory naturally includes the edge states when quantized

14 See also the extensive and nice discussion in [43].

15 In particular, in $1+1$ gauge field theories it is also known as the "chiral anomaly".

on a compact surface under the request of gauge invariance. In this section we will present a simple construction of the Chiral LuL Hamiltonian due to Wen [2].

Consider the system depicted in Fig. (5). We assume the bulk region Ω to be filled with an incompressible electron liquid at filling fraction ν. The edge Σ of the system sets the boundary between the QH state and the normal state. The electron liquid is confined in the QH bar by a confinement field E due to an electrostatic potential. Since by assumption the bulk is in an incompressible state, the only gapless excitations can be surface waves due to deformations of the boundary. We can introduce the displacement field $h(x)$ and compute the energy cost of a deformation

$$H = \int_x \int_0^{h(x)} dy\, n_e\, f_{ext}\, y, \tag{1.5.2}$$

where $f_{ext} = e\,E$ is the external force acting on the edge and n_e is the constant electron density. We can connect the displacement field to the electron density of the wave by defining $\rho(x) = n_e\, h(x)$ and use Eq. (1.1.4) to relate the electron density to the filling fraction of the QH state $n_e = e\nu\, B/(2\pi c)$:

$$H = \frac{\pi}{\nu}\int_x \rho^2(x)\frac{E\,c}{B}. \tag{1.5.3}$$

The above equation must be supplemented by a boundary condition coming from the edge dynamics, namely that the total force acting on the boundary should be zero $\delta f = f_{int} - f_{ext} = 0$, where $f^y_{int} = (-e/c)\mathbf{u} \wedge \mathbf{B}$. This tells us that there are states moving in the x direction at velocity

$$u_x = \pm\frac{E\,c}{B_z}, \tag{1.5.4}$$

where the $\pm$ sign refers to the direction of propagation on the two different edges of the sample. A perhaps more familiar example of this phenomenon in classical physics is a Hurricane [43]. In this case the magnetic field is replaced by the angular velocity of the Earth and Lorentz force is replaced by the Coriolis force. Finally, the confinement field is replaced by the gradient of air pressure surrounding the Hurricane. Since the edge current is conserved, we also have as an additional constraint the continuity equation

$$(\partial_t + u_x\partial_x)\rho(x) = 0, \tag{1.5.5}$$

where we have used $j(x) = u_x\,\rho(x)$. In order to canonically quantize the Hamiltonian, we move to momentum space

$$H = \frac{2\pi u_x}{\nu}\sum_k \rho_k\rho_{-k} \tag{1.5.6}$$

$$\dot{\rho}_k = -\imath u_x\, k\,\rho_k. \tag{1.5.7}$$

If we interpret ρ_k as the generalized coordinate q, then we need to choose the canonical momentum in such a way that it reproduces the correct equations of motion

$$\dot{\Pi} = -\frac{\partial H}{\partial q} \quad , \quad H = \Pi\dot{q} - L. \tag{1.5.8}$$

Choosing $\Pi = \imath 2\pi\rho_{-k}/(\nu\, k)$, Eq. (1.5.8) is correctly reproduced and the density fields satisfy the canonical commutation relation

$$\left[\rho_k, \frac{\imath 2\pi}{\nu k'}\rho_{k'}\right] = \frac{\nu}{2\pi} k\, \delta_{k,k'}. \tag{1.5.9}$$

As we will show in the next chapter, the above commutator describes the Kac-Moody Algebra of chiral bosons.

2 BOSONIZATION

CONTENTS

We ended the last section showing that a general QH state presents gapless excitations at the boundary of the sample. We showed that those one dimensional excitations can be described in terms of a chiral bosonic theory, and they account for the measured QH conductance. However it should be reminded that the original theory was written in terms of fermions; this "transmutation" of the statistics for a $1+1$ dimensional system and the related technique goes under the name of bosonization and will be the main focus of this chapter. We will start introducing the main concepts and tools of the standard bosonization approach in operator formalism, show how the Luttinger Liquid (LuL) model is derived and highlights its main properties. We will show that in $1+1$ dimensions a strongly interacting fermionic system can be mapped onto a non-interacting bosonic one, allowing in this way for an exact solution of a many-body problem. Recently it has been realized that for some non-equilibrium configurations the standard bosonization approach does not lead to an exact solution of the many-body fermionic problem [6–9]. We will use non-equilibrium bosonization techniques in chapter (5) and introduce them here by means of a functional approach. The functional approach will prove particularly useful since it treats fermions and bosons on equal footing and it highlights the various assumptions involved in the bosonization machinery.

2.1 BOSONIZATION IN A NUTSHELL

In this section we review some of the central bosonization formulas and the key concepts to be used later on in this thesis. Different formulations of bosonization exist in the literature, here we present the so called "constructive" (or operator based) approach pioneered by Mattis

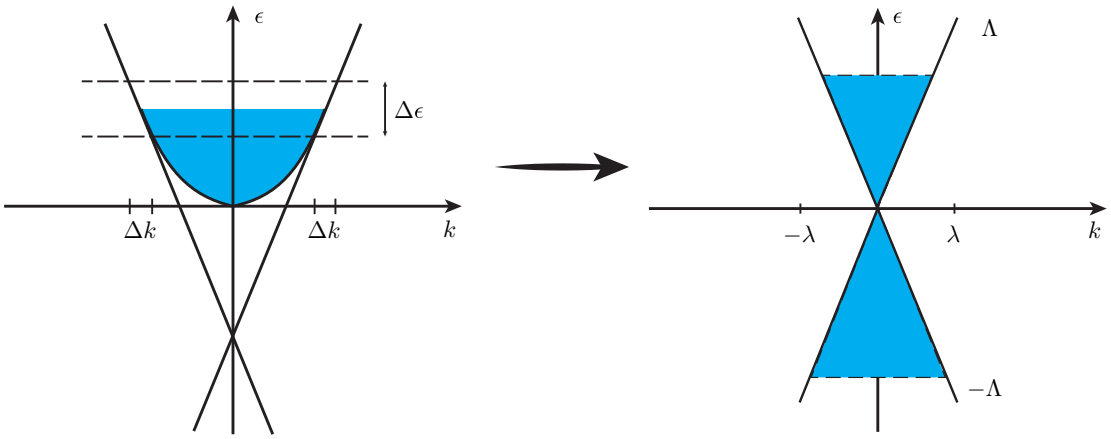

Figure 6: One Dimensional dispersion relation and low energy approximation. (Left) parabolic dispersion in one dimension. The blue area describes the filled Fermi sea. The low energy and momentum intervals around the two Fermi points are also shown. (Right) linear approximation of the dispersion relation in the neighborhood of the two Fermi points. The cut-offs λ and Λ originate respectively from the Δk and $\Delta\epsilon$ intervals defined in the left picture.

and Lieb [44] in the notation introduced by Haldane [45]. Most of this section is based on references [19, 46–48].

2.1.1 The Tomonoga-Luttinger model

Consider a one dimensional system of interacting electrons. The Hamiltonian density for such system is $\mathscr{H} = \mathscr{H}_0 + \mathscr{H}_I$, where

$$\begin{aligned} \mathscr{H}_0 &= \sum_{\sigma=\uparrow,\downarrow} \psi^\dagger_\sigma(x)\left(-\frac{\hbar^2}{2m}\partial_x^2 - \mu\right)\psi_\sigma(x) \\ \mathscr{H}_I &= \sum_{\sigma,\sigma'=\uparrow,\downarrow} \psi^\dagger_\sigma(x)\psi_\sigma(x)U(x-x')\psi^\dagger_{\sigma'}(x')\psi_{\sigma'}(x'), \end{aligned} \tag{2.1.1}$$

where $U(x-x')$ is the electon-electron interaction potential that can be Coulomb or short-ranged, and σ is the spin index. We are interested in deriving a low energy theory of the one dimensional electron gas. Let us start considering the free theory $\mathscr{H}_0$; the crucial observation is that in one spatial dimension instead of a Fermi surface there are at least two Fermi points situated at $\pm k_F$. If we are interested in the long-distance behavior of this system we can focus on states close to the Fermi energy and linearize the original parabolic electron dispersion relation around the two Fermi points (here u_F is the Fermi velocity)

$$\epsilon_k \simeq \epsilon_F + (|k| - k_F)u_F + \ldots \tag{2.1.2}$$

In Fig. (6) the linearization procedure is sketched together with the definition of the momentum and energy cut-off, respectively $\lambda \sim \Delta k$ and $\Lambda \sim \Delta\epsilon$. Consider then the Fourier expansion of the fermionic field around the two Fermi points:

$$\begin{aligned}\psi_\sigma(x) &\simeq \int_{-\lambda}^{\lambda} \frac{dk}{2\pi} e^{\imath(k+k_F)x}\psi_\sigma(k+k_F) + \int_{-\lambda}^{\lambda} \frac{dk}{2\pi} e^{\imath(k-k_F)x}\psi_\sigma(k-k_F) \\ &= e^{\imath k_F x}\psi_{\sigma,R}(x) + e^{-\imath k_F x}\psi_{\sigma,L}(x).\end{aligned} \tag{2.1.3}$$

In the above expression we have defined the right and left moving pieces of the original fermionic field. The linearized one-dimensional Hamiltonian is simply the Dirac Hamiltonian with the velocity of light replaced by the Fermi velocity[1]:

$$\mathscr{H}_0 = -\imath u_F \sum_{\sigma=\uparrow,\downarrow} \Psi^\dagger_\sigma(x)\sigma_3\partial_x\Psi_\sigma(x), \tag{2.1.4}$$

where we have set the Fermi energy to zero and introduced the spinor components

$$\Psi_\sigma(x) = \begin{pmatrix} \psi_{\sigma,R}(x) \\ \psi_{\sigma,L}(x) \end{pmatrix} \quad , \quad \sigma_3 = \begin{pmatrix} 1 & 0 \\ 0 & -1 \end{pmatrix} \tag{2.1.5}$$

In Dirac theory it is customary to define the γ matrices in terms of the Pauli matrices: $\gamma_0 = \sigma_1$, $\gamma_1 = -\imath\sigma_2$ and $\gamma_5 = \gamma_0\gamma_1 = \sigma_3$. Since we will be mainly interested in spinless electrons, we can drop the spin index and define the fermionic current as ($u_F = 1$):

$$j_\mu = \Psi^\dagger\gamma_0\gamma_\mu\Psi. \tag{2.1.6}$$

The zero component of this operator gives the total fermion density $j_0(x) = \rho(x)$ while the spatial component gives the difference between right and left moving fermions, i.e. a particle current. The γ_5 matrix is related to chiral symmetry and we can use it to define an additional bilinear function of fermionic fields called the chiral (or axial) current:

$$j^5_\mu = \Psi^\dagger\,\gamma_0\gamma_\mu\gamma^5\,\Psi. \tag{2.1.7}$$

A chiral transformation of the fields is defined as a rotation $\psi'_\alpha = (e^{\imath\gamma_5\theta})_{\alpha\beta}\psi_\beta$, with θ a constant angle. Both the Hamiltonian Eq. (2.1.4) and the fermionic current Eq. (2.1.7) are invariant with respect to chiral transformations. To see this we use $\psi'^\dagger_\alpha\gamma_0 = (\psi)^\dagger_\beta(e^{-\imath\gamma_5\theta})_{\alpha\beta}\gamma_0$ together with the anti-commutation relation $\{\gamma_\mu,\gamma_5\} = 0$. From a direct inspection we can verify that $\sigma_3 e^{\imath\gamma_5\theta} = e^{-\imath\gamma_5\theta}\sigma_3$, from which $\psi'^\dagger_\alpha\gamma_0 = (\psi)^\dagger_\beta\gamma_0(e^{\imath\gamma_5\theta})_{\alpha\beta}$. Using these transformations, the invariance of the Hamiltonian and the chiral current follows. As a concluding remark we would like to mention that the chiral current is not conserved at the quantum level, a phenomenon known as the chiral anomaly[2].

1 This is an example of emerging Lorentz structure. Even though the original system does not describe relativistic fermions, its low energy expression does ! Another famous example is Graphene, where linearization around the Dirac points leads to a two dimensional Dirac Hamiltonian.

2 The term anomaly is used in QFT to describe a symmetry of the classical system that is not preserved at the quantum level. An elegant and easy way of observing the appearance of the anomaly in Gauge theories is using

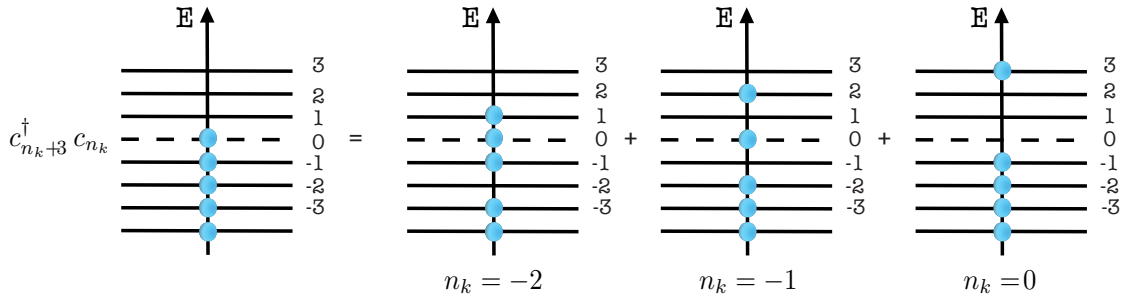

Figure 7: Particle-hole excitations on a N-particles Hilbert space. The cartoon shows the action of the "particle-hole operator" on a N-particle Hilbert space for discrete momentum quantum number $n_q = 3$. If $n_k = -3$ no excited states are created. For $n_k > -3$ there are 3 possible configurations with the same energy.

2.1.2 Structure of the Hilbert space

Now that the model has been defined we need to consider its related observables and the algebra of its operators. To our purpose it is convenient to introduce a set of creation and annihilation operators acting on the many-body state and related to the fermionic fields by

$$\psi_\eta(x) = \sqrt{\frac{2\pi}{L}} \sum_{k=-\infty}^{\infty} e^{\imath s_\eta k x} c_\eta(s_\eta k), \tag{2.1.8}$$

where $\eta = 1, 2, ..., n$ is an additional quantum number specifying the different fermionic species, $s_\eta = \pm$ respectively for right and left moving electrons. The canonical ladder operators satisfy

$$\left\{ c_{k,\eta}, c^\dagger_{k',\eta'} \right\} = \delta_{k,k'}\delta_{\eta,\eta'} \quad , \quad k \in [-\infty, \infty]\,. \tag{2.1.9}$$

In what follows we will consider spinless electrons, so $\eta = 2$ labels right and left moving electrons. It is convenient to define the system on a compact space such that momentum is quantized. For example let us work with a right moving field (hereafter we will often omit the chirality index for practical purpose) on a circle of radius L and impose periodic boundary conditions $\psi(x + L) = \psi(x)$, then $k = (2\pi/L)n_k$ ($n_k \in \mathbb{Z}$). When computing observables, we will take the $L \to \infty$ limit at the end of the calculation in order to work with a system defined on a line. The second step consists in defining the many-body Fock space

$$\mathscr{F} = \sum_{\oplus N} H_N, \tag{2.1.10}$$

a path integral method developed by Fujikawa [49]. Even though the classical action corresponding to Eq. (2.1.4) is left invariant under a gauge or a chiral transformation, the measure of the path integral changes by a Jacobian factor $\mathscr{D}[\Psi, \Psi^\dagger] = \mathscr{J}\mathscr{D}[\Psi', \Psi'^\dagger]$. As a consequence one finds that the quantum effective action of a single chiral fermion is not gauge invariant. Luckily enough, the total (i.e. involving the two chiralities) quantum action is indeed gauge invariant. However, the quantum action is not invariant under a chiral transformation, from which the non-conservation of the chiral current follows.

where H_N are many-body Hilbert spaces at fixed particle number N. The Fock space contains infinitely many states corresponding to different configurations of particle-holes excitations. We define the N−particle ground state $|N\rangle_0$ as the one containing no particle-hole (p-h) excitations. A p-h excitation of momentum q is obtained by summing over all the available electronic states generated by $c^\dagger_{k+q}c_k$ (see Fig. 7) and it can be diagrammatically visualized in terms of Feynman diagrams as the "bubble" of Fig. (8). In one dimension these p-h excitations have a full bosonic character, therefore we can define creation and annihilation bosonic operators as:

$$\begin{aligned} b^\dagger_{q,\eta} &= \imath\sqrt{\frac{2\pi}{Lq}}\sum_{k=-\infty}^{\infty} c^\dagger_{k+q,\eta}c_{k,\eta} \\ b_{q,\eta} &= -\imath\sqrt{\frac{2\pi}{Lq}}\sum_{k=-\infty}^{\infty} c^\dagger_{k-q,\eta}c_{k,\eta}. \end{aligned} \tag{2.1.11}$$

where $q = (2\pi/L)n_q$, $n_q \in \mathbb{Z}^+$. It can be shown (B.1) that the above definition reproduces the correct bosonic commutation relations

$$[b_{qs_\eta}, b^\dagger_{q's_{\eta'}}] = \delta_{q,q'}\delta_{s_\eta s_{\eta'}} \quad , \quad [b_{qs_\eta}, b_{q's_{\eta'}}] = [b^\dagger_{qs_\eta}, b^\dagger_{q's_{\eta'}}] = 0. \tag{2.1.12}$$

The key point is that for every N−particle Hilbert space, $|N\rangle_0$ serves as the vacuum state of the bosonic excitations, i.e. $b_{q,\eta}|N\rangle_0 = 0$ for every q and η simply because there are no p-h excitations to destroy. A generic state $|N\rangle \in H_N$ can be obtained via repetitive application of a bilinear function of fermionic operators $|N\rangle = g(c, c^\dagger)|N\rangle_0$. The non trivial statement is that $\exists\, g(b^\dagger) : |N\rangle = g(b^\dagger)|N\rangle_0$, that means the bosonic ladder operators span the complete N−particle Hilbert space. This equivalence between the fermionic and the bosonic Hilbert space can be proven by counting the number of states in the fermionic and in the bosonic representation and showing their equivalency. Haldane [45] proved this statement by evaluating the partition function in the two representations and showing their equivalency (see also [50]). Since the bosonic operators create p-h excitations in one of the Hilbert spaces with fixed particle numbers H_N, a faithful representation of the fermionic fields is obtained by introducing the ladder operators connecting different N−particle Hilbert spaces:

$$H_1 \xrightarrow{F^\dagger} H_2 \xrightarrow{F^\dagger} H_3 \xrightarrow{F^\dagger} \dots \tag{2.1.13}$$

These operators are known as Klein factors and they raise or lower the total fermionic number by one. Moreover, they ensure that fermionic fields of different species anti-commutes. These operators commute with every bosonic operator, they are unitary ($F_\eta^{-1} = F_\eta^\dagger$) and they obey the anti-commutation relation $\left\{F_{\eta'}, F_\eta^\dagger\right\} = 2\delta_{\eta,\eta'}$. Following Fabrizio and Gogolin [51], we can represent the Klein factor as: $F_\eta = \chi_\eta e^{\imath\theta_\eta}$, where χ_η is a Majorana fermionic field satisfying:

$$\{\chi_\eta, \chi_{\eta'}\} = 2\delta_{\eta,\eta'} \quad , \quad \chi_\eta^2 = 1 \tag{2.1.14}$$

and θ_η is the phase operator canonically conjugate to $\Delta N_\eta = N_\eta - N_{0,\eta}$

$$\left[\Delta N_\eta, \imath\theta_{\eta'}\right] = \delta_{\eta,\eta'}. \tag{2.1.15}$$

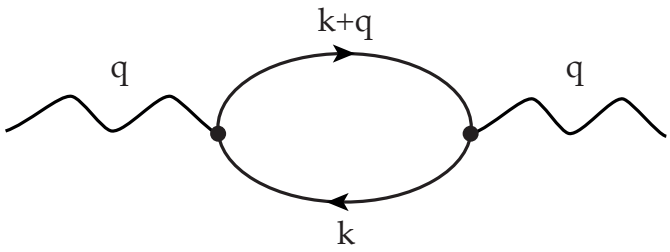

Figure 8: "Bubble" diagram. Momentum space Feynman diagram representation of a particle-hole excitation. The wiggled lines represent the incoming and outgoing external momentum while the solid lines represent the electron-hole pair.

Note that ΔN_η measures the extra number of electrons with respect to the ground state value $N_{0,\eta}$. As a concluding remark, we would like to stress that the action of $F^\dagger$ can be seen as "pushing up" all electron states by one position or equivalently "pushing down" by one position the Fermi energy. The latter picture corresponds to adding a chemical potential term $\epsilon_F - \mu$, and it is the one we will adopt. Similarly to the Fourier representation of fermionic fields, we can define the bosonic ones as:

$$\begin{aligned} \varphi_\eta(x) &= \sum_{q>0} \sqrt{\frac{2\pi}{qL}} e^{-q\alpha/2} e^{\imath s_\eta q x} b_\eta(s_\eta q) \\ \phi_\eta(x) &= \varphi(x)_\eta + \varphi_\eta^\dagger(x), \end{aligned} \tag{2.1.16}$$

where we have introduced the regularization parameter $\alpha > 0$ ($\alpha = \lambda^{-1}$) needed to regularize the ultraviolet ($q \to \infty$) divergent sums arising when considering certain expectation values. We can now express the electron density operator in terms of the bosonic field as follows (again we show it for right movers):

$$\begin{aligned} \rho(x) &= \psi^\dagger(x)\psi(x) = \frac{1}{L}\sum_{k,k'} e^{-\imath(k'-k)x} c_{k'}^\dagger c_k \\ &= \frac{1}{L}\sum_{k,q} e^{-\imath q x} c_{k+q}^\dagger c_k \\ &= \frac{1}{L}\sum_{k} c_k^\dagger c_k + \frac{1}{L}\sum_{k,q>0} e^{-\imath q x} c_{k+q}^\dagger c_k + \frac{1}{L}\sum_{k,q>0} e^{\imath q x} c_{k-q}^\dagger c_k \\ &= \frac{\Delta N_k}{L} + \frac{1}{2\pi}\partial_x \phi(x). \end{aligned} \tag{2.1.17}$$

In the first line we have just used the definition of the density operator in the fermionic representation and then defined the transferred momentum $q = k' - k$ to get to the second line. In the third line we have separated the $q = 0$ (zero mode) contribution from the $q > 0$ and $q < 0$ ones. In order to obtain the first term proportional to ΔN_k we have used the definition of the fermionic number operator paying attention that it should always be defined with respect to its ground state value. Finally we have used definitions (2.1.11), (2.1.16) to

express everything in terms of the bosonic field operators. Using the definitions of Eq. (2.1.16) we can derive the commutation relations of the bosonic field operators. We first evaluate

$$\begin{aligned}\left[\varphi^\dagger(x),\varphi(0)\right] &= \sum_{q>0}\frac{2\pi}{qL}e^{-q\alpha}e^{-\imath qx}[b_q^\dagger,b_q] \\ &= -\sum_{n_q=1}^{\infty}\frac{\left(e^{-\imath\frac{2\pi}{L}(x-\imath\alpha)}\right)^{n_q}}{n_q} \\ &= \log(1-e^{-\imath\frac{2\pi}{L}(x-\imath\alpha)}),\end{aligned} \tag{2.1.18}$$

and its complex conjugate. In the second line we have discretized momentum and in the third line we have computed the converging sum [3]. To work with a system defined on a line, we now take the $L >> x$ limit

$$\begin{aligned}[\phi(x)),\phi(0)] &\simeq \log\left(1-1+\imath\frac{2\pi}{L}(x-\imath\alpha)+...\right)-\log\left(1-1-\imath\frac{2\pi}{L}(x+\imath\alpha)\right) \\ &= \log\left(\frac{\imath x+\alpha}{-\imath x+\alpha}\right)=2\imath\arctan(x/\alpha).\end{aligned} \tag{2.1.19}$$

In the $\alpha\to 0$ limit we obtain

$$[\phi(x),\phi(0)]=\imath\pi\,\mathrm{sgn}(x), \tag{2.1.20}$$

that is the anomalous commutator of the level 1 Kac-Moody algebra. Another useful relation involving the bosonic and the density field is

$$\left[\phi(x),\rho(x')\right]=\imath\delta(x-x'), \tag{2.1.21}$$

where we used $\partial_x\mathrm{sgn}(x)=2\delta(x)$ and $\rho(x)=1/(2\pi)\partial_x\phi(x)$.

2.1.3 Bosonization Rules

Let us get back to the problem of bosonizing the one dimensional free Hamiltonian (2.1.4); here we present a simple argument based on the current algebra, a more accurate proof can be found in [50]. In section (2.1.1) we have defined the fermionic current j_μ, where the time-like component corresponds to the sum of right and left-moving density operators and the spatial component corresponds to the difference of the two. Consider then the commutation relation of the current operators

$$\begin{aligned}\left[j_0(x),j_1(x')\right] &= \left[\rho_R(x)+\rho_L(x),\rho_R(x')-\rho_L(x')\right]=-\frac{\imath}{\pi}\partial_x\delta(x-x') \\ \left[j_0(x),j_0(x')\right] &= \left[j_1(x),j_1(x')\right]=0.\end{aligned} \tag{2.1.22}$$

The first commutator is known in the high energy community as a Schwinger term and it can be obtained through a procedure known as point splitting [4][19]. However, in the

3 Note that we could have evaluated the same term in the continuum form moving from a sum over q to a principal value integral, where the $q=0$ term is excluded from the integration path.

4 As noted in [47], there is a simple way of understanding the origin of the Schwinger term, starting from the non-relativistic model (2.1.1). In the non-relativistic case, the density and current operators read : $\rho=\psi^\dagger\psi$ and

previous section we found that the fermionic density field can be written in terms of the spatial derivative of a bosonic field. What about the spatial component of the current operator then ? To answer this question in the context of the (non-chiral) current algebra defined above, we need first to define a non-chiral bosonic phase field $\Phi(x) = \phi_R(x) + \phi_L(x)$. In order for $\Phi(x)$ to be a canonical bosonic field, it should satisfy the canonical commutation relation

$$\left[\Phi(x), \Pi(x')\right] = \imath\delta(x - x'), \tag{2.1.23}$$

where $\Pi(x)$ is the canonical momentum conjugate to $\Phi(x)$. From the current algebra (2.1.22) we then have

$$\left[j_0(x), j_1(x')\right] = \frac{1}{\pi}\left[\partial_x\Phi(x), j_1(x')\right] = \frac{-1}{\pi}\left[\partial_x\Phi(x), \Pi(x')\right] = -\frac{\imath}{\pi}\partial_x\delta(x - x'). \tag{2.1.24}$$

Above, we have identified $j_1(x') = -\Pi(x')$. In this way, the Schwinger term Eq. (2.1.22) and the canonical commutation relation of Eq. (2.1.25) are simultaneously satisfied. Since bosonization relates $j_0 \to \partial_1\Phi$, we may argue that

$$j_1(x) = -\frac{1}{\pi}\partial_t\Phi(x). \tag{2.1.25}$$

In compact notation, the two components of the current assume the form of the topological current

$$j^\mu = \frac{1}{\pi}\epsilon^{\mu\nu}\partial_\nu\Phi. \tag{2.1.26}$$

This is exactly the same term found in (A.4) when deriving the chiral action at the edge of a QH system from the gauge field theory. The current conservation relation is here a mathematical identity that does not depend on the dynamics of the system, as opposed to the standard Noether current. In the free theory, left and right-moving fermions are independently conserved, that means also the chiral current (2.1.7) must be conserved. Using the identity $\gamma_\mu\gamma_5 = \epsilon_{\mu\nu}\gamma^\nu$, we see that the topological current is related to the chiral one by : $j^5_\mu = \epsilon_{\mu\nu}j^\nu$. Then, conservation of the chiral current (at the classical level) implies :

$$\partial_\mu j^\mu_5 = \frac{1}{\pi}\epsilon^{\mu\nu}\epsilon_{\nu\lambda}\partial_\mu\partial^\lambda\Phi = \frac{1}{\pi}\partial^2\Phi = 0, \tag{2.1.27}$$

where we have used the identity $\epsilon^{\mu\nu}\epsilon_{\nu\lambda} = \delta^\mu_\lambda$. Eq. (2.1.27) is the equation of motion for a field $\Phi(x)$ satisfying the Lagrangian density

$$\mathscr{L}_0 = \frac{1}{2\pi}[\partial_\mu\Phi(x)]^2 = \frac{1}{2\pi}\left\{[\partial_t\Phi(x)]^2 - [\partial_x\Phi(x)]^2\right\}, \tag{2.1.28}$$

that is the well known Lagrangian density of free bosons. This last expression shows that a system of one dimensional Dirac fermions can be mapped onto a system of free bosons having the quadratic Lagrangian density $\mathscr{L}_0$. It is worth noting that $\mathscr{L}_0$ is invariant under $\Phi \to \Phi + \theta$, with θ an arbitrary constant, as a consequence of chiral invariance. Physically,

$j = \frac{-\imath}{2m}(\psi^\dagger\partial_x\psi - (\partial_x\psi^\dagger)\psi)$. In the limit $m \to \infty$ and $k_F \to \infty$, with $u_f = k_F/m$ fixed, fluctuations of $\psi^\dagger\psi/m$ are suppressed and we can replace this term with its average value $k_F/\pi m$. Taking this limit in the commutator between ρ and j reproduces the Schwinger term.

this corresponds to the invariance of the original fermionic system under a rigid displacement of the density field. As a consequence, the system supports long lived fluctuations (called kinks) that propagate with no damping. The above Lagrangian density can also be used as a consistency check concerning our "guess" for the current operator (2.1.25); in fact, the canonical momentum resulting from Eq. (2.1.28) has the form

$$\Pi(x) = \frac{\delta \mathscr{L}_0}{\delta \partial_t \Phi(x)} = \frac{1}{\pi} \partial_t \Phi(x). \tag{2.1.29}$$

The resulting Hamiltonian density is then given by (here we reinstate the Fermi velocity)

$$\mathscr{H}_0 = \frac{u_F}{2\pi} \left\{ [\pi \Pi(x)]^2 + [\partial_x \Phi(x)]^2 \right\}. \tag{2.1.30}$$

Before introducing the "central bosonization identity" relating the original fermionic fields to the bosonic ones, it is convenient to introduce the dual form of the topological current (2.1.26). As usual, the dual form of a tensor can be constructed using the Levi-Civita tensor [36, 48]

$$j_\mu(x) = \epsilon_{\mu\nu} j^\nu(x) \to \partial_\mu \Phi(x) = \epsilon_{\mu\nu} \partial^\nu \Theta(x), \tag{2.1.31}$$

where $\Theta(x)$ is the dual field related to the dual current. As a consequence of the above relation, the conjugate momentum admits the dual representation

$$\Pi(x) = \frac{1}{\pi} \partial_x \Theta(x). \tag{2.1.32}$$

Using the above dual representation and the commutation relation (2.1.23), we can find the commutator of the two dual fields

$$\left[\Phi(x), \frac{1}{\pi} \partial_{x'} \Theta(x') \right] = \imath \delta(x - x') \to \left[\Phi(x), \Theta(x') \right] = \imath \frac{\pi}{2} \mathrm{sgn}(x - x') \tag{2.1.33}$$

consistent with the algebra of chiral fields found in Eq. (2.1.20). Let us get back to the problem of deriving the relation between the original fermionic fields and the bosonic ones. Here, we give a physically intuitive argument for the construction of such relation, we leave a "constructive" proof to appendix (B.1.1). Consider first the bosonized form of the density operator; if we invert this relation we obtain

$$\Phi(x) = \pi \int_{-\infty}^{x} dx' \, j_0(x'). \tag{2.1.34}$$

The above relation states that creating a fermion at x' increases the field $\Phi(x)$ of a factor π. Stated otherwise, adding a fermion corresponds to a π kink[5] in the field configuration, see Fig. (9). Generally, in quantum mechanics the shift of some operator by a certain amount is obtained by the action of the exponential of the conjugate operator. In our case, the shift of $\Phi(x)$ by π is obtained by the action of the exponential of the conjugate momentum. We may identify this operator with the coherent state, bosonic representation of a fermionic field

$$\psi(x) \sim e^{\imath \pi \int_{-\infty}^{x} dx' \Pi(x')} = e^{\imath \Theta(x)}, \tag{2.1.35}$$

5 Kink is the name used to designate a soliton in $1+1$ dimensions. For example, vortices are solitons in $2+1$ dimensions. Solitonic terms appearing in non-abelian gauge theories are called instantons.

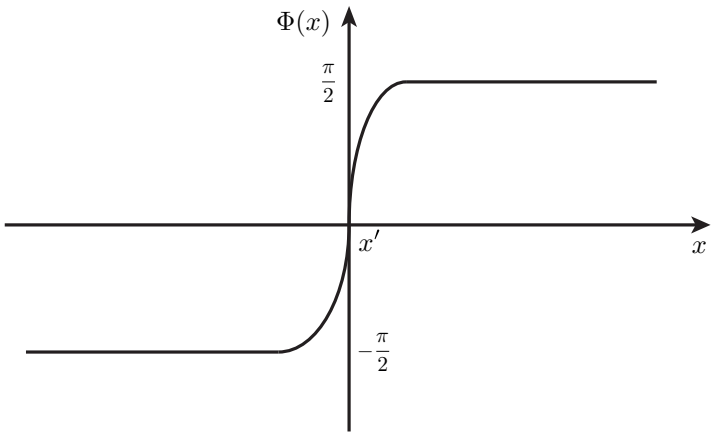

Figure 9: Kink configuration. Creating a fermion at x' corresponds to a π jump in the field configuration.

where we have used the dual representation of the conjugate momentum. We can also understand Eq. (2.1.35) by referring to Fig. (7), where the action of the p-h operator on the N-particles Hilbert space is sketched. If we power expand the exponential in Eq. (2.1.35) we see that this is exactly a sum over all the possible p-h excitations of the system. We conclude this section by deriving the chiral representation of the Hamiltonian (2.1.30). We have seen that $\Phi(x)$ admits a chiral a representation in terms of a sum of right and left-moving fields. Since by construction $\partial_x\Theta(x)$ is related to the spatial component of the current operator, it will admit a chiral representation in terms of a difference between left and right-moving fields. Here we choose the normalized combination $\Theta(x) = (\phi_R(x) - \phi_L(x))/2$ and $\Phi(x) = (\phi_R(x) + \phi_L(x))/2$. Using the chiral decomposition in Eq. (2.1.30), we arrive at

$$\begin{aligned} \mathscr{H}_0 &= \frac{u_F}{4\pi}\left\{[\partial_x\phi_R(x)]^2 + [\partial_x\phi_L(x)]^2\right\} \\ &= u_F\pi\left\{\rho_R^2(x) + \rho_L^2(x)\right\}. \end{aligned} \tag{2.1.36}$$

In the chiral representation, the free Hamiltonian density is simply given by the sum of the two chiral bosonic densities. From Eq. (2.1.35), the most general expression for the chiral fermionic fields (we will refer to this as a vertex operator) is found to be :

$$\psi_\eta(x) = \frac{\chi_\eta}{\sqrt{2\pi\alpha}} e^{\imath s_\eta \theta_\eta} e^{\imath \frac{\pi x}{L}\Delta N_\eta} e^{\imath s_\eta \phi_\eta(x)}. \tag{2.1.37}$$

In the above expression we have added a normalization factor proportional to the short distance cut-off α, the zero mode contribution and the Klein factor introduced in section (2.1.2).

2.1.4 Computing observables

Once the bosonization identities have been defined, we are able to compute various observables. Here we focus our attention on the evaluation of the equal time propagator for the right moving fields (we omit hereby the chirality index)

$$C_\psi(x) = \mathrm{Tr}\left\{\hat{\rho}_F \psi^\dagger(x,t)\psi(0,t)\right\} \tag{2.1.38}$$

for free fermions. Our goal is to show that this procedure reproduces the correct propagator derived directly from a fermionic approach. In Eq. (2.1.38), $\hat{\rho}_F = Z^{-1}e^{-\beta\mathscr{H}_0}$ is the equilibrium density matrix of the electrons and Z is the partition function. As a first step we make use of the bosonic representation of the fermionic fields, and rewrite $C_\psi(x)$ as:

$$C_\psi(x) = \frac{1}{2\pi\alpha}\mathrm{Tr}\left\{\hat{\rho}_B e^{-\imath\phi(x)}e^{\imath\phi(0)}\right\}. \tag{2.1.39}$$

We are left evaluating averages of bosonic fields together with the correct density matrix. In this step we have used the fact that in equilibrium $\hat{\rho}_F \to \hat{\rho}_B$; in the next section we will show that this assumption is not correct when we consider a system out of equilibrium. As a next step it is convenient to use the Baker-Haussdorf formula $e^A e^B = e^{[A,B]/2}e^{A+B}$ (provided $[A,B]$ is a c-number) in order to obtain

$$C_\psi(x) = \frac{1}{2\pi\alpha}e^{[\phi(x),\phi(0)]/2}\mathrm{Tr}\left\{\hat{\rho}_B e^{-\imath[\phi(x)-\phi(0)]}\right\}. \tag{2.1.40}$$

The first term is a commutator and it does not depend on the specific density matrix we use. Using Eq. (2.1.16) we can write the difference of bosonic fields as:

$$\begin{aligned} -\imath[\phi(x)-\phi(0)] &= \sum_{q>0}\sqrt{\frac{2\pi}{qL}}e^{-q\alpha/2}\left\{-\imath\left(e^{\imath qx}-1\right)b_q - \imath\left(e^{-\imath qx}-1\right)b_q^\dagger\right\} \\ &= \sum_{q>0}\lambda_q^*(x)b_q^\dagger - \sum_{q>0}\lambda_q(x)b_q \\ \lambda_q(x) &= \imath\sqrt{\frac{2\pi}{qL}}\left(e^{\imath qx}-1\right)e^{-q\alpha/2}. \end{aligned} \tag{2.1.41}$$

Using again the Baker-Haussdorf formula we can evaluate the average of exponential of bosonic operators and find

$$C_\psi(x) = \frac{1}{2\pi\alpha}e^{[\phi(x),\phi(0)]/2}e^{-\sum_q\lambda^*\lambda/2}e^{-\sum_q\lambda^*\lambda\mathrm{Tr}(\hat{\rho}_B b_q^\dagger b_q)}. \tag{2.1.42}$$

The proof of the above formula will be given in (B.1.2); however it is easy to understand the above result noting that in equilibrium the expectation value of exponentials of bosonic fields reduces to the evaluation of a Gaussian term. This means that in a cumulant expansion of the vertex operators only the quadratic term will be non zero. In the fermionic approach this is equivalent to saying that the random phase approximation in one spatial dimension is indeed exact. This peculiar fact makes possible to evaluate exactly expectation values of

vertex operators even in the presence of strong interactions. In the next section we will look at this Gaussian feature of the theory from a different point of view and we will show how in a system out of equilibrium, terms beyond the Gaussian one do not vanish. For the moment let us get back to the equilibrium case and consider for simplicity the zero temperature case (we consider the finite temperature case in B.1.3). In this case the exponent containing the trace of bosonic operators (i.e. the bosonic distribution function) is zero and we are left with evaluating

$$\sum_{q>0} \lambda^* \lambda/2 = \frac{1}{2}\sum_{q>0}\frac{2\pi}{qL}(1-\cos qx)e^{-q\alpha} = \sum_{n_q=1}^{\infty}\frac{1}{n_q}(1-\cos\frac{2\pi}{L}n_q x)e^{-\frac{2\pi}{L}n_q\alpha} \quad (2.1.43)$$

$$= \frac{1}{2}\log\left(1-e^{\imath\frac{2\pi}{L}(x+\imath\alpha)}\right)+\frac{1}{2}\log\left(1-e^{-\imath\frac{2\pi}{L}(x-\imath\alpha)}\right)-\log\left(1-e^{\frac{2\pi}{L}\alpha}\right)$$

$$\simeq \frac{1}{2}\log\left(\frac{x^2+\alpha^2}{\alpha^2}\right) \quad (2.1.44)$$

where in the last step we considered the $L >> x$ limit. Using this result and Eq. (2.1.19) and (2.1.42) we finally find

$$C_\psi(x) = \frac{\imath}{2\pi}\frac{1}{(x+\imath\alpha)}, \quad (2.1.45)$$

that reproduces the well known result of the fermionic approach. The energy distribution function is defined as the Fourier transform of the real space propagator

$$f(\epsilon_k) = \int_{-\infty}^{\infty} dx\, e^{\imath kx} C_\psi(x) = \theta(-k) \quad (2.1.46)$$

where the $\alpha \to 0$ limit has been taken at the end of the calculation.

2.1.5 The interacting electron gas

Up to now we have shown the equivalency between the fermionic and the bosonic free theories. However, where the bosonization machinery really comes in handy is the interacting case. It turns out that in one dimension perturbation theory breaks down. Intuitively we can understand this failure of perturbation theory by considering a system of electrons constrained to move on a line; if we want to create an excitation the electrons necessarily have to "bump" into each others so that no individual motion is possible but only a collective one. In this case we say that the system is strongly correlated. This is in stark contrast with the higher dimensional case where it is possible to treat excitations in terms of weakly interacting quasi-particles in the so called Fermi Liquids framework. The low energy form of the interacting Hamiltonian (2.1.1) is readily found to be

$$\mathscr{H}_I \simeq \pi\left\{g_2\rho_R(x)\rho_L(x)+g_4\left(\rho_R(x)^2+\rho_L(x)^2\right)\right\}, \quad (2.1.47)$$

where following standard notation we have defined $g_2 = \tilde{U}(0)-\tilde{U}(2k_F)$ and $g_4 = \tilde{U}(0)/2$ in terms of the Fourier transform of the interaction potential, Fig. (10). The g_4 term describes

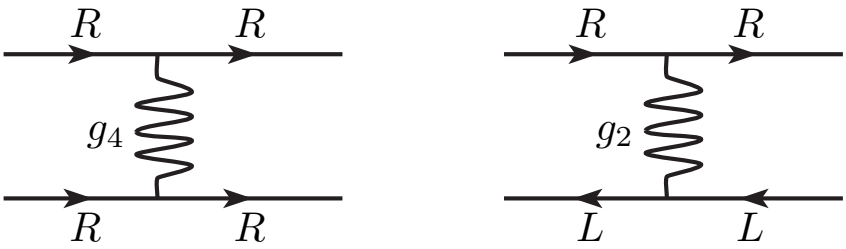

Figure 10: Interactions in spinless Luttinger Liquids. The g_4 term involves only electrons of the same species and gives rise to forward scattering. The g_2 term on the other hand scatters electrons of different species.

forward electron scattering and therefore it preserves chiral symmetry. We see that this term can be shifted into a redefinition of the velocity $u = (u_F + g_4/\pi)$ and it does not change the form of the free Hamiltonian. On the other hand, the g_2 term mixes the right and left moving components. It is worth stressing that even though a backward scattering term is present, the model is still integrable due to the strictly linear electron dispersion relation, that imposes joint energy-momentum conservation. The Hamiltonian $\mathscr{H} = \mathscr{H}_0 + \mathscr{H}_1$ can be diagonalized by means of a canonical Bogoliubov transformation[6]. In operator space the transformation matrix can be represented as

$$\begin{pmatrix} \rho_R \\ \rho_L \end{pmatrix} = \begin{pmatrix} \cosh\theta & \sinh\theta \\ \sinh\theta & \cosh\theta \end{pmatrix} \begin{pmatrix} \tilde{\rho}_R \\ \tilde{\rho}_L \end{pmatrix}, \tag{2.1.48}$$

where θ is the mixing angle between the original eigenstates. The rotated Hamiltonian then reads:

$$\begin{aligned} \tilde{\mathscr{H}} &= \pi\{\tilde{\rho}_R^2 \left(u\cosh^2\theta + u\sinh^2\theta + 2g_2\cosh\theta\sinh\theta\right) \\ &+ \tilde{\rho}_L^2 \left(u\sinh^2\theta + u\cosh^2\theta + 2g_2\cosh\theta\sinh\theta\right) \\ &+ \tilde{\rho}_R\tilde{\rho}_L \left(2u\sinh 2\theta + 2g_2\cosh 2\theta\right)\}. \end{aligned} \tag{2.1.49}$$

Demanding the last term to be zero, we find the value of the mixing angle:

$$\tanh 2\theta = -\frac{g_2}{u}. \tag{2.1.50}$$

Now we can extract the value of the effective Luttinger parameter (g) using the constraint enforced by the canonical property of the Bogoliubov transformation, assured by the trigonometric identity:

$$\cosh^2\theta - \sinh^2\theta = 1. \tag{2.1.51}$$

One possible choice of the parametrization is therefore:

$$\cosh\theta = \frac{g+1}{2\sqrt{g}} \quad , \quad \sinh\theta = \frac{g-1}{2\sqrt{g}}. \tag{2.1.52}$$

6 We will often refer to this transformation as a rotation in operator space. This nomenclature is due to the form of the transformation matrix.

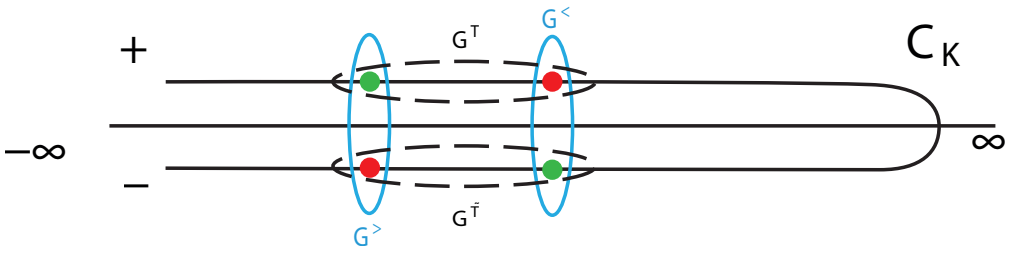

Figure 11: The time-loop contour. The cartoon represents the time loop contour and the definition of the four different Green functions. The dots corresponds to the time arguments of the Green functions. When both fields are defined over the upper contour, their correlator is time ordered while the same situation over the lower contour defines the anti-time ordered correlator. Fields defined on both branches of the contour corresponds to "lesser" and "greater" Green functions.

Finally, g can be extracted using the following trigonometric identities:

$$\tanh\theta = \frac{g-1}{g+1} \quad , \quad \tanh 2\theta = \frac{2\tanh\theta}{1+\tanh^2\theta}, \tag{2.1.53}$$

from which

$$g = \sqrt{\frac{u-g_2}{u+g_2}} \tag{2.1.54}$$

Using (2.1.54) and (2.1.52) in (2.1.49) we find the diagonal form of the rotated Hamiltonian :

$$\begin{aligned} \tilde{\mathscr{H}} &= \pi\tilde{u}\left(\tilde{\rho}_R^2 + \tilde{\rho}_L^2\right) \\ \tilde{u} &= \sqrt{u^2 - g_2^2}. \end{aligned} \tag{2.1.55}$$

The rotated Hamiltonian describes a system of two free counter-propagating chiral bosons, moving with the renormalized velocity $\tilde{u}$.

2.2 NON-EQUILIBRIUM BOSONIZATION

In this section we will take a different approach to the bosonization procedure using the so called "functional bosonization". The scope of this section is not to repeat what we have already found in the previous section, but to clarify the origin of the difference between the standard equilibrium and the non-equilibrium situation; here we will mostly follow the original article by Gutman, Gefen and Mirlin [6]. The starting point is the Dirac action related to Eq. (2.1.4)

$$S_0 = \int_{C_K} dt \int dx \sum_{\eta=R,L} \psi_\eta^\dagger \imath\partial_\eta \psi_\eta, \tag{2.2.1}$$

where we have defined $\partial_{R/L} = \partial_t \pm u_F \partial_x$ and the time integral is over the Schwinger-Keldysh time loop contour of Fig. (11) in order to tackle the non-equilibrium properties of the system

[52]. It is worth noting that this is indeed the most natural choice of the time evolution of a state. The many-body system is in fact prepared in some initial equilibrium state at $t = -\infty$, where it is described by an equilibrium density matrix $\hat{\rho}(-\infty)$. The system is then driven out of equilibrium by means of an external perturbation and its density matrix evolves accordingly in time. The time evolution is governed by the Von Neumann equation $\partial_t \hat{\rho} = -\imath [H(t), \rho(t)]$, whose formal solution is $\hat{\rho} = U(t, -\infty)\hat{\rho}(-\infty)U(-\infty, t)$, U being a unitary evolution operator[7]. Let us go back to our problem, we fix $\eta = R$ and omit this label afterwards. Defining explicitly the fields over the $\pm$ branches of the time-loop contour, we can rewrite the action as

$$S_0 = \int_{t,x} \Psi^\dagger \imath \sigma_3 \partial \Psi \quad , \quad \Psi = \begin{pmatrix} \psi_+ \\ \psi_- \end{pmatrix}. \tag{2.2.2}$$

As shown in Fig. (11) expectation values of fields over C_K define four different types of Green functions

$$\begin{aligned}
\langle \psi_+(t)\psi_-^\dagger(t')\rangle &= \imath G^<(t,t') \\
\langle \psi_-(t)\psi_+^\dagger(t')\rangle &= \imath G^>(t,t') \\
\langle \psi_+(t)\psi_+^\dagger(t')\rangle &= \imath G^T(t,t') = \theta(t-t')\imath G^>(t,t') + \theta(t'-t)\imath G^<(t,t') \\
\langle \psi_-(t)\psi_-^\dagger(t')\rangle &= \imath G^{\tilde{T}}(t,t') = \theta(t'-t)\imath G^>(t,t') + \theta(t-t')\imath G^<(t,t').
\end{aligned} \tag{2.2.3}$$

However, not all of the four Green functions are independent. This is most easily seen by performing a "Keldysh rotation" using the linear operator

$$U = \frac{1}{\sqrt{2}} \begin{pmatrix} 1 & 1 \\ 1 & -1 \end{pmatrix}, \tag{2.2.4}$$

and new fields

$$\tilde{\Psi} = U\Psi \quad , \quad \tilde{\Psi}^\dagger = \Psi^\dagger \sigma_3 U^{-1} \quad , \quad \tilde{\Psi} = \begin{pmatrix} \psi_1 \\ \psi_2 \end{pmatrix}, \tag{2.2.5}$$

so that we can rewrite the action in its final form

$$S_0 = \int_{t,x} \tilde{\Psi}^\dagger \hat{G}_0^{-1} \tilde{\Psi} \quad , \quad \hat{G}_0 = \begin{pmatrix} G_0^r & G_0^K \\ 0 & G_0^a \end{pmatrix}. \tag{2.2.6}$$

Where the retarded (r), advanced (a) and Keldysh (K) components of the Green function are found to be :

$$G_{0,\eta}^{r,a} = \frac{1}{\epsilon - \eta u p \pm \imath 0^+} \quad , \quad G_{0,s_\eta}^K = (1 - 2f_\eta(\epsilon)) \left\{ G_{0,\eta}^r - G_{0,\eta}^a \right\}, \tag{2.2.7}$$

$s_\eta = \pm$ respectively for right and left moving electrons and 0^+ is a positive converging factor. The key observation is that the fermionic distribution function $f_\eta(\epsilon)$ only appears in the Keldysh component, so that all the information about non-equilibrium is contained here. The retarded and advanced functions on the other hand only contain informations concerning the spectral properties of the system.

7 In equilibrium it is possible to deform the time-loop contour into the familiar one defined over $t \in [-\infty, \infty]$ (see [52] for details)

2.2.1 Source terms and correlation functions

In order to generate the density-density correlation functions we introduce the following source term in Keldysh space:

$$S_V = \int_{t,x} V_{cl}\tilde{\Psi}^\dagger\sigma_0\tilde{\Psi} + V_q\tilde{\Psi}^\dagger\sigma_1\tilde{\Psi}, \tag{2.2.8}$$

where $V_{cl/q} = 1/2(V_+ \pm V_-)$ are the classical and quantum components of the source fields, obtained by a Keldysh rotation of the original fields defined on the upper and lower contour. The next step consists in obtaining the generating functional of the density correlation functions

$$\begin{aligned} Z[V_q, V_{cl}] &= \langle e^{\imath S_V}\rangle_{S_0} = Z_0^{-1}\int \mathscr{D}\tilde{\Psi}^\dagger\mathscr{D}\tilde{\Psi} e^{\imath\int\tilde{\Psi}^\dagger(\hat{G}_0^{-1}+V_{cl}\sigma_0+V_q\sigma_1)\tilde{\Psi}} \\ &= Z_0^{-1}\det[\hat{G}_0^{-1} + V_{cl}\sigma_0 + V_q\sigma_1] \\ &= \det[1 + \hat{G}_0(V_{cl}\sigma_0 + V_q\sigma_1)], \end{aligned} \tag{2.2.9}$$

where $Z_0 = \det[\hat{G}_0^{-1}]$ is the partition function of the free system. Now we can re-exponentiate the determinant and power expand the logarithm in the exponent[8]

$$Z[V_q, V_cl] = \exp\left\{\sum_{n=1}^{\infty}\frac{(-1)^{n+1}}{n}\mathrm{Tr}\left(\hat{G}_0\left(V_{cl}\sigma_0 + V_q\sigma_1\right)\right)^n\right\}. \tag{2.2.10}$$

This is also known as the loop expansion of the generating functional. The $n = 1$ term cancels against the homogenous background. For $n = 2$ the correlation functions are of the type depicted in Fig. (8) and we obtain the polarization operators (B.2)

$$\begin{aligned} \Pi_\eta^{r,a}(\omega, q) &= \frac{1}{2\pi}\frac{\eta q}{\eta u q - \omega \mp 0^+} \\ \Pi_\eta^K(\omega, q) &= \left[\Pi_\eta^r(\omega, q) - \Pi_\eta^a(\omega, q)\right] B_\eta(\omega). \end{aligned} \tag{2.2.11}$$

As a check, we notice that the advanced and retarded components obtained above can be equivalently obtained from the Fourier space expression of the electron propagator Eq. (2.1.45)[9]. Since they do not depend on the distribution function, these two correlators do not change their form out of equilibrium. The Keldysh component however depends explicitly on the distribution function

$$B_\eta(\omega) = \frac{1}{\omega}\int_\epsilon f_\eta(\epsilon)\{2 - f_\eta(\epsilon+\omega) - f_\eta(\epsilon-\omega)\}. \tag{2.2.12}$$

When $f(\epsilon)$ describes a system of fermions at equilibrium, Eq. (2.2.12) reproduces the equilibrium bosonic distribution. However, when $f(\epsilon)$ is a non-equilibrium distribution, then $B(\omega)$ becomes a complicated out-of-equilibrium bosonic distribution. Retaining only the $n = 2$

8 Here we use the identity $\log\det = \mathrm{Tr}\log$ and the expansion of the $\log(1+x) = \sum_{n=1}^{\infty}\frac{(-1)^{n+1}}{n}x^n$.

9 More correctly, instead of the equal time correlator of Eq. (2.1.45), we should consider the full space-time correlator. This amounts to the substitution $x \to x - u\,t$ in the electron propagator.

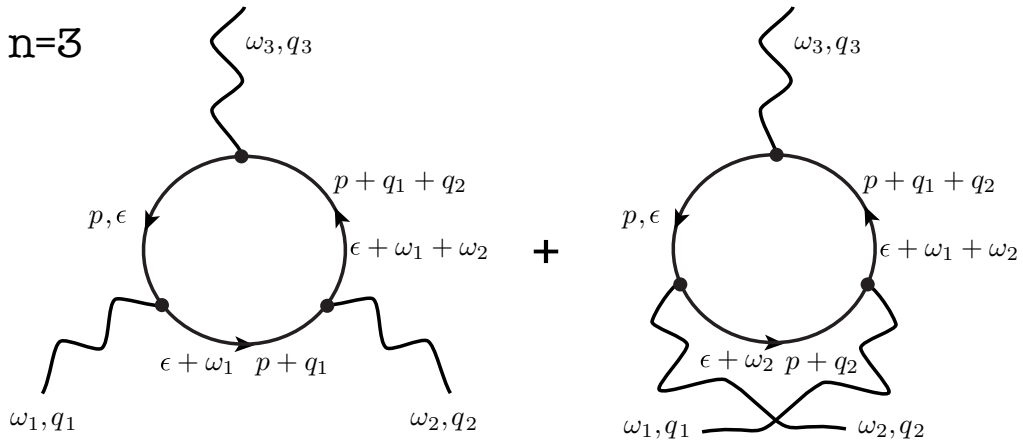

Figure 12: Example of a third order term in the loop expansion. Solid lines represent fermionic Green functions. In Keldysh space every diagram contains different combinations of retarded, advanced and Keldysh Green functions. The wiggled lines represent interactions with the external source fields and dots represent interaction vertices.

terms corresponds to the well known random phase approximation (RPA). In equilibrium one-dimensional systems however RPA turns out to be exact due to the cancellation of all higher order contributions [53–55]. Intuitively this can be understood by looking at Fig. (12) where a third order Feynman diagram is represented. When evaluating the diagrams in the loop expansion, there are $(n-1)!$ permutations of the space-time indices; so for $n = 2$ only one bubble diagram is present. For $n = 3$ there are two bubble diagrams whose internal momentum "flow" in opposite directions, and the two diagrams cancel against each other. It can be proven that such cancelation involves every term with $n > 2$ in the loop expansion, and the resulting theory is Gaussian. We can rewrite the generating functional as

$$\begin{aligned} Z_\eta[V_{cl}, V_q] &= \exp\left(\imath V_{q,\eta}\Pi^a_\eta V_{cl,\eta} + \imath V_{cl,\eta}\Pi^r_\eta V_{q,\eta} + \sum_{n=2}^{\infty}\frac{1}{n!}V^n_{q,\eta}\mathscr{S}_{n,\eta}\right) \\ \mathscr{S}_{n,\eta} &= \langle \rho(x_1,t_1)\rho(x_2,t_2)\dots\rho(x_n,t_n)\rangle, \end{aligned} \tag{2.2.13}$$

where $\mathscr{S}_{n,\eta}$ are irreducible density correlation functions and integration over space-time coordinates is everywhere implied. As we said, in equilibrium $\mathscr{S}_{2,\eta} = \Pi^K_\eta$ is the only non-zero term. However out of equilibrium this is not anymore true. In appendix we compute $\mathscr{S}_{3,\eta}$ and find

$$\mathscr{S}_{3,\eta} \propto \int_\epsilon f_\eta(\epsilon+\omega_1+\omega_2)[1-f_\eta(\epsilon)][1-f_\eta(\epsilon+\omega_1)-f_\eta(\epsilon+\omega_2)]. \tag{2.2.14}$$

If $f(\epsilon)$ is an equilibrium fermionic distribution, than Eq. (2.2.14) is zero. However this term is not vanishing for a general non-equilibrium configuration. This is also true for higher order terms in the loop expansion and it means that RPA is not anymore exact out of equilibrium ! To conclude this section, we derive the bosonized action corresponding (at equilibrium) to

Eq. (2.1.27). In order to do that we use the following functional Fourier transform identity of Eq. (2.2.8) and use the definition of the density operators $\rho = \tilde{\Psi}^\dagger\tilde{\Psi}$:

$$e^{-\imath S_0[\rho_q,\rho_{cl}]} = \int \mathscr{D}V_q \mathscr{D}V_{cl} Z[V_q, V_{cl}] e^{-\imath V_{cl}\rho_q - \imath V_q \rho_{cl}}. \tag{2.2.15}$$

After integrating out the source fields, the bosonized action is finally obtained

$$\begin{aligned} S_0[\rho_q,\rho_{cl}] &= -\rho_{cl}(\Pi^a)^{-1}\rho_q - \rho_q(\Pi^r)^{-1}\rho_{cl} - \imath \log Z[\chi_q] \\ \imath \log Z[\chi_q] &= \sum_{n=2}^{\infty} \imath^{n+1}\chi_q \mathscr{S}_{n,\eta}/n!, \end{aligned} \tag{2.2.16}$$

where $\chi_q = ((\Pi^a)^{-1}\rho_q + (\Pi^r)^{-1}\rho_q)$ acts as an external quantum field [6]. We would like to stress that even thought the theory looks like an interacting one, we are still working in the absence of Coulomb interaction. A hint to the full solution of the non-equilibrium problem comes from noting that transport properties in the Keldysh formalism are only related to the quantum components of the generating function. For example, the average current is defined as

$$\langle I \rangle = -\frac{1}{2}\left.\frac{\delta \log Z[V_q, V_{cl}]}{\delta V_q}\right|_{V_q=0}. \tag{2.2.17}$$

This definition gives the correct Kubo formula for the current [52]. Current fluctuations around this mean value are known as current noise. By functionally differentiating twice we obtain the properly symmetrized noise power

$$S(\omega) = -\frac{1}{2}\left.\frac{\delta^2 \log Z[V_q, V_{cl}]}{\delta V_q(\omega)\delta V_q(-\omega)}\right|_{V_q=0}. \tag{2.2.18}$$

We see that taking higher order terms in the loop expansion is equivalent to computing higher order current cumulants. It turns out that in one dimension, and under appropriate conditions, it is possible to exactly evaluate the sum of all current cumulants, a problem known as full counting statistics.

2.2.2 Full Counting Statistics

A particle current is defined as the number of particles passing through a reference point within some time interval δt. As shown in Fig. (13), the particle number is usually fluctuating in time according to some probability distribution and what we usually measure is its value averaged over the time interval δt. However, fluctuations around this mean value bear important informations about the shape of the original distribution, or can give us informations about the charge of the carriers [56]. Let us say we know the average time τ separating the detection of two particles, then the total number of events $N = \delta t/\tau$. Generally, we would like to know the probability distribution $P_N(m)$ of measuring m electrons out of the N trials. There is another useful way of looking at this problem that consists in modeling the measurement process as the outcome ξ of a random variable X_i ($i = 1, 2, ..., N$), of the single

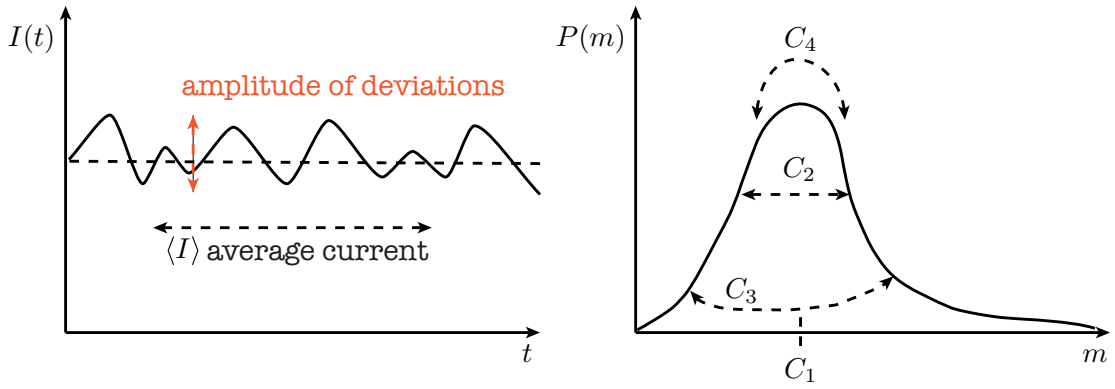

Figure 13: Current cumulants. (Left) Current as a function of time. The measured average current and the fluctuations around the mean value are shown. Fluctuations give rise to current noise. (Right) A general probability distribution as a function of the number of successful events m. C_1 gives the average value, C_2 the width, C_3 the asymmetry and C_4 the sharpness of the distribution.

event. We can assign a probability p_j for every possible outcome ξ, and define the probability density (this terminology will be clear shortly below) $P_{X_i}(\xi)$ for every trial. The probability density is related to the generating function[10] via a Fourier transform

$$\Delta_{X_i}(\lambda) = \langle e^{\imath\lambda\xi}\rangle = \int_{-\infty}^{\infty} d\xi\, P_{X_i}(\xi) e^{\imath\lambda\xi} \tag{2.2.19}$$

where λ is called a "counting field" [57]. Usually it is convenient to work with the cumulant generating function

$$\Phi_{X_i}(\lambda) = \log \Delta_{X_i}(\lambda) = \sum_{n=1}^{\infty} \frac{(\imath\lambda)^n}{n!} \langle \xi^n \rangle_c, \tag{2.2.20}$$

where $\langle ... \rangle_c$ means we are evaluating the connected correlation functions. The cumulants can be generated by differentiating Eq. (2.2.20) with respect to the counting field

$$\langle \xi^n \rangle_c = (-\imath)^n \frac{\partial^n}{\partial \lambda^n} \Phi_{X_i}(\lambda)\Big|_{\lambda=0}. \tag{2.2.21}$$

In this way we find for example

$$\begin{aligned} C_1 &\equiv \langle \xi \rangle_c = \langle \xi \rangle \\ C_2 &\equiv \langle \xi^2 \rangle_c = \langle \xi^2 \rangle - \langle \xi \rangle^2 \\ C_3 &\equiv \langle \xi^3 \rangle_c = \langle \xi^4 \rangle - 3\langle \xi^2 \rangle^2 - 4\langle \xi \rangle \langle \xi^3 \rangle + 12 \langle \xi \rangle^2 \langle \xi^2 \rangle - 6 \langle \xi \rangle^4 \end{aligned} \tag{2.2.22}$$

The first four cumulants are named mean, variance, skewness and kurtosis. As shown in Fig. (13), they characterize respectively the position of the peak, the width, the asymmetry and the sharpness of the distribution. Knowing the generating function gives us a complete

10 In the mathematical literature the name "characteristic function" is often use.

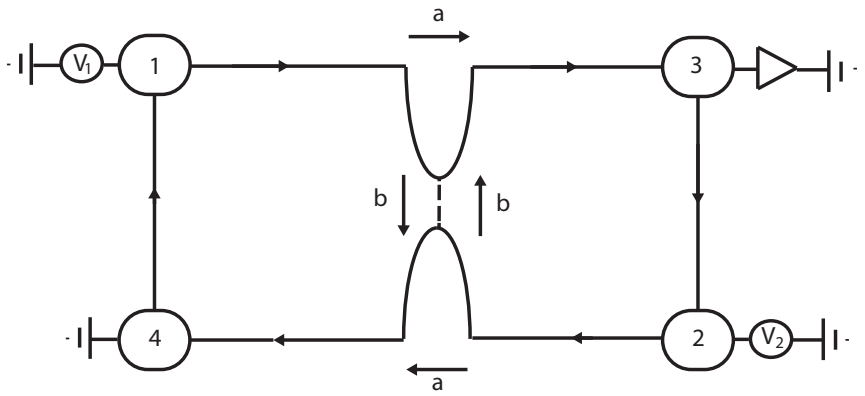

Figure 14: Mesoscopic sample with a QPC. A typical situation in mesoscopic physics, where current carrying channels are biased at contacts 1 and 2. A QPC is partitioning the current and gives rise to shot-noise, measured at contact 3. Here a is the transmission probability at the QPC while b is the reflection probability. Since total charge is a conserved quantity, we must have $b = 1 - a$.

knowledge of all the cumulants and therefore the probability distribution. From the above definitions it is easy to see the connection with the statistical mechanics quantities we have previously defined. The generating function corresponds to the partition function $Z[V_{cl}, V_q]$, the cumulant generating function is connected to the effective action Eq. (2.2.16) (or more generally to the the Helmotz free energy) and Eq (2.2.21) corresponds to Eq. (2.2.17), (2.2.18). As an insightful application, consider the mesoscopic setup depicted in Fig. (14). Here, a quantum point contact (QPC) is partitioning the current carried by the upper and lower channel, emanating from their respective contacts. The two contacts serve as electron reservoirs held at potentials V_1 and V_2 and current noise is measured at contact 3. An electron arriving at the QPC, say from contact 1, can either be transmitted with probability a or reflected with probability b. If we assign the values $\xi = 1$ to the transmission event and $\xi = 0$ to the reflection, then the probability density for the single transmission event is

$$P_{X_i}(\xi) = b\,\delta(\xi) + a\,\delta(\xi - 1). \tag{2.2.23}$$

Using the above expression in Eq. (2.2.19), we find the generating function

$$\Delta_{X_i}(\lambda) = b + a\,e^{i\lambda}. \tag{2.2.24}$$

If successive electron tunneling are uncorrelated, then the total generating function $\Delta_X(\lambda)$ is simply given by the product of the generating functions of the N single trials. Here $X = X_1 + X_2 + ... + X_N$ is the random variable describing the additive outcome of the N trials. In this way we find the generating function of the Binomial distribution

$$\Delta_X(\lambda) = (1 - a + a\,e^{i\lambda})^N, \tag{2.2.25}$$

where we have used $b = 1 - a$, coming from the probability normalization condition.

Moving to the quantum realm, Levitov and Lesovik [58] found that for a quantum mesoscopic system the most general expression for the generating function of electron counting statistics (in the long time limit) is (B.3)

$$\Delta(\lambda) = \det\left[1 + \hat{f}(\epsilon)(\hat{S}^{\dagger}e^{\imath q\lambda}\hat{S}e^{-\imath q\lambda} - 1)\right]. \tag{2.2.26}$$

In the above formula $\hat{f}(\epsilon)$ is a $d \times d$ diagonal matrix of fermionic distributions in the d current channels and $\hat{S}$ is the scattering matrix describing the transmission of electrons through the mesoscopic device. When evaluated for the setup depicted in Fig. (14), Eq. (2.2.26) results in the Binomial generating function (2.2.25) (see also section B.3.2).

To get back to the non-equilibrium bosonization problem, we discuss now a formal expression for the Green function. Consider for example the equal space Green function

$$G_0^{>}(\tau) = \frac{1}{2\pi\alpha}\langle T_K e^{\imath\phi(0,\tau)}e^{-\imath\phi(0,0)}\rangle, \tag{2.2.27}$$

where T_K is the time ordering operator over the Schwinger-Keldysh contour and we have used Eq. (2.1.37). As usual, the Green function can be obtained by the functional integral [6]

$$\begin{aligned} G_0^{>}(\tau) &= \frac{1}{2\pi\alpha}\int \mathscr{D}\rho_q \mathscr{D}\rho_{cl} e^{\imath S_0[\rho_q,\rho_{cl}]} e^{\frac{\imath}{\sqrt{2}}(\varphi_{cl}(0,\tau)-\varphi_{cl}(0,0)-\varphi_q(0,\tau)-\varphi_q(0,0))} \\ &= \frac{1}{2\pi\alpha}\frac{1}{(-\imath\tilde{u}\tau+\alpha)}\bar{\Delta}(\lambda_\tau). \end{aligned} \tag{2.2.28}$$

To derive this expression we have used the fact that integration over the classical components can be easily performed thanks to their Gaussian nature. As a result of this integration, a constraint over the quantum component is obtained [6]. Resolving the constraint and using Eq. (2.2.26) to express exactly the sum over all the quantum loops, we arrive at the second line. In chapter (5) we will use the non-equilibrium bosonization formalism to study energy relaxation and quantum shot noise in a $\nu = 2$ QH system. There, we will derive an explicit expression for the Fredholm determinant Eq. (2.2.26) and its relation to the bosonized, interacting Green function.

3 NON-EQUILIBRIUM ELECTRON SPECTROSCOPY OF LUTTINGER LIQUIDS

CONTENTS

In the previous chapters we have learned about the chiral and non-chiral Luttinger Liquid model as useful tools for studying low energy properties of strongly-interacting, one dimensional electron systems. A fundamental feature of the Luttinger model is its integrability. In classical mechanics, integrability corresponds to the existence of the so called integrals of motion (i.e. conserved quantities) that allow to solve exactly the equation of motions[1]. In an integrable quantum field theory there is an infinite number of conserved quantities and an exact evaluation of all the quantities of interest is therefore possible. The existence of an infinite number of conserved quantities also means that thermalization of the system from an arbitrary excited state is precluded, since no energy (and momentum) redistribution is possible between the different degrees of freedom of the system. Understanding energy relaxation in integrable systems has been the focus of many recent theoretical studies involving different communities both in condensed matter and statistical physics [60–63].

In the present chapter we address the issue of energy relaxation in integrable systems in the context of the Luttinger liquid model (LuL), for a setup that can be particularly relevant for experiments[2]. In the specific, we consider a chiral and a standard Luttinger Liquid (CLuL and LuL respectively), driven out of equilibrium by local injection of high-energy electrons, far away from any contacts, at a fixed energy. The spectral properties of the electrons, locally injected from the resonant level of a first quantum dot (QD), are then extracted at another spatial point some distance away by evaluating the average tunneling current from the Lut-

1 In classical mechanics, the existence of a certain number of integrals of motion allows a canonical transformation to the so called action-angle variables that in turns allows for an exact solution of the equation of motions. See e.g. [59].

2 Recently, the setup described in this chapter has been experimentally realized [64]. However, in this work the authors have investigated energy transfer along a reconstructed QH edge at filling $\nu = 2$.

tinger liquid into an empty resonant level of a second QD with tunable energy. For a realistic parameter range, we find that the current in general has two contributions: an elastic one at the injected energy, and a broad inelastic contribution which shows evidence of energy relaxation. For a CLuL, an essentially exact calculation of the tunneling current is possible. In striking contrast to the decreasing spectral function in an equilibrium CLuL, the inelastic part of the current increases monotonically as the probe energy is lowered from the injection energy toward the chemical potential of the wire. For probe energies slightly below the injection energy, the current rises linearly as a function of the difference between the injection and probe energies. This linear upturn feature appears to be universal for all fractional quantum Hall states with Laughlin filling fractions, $\nu = 1/q$ with q odd. We also show that the same setup with a slight modification can be used to extract the electron energy distribution and spectral function inside the wire. For probe energies slightly below the injection energy, the energy distribution also has a contribution that rises linearly as a function of the energy difference, reflecting the similar behavior observed in the current. Surprisingly, there are strong non-equilibrium corrections close to the chemical potential of the CLuL, where the electron spectral function approaches a finite value and the distribution function saturates at unity. Remarkably, the results reveal that the chiral nature of the excitations plays an important role in how the electrons relax. For the standard LuL, we find that the inelastic component of the current shows a power law behavior as a function of the energy difference with an exponent that continuously evolves as the interaction parameter is varied. This is in contrast to the chiral solution where the linear upturn behavior appears to be independent of the LuL's parameter determined by the inverse filling fraction. In the setup considered in this chapter, relaxation is possible due to the locality of the injection process that partially breaks the translational invariance of the system. For the case of the LuL we explicitly show by means of a diagrammatic approach, how relaxation is possible because the locality of the injection process allows the injected electrons to emit plasmons in the vicinity of the tunneling site through a series of virtual states.

3.1 SYSTEM SETUP

Hot electrons with charge e_0 are injected into the LuL from a resonant level of a QD (source) with energy $E_1 \equiv e_0 V_1 > 0$ at position $x = 0$, see Fig. (15). The relaxation is studied by coupling the system to a resonant level of a second QD (probe) with energy $E_2 \equiv e_0 V_2 > 0$ located downstream at $x = L$, and by computing the tunneling electron current between the edge and the level. The two levels are coupled to the edge via tunneling amplitudes η_1 and η_2, respectively. The source (probe) dot is also coupled to reservoir 1 (2) held at chemical potential μ_1 (μ_2) via tunneling amplitude λ_1 (λ_2), and the chemical potential of the edge is taken to be zero. We assume the level broadening due to tunnel couplings to be small in comparison to both E_1 and E_2, and therefore consider the current in the sequential-tunneling regime, i.e. transport is dominated by independent electrons hops from the QD into the LuL.

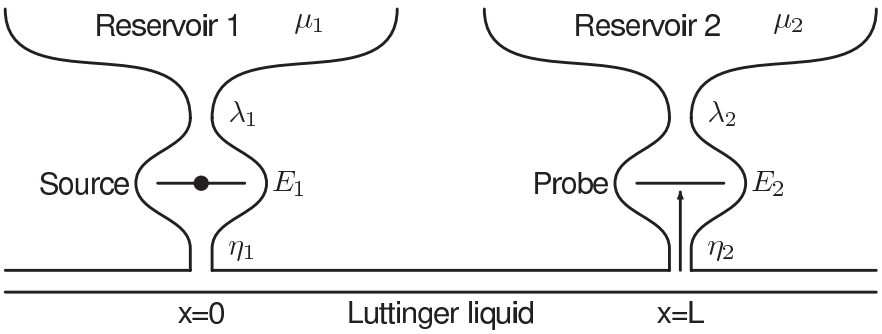

Figure 15: The proposed experimental setup. Hot electrons are injected from the source resonant level at $x = 0$, and are collected at the probe resonant level at $x = L$. System parameters are set (see text) so that the source (probe) occupancy is fixed to be full (empty). Spectral properties of the injected electrons are extracted by measuring the tunneling current between the edge and the probe (indicated by the arrow).

We assume $\lambda_1 \gg \eta_1$ with $\mu_1 > E_1$ so that the source occupancy is constrained to one (in other words, as soon as an electron tunnel from the QD into the LuL, another electron takes his place). Likewise, we assume $\lambda_2 \gg \eta_2$ with $\mu_2 < E_2$ so that the probe occupancy is fixed at zero.

3.2 TUNNELING CURRENT IN THE CHIRAL CASE

The system is modeled by the Hamiltonian $H = H_{0,edge} + H_{0,dot} + H_T$, where $H_{0,edge}$ models the edge state, $H_{0,dot} = E_1\psi_1^\dagger\psi_1 + E_2\psi_2^\dagger\psi_2$ the two resonant states, and $H_T = H_{T1} + H_{T2}$ describes the tunneling of electrons between the edge and the two resonant levels. ψ_1 (ψ_2) are electron operators of the source (probe) with occupation numbers

$$\langle\psi_1^\dagger\psi_1\rangle = 1 \quad , \quad \langle\psi_2^\dagger\psi_2\rangle = 0. \tag{3.2.1}$$

The Hamiltonian for the single chiral edge mode is given by

$$H_{0,edge} = \frac{u}{4\pi\nu}\int dx\,[\partial_x\phi(x)]^2\,. \tag{3.2.2}$$

The one-dimensional electron density is given by $\rho(x) = \partial_x\phi(x)/2\pi$, u denotes the edge velocity, ν the filling fraction, and $\phi(x)$ is the bosonic phase field satisfying the Kac-Moody algebra $[\phi(x), \phi(x')] = \imath\pi\nu\,\mathrm{sgn}(x - x')$ (2.1.20). In order to simplify notation, we use units with $\hbar = 1$ and $k_B = 1$. The interaction picture tunneling Hamiltonian density is

$$\begin{aligned} H_{T1} &= \eta_1 e^{\imath E_1 t}\psi_1\psi^\dagger(x = 0) + h.c. \\ H_{T2} &= \eta_2 e^{\imath E_2 t}\psi_2\psi^\dagger(x = L) + h.c. \end{aligned} \tag{3.2.3}$$

Using bosonization, the edge electron operator is related to the chiral bosonic field in Eq. (3.2.2) by $\psi(x) = e^{i\phi(x)/\nu}/\sqrt{2\pi\alpha}$, where α is a short distance cutoff on the scale of the magnetic length. The tunneling current operator at the second QD can be derived in interaction picture by evaluating the Heisenberg equation of motion

$$\hat{I}(L,t_1) = -\imath e_0[\psi_2^\dagger\psi_2, H_{T2}] = \imath e_0\left(\eta_2 e^{\imath E_2 t_1}\psi^\dagger\psi_2 - \eta_2^* e^{-\imath E_2 t_1}\psi_2^\dagger\psi\right), \tag{3.2.4}$$

where t_1 is the measurement time. The expectation value of the current reads

$$\langle I(t_1)\rangle = \langle T_K\{\hat{I}(t_1)e^{-i\int_{C_K} dt\, H_T(t)}\}\rangle_0, \tag{3.2.5}$$

where all operators are expressed in the interaction picture with respect to $H_{0,edge} + H_{0,dot}$. The current is computed using the non-equilibrium Keldysh technique [65], and T_K indicates time-ordering of the operators on the time-loop contour C_K, see Fig. (11). Here $\langle ...\rangle_0$ is the expectation value evaluated in the absence of interactions. In order to evaluate the tunneling current at the second QD it is convenient to define the operator [66]

$$O_i^\pm(t) = \frac{1}{\sqrt{2\pi\alpha}} e^{\mp\imath\phi(t,x_i)/\nu}\psi_i^\pm(t,x_i) \tag{3.2.6}$$

where $x_1 = 0$ and $x_2 = L$ define the spatial coordinate, $i = 1,2$ and we have introduced the notation $\psi^+ = \psi$ and $\psi^- = \psi^\dagger$. Using Eq. (3.2.6) we can re-write the current (3.2.4) and the tunneling operators (3.2.3) in the following compact form :

$$I(t) = \imath e_0\eta_2 \sum_{s_1=\pm} s_1 e^{\imath s_1 E_2 t} O_2^{s_1}(t) \tag{3.2.7}$$

$$H_{T1}(t) = \eta_1 \sum_{s_3=\pm} e^{\imath s_3 E_1 t} O_1^{s_3}(t)$$

$$H_{T2}(t) = \eta_2 \sum_{s_2=\pm} e^{\imath s_2 E_2 t} O_2^{s_2}(t), \tag{3.2.8}$$

where we have introduced the index $s_i = \pm$. In the perturbative expansion of Eq. (3.2.5), the zeroth order term is zero since the expectation value $\langle O_2^{s_1}(t_1)\rangle_0 = 0$. The first order term (in the perturbative expansion) is given by

$$\begin{aligned}\langle J_1(t_1)\rangle &= -\imath\left\langle T_K\left\{I(t_1)\int_{C_K} dt_2\, H_T(t_2)\right\}\right\rangle_0 \\ &= (-\imath)\imath e_0|\eta_2|^2 \sum_{s_1,s_2=\pm} s_1 \int_{C_K} dt_2\, e^{\imath E_2(s_1t_1+s_2t_2)}\left\langle T_K O_2^{s_1}(t_1)O_2^{s_2}(t_2)\right\rangle_0,\end{aligned} \tag{3.2.9}$$

that is already second order in the tunneling coupling η_2. Using the fact that expectation values of bosonic exponents satisfy the condition $s_1 + s_2 = 0$ (B.1.25), imposing the constraint (3.2.1) on the resonant level occupancy and setting $t_1 = 0$ (the measurement time is arbitrary), we find (C.1)

$$\begin{aligned}\langle J_1(0)\rangle &= e_0|\eta_2|^2 2\int dt_2 e^{-\imath E_2 t_2}\left(\imath G^>_{1/\nu}(-t_2) - \imath G^<_{1/\nu}(-t_2)\right) \\ &= -e_0|\eta_2|^2 \frac{(2\alpha\pi T)^{1/\nu-1}}{2\pi u^{1/\nu}} \quad \frac{\Gamma[\frac{1}{2\nu} - \imath\frac{E_2}{4\pi T}]\Gamma[\frac{1}{2\nu} + \imath\frac{E_2}{4\pi T}]}{\Gamma[1/\nu]}\, e^{-E_2/2T},\end{aligned} \tag{3.2.10}$$

ror $E_2 > 0$. Above, the factor of correlation functions,

$$\imath G^{\gtrless}_{\beta}(t) = \pm \frac{1}{2\pi\alpha} \frac{(\pi T \alpha/u)^{\beta}}{[\sin \pi T(\alpha/u \pm \imath t)]^{\beta}}, \tag{3.2.11}$$

can be interpreted as the tunneling in and out density of states. We find that the first non-zero order contribution $\langle J_1(t_1)\rangle$ to the tunneling current represents tunneling of electrons into the probe, solely due to thermal fluctuations; at low temperatures ($T \ll E_2$) this contribution is exponentially suppressed and we will neglect it hereafter.

We then evaluate the perturbative expansion of Eq. (3.2.5) looking for terms proportional both to η_1 and η_2. The leading order term (first perturbative order in η_2 and second in η_1) gives

$$\begin{aligned} \langle I(t_1)\rangle \;&\simeq\; -e_0 \frac{|\eta_1|^2|\eta_2|^2}{2} \sum_{\{s_k\}} s_1 \int_{C_K} d^3t\, e^{\imath E_2(s_1t_1+s_2t_2)+\imath E_1(s_3t_3+s_4t_4)} \\ &\times\; \left\langle T_K O_2^{s_1}(t_1) O_2^{s_2}(t_2) O_1^{s_3}(t_3) O_1^{s_4}(t_4)\right\rangle_0 . \end{aligned} \tag{3.2.12}$$

If the propagation time L/u between the dots is much larger than the maximum of the dwell time $\tau_i = 1/(\lambda_i^2 + \eta_i^2)$, processes at the probe dot occur at later times than processes at the source dot, and the time ordering over the Keldysh contour is fixed accordingly [66]. Moreover, upon imposing the constraints (3.2.1) on the resonant level occupancies and taking the limit of large inter-dot separation, the time of propagation L/u drops out of the final expression and we arrive at the following expression for the steady state current to leading order in η_1 and η_2 (C.1)

$$\langle I(0)\rangle = e_0|\eta_1|^2|\eta_2|^2 \int_{-\infty}^{\infty} d^3t\, e^{-\imath E_2 t_2 + \imath E_1 t_{34}} \left(\imath G^{<}_{1/\nu}(-t_2)\right)\left(\imath G^{>}_{1/\nu}(t_{34})\right)\left\{\Pi^{<>}_{1/\nu} - \Pi^{<<}_{1/\nu}\right\}, \tag{3.2.13}$$

where $t_{ij} = t_i - t_j$ and $d^3t = dt_1\, dt_2, dt_3$. The Π-matrices

$$\Pi^{\rho\sigma}_{\beta} = \frac{G^{\rho}_{\beta}(t_{23}) G^{\sigma}_{\beta}(-t_4)}{G^{\rho}_{\beta}(-t_3) G^{\sigma}_{\beta}(t_{24})}, \tag{3.2.14}$$

describe the propagation of electrons along the edge. It is instructive to consider first the case of a non-interacting chiral Fermi liquid, which describes the edge excitations of an integer quantum Hall state. In this case we expect no relaxation in the system. This simple example is also useful to show the general strategy for evaluating the current in the interacting case. Choosing $\nu = 1$ in Eq. (3.2.13), and scaling out the temperature dependence into the time variable, $\pi T t_i \to t_i$ the tunneling current is given by

$$\begin{aligned} \langle I(0)\rangle \;&=\; -e_0 \frac{|\eta_1|^2|\eta_2|^2}{4\pi^2 u^2 (\pi T)} \int_{-\infty}^{\infty} d^3t \frac{e^{-iX_2t_2/\pi + iX_1t_{34}/\pi}}{\sin(\alpha/u + \imath t_2)} \frac{-1}{\sin(\alpha/u + \imath t_{34})} \\ &\times\; \frac{\sin(\imath t_3)\sin(\imath t_{24})}{\sin(\alpha/u - \imath t_{23})} \left\{\frac{1}{\sin(\alpha/u + \imath t_4)} + \frac{1}{\sin(\alpha/u - \imath t_4)}\right\}, \end{aligned} \tag{3.2.15}$$

where $X_i = E_i/k_B T$. In order to solve the above integral, we note that the term in parenthesis is a representation of a Dirac delta function

$$\left\{\frac{1}{\sin(\alpha/u + \imath t_4)} + \frac{1}{\sin(\alpha/u - \imath t_4)}\right\} = -\pi\delta(t_4). \tag{3.2.16}$$

This simplifies the integral to

$$\begin{aligned}\langle I(0)\rangle &= -e_0\frac{|\eta_1|^2|\eta_2|^2}{4\pi u^2(\pi T)}\int dt_2 dt_3 \frac{e^{-\imath X_2 t_2/\pi+\imath X_1 t_3/\pi}}{\sin(\alpha/u-\imath t_{23})} \\ &= -e_0\frac{|\eta_1|^2|\eta_2|^2}{4u^2(\pi T)}\delta(\Delta X)\int dt_2 \frac{e^{-\imath X_2 t_2/\pi}}{\sin(\alpha/u-\imath t_2)}.\end{aligned} \tag{3.2.17}$$

In the second line we have performed the shift $t_2 \to t_2 + t_3$ and defined $\Delta X = X_1 - X_2$. An easy way to evaluate the integral above is by performing a shift in the time variable $t_2 \to t_2 + \imath\pi/2$ in order to move the poles of the integral over the imaginary axes (C.1.1). In this way we arrive to

$$\langle I(0)\rangle = -e_0\pi\frac{|\eta_1|^2|\eta_2|^2}{4u^2\hbar^3}\frac{e^{E_2/(2k_BT)}}{\cosh\left[E_2/(2k_BT)\right]}\delta(\Delta E), \tag{3.2.18}$$

where $\hbar$ and k_B have been reistated. Equation (3.2.18) shows that hot electrons do not relax when many-body interactions are absent. In addition, the weight of the elastic peak is reduced as the temperature is increased. This reduction is due to Pauli blocking of states by thermally excited edge electrons residing above the chemical potential.

Next we focus our attention on the strongest fractional quantum Hall state at filling fraction $\nu = 1/3$, where the area occupied by one electron is threaded by three quanta of magnetic flux. In this case the integrals in equation (3.2.13) can be evaluated exactly following a procedure similar to the one presented for the non-interacting case (see C.1.1 for details)

$$\begin{aligned}\langle I(0)\rangle &= -e_0\frac{\pi^3|\eta_1|^2|\eta_2|^2\alpha^4(k_BT)^3}{4u^6\hbar^7}\left\{\frac{X_1^2 e^{\frac{X_1}{2}}}{\cosh(X_1/2)}\left(1+\frac{X_1^2}{\pi^2}\right)\delta(\Delta X)\right. \\ &+ \left.\frac{3\Delta X e^{\Delta X/2}}{\sinh(\Delta X/2)}\sum_{i=1}^{2}\frac{e^{X_i/2}}{\cosh(X_i/2)}\left(1+\frac{X_i^2}{\pi^2}\right)\right\}.\end{aligned} \tag{3.2.19}$$

At zero temperature, the expression for the current simplifies to

$$\langle I(0)\rangle = -e_0\frac{\pi|\eta_1|^2|\eta_2|^2\alpha^4}{4u^6\hbar^7}\left(E_1^4\delta(\Delta E)+6\theta(\Delta E)(E_1^2+E_2^2)\Delta E\right), \tag{3.2.20}$$

where $\Delta E = E_1 - E_2$. The current, plotted for both zero and finite temperatures in Fig. (16), has two main contributions: an elastic and an inelastic one. The elastic peak is due to electrons that were elastically transported from the source to the probe. Its broadening is included in the figure to reflect the finite width of the resonant levels due to the couplings to the reservoirs and the wire. Second, there is a broad inelastic contribution that extends over the range $E_2 < E_1$ that grows monotonically as E_2 is lowered. This signals the presence of energy relaxation as hot electrons are transported from the source to the probe. For $E_2 \lesssim E_1$, the current increases linearly with ΔE.

We have confirmed that an inelastic contribution to the current is also present for Laughlin filling fraction of $\nu = 1/5$. In this case, an exact computation at zero temperature shows again that $I_{inel} \propto \Delta E$ for $E_2 \lesssim E_1$. This suggests that the linear upturn in the current below E_1 may be a generic feature at all Laughlin filling fractions.

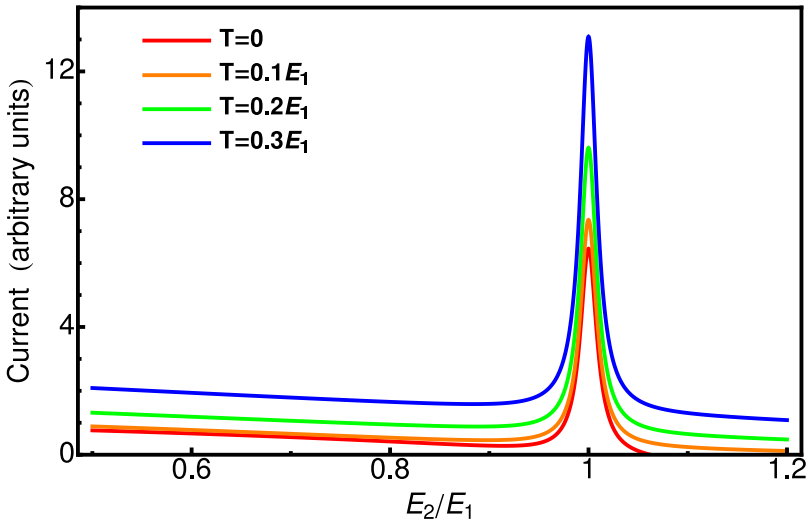

Figure 16: Tunneling current for the chiral case at various temperatures. The current shows an elastic contribution at $E_1 = E_2$, and an inelastic contribution for $E_2 < E_1$ which increases as energy transfer is increased. In the regime of small E_2 ($0 \lesssim E_2 \ll E_1$) the sequential-tunneling assumption is expected to break down. A level broadening of $0.001\,E_1$ is used for the elastic peak.

In the presence of interactions, Fig. (16) shows an overall increase in the elastic current with temperature. This reflects the increase in the tunneling density of states with temperature and constitutes a clear signature of Luttinger liquid physics.

The setup of Fig.(15) is ideal for directly extracting the electron energy distribution, $f(E)$, and spectral function, $A(E)$, inside the wire at a spatial point far from the injection site. With the probe occupancy constrained to be empty, the tunneling current is given by [67]

$$I_{\text{empty}} = \imath e_0 |\eta_2|^2 G^<(E), \tag{3.2.21}$$

while a similar evaluation with probe occupation held full gives

$$I_{\text{full}} = \imath e_0 |\eta_2|^2 G^>(E). \tag{3.2.22}$$

Once the two currents are obtained, both $f(E)$ and $A(E)$ can be extracted by expressing the lesser and greater Green functions, $G^<(E) = \imath f(E)A(E)$ and $G^>(E) = -\imath(1-f(E))A(E)$, in terms of electron distribution function and spectral weight. At zero temperature and for $\nu = 1/3$, $f(E_2)$ and $A(E_2)$ valid for $0 < E_2 < E_1$ read

$$A(E_2) = \frac{\alpha^2}{2u^3\hbar^4}\left[E_2^2 + (E^*)^2\,\frac{\Delta E}{E_1}\right], \tag{3.2.23}$$

$$f(E_2) = \frac{\left[1+\left(\frac{E_2}{E_1}\right)^2\right]\frac{\Delta E}{E_1}}{\left(\frac{E_2}{E^*}\right)^2 + \frac{\Delta E}{E_1}}, \tag{3.2.24}$$

where $E^* = \sqrt{6\pi|\eta_1|^2\alpha^2 E_1^3/u^3\hbar^3}$ separates two energy regimes. In the high-energy regime and for small energy transfers ($E^* < E_2 \lesssim E_1$), $f(E_2) \approx 12\pi|\eta_1|^2\alpha^2\Delta E/u^3\hbar^3$, which shows that the linear upturn in the current below E_1 is also reflected in the energy distribution. In the same regime, we find that the spectral function does not deviate strongly from its equilibrium expression (with $\eta_1 = 0$). In the low-energy regime ($0 \lesssim E_2 < E^*$), $f(E_2)$ smoothly approaches one and the spectral function approaches a finite value. The latter is in stark contrast to the equilibrium case.

3.3 THE CURRENT IN THE STANDARD LL

The setup depicted in Fig. (15), can also be used to study energy relaxation in a standard LuL. In this case, there is scattering between electrons moving in the same direction near the Fermi points with amplitude g_4, and between electrons moving in opposite direction with amplitude g_2 (2.1.5). In this case, the standard LuL Hamiltonian is expressed in the chiral form as (2.1.36)

$$H_{LL} = \frac{u}{4\pi g}\int dx\left\{[\partial_x\phi_R(x)]^2 + [\partial_x\phi_L(x)]^2\right\}, \tag{3.3.1}$$

where $g < 1$ is the LL parameter, $\rho_{R,L} = \pm\partial_x\Phi(x)_{R,L}/2\pi$ and the chiral boson operators satisfy $[\phi_R(x),\phi_R(x')] = -[\phi_L(x),\phi_L(x')] = i\pi\, g\,\mathrm{sgn}(x-x')$. The tunneling Hamiltonian is identical to equation (3.2.3), where the electron operator is now given by $\psi(x) = \psi_R(x) + \psi_L(x)$, and

$$\psi_{R,L}(x) = \exp[\imath(g_\pm\phi_R(x) + g_\mp\phi_L(x))]/\sqrt{2\pi\alpha} \tag{3.3.2}$$

$$g_\pm = (g^{-1}\pm 1)/2 \tag{3.3.3}$$

$$g = \sqrt{\frac{u_F + (g_4-g_2)/2\pi}{u_F + (g_4+g_2)/2\pi}}. \tag{3.3.4}$$

Note that the above definitions differ from the ones in section (2.1.5) by a normalization factor. For notational convenience we have also used $\tilde{u} \equiv u$. Following similar steps as in the chiral calculation yields

$$\begin{aligned}\langle I(0)\rangle &= e_0|\eta_1|^2|\eta_2|^2\int d^3t e^{-\imath E_2 t_2 + \imath E_1 t_{34}}[\imath G^<_{2\gamma+1}(-t_2)][\imath G^>_{2\gamma+1}(t_{34})] \\ &\times \{\Pi^{<>}_{1+\gamma} - \Pi^{<<}_{1+\gamma} + \Pi^{<>}_{\gamma} - \Pi^{<<}_{\gamma} + 2\Pi^{<>}_{\gamma'} - 2\Pi^{<<}_{\gamma'}\},\end{aligned} \tag{3.3.5}$$

where $\gamma = g_-^2 g$ and $\gamma' = (g_-^2 + g_-)g$. The correlation functions and the Π-matrices are given by equations (3.2.11) and (3.2.14). In principle, the Π-matrices contain both left and right moving Green's functions. However, in the limit where $L \gg u/\Delta E$, all dependence on left moving Green's functions cancels out.

Unfortunately Eq. (3.3.5) does not allow for an easy analytical solution. Comparing this result with the one obtained for the CLuL, we see that the main difference consists in the

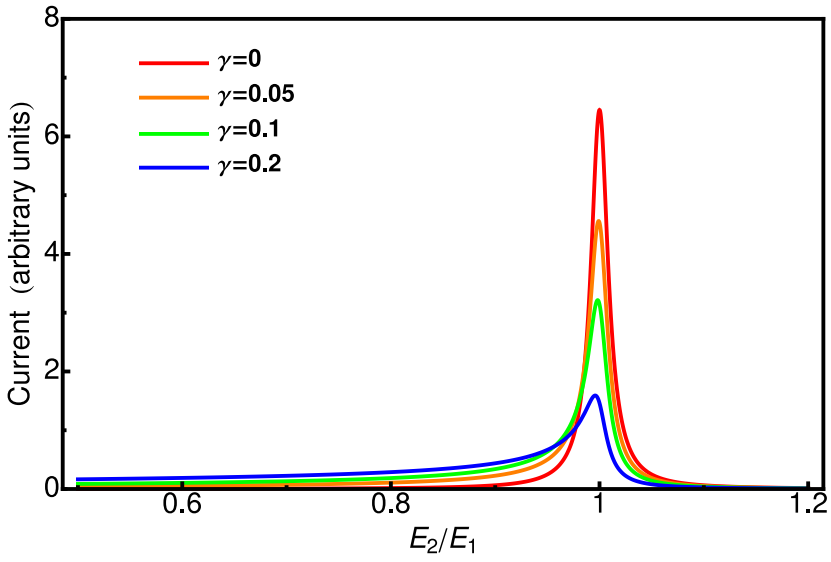

Figure 17: Tunneling current for the standard LuL, for various interaction parameters γ. The current is plotted for zero temperature and includes the leading contribution in $\Delta E/E_1$. The inelastic contribution for $E_2 < E_1$ shows a power law decay as a function of increasing ΔE with an exponent that depends on the interaction parameter (see text). A level broadening of $0.001\,E_1$ is used for the elastic peak.

value of the interaction parameters γ and γ'. While in the chiral case the interaction parameter is universal and integer valued, here it is a non-universal rational number. Therefore it would be desirable to obtain a general expression for the tunneling current as a function of the interaction parameter. We find that at zero temperature the above formal expression for the current can be evaluated for any value of the interaction parameter to leading order in $\Delta E/E_1 \ll 1$ (C.2):

$$\langle I(0)\rangle = -\frac{2\pi e_0}{\hbar}\frac{|\eta_1|^2|\eta_2|^2\theta(\Delta E)}{u^2\hbar^2 E_1\Gamma^2(1+\gamma)}\left(\frac{\alpha E_1}{u\hbar}\right)^{4\gamma}\left[\frac{(\Delta E/E_1)^{2\gamma-1}}{\Gamma(2\gamma)}\right], \tag{3.3.6}$$

where $\Gamma(x)$ is the gamma-function and $\gamma \geqslant 1$. In order to derive the above result we have considered $E_1 = 1/\alpha$, i.e. we have taken the energy of the injected electrons to be of the order of the high energy cut-off scale.

In order to check the validity of our result, we consider Eq. (3.3.6) in the non-interacting limit ($\gamma \to 0$). In this limit, the quantity in the square brackets is a representation of the delta-function, and Eq. (3.3.6) correctly reduces to the zero temperature form. When the interactions are turned on, the elastic peak gradually broadens to give rise to an inelastic contribution (see Fig.17) which shows a power law decay as a function of increasing ΔE with an exponent that continuously evolves as a function of the interaction parameter. For strong enough interactions with $\gamma > 1/2$, the elastic peak vanishes and the remaining inelastic contribution monotonically increases with a power law which again evolves as a function of the interaction parameter. Eq. (3.3.6) is plotted in Fig. (17), where a broadening of the peak

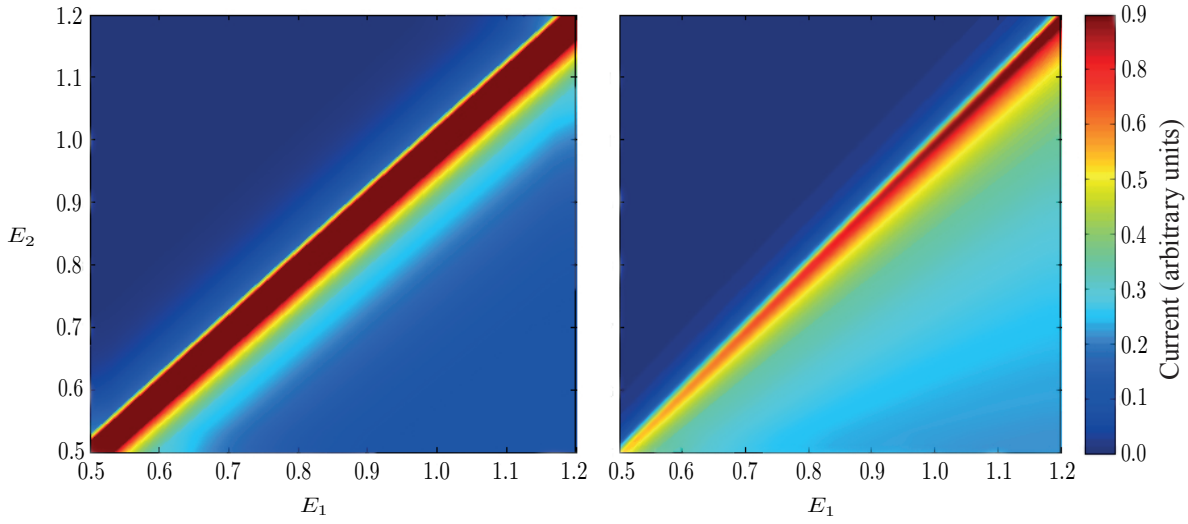

Figure 18: Tunneling current for the standard LuL as a function of the injection and extraction energy . The tunneling current is plotted as a function of the injection (E_1) and extraction (E_2) energy. The color scale on the right expresses the magnitude of the current. The two plots refer to different values of the interaction parameter: $\gamma = 0.1$ (left) and $\gamma = 0.3$ (right).

has been included to reflect the finite width of the resonant levels due to the coupling to the reservoirs and the wire. Finally, we can expand Eq. (3.3.6) for $\gamma \ll 1$, i.e. for small g_2 interaction. In this limit we obtain

$$\begin{aligned} I &\simeq -\frac{4\pi e_0}{\hbar}\frac{|\eta_1|^2|\eta_2|^2\theta(\Delta E)}{u^2\hbar^2}\frac{\gamma}{\Delta E} \\ \gamma &\simeq \frac{g_2^2}{(4\pi u\hbar)^2}, \end{aligned} \tag{3.3.7}$$

where we have expanded γ for small g_2 using the definitions in Eq. (3.3.2) to the first non zero order. The nice feature of this result is that we can check its validity by developing a perturbative approach. The perturbative approach not only allows us to verify the correctness of Eq. (3.3.7), but can also shed some light on the nature of the relaxation process, at least for small interaction strengths. We present the perturbative approach in the next section.

Before concluding this section, we would like to stress that the results obtained in this section are in contrast with what obtained in the chiral case, where the linear upturn may be a ubiquitous feature for all Laughlin states.

3.4 DIAGRAMMATIC ANALYSIS

In the limit of weak interactions ($0 < \gamma \ll 1$) and for finite energy transfer ($\Delta E > 0$) equation (3.3.6) can be interpreted using a diagrammatic method that also provides an intuitive picture for the relaxation process. Out of the two scattering processes in the LuL,

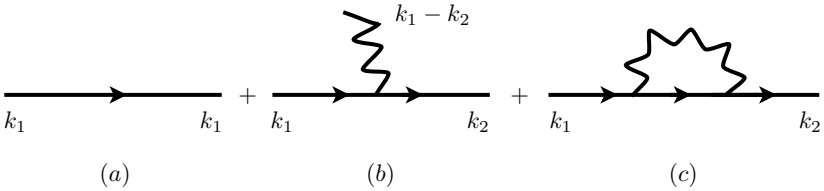

Figure 19: The three diagrams considered in the process. (a) the electron propagates without emitting any plasmon; this correspond to the elastic contribution. (b) the electron emits a plasmon of energy $\Delta E = u\hbar|k_1 - k_2|$ while in the virtual state; this term correspond to the inelastic part. (c) the electron emits and then reabsorb a plasmon; this term renormalizes the elastic one.

the g_4-interaction merely renormalizes the fermion and plasmon velocities and cannot give rise to relaxation (2.1.5). In a spatially homogenous LuL, the g_2-process cannot give rise to energy relaxation either due to the simultaneous requirement of momentum and energy conservation. However, because of the local nature of injection and collection processes considered here, an electron is capable of exploring virtual momentum states in connection with tunneling, and a consecutive inelastic process can both conserve momentum and produce a final state with the same total energy as the initial state. Here, we consider the lowest order inelastic process proportional to $\gamma \propto g_2^2$ at zero temperature.

The model is defined by the non-interacting Hamiltonian H_0 (2.1.4) and the perturbation $H_{int} = H_{g_2} + H_{T1} + H_{T2}$. The free Hamiltonian describes the right- and left- moving chiral fermions

$$H_0 = -\imath u_F \int dx \left\{ \psi_R^\dagger(x)\partial_x\psi_R(x) - \psi_L^\dagger(x)\partial_x\psi_L(x) \right\}, \tag{3.4.1}$$

where u_F is the Fermi velocity. The g_4 interaction involves only fermions of the same chirality

$$H_{g_4} = \frac{g_4}{2} \int dx \psi_R^\dagger(x)\psi_R(x)\psi_R^\dagger(x)\psi_R(x), \tag{3.4.2}$$

while the g_2 interaction involves fermions of both chiralities

$$H_{g_2} = g_2 \int dx \psi_R^\dagger(x)\psi_R(x)\psi_L^\dagger(x)\psi_L(x). \tag{3.4.3}$$

Finally, the tunneling between the dots and the LuL is described by

$$H_{T1} = \int \frac{dk}{2\pi} \{\eta_1 \psi_1 c_k^\dagger + h.c.\} \tag{3.4.4}$$

$$H_{T2} = \int \frac{dk}{2\pi} \{\eta_2 \psi_2 c_k^\dagger e^{-\imath kL} + h.c.\}, \tag{3.4.5}$$

where ψ_1 and ψ_2 are the fermionic fields of the source and the probe, respectively. Here, c_k is the right-moving fermion operator in the occupation number representation. When bosonizing (2.1.5) the Hamiltonian, the g_4 interaction renormalizes the Fermi velocity $u =$

$(u_F + g_4/2\pi)$[3]. Moving to Fourier space and using the bosonization identity Eq. (2.1.11), the g_2-Hamiltonian, involving right-moving fermions and a left-moving plasmons, is given by

$$H_{g_2} = g_2 \int \frac{dp}{2\pi}\frac{dk}{2\pi}\sqrt{|p|}\theta(-p)[c_k^\dagger c_{k+p} b_p^\dagger + c_k^\dagger c_{k-p} b_p], \tag{3.4.6}$$

where b_p is the left moving plasmon operator with momentum p [50]. Consider first the inelastic component of the current, given by diagram (b), in which an electron is transported from the source to the probe while emitting a single plasmon inside the wire. In the first step, the electron in the source ($|i\rangle = \psi_1^\dagger|0\rangle$) tunnels into a right moving momentum eigenstate of energy $\epsilon_{k_1} = u\hbar k_1$. In the second step, a left moving plasmon with energy $\Delta E = u\hbar|k_1 - k_2|$ is emitted via a g_2-process, and the right moving electron is scattered into another wire state such that momentum is conserved. In the third and final step, the electron tunnels into the probe ($|f\rangle = \psi_2^\dagger b_p^\dagger|0\rangle$). The matrix element for this process is given by

$$\mathcal{M} = \langle f|H_{int}\frac{1}{E_i - H_0 + i0^+}H_{int}\frac{1}{E_i - H_0 + i0^+}H_{int}|i\rangle, \tag{3.4.7}$$

that yields

$$|\langle f|i\rangle_{\text{eff}}^{\text{inel}}|^2 = |\eta_1\eta_2^*|^2 g_2^2 \frac{\theta(-p)\sin^2(pL)}{|p|(\hbar u)^4}. \tag{3.4.8}$$

In the above expression an oscillatory L dependence is still present in the limit $L \gg u\hbar/E_1$ and $L \ll u\hbar/E_2$, physically describing the interference between processes with plasmon emission at the source and at the probe dot, respectively. However, this interference disappears once the energy loss ΔE is averaged over the widths $\hbar/\tau_i$ of the dot levels. For $L/u \gg \tau_i$, this energy average leads to a replacement of the $\sin^2(pL)$ factor by its average of $1/2$. It is interesting to note that the criterion on L for the disappearance of the oscillatory factor agrees with the criterion for fixing the time ordering over the Keldysh contour used to derive Eq. (3.2.13).

Eq (3.4.8) shows that the transition amplitude scales as $1/\sqrt{|\Delta E|}$. This behavior can be intuitively understood as a competition between two factors: while the phase space for plasmon emission increases as $\sqrt{|\Delta E|}$, the time scale in which this emission can occur diminishes as $1/|\Delta E|$ due to the energy-time uncertainty principle. The resulting current can then be computed using Fermi's golden rule ($E_p = \hbar u|p|$)

$$\begin{aligned} I &= -\frac{2\pi e_0}{\hbar}\int_{-\infty}^{\infty}\frac{dp}{2\pi\hbar}|\langle f|i\rangle_{\text{eff}}^{\text{inel}}|^2\delta(\Delta E - E_p) \\ &= -\frac{4\pi e_0}{\hbar}\frac{|\eta_1|^2|\eta_2|^2\theta(\Delta E)}{u^2\hbar^2}\left(\frac{g_2^2}{(4\pi u\hbar)^2}\right)\frac{1}{\Delta E}, \end{aligned} \tag{3.4.9}$$

that correctly reproduces equation (3.3.7) upon identifying γ.

Finally, consider the remaining two diagrams (a), (c). They take into account the elastic components of the process. The first diagram, where no interactions take place, can be easily computed and reproduce the Fermi Liquid result. The second diagram takes into account

3 Note that this differs from the definition used in section (2.1.5) by a normalization factor.

the elastic peak renormalization due to a plasmon emission/absorption process and must be taken into account in order to obtain a finite, integrated, elastic current. In this case the matrix element is given by :

$$\mathcal{M} := \langle f|H_{T_2}\frac{1}{E_i - H_0 + \imath 0^+}H_{g_2}\frac{1}{E_i - H_0 + \imath 0^+}H_{g_2}\frac{1}{E_i - H_0 + \imath 0^+}H_{T_1}|i\rangle. \tag{3.4.10}$$

Combining the resulting expressions with the matrix element for diagram (a) finally gives :

$$|\langle f|i\rangle^{el}_{eff}|^2 = \frac{|\eta_1\eta_2^*|^2}{(\hbar u)^2}\left\{1 - \frac{g_2^2}{4\pi(\hbar u)^2}\ln\left[\frac{2L}{\alpha}\right]\right\} + \mathcal{O}(g_2^4). \tag{3.4.11}$$

3.5 PERTURBATIVE EXPANSION OF THE CHIRAL RESULT

The perturbative approach presented in the previous section gives an intuitive picture of the relaxation process taking place in the wire. We may then wonder if such approach can also be used to understand the behavior of the chiral result derived in section (3.2). We may try to expand Eq. (3.2.13) with respect to the interaction parameter $g = \nu$, close to the non-interacting system: $g = 1 - \eta$. Since now on, η will play the role of the small parameter; at zero temperature the Green function, up to first order in η, is readily found to be:

$$G^{\pm}_{1/\nu}(t_{ij}) = \frac{\alpha^{1/(1-\eta)-1}}{[(\alpha \pm \imath t_{ij})]^{1/(1-\eta)}} = \frac{1}{(\alpha \pm \imath t_{ij})}\left[1 - \eta\,\log\left(1 \pm \imath\frac{t_{ij}}{\alpha}\right) + O(\eta^2)\right]. \tag{3.5.1}$$

Using the above expansion in Eq. (3.2.13) and keeping only terms up to first order in η (see C.3) and in α, for small ΔE we observe no relaxation. This result highlights the difference between the chiral and the standard Luttinger liquid model. This "stability" of the chiral model with respect to small perturbations can be understood as a consequence of the topological nature of the exponent. As we have previously mentioned, the Chiral LuL model describes the low energy behavior of the edges of a fractional quantum Hall system, where the exponents appearing in the propagators are related to the bulk filling fraction of the QH effect. A Laughlin state contains only one component of incompressible fluid and the exponent $m = 1/\nu$ is an odd integer topological quantum number that describes the strong electron-electron interaction in the QH system. In this picture it is clear that we can not continuously vary m since its value is quantized [68].

3.6 CONCLUSIONS

In this chapter we have considered the problem of energy relaxation of high energy electrons locally injected in a one dimensional system. As a specific model of a one-dimensional system we have considered a chiral Luttinger liquid, as found at the edges of a FQH state, and a standard LuL containing both chiral branches (i.e. left and right moving states). Our

interest in this problem originates from the fact that the Luttinger model is an integrable quantum field theory and therefore relaxation from an arbitrarily excited state should be precluded. However, it is not a priori clear how these considerations apply when the system is driven out of equilibrium. In order to understand this issue we have proposed an electron spectroscopy experiment where the Luttinger liquid is weakly coupled to the resonant levels of two quantum dots, one used for injecting the high energy electrons and the other one to extract them. We have theoretically considered the proposed experimental setup and found that both for the CLuL and the LuL, injected electrons do relax. In our model, energy relaxation is due to the locality of the injection and extraction process that breaks the global translational invariance of the system. Even though energy relaxation is observed in both the chiral and the standard Luttinger liquid model, the detailed nature of the relaxation process is deeply different. For the standard LuL, we found that the inelastic component of the current shows a power law behavior as a function of the energy difference with an exponent that continuously evolves as the interaction parameter is varied. This is in stark contrast to the chiral case, where the linear upturn behavior appears to be independent of the CLuL's parameter determined by the inverse filling fraction. For the case of the LuL we have explicitly shown by means of a diagrammatic approach, how relaxation is possible because the locality of the injection process allows the injected electrons to emit plasmons in the vicinity of the tunneling site through a series of virtual states. Unfortunately a similar intuitive picture for the CLuL case is still missing.

4 ENERGY TRANSPORT AND THERMAL NOISE IN FQH LINE JUNCTIONS

CONTENTS

4.1 OVERVIEW

In chapter (2.2.2), we have briefly mentioned how the statistics of tunneling current at a QPC and the charge of quasi-particles can be extracted by studying current fluctuations. In particular, the second moment of the tunneling current (the variance), is proportional to current noise (see also section B.3.2). Current noise has two contributions: an equilibrium and a non-equilibrium one. The former is due to thermal fluctuations in the distribution of the charge carriers and at the classical level is described by the Johnson–Nyquist formula

$$S_{Th} = 4\, G\, k_B T. \tag{4.1.1}$$

Here, k_B is the Boltzmann constant, G is the conductance and T is the temperature. The non-equilibrium contribution is known as shot noise and it is due to the random transmission of the charge carriers at finite bias voltage, in the low frequency limit. Classically, this contribution is described by the Schottky formula

$$S(\omega \to 0) = 2q\, I, \tag{4.1.2}$$

where q is the charge of the carriers and I the measured current. This formula can be obtained considering transmission of charge carriers according to a Poissonian distribution in the limit in which the energy scale set by the bias voltage is bigger than the energy of the

thermal fluctuations ($eV \gg k_B T$). Remarkably, this formula shows that we can extract the charge of the carriers by measuring the shot noise. Moreover, it treats the carriers as discrete objects[1]. For fermions transmitted through a single quantum channel, the above formulas are modified as

$$\begin{aligned} S_{Th} &= 4\frac{e^2}{h} k_B T \\ S(\omega \to 0) &= 2q \langle I \rangle (1-a), \end{aligned} \tag{4.1.3}$$

where the quantum of conductance $G = e^2/h$ can be seen as a bandwidth limitation imposed by the energy time uncertainty (see the discussion on scattering states in section B.3.2) and a is the transmission probability of the carriers. As we discuss in section (B.3.2), the $(1-a)$ factor is due to Pauli blocking. Note that in the weak transmission limit $a \ll 1$, the Poissonian result is recovered.

In the FQH regime, quasi particles are predicted to carry fractional charges; however, the detection of fractional charges by means of transport experiments proves particularly challenging. While the bulk states have a finite gap, edge states support gapless excitations (1.5) and it is generally believed that they are responsible for the measured value of the QH conductance. However, being attached to Fermi liquids leads, the edge excitations do not allow for a direct observation of the predicted fractional charges. It has been shown that shot noise provides a way of overcoming this problem, allowing for a direct access to the measurement of fractional charges [69, 70]. As we have mentioned earlier, shot noise can be induced by bringing the two opposite edge states close to each other at some spatial point. Experimentally, this can be achieved by gating the QH bar at some point in space, creating in this way a QPC [71]. The strength of tunneling between the two counter-propagating edge states is proportional to their spatial separation and it can be controlled via the gate potential V_g. At finite temperature, the quantum shot noise is given by the following expression [56, 69, 72]:

$$\begin{aligned} S(\omega \to 0) &= 2\,e\,I_{imp}\,a(1-a)\left\{\coth\left(\frac{e^*V}{2k_BT}\right) - \frac{2k_BT}{e^*V}\right\} \\ I_{imp} &= \nu\frac{e^2}{h}. \end{aligned} \tag{4.1.4}$$

Here, e^* is the fractional charge and I_{imp} stands for the current impinging on the QPC. The above formula reduces to Eq. (4.1.3) in the $e^*V \gg k_B T$ limit.

As mentioned above, V_g controls the spatial separation of the two counter propagating edge states via a continuous depletion of the underlying two dimensional electron gas (2DEG). A local change of density in the 2DEG corresponds to a local change of the filling fraction ν_c in the constriction. In the weak backscattering limit, the two edge states are weakly coupled and $\nu_c \sim \nu_b$, where ν_b is the bulk filling fraction. In this case, only quasiparticles sharing the same topological numbers of the bulk state can tunnel from one side

1 We would like to stress that the derivation of this formula only assumes the discreteness of the carriers and that tunneling can be described in terms of independent random events. For example, the same concept has been applied to photon counting in optical devices. In this case, shot noise is related to the discrete nature of photons.

to the other, probing in this way the bulk fractional charge. In the opposite limit of strong backscattering, the constriction is completely pinched off and $\nu_c \sim 0$. In this case, only electrons can tunnel through vacuum[2]. For intermediate regimes however, ν_c can be different from the bulk filling fraction [72, 74], a fact that has some interesting physical consequences [75–77]. In particular, A.Bid et al. [72] measured a temperature dependent, but otherwise universal fractional charge. In this work the authors measure a 2/3 charge at low temperatures and a 1/3 charge at high temperatures. Moreover, shot noise was also found on the clear 1/3 plateau. We argue that a diffusive behavior of the system may explain this peculiar findings. It was shown by Nagaev [78], that strong electron-electron interaction and diffusion change the value of shot noise in a wire. More specifically, without electron-electron interaction, shot noise in a diffusive wires with purely elastic scattering is 1/3 of the classical Poissonian result. In the presence of strong electron-electron scattering, the electron distribution can be described in terms of a local temperature $T_e(x)$. Once the local temperature is known, noise can be evaluated using [78]

$$S(\omega \to 0) = \frac{4}{RL}\int_0^L dx \int d\epsilon\, f(\epsilon, x)[1 - f(\epsilon, x)], \tag{4.1.5}$$

where L is the linear dimension of the wire and R is the contact resistance. It is worth noting [78] that Eq. (4.1.5) remains valid also when impurity scattering coexists with electron-electron or electron-phonon scattering. Provided that the elastic scattering time τ is energy independent near the Fermi surface, electron-electron scattering cannot give rise to current fluctuations due to the total conservation of momentum in the collisions. As for phonons, at low temperatures, their contributions to fluctuations is small as compared to electron-impurity scattering. For a diffusive wire, Nagaev found a universal increase in the noise power due to the joint effect of diffusion and electron-electron interaction:

$$S(\omega \to 0) = \frac{\sqrt{2}}{3}\frac{eV}{R}. \tag{4.1.6}$$

As we discuss below, transport between counter propagating edge modes at different filling fractions leads to a non quantized value of the QH conductance as a consequence of the inter-mode interaction. Kane and Fisher [79–81] showed that impurity scattering is essential to obtain a correctly quantized QH conductance. In general, it is well known that at low temperatures impurity scattering provides the main relaxation mechanism in the electron system and it is responsible for the observed finite charge current. However, current relaxation leads to Joule heating and consequently heat currents propagate through the system. Looking at Eq. (4.1.4), we may wonder if shot noise measurement (and therefore the quasi-particle charge) is affected by the emergence of local temperatures in the QH system as it is in the diffusive quantum wire studied by Nagaev. In this case, a universal increase in the noise could explain the findings of A.Bid et al. [72].

2 Most interestingly, it has been shown that this two regimes are related by an exact duality transformation [20, 73].

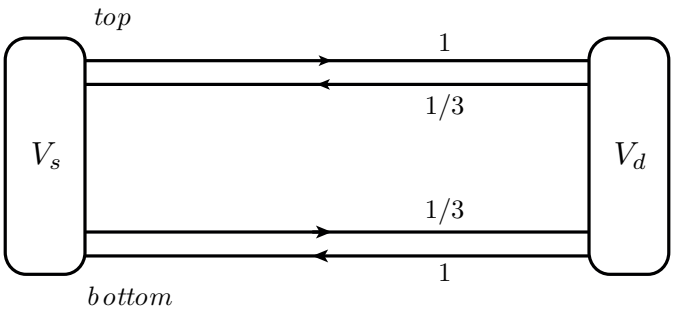

Figure 20: Edge states at $\nu = 2/3$. The sketch represents the edge states of a $\nu = 2/3$ QH state connected to two Fermi liquid reservoirs. According to the K-matrix classification (A.3), the edges support two counter propagating edge modes at fillings $\nu_1 = 1$ and $\nu_2 = 1/3$.

In this chapter we consider a QH system at bulk filling fraction $\nu_b = 2/3$ and a local filling $\nu_c = 1/3$ in the QPC. First we briefly explain the need for random impurity scattering in FQH states presenting multiple, counter propagating edge modes at different filling fractions. We will use the $\nu = 2/3$ state as an example, being the simpler state presenting counter propagating edge modes. Next, we will consider thermal transport in the FQH regime and highlights the difference between the QH thermal conductance and conductivity.

4.1.1 Clean QH edge at $\nu = 2/3$

The polarized $\nu = 2/3$ QH state belongs to the class of states whose filling fraction can be generically represented as $\nu = 1 - 1/n$, with n an odd integer [2], in both the Haldane-Halperin and the Jain's hierarchical contruction. As we discuss in appendix (A.4), the topological order of the QH state is characterized in terms of an integer, symmetric matrix $\mathbf{K}$ whose eigenvalues determine the direction in which the chiral states propagate. When brought in diagonal form (A.4.1), the K-matrix for the $\nu = 2/3$ state reads

$$\mathbf{K} = \begin{pmatrix} 1 & 0 \\ 0 & -3 \end{pmatrix}. \tag{4.1.7}$$

The above matrix describes two chiral edge modes, one at filling fraction $\nu_1 = 1$ and a second, counter propagating one, at $\nu_2 = 1/3$. The effective action for this state is

$$\begin{aligned} S &= \frac{1}{4\pi}\int_{x,\tau}\{\partial_x\phi_1(\imath\partial_\tau + u_1\partial_x)\phi_1 + 3\partial_x\phi_2(-\imath\partial_\tau + u_2\partial_x)\phi_2 + 2u_{12}\partial_x\phi_1\partial_x\phi_2\} \\ &+ \frac{1}{2\pi}\int_{x,\tau} q\epsilon^{\mu\nu}A_\mu\partial_\nu(\phi_1+\phi_2) = S_0 + S_A, \end{aligned} \tag{4.1.8}$$

where u_1 and u_2 are the velocities of the two edge modes[3], and q is the electron's charge. The two edge modes interact via a contact density-density interaction of strength u_{12}, that

3 According to (A.4.1), the velocities here are not the original ones, since the transformation $\mathbf{M}_1$ that diagonalizes $\mathbf{K}$ also affects the velocity matrix $\mathbf{U}$. However, $\mathbf{M}_1$ does not diagonalize the velocity matrix and we can just rename the matrix elements to bring them back in standard form.

corresponds to the usual g_2 interaction in the "g-ology" nomenclature of standard Luttinger liquids, see (2.1.5). Let us consider the situation depicted in Fig. (20), where the QH bar is connected to Fermi liquid contacts. Consider first the simpler (and somehow unrealistic) case in which the two edge modes do not interact at all ($u_{12} = 0$). According to the Landauer picture, every current channel contributes to the (two terminal) conductance as $g_i = \nu_i e^2/h$. Therefore, the current flowing in the top (t) and bottom (b) edge is

$$\begin{aligned} I_t &= \frac{e^2}{h}\left(V_s - \frac{1}{3}V_d\right) \\ I_b &= \frac{e^2}{h}\left(\frac{1}{3}V_s - V_d\right). \end{aligned} \tag{4.1.9}$$

The total current is readily found by summing the contributions coming from the top and bottom edge

$$I = I_t + I_b = \frac{4}{3}\frac{e^2}{h}\left(V_s - V_d\right). \tag{4.1.10}$$

The two terminal QH conductance is proportional to 4/3 instead of the expected 2/3. The above argument can be extended to a four terminal setup, for which the conductance is still found to be proportional to 4/3 [80]. Things do not get any better when adding the density-density interaction term. We can see this explicitly by diagonalizing the action (4.1.8). The general procedure is shown in (A.4.1); here we use as a representation of the transformation matrix $\mathbf{M} = \mathbf{M}_3\mathbf{M}_2$

$$\begin{pmatrix} \phi_1 \\ \phi_2 \end{pmatrix} = \begin{pmatrix} \cosh\theta & \sinh\theta \\ \frac{1}{\sqrt{3}}\sinh\theta & \frac{1}{\sqrt{3}}\cosh\theta \end{pmatrix} \begin{pmatrix} \tilde{\phi}_1 \\ \tilde{\phi}_2 \end{pmatrix}, \tag{4.1.11}$$

where θ is the mixing angle between the original eigenstates

$$\tanh 2\theta = -\frac{2u_{12}}{\sqrt{3}(u_1 + u_2)} = -c. \tag{4.1.12}$$

The value of the effective Luttinger parameter can be extracted following the method of section (2.1.5):

$$g = \sqrt{\frac{1-c}{1+c}} \tag{4.1.13}$$

In terms of the new fields, the action assumes the diagonal form

$$\begin{aligned} S &= \frac{1}{4\pi}\int_{x,\tau}\left\{\partial_x\tilde{\phi}_1(\imath\partial_\tau + \tilde{u}_+\partial_x)\tilde{\phi}_1 + \partial_x\tilde{\phi}_2(-\imath\partial_\tau + u_-\partial_x)\tilde{\phi}_2\right\} \\ &+ \frac{1}{2\pi}\int_{x,\tau} q\epsilon^{\mu\nu}\tilde{A}_\mu\left\{\left(\frac{g+1}{2\sqrt{g}} + \frac{1}{\sqrt{3}}\frac{g-1}{2\sqrt{g}}\right)\partial_\nu\tilde{\phi}_1 + \left(\frac{1}{\sqrt{3}}\frac{g+1}{2\sqrt{g}} + \frac{g-1}{2\sqrt{g}}\right)\partial_\nu\tilde{\phi}_2\right\} \\ &= \tilde{S}_0 + \tilde{S}_A. \end{aligned} \tag{4.1.14}$$

Here, $\tilde{S}_0$ represents two non interacting edge modes, propagating in opposite directions with velocities

$$u_\pm = \frac{(u_1+u_2)}{2}\left\{\frac{1+c^2}{\sqrt{1-c^2}} \pm \frac{u_1-u_2}{u_1+u_2}\right\}. \tag{4.1.15}$$

Even though the interactions do not appear anymore in $\tilde{S}_0$, they do appear in $\tilde{S}_A$. Note that also the gauge field $\tilde{A}_\mu$ is is affected by the transformation since it now couples to the rotated bosonic fields; more precisely, the gauge field should satisfy modified boundary conditions with respect to the original A_μ field, as we show below. In appendix (A.4.2) we show how to evaluate the two terminal QH conductance from the single mode effective action. This analysis can be extended to multiple edge modes; in this case Eq. (A.4.20) reads

$$\left\langle J^1(x)\right\rangle = \int_{x'} \lim_{\omega\to 0} \Pi^{10}(x-x',\omega)\tilde{A}_0(x'). \tag{4.1.16}$$

The polarization tensor can be obtained by an analytic continuation to real frequencies ($\omega_n \to \omega + \imath\epsilon$) of the Matsubara tensor

$$\Pi^{10}(x-x',\omega_n) = \frac{(-e)^2}{3\pi}\int_k \frac{e^{\imath k(x-x')}}{2\pi}\left\{(\Delta+1)\frac{\omega_n}{\omega_n+\imath u_+ k} - (\Delta-1)\frac{\omega_n}{\omega_n-\imath u_- k}\right\}, \tag{4.1.17}$$

where ω_n are Matsubara (bosonic) frequencies. In Eq. (4.1.17) we have used the parameter $\Delta \pm 1$ following definitions for the

$$\begin{aligned}
\left\{\frac{g+1}{2\sqrt{g}} + \frac{1}{\sqrt{3}}\frac{g-1}{2\sqrt{g}}\right\}^2 &= \frac{1}{2}\left\{\left(1+\frac{1}{\sqrt{3}}\right)g^{1/2} + \left(1-\frac{1}{\sqrt{3}}\right)g^{-1/2}\right\} \\
&= \frac{1}{3}\left\{\frac{2-\sqrt{3}c}{\sqrt{1-c^2}}+1\right\} = \frac{1}{3}(\Delta+1) \\
\left\{\frac{1}{\sqrt{3}}\frac{g+1}{2\sqrt{g}} + \frac{g-1}{2\sqrt{g}}\right\}^2 &= \frac{1}{3}(\Delta-1).
\end{aligned}$$

After integrating over momenta, we substitute the resulting expression into (4.1.16) and impose the following boundary condition for the gauge field: $\theta(\eta(x-x'))\tilde{A}_0(x') = \eta(V_1 - V_2)$, with $\eta = \pm$ respectively for right and left moving fields. As a result, the two terminal conductance reads

$$G = \frac{2}{3}\Delta\frac{e^2}{h}. \tag{4.1.18}$$

The conductance is correctly quantized only if $\Delta = 1$, that means $c = \sqrt{3}/2$ [79]. This is a very specific value that should result from a fine tuning of the non-universal velocity matrix, and therefore unlikely to happen in an experiment. Moreover, the inter-mode interaction gives rise to a non universal quasi-particle charge. To see this, consider a QPC pinching the QH bar and inducing scattering between the top and the bottom edge. A general tunneling operator has the form $V = \exp(\imath l_1\phi_1 + \imath l_2\phi_2)$, adding l_1 electrons to the mode ϕ_1 and l_2, 1/3-charged Laughlin quasi-holes to mode ϕ_2. Since charge must be conserved during inter edge tunneling, the most relevant operator (i.e. the one with the smallest scaling dimension) has $l_1 = 1$ and $l_2 = 3$. The effect of the QPC is taken into account by adding to the action (4.1.8) and additional term

$$S_{QPC} = \int_{x,\tau}\left(t_Q e^{\imath\phi_1 + 3\imath\phi_2} + \text{h.c.}\right), \tag{4.1.19}$$

where t_Q is the transmission amplitude of the QPC. The pair correlation function of the tunneling operator is evaluated in the diagonal basis by using the quadratic action $\tilde{S}_0$, Eq. (4.1.14):

$$\left\langle V^\dagger(x,\tau)V(x,0)\right\rangle \sim \tau^{-(\Delta+1)}\,\tau^{-(\Delta-1)}. \tag{4.1.20}$$

Since we would like to extract the quasi-particle charge through a noise measurement, Eq. (4.1.20) would imply a non-universal quasi-particle charge.

4.1.2 The disordered QH edge at $\nu = 2/3$

Since a conductance $G = (2/3)e^2/h$ is experimentally observed, a relaxation mechanism not present in Eq. (4.1.8) should be responsible for its observed value. Kane and Fisher [79] showed that random impurity scattering is responsible for an edge phase transition towards a disorder dominated phase characterized by a $G = (2/3)e^2/h$ QH conductance. To see this, we first add the random inter-mode tunneling term, describing the effect of disorder

$$S_I = \int_{x,\tau} \left(\xi(x)e^{\imath\phi_1+3\imath\phi_2} + \text{c.c.}\right), \tag{4.1.21}$$

to the action (4.1.8). This term is similar to the one considered in Eq. (4.1.19) for scattering at a QPC. However, here t_Q has been substituted by the spatially dependent, complex valued parameter $\xi(x)$. We take ξ to be a Gaussian random variable with variance $\overline{\xi^*(x)\xi(x')} = W\delta(x-x')$, with W the disorder strength. The relevancy of disorder scattering can be determined by the following renormalization group (RG) equation [79]:

$$\frac{dW}{dl} = (3-2\Delta)W. \tag{4.1.22}$$

Hence, for $\Delta > 3/2$ small randomness is irrelevant and the non universal conductance Eq. (4.1.18) is found. For $\Delta = 3/2$ weak disorder is marginal. Finally, for $\Delta < 3/2$ weak disorder is relevant. In this case, at zero temperature the RG flows is towards the fixed line $\Delta = 1$; only a single charge mode propagates ballistically and gives a quantized Hall conductance of $G = (2/3)e^2/h$. This can be seen by moving to the charge (ρ) and neutral mode (σ) basis

$$\phi_\rho = \sqrt{\frac{3}{2}}(\phi_1+\phi_2) \quad , \quad \phi_\sigma = \sqrt{\frac{1}{2}}(\phi_1+3\phi_2). \tag{4.1.23}$$

In this basis, the total action $S = S_\rho + S_\sigma + S_{\text{int}}$ reads:

$$\begin{aligned} S_\rho &= \int_{x,\tau}\left\{\frac{1}{4\pi}\partial_x\phi_\rho(\imath\partial_\tau + u_\rho\partial_x)\phi_\rho + \frac{q}{2\pi}\sqrt{\frac{2}{3}}\epsilon^{\mu\nu}A_\mu\partial_\nu\phi_\rho\right\} \\ S_\sigma &= \int_{x,\tau}\left\{\frac{1}{4\pi}\partial_x\phi_\sigma(-\imath\partial_\tau + u_\sigma\partial_x)\phi_\sigma + \xi(x)e^{\imath\sqrt{2}\phi_\sigma} + \text{c.c.}\right\} \\ S_{\text{int}} &= \frac{u}{4\pi}\int_{x,\tau}\partial_x\phi_\rho\partial_x\phi_\sigma. \end{aligned} \tag{4.1.24}$$

The advantage of this basis is that only the charge mode couples to the external gauge field (hence the name), while the neutral mode only couples to impurities. The last term is the

density-density interaction between the two modes. the new velocities are related to the old ones as:

$$\begin{aligned} u_\rho &= \frac{3}{2}u_1 + \frac{1}{2}u_2 - u_{12} \\ u_\sigma &= \frac{1}{2}u_1 + \frac{3}{2}u_2 - u_{12} \\ u &= \frac{4}{\sqrt{3}}\left(u_{12} - \frac{3}{4}(u_1 - u_2)\right). \end{aligned} \tag{4.1.25}$$

In particular, for $\Delta - 1$ small a simple relation between the three velocities is found:

$$u = (u_\rho + u_\sigma)\sqrt{\frac{\Delta - 1}{2}}. \tag{4.1.26}$$

In this form, it can be seen that at $\Delta = 1$ the charge and neutral sector decouples. The decoupled edge problem can be exactly solved [79, 80] and yields a propagating charge mode (with a correctly quantized QH conductance) and a counter propagating neutral mode. Even though the neutral mode does not carry any charge, it carries energy. We discuss energy transport in the next section.

4.1.3 Thermal transport

As a result of Joule heating, local (i.e. space dependent) temperatures can set in the system. More in general, in QH devices the points where energy is dissipated are called hot spots. Usually, in a QH bar without a QPC, these hot spots are located at the opposite corners of the device, exactly at the contact region[4] [82–84]. This result is somehow easy to understand in the Landauer picture, where dissipation can only take place at the contacts of the mesoscopic sample [85]. The presence of the hot spots, also implies the presence of thermal currents in the sample. Here we briefly review the theory of thermal transport in QH systems [86]. Consider the Lagrangian density for the (single) edge of a general (abelian) QH state in the diagonal basis[5], Eq. (A.4.13)

$$\mathscr{L} = \frac{1}{4\pi}\sum_{i=1}^{n} \partial_x \phi_i \left(\eta_i \, \partial_t \phi_i - u_i \, \partial_x \phi_i\right), \tag{4.1.27}$$

where i labels different edge modes. Here, $\eta_i = \pm 1$ specifies the direction of propagation of the chiral modes. A nice way of deriving the energy current associated with the above Lagrangian density is to use the energy-momentum tensor

$$T^{\mu\nu} = \frac{\partial \mathscr{L}}{\partial(\partial_\mu \phi)}\partial_\nu \phi - \delta_{\mu\nu}\mathscr{L}. \tag{4.1.28}$$

4 This is also true for systems in the IQH regime and in FQH states with only co-propagating edge states.
5 In order to simplify the notation, here we use ϕ instead of $\tilde{\phi}_3$.

The existence of the tensor follows from Noether's theorem and the request of invariance of the Lagrangian under a general coordinate transformation [23]. The relation between the energy momentum tensor and the thermal current density is

$$\begin{aligned}\langle j_Q \rangle &= \sum_{i=1}^{n} u_i \langle T_i^{01} \rangle = \sum_{i=1}^{n} u_i \left\langle \frac{\partial \mathscr{L}_i}{\partial(\partial_0 \phi_i)} \partial_1 \phi_i \right\rangle = \sum_{i=1}^{n} u_i \eta_i \left\langle \frac{\partial_x \phi_i \partial_x \phi_i}{4\pi} \right\rangle \\ &= \sum_{i=1}^{n} u_i \eta_i \left\langle \frac{\mathscr{H}_i}{u_i} \right\rangle .\end{aligned} \tag{4.1.29}$$

Above, we have used the definition of the Hamiltonian density. Since in the diagonal basis the "new" bosons are independent, the current density results from summing the contribution of the energy densities in every single channel. Moreover, the non-universal velocities cancels from the expression of the current. The energy density in channel i is readily found as

$$\langle \mathscr{H}_i \rangle = \int_0^\infty \frac{d\epsilon_i}{2\pi} \epsilon_i \, n(\epsilon_i) = \frac{\pi^2}{6} \frac{k_B^2}{h} T^2, \tag{4.1.30}$$

where $n(\epsilon_i)$ is the Bose-Einstein distribution function in channel i and T is the related bosonic temperature[6], the same for every edge mode. The thermal Hall conductance can be extracted from Eq. (4.1.30) and (4.1.29)

$$K_H = \frac{\partial J_Q}{\partial T} = \nu_Q \frac{\pi^2}{3} \frac{k_B^2}{h} T. \tag{4.1.31}$$

The coefficient $\nu_Q = \sum_i \eta_i$ plays the role of the "filling fraction"; its value is given by the difference in the number of upstream and downstream edge modes. Analogously to the filling fraction of the charged Hall conductance, ν_Q shares the same topological stability[7]. It is interesting to note that for QH states having an equal number of downstream and upstream modes, the thermal QH conductance is identically zero. Kane and Fisher [86] showed that impurity scattering is necessary to equilibrate the different edge modes and gives rise to a single, propagating charge mode, see section (4.1.2). In the case of the heat mode, random impurity scattering in states characterized by $nu_Q \neq 0$, do not modify the result found for the clean edge: a single heat mode propagates. This heat mode is characterized by the quantized thermal QH conductance K_H defined in Eq. (4.1.31). We mentioned that K_H vanishes for FQH states having an equal number of upstream and downstream edge modes. In this case, random impurity scattering gives rise to a diffusive mode characterized by a, non-universal, QH thermal conductivity $\kappa = C D_Q$. Here, $C = (\pi^2/3) T \sum_i \nu_i^{-1}$ is the edge heat capacity and D_Q is the diffusion constant whose form depends on the details of the impurity scattering.

6 The general expression for this type of integrals is : $F_n = \int_0^\infty dx \frac{x^n}{e^x - 1} = \Gamma(n+1)\xi(n+1)$, where $\Gamma(n)$ is the Euler gamma function and $\xi(n)$ is the Riemann zeta function.

7 The connection between the thermal QH effect and the gravitational anomaly in $1+1$ conformal field theories has been investigated in [87]. Recently, it has been proposed by various authors to use the gravitational anomaly and the related thermal QHE to classify different topological insulators and superconductors [88–90].

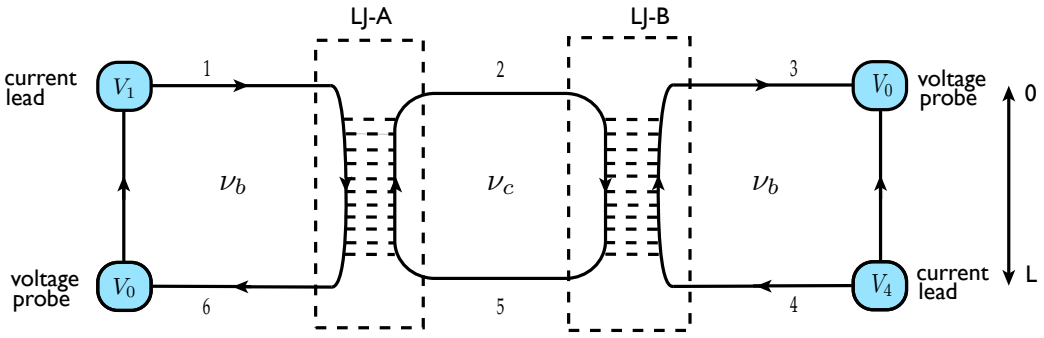

Figure 21: Sketch of a Hall bar with a low density region. The interaction between the edge states at bulk filling ν_b and the ones at the constriction filling ν_c is modeled in terms of two line junctions. Dashed, horizontal lines represent random impurity scattering. We isolate the two line junctions region and name them LJ-A and LJ-B. Numbers label voltages and edge currents flowing in the i-th edge modes, $i = 1...6$. Note that this representation in only valid when ν_b and ν_c do not belong to the same hierarchy [75].

4.2 CHARGE CURRENTS AND DISSIPATION

In this section we consider the setup depicted in Fig. (21). Following [75, 91], we model the interaction between the low density constriction and the bulk in terms of two line junctions (LJ) [92]. We consider ν_c in the principal Laughlin sequence, while ν_b can be extended to the hierarchical case. As a consequence, the bulk section of the QH bar supports multiple edge modes. In the specific case of $\nu_b = 2/3$, there are two counter-propagating edge modes, one at filling $\nu = 1$ and the other at filling $\nu = 1/3$, see Fig(20). Therefore, for $\nu_c = 1/3$ LJ-A will support three edge modes: a $\nu = 1$ mode propagating downwards (from 0 to L) and two $\nu = 1/3$ modes propagating upwards. The same situation takes place in LJ-B, with edge modes propagating in the opposite direction with respect to the configuration in LJ-A. In this chapter we consider a regime in which weak impurity scattering is relevant and the LJ supports a single charge and energy mode, as discussed in the introductory section. We start this analysis by studying charge current equilibration in a single LJ setup using an hydrodynamic approach; then we use a mesoscopic, scattering approach, to study electrical power dissipation in the single and in the double LJ setup. Finally, we determine the position of the hot-spots and their temperatures as a function of the LJ transmission.

4.2.1 Equilibration in a single LJ: hydrodynamical approach

In this section we analyze mode equilibration in the line junction using a simple hydrodynamic approach. Consider the setup depicted in Fig. (22); the schematic represents a single LJ between two partitions of a FQH fluid at two different filling fractions, ν_b and ν_c. The system is coupled to ideal ohmic contacts kept at potentials $V_1 > V_3 \neq 0$ that act as electrons

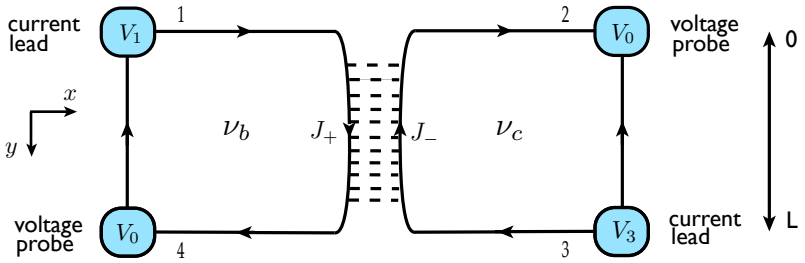

Figure 22: Single line junction setup between two different filling fractions. Numbers label currents, voltages and electrical power flowing in the i-th edge modes, $i = 1...4$. $J_\pm$ are currents flowing through the LJ as a result of a potential difference between the bulk and the constriction. Here we also show explicitly our convention on the signs of the currents moving in the x and y direction.

reservoirs, while $V_2 = V_4 = V_0$ act as a voltage probe. The numbers on the edges specify the values of the charge current I_i flowing in the i-th edge mode ($i = 1...4$) and the potentials V_i. Arrows specify the chirality of the edge mode and J_+, J_- are the currents flowing through the LJ. For an ideal contact, edge modes originate in equilibrium at the contact's voltage. In the FQH regime, the currents flowing in each edge mode are

$$\begin{aligned} I_i &= \nu_i \frac{e^2}{h} V_i \\ \nu_i &= \begin{cases} \nu_b & i = 1,4 \\ \nu_c & i = 2,3 \end{cases} \end{aligned} \tag{4.2.1}$$

As a first step, we need to find the two terminal LJ conductance and then relate it to the two terminal (source to drain) conductance of the quantum Hall bar. As a result of impurity scattering, transport between the two edges in the LJ is characterized by a tunneling conductivity per unit length σ [92], whose value depends on the details of the impurity potential. In order to study current equilibration, we can use the continuity equation for the currents flowing in the LJ in stationary regime. The source term is due to the steady state tunneling currents between J_+ and J_-:

$$\pm \partial_x J_\pm(x) = \sigma(V_\mp(x) - V_\pm(x)), \tag{4.2.2}$$

where σ is space independent. Assuming local equilibrium on the edge, we can relate the edge potentials to the currents by inverting Eq. (4.2.1):

$$\begin{aligned} V_+(x) &= \frac{h}{\nu_b} J_+(x) \\ V_-(x) &= \frac{h}{\nu_c} J_-(x). \end{aligned} \tag{4.2.3}$$

It is worth stressing that Eq. (4.2.1) defines global (i.e. space independent) currents, while Eq. (4.2.3) only holds locally. Using Eq. (4.2.3) in Eq. (4.2.2) we obtain two coupled, non homogeneous differential equations:

$$\begin{aligned} \partial_x J_+(x) &= \frac{\sigma h}{e^2}\left(\frac{J_-(x)}{\nu_c} - \frac{J_+(x)}{\nu_b}\right) \\ \partial_x J_-(x) &= \frac{\sigma h}{e^2}\left(\frac{J_-(x)}{\nu_c} - \frac{J_+(x)}{\nu_b}\right). \end{aligned} \tag{4.2.4}$$

The total (non chiral) current flowing through the junction is constant, i.e. $\partial_x(J_+ - J_-) = 0$. To complete the Cauchy problem, we need to specify the boundary conditions: $J_+(0) = I_1$ and $J_-(L) = I_3$. Solving the coupled differential equations, we find the currents flowing in the LJ:

$$J_+(x) = \frac{I_1\left(\nu_b - \nu_c\, e^{(x-L)/l}\right) + I_3\nu_b\, e^{-L/l}\left(e^{x/l} - 1\right)}{\nu_b - e^{-L/l}\nu_c} \tag{4.2.5}$$

$$J_-(x) = \frac{I_1\,\nu_c\left(1 - e^{(x-L)/l}\right) + I_3\, e^{-L/l}\left(e^{x/l}\nu_b - \nu_c\right)}{\nu_b - e^{-L/l}\nu_c}. \tag{4.2.6}$$

Where we have defined the equilibration length $l = (h\sigma/e^2)(\nu_b\nu_c)/(\nu_b - \nu_c)$. The total current through the junction is then given by:

$$J_+(x) - J_-(x) = (\nu_b - \nu_c)\frac{I_1 - I_3\, e^{-L/l}}{\nu_b - \nu_c\, e^{-L/l}}. \tag{4.2.7}$$

The above expression generalizes the result of [92] to the case of a LJ between two different filling fractions. If we set $V_3 = 0$ and $V_1 = V$ the LJ conductance reads

$$G_{LG} = \frac{e^2}{h}\frac{\nu_b - \nu_c}{1 - \frac{\nu_c}{\nu_b}\, e^{-L/l}}. \tag{4.2.8}$$

From the above equation we see that the LJ two terminal conductance is not quantized for $L \ll l$. However, in the opposite limit $L \gg l$, corresponding to a fully equilibrated junction, a correctly quantized two terminal LJ conductance is obtained

$$G_{LJ} = \frac{e^2}{h}(\nu_b - \nu_c). \tag{4.2.9}$$

Using the two terminal LJ conductance, we are now able to compute the source to drain conductance of the quantum Hall bar. In the following, we will set $V_3 = 0$ and $V_1 = V$. Let $I_{LJ} = G_{LJ}V$ be the current passing through the LJ, so the current and the voltage at the drain contact ($y = 0$) is

$$I_2 = I_1 - I_{LJ} = \frac{e^2}{h}\nu_c V = \frac{\nu_c}{\nu_b} I_1 \tag{4.2.10}$$

$$V_2 = V. \tag{4.2.11}$$

As for the current and voltage at the other drain contact ($y = L$):

$$I_4 = I_{LJ} = \frac{e^2}{h}(\nu_b - \nu_c)V \tag{4.2.12}$$

$$V_4 = \left(1 - \frac{\nu_\beta}{\nu_\alpha}\right)V. \tag{4.2.13}$$

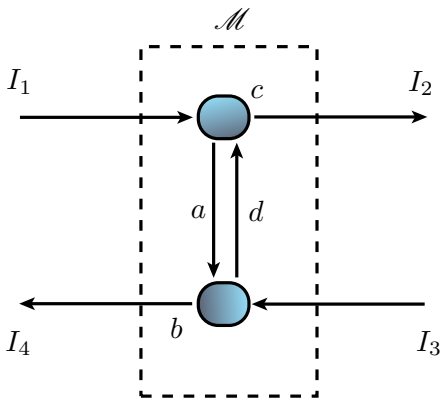

Figure 23: Branching matrix. Schematic representation of the branching matrix, relating incoming and outgoing currents at the junction.

4.2.2 Mesoscopic approach

In this section we will consider a mesoscopic transport approach to compute voltages, currents and electrical power in the line junction [77, 91]. The aim of this approach is to relate the quantities previously found from the hydrodynamical analysis, to the transmission coefficient of the LJ.

At the LJ, currents coming from the two current leads can either be transmitted or reflected. In order to relate the incoming and outgoing currents in the LJ, we construct the branching matrix $\mathscr{M}$ as follows[8]:

$$\begin{pmatrix} I_4 \\ I_2 \end{pmatrix} = \begin{pmatrix} a & b \\ c & d \end{pmatrix} \begin{pmatrix} I_1 \\ I_3 \end{pmatrix}. \tag{4.2.14}$$

In the above definitions we have introduced the transmission probabilities c and b and the reflection ones a and d, see Fig. (23). If the sample is unbiased, all the voltages on the edges must be the same: $V_1 = V_3 \to V_2 = V_4$, and no net current flows through the system. This neutrality condition yields:

$$\begin{pmatrix} \nu_b \\ \nu_c \end{pmatrix} = \mathscr{M} \begin{pmatrix} \nu_b \\ \nu_c \end{pmatrix} \qquad \text{or} \quad \underline{\nu} = \mathscr{M}\underline{\nu}. \tag{4.2.15}$$

Condition (4.2.15) says that $\underline{\nu}$ is an eigenvector of $\mathscr{M}$, and yields a restriction on the values of the transmission and reflection probabilities:

$$\begin{aligned} b &= (\nu_b/\nu_c)(1-a) \\ c &= (\nu_c/\nu_b)(1-d). \end{aligned} \tag{4.2.16}$$

8 Even though similar in structure, the branching matrix $\mathscr{M}$ is conceptually different from the scattering Matrix S, that relates instead the microscopic quantum mechanical amplitudes for transmission and reflection. Even though S and $\mathscr{M}$ are related, the first one is defined in terms of microscopic quantities, while the second one relates on macroscopic ones.

A second constraint on $\mathscr{M}$ is imposed by Kirchoff's law (current conservation):

$$I_1 + I_3 = I_2 + I_4, \tag{4.2.17}$$

that implies that the matrix elements of $\mathscr{M}$ belonging to the same column, should sum up to one. Using Eq. (4.2.16) and (4.2.17), we obtain:

$$\mathscr{M} = \begin{pmatrix} 1 - \frac{\nu_c}{\nu_b}(1-d) & 1-d \\ \frac{\nu_c}{\nu_b}(1-d) & d \end{pmatrix}. \tag{4.2.18}$$

In order to define the transmission coefficient of the LJ, we tune V_3 in order to obtain $I_3 = I_1$. In this way, we obtain the same incident current on the junction:

$$\begin{aligned} I_4 &= \left(1 - \frac{\nu_c}{\nu_b}(1-d) + (1-d)\right) I_1 \\ &= \nu_b \frac{e^2}{h}\left(1 - \frac{\nu_b + \nu_c}{\nu_b}(1-d)\right) V_1. \end{aligned} \tag{4.2.19}$$

According to Landauer's formula, we can define the transmission coefficient [9]:

$$t = \frac{\nu_b + \nu_c}{2\nu_b}(1-d), \tag{4.2.20}$$

so that the branching matrix is parametrized by a single parameter specifying the strength of the constriction. Using Eq. (4.2.20) in Eq. (4.2.18), we obtain the final expression for the branching matrix:

$$\mathscr{M} = \begin{pmatrix} 1 - t\frac{2\nu_c}{\nu_b+\nu_c} & t\frac{2\nu_b}{\nu_b+\nu_c} \\ t\frac{2\nu_c}{\nu_b+\nu_c} & 1 - t\frac{2\nu_b}{\nu_b+\nu_c} \end{pmatrix}. \tag{4.2.21}$$

Eq. (4.2.14) can now be expressed in the useful form

$$\begin{pmatrix} I_4 \\ I_2 \end{pmatrix} = \begin{pmatrix} G_1 - G_t & G_t \\ G_t & G_3 - G_t \end{pmatrix} \begin{pmatrix} V_1 \\ V_3 \end{pmatrix}, \tag{4.2.22}$$

where we have defined the tunneling conductance of the LJ

$$G_t = 2\frac{e^2}{h} t \left(\frac{\nu_c \nu_b}{\nu_b + \nu_c}\right). \tag{4.2.23}$$

When written in components, the two currents read:

$$\begin{aligned} I_4 &= G_1 V_1 + G_t(V_3 - V_1) \\ I_2 &= G_3 V_3 + G_t(V_1 - V_3). \end{aligned} \tag{4.2.24}$$

We correctly obtain that in equilibrium, i.e. for $V_3 = V_1$, the contribution of the LJ vanishes.

At this point we are able to relate the hydrodynamical results of section (4.2.1), to what obtained in Eq. (4.2.14) and (4.2.23) (we set $V_3 = 0$ and $V_1 = V$). Comparing Eq. (4.2.10),

9 The factor of two in the denominator has been chosen such that $t = (1-d)$ when $\nu_\alpha = \nu_\beta$.

obtained in the limit of a fully equilibrated LJ, with Eq. (5.4.1) for I_2, we can identify the effective transmission coefficient of the LJ

$$t_e = \frac{1}{2}\left(1 + \frac{\nu_c}{\nu_b}\right). \tag{4.2.25}$$

For the case considered in this chapter with $\nu_c = 1/3$ and $\nu_b = 3/2$, the effective transmission coefficient is $t_e = 3/4$.

4.2.3 Power dissipation and Joule heating

The electrical power flux in the i-th edge mode (or electrical energy flux) is given by the following equivalent expressions:

$$P_i = \frac{1}{2} I_i V_i = \frac{1}{2} I_i^2 G^{-1} = \frac{1}{2} G V_i^2. \tag{4.2.26}$$

Note that the first equality is more general, while the second and third assume a system characterized by a conductance. The "conservation law" for P_i is simply $P_{in} = P_{out} = P_j$, where P_{in} is the total energy flux entering the system, P_{out} is the one leaving the system and P_j is the power dissipated in the system through Joule heating. For the setup of Fig. (22) we find:

$$P_1 + P_3 - P_2 - P_4 = P_j. \tag{4.2.27}$$

We can compute this expression explicitly using Eq. (4.2.26). We also use $G_1 = G_4$ $G_2 = G_3$:

$$\begin{aligned} P_j &= \frac{1}{2}\{G_1 V_1^2 - G_3^{-1}(G_3 V_3 + G_t(V_1 - V_3))^2 + G_3 V_3^2 \\ &- G_1^{-1}(G_1 V_1 - G_t(V_1 - V_3))^2\} = G_t(1-t)(V_1 - V_3)^2. \end{aligned} \tag{4.2.28}$$

Correctly, we find that for perfect reflection or transmission, i.e. for $t = 0, 1$ respectively, no power is dissipated. Consider now the case $\nu_c = 1/3$ and $\nu_b = 2/3$. As discussed in section (4.1.1), the 2/3 state consists of two counter propagating edge modes, one at filling fraction $\nu = 1$ and the other at filling $\nu = 1/3$. In Fig. (24), we show explicitly the three edge modes in the junction; the two 1/3 modes co-propagate upwards while the $\nu = 1$ mode propagates downwards. According to Eq. (4.1.31), their thermal Hall conductance K_H is characterized by the topological number $\nu_Q = 1 - 1 - 1 = -1$. As a preliminary analysis, we consider the case where all the contacts in the system are held at $T = 0$. According to Eq. (4.1.31), a single thermal mode propagates towards the negative y direction. As a result, a heat flux increases the local temperature at the end of the junction on the $y = 0$ axes. Note that we are assuming a point-like hotspot. In this approximation we are neglecting the fact that, within the equilibration length l, a conductivity per unit-length σ exists, together with a temperature gradient. In the next section we will study how heat is transported away from the hot-spot. For the moment we can determine the local temperature at the hotspot using Eq. (4.2.28) and the expression for the energy flux

$$j_Q = K_H T = P_J \quad \rightarrow \quad T(t) = \sqrt{\frac{3G_t(1-t)}{\pi^2}\frac{h}{k_B^2}}\,(V_1 - V_3). \tag{4.2.29}$$

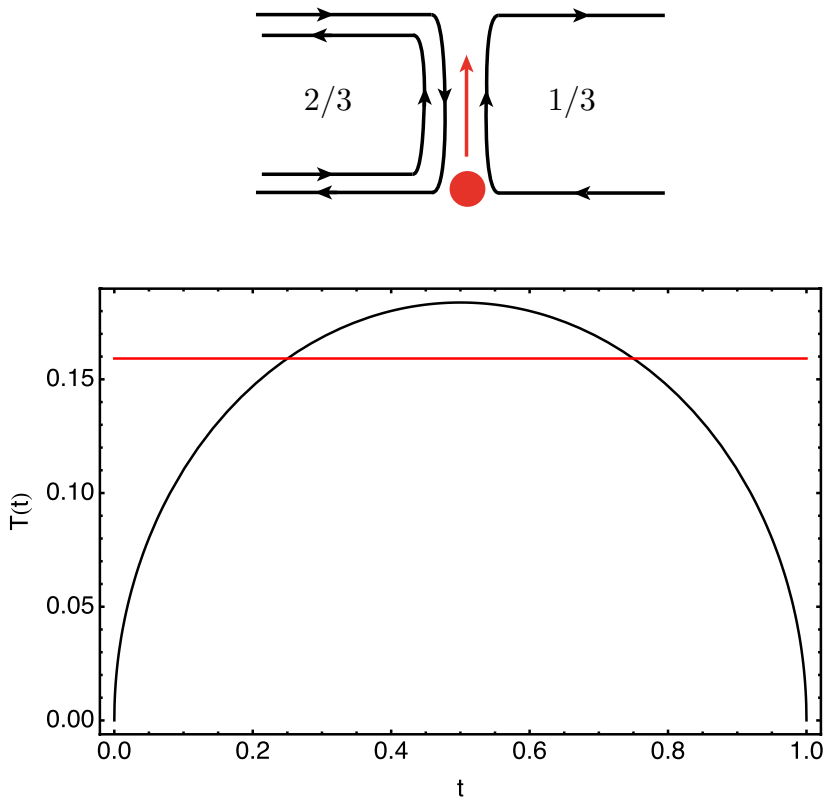

Figure 24: Joule heating in a LJ. (top) The schematic represents a LJ between a $\nu_b = 2/3$ and a $\nu_c = 1/3$ QH state. The edge modes for the two bulk filling fractions are shown together with their chiralities. The red arrow represents the direction in which the heat flux propagates. The red dot represents the hotspot. (bottom) Temperature of the hotspot as a function of the LJ transmission coefficient t, Eq.(4.2.20). The plot is evaluated for $V_1 = 1V$, $V_3 = 0$ in natural units. The red line represents the temperature evaluated at the effective transmission t_e (4.2.25), corresponding to the equilibrated edge. For $\nu_b = 2/3$ and $\nu_c = 1/3$, $t_e = 3/4$.

4.2.4 Multiple LJ setup

We can now generalize what we obtained so far to the double LJ setup of Fig. (21). The double LJ setup can be obtained by "glueing" together two copies of the single LJ setup analyzed so far. However, the r.h.s of the LJ (LJ-B) has chiralities inverted with respect to the l.h.s. (LJ-A). However, as shown in Fig. (25), we can map one section into the other simply by permuting the "labels" of the filling fractions. So we can obtain the branching matrix $\mathscr{M}_B$ for LJ-B by exchanging ν_b and ν_c in (4.2.21). Defining $\mathscr{M}_A = \mathscr{M}$, we can formally represent this operation as

$$\hat{\nu}_{ex}\mathscr{M}_A = \mathscr{M}_B, \tag{4.2.30}$$

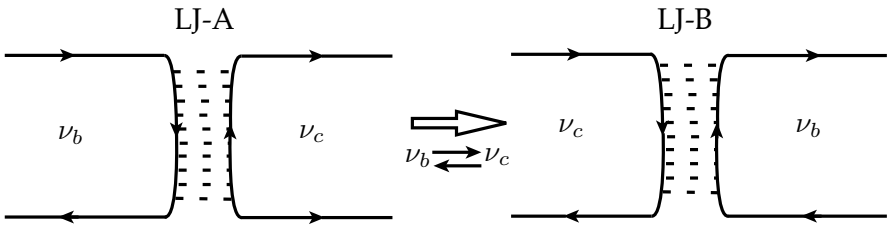

Figure 25: Relation between the two LJs. The two LJs can be related through a relabeling of the filling fractions.

where $\hat{\nu}_{ex}$ is the filling fraction exchange operator. According to Eq. (4.2.21), we can denote the matrix elements of the branching matrix as:

$$\begin{aligned} r_c &= 1 - t\frac{2\nu_c}{\nu_b+\nu_c} \quad , \quad \Theta_b = t\frac{2\nu_b}{\nu_b+\nu_c} \\ \Theta_c &= t\frac{2\nu_c}{\nu_b+\nu_c} \quad , \quad r_b = 1 - t\frac{2\nu_b}{\nu_b+\nu_c} \end{aligned} \tag{4.2.31}$$

Using this notation, the two branching matrices read:

$$\mathscr{M}_A = \begin{pmatrix} r_c & \Theta_b \\ \Theta_c & r_b \end{pmatrix} \quad , \quad \mathscr{M}_B = \begin{pmatrix} r_b & \Theta_c \\ \Theta_b & r_c \end{pmatrix}. \tag{4.2.32}$$

Currents in the two sections are given by:

$$\begin{pmatrix} I_6 \\ I_2 \end{pmatrix} = \mathscr{M}_A \begin{pmatrix} I_1 \\ I_5 \end{pmatrix} \quad , \quad \begin{pmatrix} I_5 \\ I_3 \end{pmatrix} = \mathscr{M}_B \begin{pmatrix} I_2 \\ I_4 \end{pmatrix}. \tag{4.2.33}$$

We can find I_2 and I_5 by solving the system above

$$\begin{aligned} I_2 &= \frac{\Theta_c}{1-r_b^2}(I_1 + r_b\, I_4) \\ I_5 &= \frac{\Theta_c}{1-r_b^2}(I_4 + r_b\, I_1). \end{aligned} \tag{4.2.34}$$

Using the above relation, and setting $D^{-1} = 1 - r_b^2$, we can obtain the relation between the incoming and outgoing currents in the system:

$$\begin{pmatrix} I_6 \\ I_3 \end{pmatrix} = \begin{pmatrix} r_c + D r_b \Theta_b \Theta_c & D\Theta_b\Theta_c \\ D\Theta_b\Theta_c & r_c + D r_b \Theta_b \Theta_c \end{pmatrix} \begin{pmatrix} I_1 \\ I_4 \end{pmatrix}. \tag{4.2.35}$$

The dissipated power at the two junctions can be found following the same reasoning of the single LJ. Let us call P_{jA} the power dissipated at LJ-A and P_{jB} the power dissipated at LJ-B, then

$$\begin{aligned} P_1 + P_5 - P_2 - P_6 &= P_{jA} \\ P_4 + P_2 - P_3 - P_5 &= P_{jB}. \end{aligned} \tag{4.2.36}$$

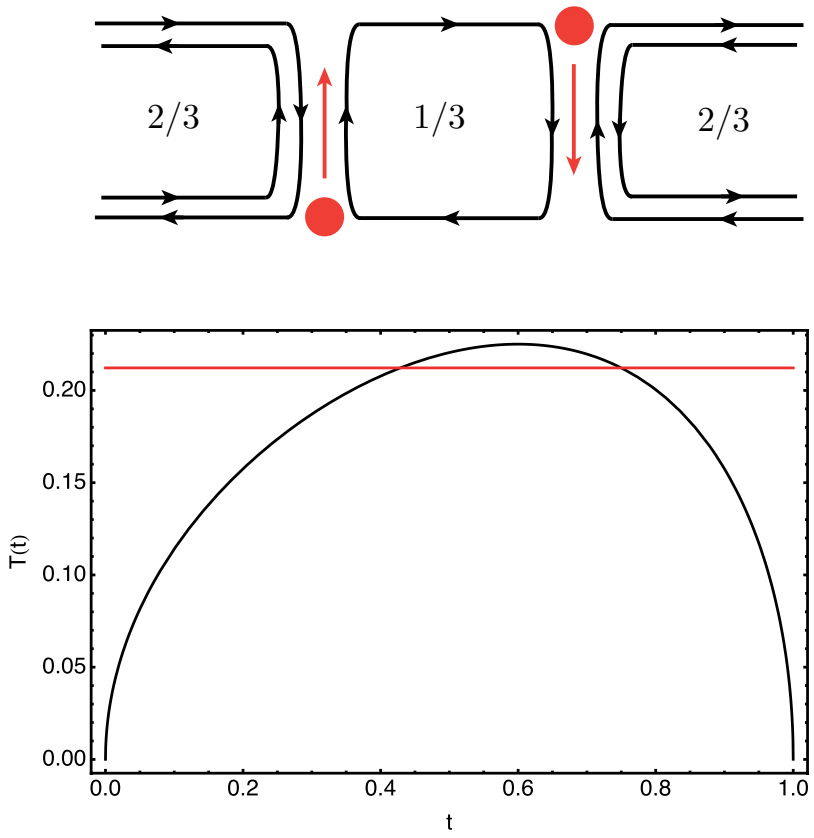

Figure 26: Joule heating in a double LJ. (top) The schematic represents the double LJ system. The edge modes for the two bulk filling fractions are shown together with their chiralities. The red arrow represents the direction in which the heat flux propagates. The red dot represents the hotspot. (bottom) Temperature of the hotspots as a function of the LJ transmission coefficient t. The plot is evaluated for $V_1 = 1V$, $V_3 = 0$ in natural units. Here, $T = T_A = T_B$. The red line represents the temperature evaluated at the effective transmission t_e (4.2.25), corresponding to the equilibrated edge. For $\nu_b = 2/3$ and $\nu_c = 1/3$, $t_e = 3/4$.

The explicit value of the dissipated power can be found using Eq. (4.2.26) together with Eq. (4.2.35)

$$P_{jA} = P_{jB} = \frac{e^2}{2h} \frac{t(1-t)(\nu_b \nu_c)}{(1+(1-t)\frac{\nu_c}{\nu_b})^2} (V_1 - V_4)^2. \tag{4.2.37}$$

From the above equation we also find the temperature at the hotspots:

$$T_A = \sqrt{\left| \frac{3}{\pi^2} P_A \right|} = T_B. \tag{4.2.38}$$

The local temperature at the hotspot is plotted as a function of the LJ transmission coefficient t in Fig. (26). As a result of the coupling between the two LJs, the t dependence of the temperature develops an asymmetry with respect to the single LJ case, where the maximum was found at $t = 1/2$.

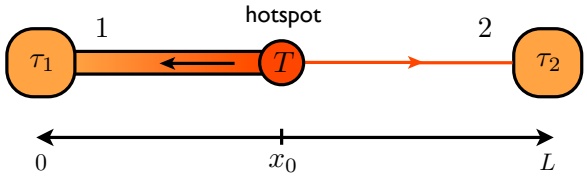

Figure 27: Heat transport in a single edge. A diffusive (1) and a ballistic (2) thermal conductors are connected to a common heat source (Hs). The temperature of the HS is due to the dissipated power P_j in the junction and is found by solving the temperature equation (4.3.9). In turn, the other sides of the conductors are connected to thermal reservoirs held at temperatures τ_i. x_0 denotes the distance between the Hs and the thermal reservoir on the diffusive side. The black arrow in the diffusive side denotes the direction of propagation of the diffusive heat current. The gradient of temperature is represented by a color gradient: red represents a higher temperature with respect to the light orange one.

4.3 HEAT CURRENTS EQUILIBRATION IN A LJ : HYDRODYNAMICAL APPROACH

In this section we consider heat currents equilibration in a mixed diffusive/ballistic conductor. This is the case when ν_b supports counter propagating edge modes and ν_c belongs to the principal sequence. We start this analysis with the following simple model: two one dimensional conductors are coupled to a common thermal source, represented by the scatterer positioned at x_0 in Fig. (27). Section "1" of the system supports two counter propagating edge modes and random impurity scattering gives rise to a diffusive heat current [86]. Section "2" of the system is a chiral conductor and disorder has no effect on the propagation of the heat current, that remains ballistic. In the electrical domain, power P_j is lost through the scatterer and "converted" into temperature "T" through Joule heating. Given P_j, which is the temperature at the scatterer (we will call this the hot spot) ? The heat currents in the two conductors are given by (here we use "J_q" for the diffusive currents and "I_q" for the ballistic ones):

$$\begin{aligned} J_{q,i} &= -K_D \partial_x T_i(x) \\ I_{q,i} &= K_H T_i, \end{aligned} \tag{4.3.1}$$

where $K_D = (\pi^2/3) l T(x) K_B^2/h$ is the thermal Hall conductivity of the diffusive system, l is the elastic mean free path set by disorder [86]. K_H is the thermal Hall conductance of the ballistic system defined in Eq. (4.1.31). In what follows we will use natural units ($K_H = h = 1$), then measuring temperature in units of energy. Heat currents are governed by Fourier's heat equation:

$$\partial_t n_q(x,t) + \partial_x J_q(x,t) = q(x,t), \tag{4.3.2}$$

where $n_q(x,t)$ is the heat density, $J_q(x,t)$ the heat current and $q(x,t)$ a heat source. Here we are interested in the steady state solution of Eq. (4.3.2). As discussed in section (4.2.3), we

consider a point like heat source, i.e. we consider a situation where the heat source is peaked at $x = x_0$. The total heat current is a discontinuous function of the space coordinates

$$J_q(x) = J_{q,1}(x)\theta(x_0 - x) + I_{q,2}\theta(x - x_0). \tag{4.3.3}$$

The steady state heat source $q(x) = P_j\delta(x - x_0)$. Equation (4.3.2) then reads:

$$\begin{aligned} \partial_x J_q(x) &= \left[\partial_x J_{q,1}(x)\right]\theta(x_0 - x) + J_{q,1}(x)\,\partial_x\theta(x_0 - x) \\ &+ \left(\partial_x I_{q,2}\right)\,\theta(x - x_0) + I_{q,2}\,\partial_x\theta(x - x_0) \\ &= P_j\delta(x - x_0). \end{aligned} \tag{4.3.4}$$

$\partial_x I_{q,2} = 0$ is by definition always satisfied. We obtain two equations:

$$\partial_x J_{q,1}(x) = 0 \qquad \text{for} \quad x < x_0, \tag{4.3.5}$$

that is true if no electrical power is dissipated in section "1" away from $x = x_0$. At the heat source we obtain

$$J_{q,1} + I_{q,2} = P_j \qquad \text{for} \quad x = x_0. \tag{4.3.6}$$

The latter equation can be solved using Eq. (4.3.1) and by defining the appropriate boundary conditions:

$$\begin{aligned} \partial_x^2 T_1^2(x) &= 0 \\ T_1^2(0) &= \tau_1^2 \\ T_1^2(x_0) &= T^2. \end{aligned} \tag{4.3.7}$$

In this way we find:

$$T_1^2(x) = \frac{x}{x_0}(T^2 - \tau_1^2) + \tau_1^2. \tag{4.3.8}$$

Using this result in Eq. (4.3.6) we finally obtain the temperature at the scatterer:

$$T^2 = \frac{(3/\pi^2)P_j + (l/2x_0)\tau_1^2}{(1 + l/2x_0)} \tag{4.3.9}$$

For an edge much longer than the mean free path l, we find: $T^2 \simeq (3/\pi^2)P_j$.

Consider now a single line junction system. In Fig. (28), the line junction of Fig. (22) is represented in the energy domain. The LJ system shares the basic feature of the simple model previously considered. We may think of the top and bottom part of the system as two connected single edges. Channel 5 connects the two heat sources and serves as a sink/source respectively for the bottom and the top section of the system. Equation (4.3.5) holds independently for the two diffusive sections of the system and we obtain the two following equations:

$$\begin{aligned} J_{q,4} + I_{q,5} &= P_j + I_{q,3} \\ J_{q,1} + I_{q,2} &= I_{q,5}. \end{aligned} \tag{4.3.10}$$

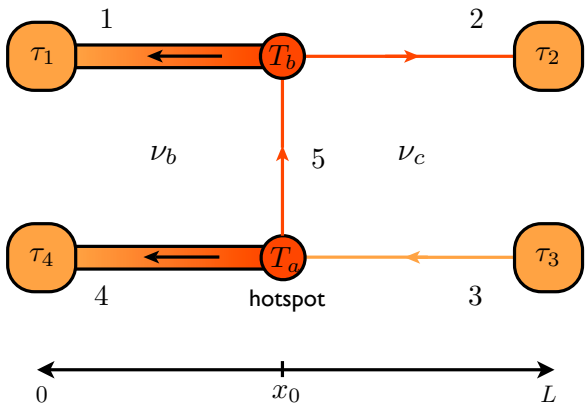

Figure 28: Heat transport in a single LJ setup. An extension of the simple model considered in Fig. (27): In this case electrical power drops at "T_a", while "T_b" gets hotter because of the heat current flowing through the LJ, here depicted by edge 5. The gradient of temperature is represented by a color gradient: red represents a higher temperature with respect to the light orange one. For an edge much longer than the mean free path l, $T_a = T_b$.

Here we consider $\tau_4 < T_a$ and $\tau_1 < T_b$. Temperatures at the scatterer can be found as we did for the single edge problem; we find:

$$T_a^2 = \frac{(3/\pi^2)P_j + \tau_3^2 + (l/2x_0)\tau_4^2}{(1 + l/2x_0)} \tag{4.3.11}$$

$$T_b^2 = \frac{(3/\pi^2)P_j + \tau_3^2 + (l/2x_0)\tau_4^2}{(1 + l/2x_0)^2} + \frac{(l/2x_0)\tau_1^2}{(1 + l/2x_0)}. \tag{4.3.12}$$

For an edge much longer than the mean free path l, we find:

$$T_a^2 = T_b^2 \simeq \frac{3}{\pi^2}P_j + \tau_3^2. \tag{4.3.13}$$

For $\tau_3 = 0$ this is in agreement with Eq. (4.2.29).

4.3.1 Heat transport in the double LJ

We now extend the analysis of heat transport to the double LJ setup depicted in Fig. (29), where ν_b supports counter propagating edge modes and ν_c a single chiral mode. We obtain the set of equations:

$$\begin{aligned} J_{q,6} + I_{q,7} &= P_{j,A} + I_{q,5} \\ J_{q,4} + I_{q,5} &= I_{q,8} \\ J_{q,3} + I_{q,8} &= P_{j,B} + I_{q,2} \\ J_{q,1} + I_{q,2} &= I_{q,7}. \end{aligned} \tag{4.3.14}$$

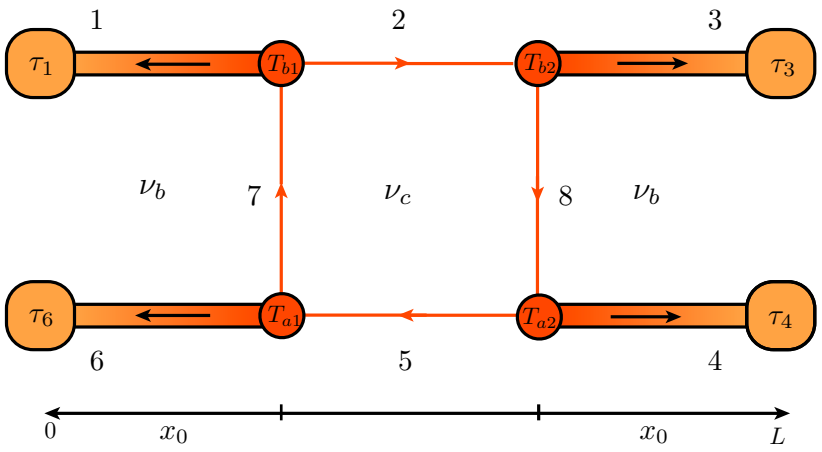

Figure 29: Heat transport in the double LJ setup. The double LJ system of Fig. (21) is here represented in the heat domain. The gradient of temperature is represented by a color gradient: red represents a higher temperature with respect to the light orange one.

from which we can find the temperatures at the links:

$$\begin{aligned} T^2_{a,1} &= \frac{(3/\pi^2)P_{j,A} + T^2_{a,2} + (l/2x_0)\tau_6^2}{(1 + l/2x_0)} \\ T^2_{a,2} &= \frac{T^2_{B,2} + (l/2x_0)\tau_4^2}{(1 + l/2x_0)} \\ T^2_{b,1} &= \frac{T^2_{A,1} + (l/2x_0)\tau_1^2}{(1 + l/2x_0)} \\ T^2_{b,2} &= \frac{(3/\pi^2)P_{j,B} + T^2_{B,1} + (l/2x_0)\tau_2^2}{(1 + l/2x_0)} \end{aligned} \tag{4.3.15}$$

In order to solve this system it is convenient to define $r = l/2x_0$ and $s = (1 + r)^{-1}$:

$$\begin{aligned} T^2_{a,1} &= \frac{1}{1 - s^4}\left\{ s\left(\frac{3}{\pi^2}P_{j,A} + r\,\tau_6^2\right) + s^3\left(\frac{3}{\pi^2}P_{j,B} + r\,\tau_2^2\right) + r\,s^2\left(\tau_4^2 + s^2\,\tau_6^2\right)\right\} \\ T^2_{b,2} &= s\left(\frac{3}{\pi^2}P_{j,B} + r\,\tau_2^2\right) + r\,s^2\tau_1^2 + s^2 T^2_{a,1}. \end{aligned} \tag{4.3.16}$$

The above expressions depend explicitly on the length of the sample, even when we consider $x_0 \gg l$. However, opposite to the case described by Nagaev [78], the space average of Eq. (4.1.5) does not trivially hold due to the "mix" nature of the system, (i.e. diffusive and ballistic). The other main difference with Nagaev's analysis is that in that case the diffusive modes were the charge ones, while in our case the charge mode propagates ballistically and it is the heat one to diffuse. The noise evaluated using Eq. (4.1.5) and Eq. (4.3.16) in the regime $x_0 \gg l$ gives a complicated expression that does not result in a universal value. One of the possible reasons of this result is that Eq. (4.1.5) does not trivially hold for this kind of system and a more detailed, microscopic analysis would be needed. For example, Nagaev's

result was originally derived using a quantum Boltzmann approach. Successively, a non-linear sigma model approach to derive the full counting statistics of diffusive conductors was developed [52]. This model could be used to derive an ab initio expression for the noise in our setup. However, such analysis is beyond the scope of this section. Another possibility is that we would need to take into account the detailed structure of the hot spot, that was here neglected in the assumption of a point-like hot-spot. Also in this case, such analysis is beyond the formalism used in this section, and it deserves further attention.

4.4 CONCLUSIONS

In this chapter we have considered the problem of heating and heat transport in QH system characterized by a low density constriction. As a result of the lower filling fraction in the constriction, interactions between counter propagating edge modes on both sides of the constriction takes place. We model the two sides of the constriction in terms of two LJs between two different filling fractions and perform a general analysis of charge current relaxation. We find a generalization of the result of [86] for the LJ conductance, Eq.(4.2.8). Using a mesoscopic analysis, we found the dissipated power and the local temperature at the two sides of the junction as a function of the LJ transmission coefficient t. For a single LJ setup, this dependence shows a maximum in the temperature for $t = 1/2$. However, for the double LJ setup, physically corresponding to the original problem, we find that the temperature dependence is modified. For both cases, we derive an expression for the effective transmission probability t_e of a fully equilibrated LJ by comparing the mesoscopic result to the hydrodynamical one. So, for an edge much longer than the mean free path l, $t \to t_e$. This can have consequences when evaluating the finite temperature shot noise. The mesoscopic approach, however, does not tell us anything about the relaxation dynamics of the heat currents. In order to address this issue we developed a hydrodynamical approach similar to the one considered in section (4.2.1). While this approach demonstrates successful for the single LJ setup, the result for the double LJ leads to a non-universal value of shot-noise.

5 SHOT NOISE SIGNATURES OF CHARGE FRACTIONALIZATION IN THE $\nu = 2$ QH EDGE

CONTENTS

5.1 OVERVIEW

In chapter (1) and appendix (A.2), (A.3) we have discussed the appearance of fractional charges in FQH states as a striking consequence of strong interactions and low dimensionality. In FQH states, the fractional charge is related to the topological properties of the state and is therefore a universal quantity. However, probing the bulk fractional charge is a challenging task and it is usually easier in mesoscopic systems to measure transport properties. A way to measure the charge of the carriers is by studying the current fluctuations due to the random tunneling at a point scatterer. In a QH system this is done by inducing scattering between the upper and the lower edge states via a QPC. The key point is that due to the bulk-edge correspondence (A.4), the edge states and the bulk share the same topological order. For this reason only particles on the edge sharing the same topological quantum numbers of the bulk can tunnel at the QPC, probing in this way the bulk topological order.

In integer QH states with multiple edge modes or in non-chiral LuL, fractionalization can appear as a consequence of the inter-edge electron-electron interaction. This means that the fractional charge will be non-universal, and it will depend on the details of the edge confining potential. Nevertheless, noise measurement in these systems can provide informations about the strongly correlated nature of these states. In the integer QH case, the

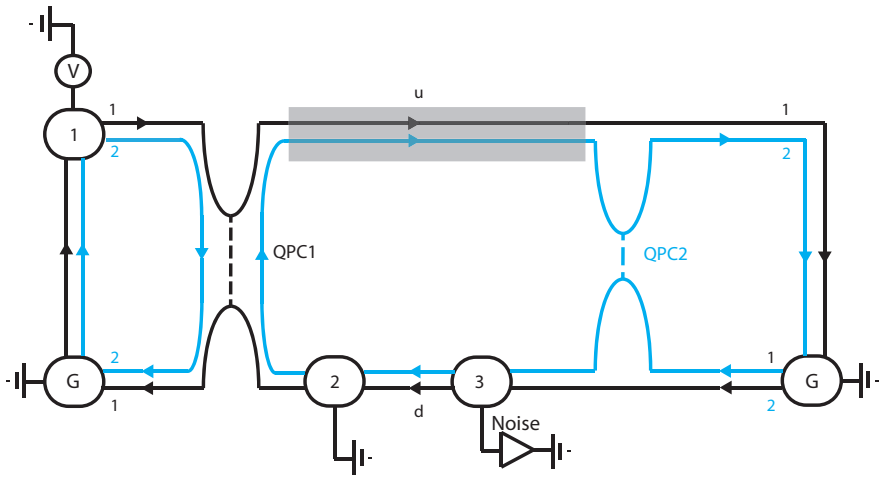

Figure 30: Sketch of a $\nu = 2$ Hall bar. The Hall bar is pinched by a QPC1, where inner modes ("2", light blue) are fully reflected, while partial transmission of outer edge modes ("1", black) is possible. At QPC2, the opposite situation is realized. The shaded area is the interaction region, where partial energy relaxation takes place. The upper edge is biased with voltage V at contact 1, current noise is measured at contact 3.

$\nu = 2$ state represents the simplest state to allow for the study of charge fractionalization. In a $\nu = 2$ QH state the Zeeman term is usually relevant and lifts the spin degeneracy. According to the hydrodynamic picture (A.4), this results in two co-propagating chiral edge modes carrying opposite spin[1] [93]. In the presence of a short range interaction between them, a pulse of charge e injected into the first edge mode decomposes into a charge pulse and a neutral pulse. The question we would like to address in this chapter is how fractional charges in the $\nu = 2$ QH state can be detected by means of a noise measurement. A related question that will be addressed in this chapter concerns the relaxation dynamics of the system due to the inter-modes interaction and how this affects the value of the fractional charge. Interactions plays in fact a crucial role in the thermalization process that drives a system through states described by the Gibbs equilibrium ensemble. Generically, the dynamics is only constrained by two integrals of motion : the total energy and the total particle number. Integrable models like the $\nu = 2$ quantum Hall edge have infinitely many integrals of motion, and therefore it is not clear if an equilibrium state can ever be reached [4, 94–97]. Consider the setup of Fig. (30) where a Hall bar supporting a $\nu = 2$ QH state is pinched by two QPCs. The outer edge mode is labeled "1" and the inner one "2". The top and bottom edges originate at zero temperature from reservoirs at voltages $V_1 = V$ and $V_2 = 0$. At QPC1, the outer modes are partially transmitted with probability a, while the inner ones are fully reflected; as a consequence, only the outer modes become noisy. After QPC1, the two edge modes interact over some distance (shaded area in Fig. (15) with length ℓ) before reaching QPC2. Here, the outer modes are fully transmitted while the inner ones are partially reflected with probability

1 Even though the two chiral edge modes carry opposite spins, in this work we will not consider explicitly the spin index since it does not play a role in the transport properties we are interested in.

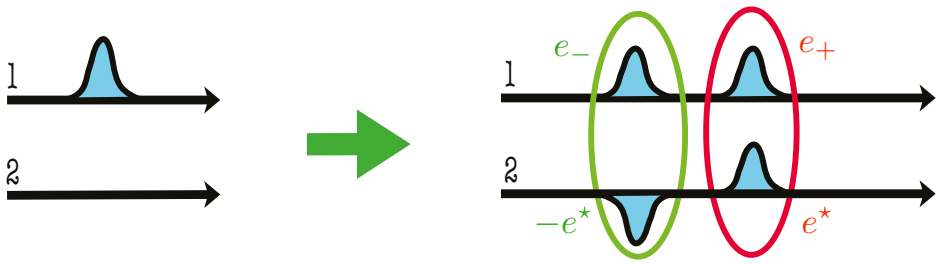

Figure 31: Charge Fractionalization in a $\nu = 2$ QH state. A charge pulse initially injected in edge mode 1 separates in a neutral (green) and charge (red) mode as a result of inter-channel interactions. The quasiparticles on edge mode 2 have charges $e^* = \sin 2\theta/2$, while the quasi particles on edge mode 1 have charges $e_\pm = e/2 \pm \sqrt{e^2/4 - (e^*)^2}$.

p. Current noise is then measured at contact 3. Using the recently developed non-equilibrium bosonization technique [6–9] within a quantum-quench model [98–100], we compute the shot noise at QPC2, with particular emphasis on its dependence on the strength of the interaction between the two edge modes. We find that the system relaxes towards a non-thermal steady state, whose distribution function determines shot noise at QPC2. The corresponding Fano factor depends on the strength of the interaction between the two edge modes, and in general neither agrees with the fractional charge e^* derived from a simple charge fractionalization model (5.2), nor with the result for two fully equilibrated edge modes. For the special case of a half open QPC1 however, the Fano factor is close to e^*/e, suggesting an interpretation in terms of charge fractionalization. Finally we would like to stress that if integrability of the $\nu = 2$ edge is broken (for example deviating from a strictly linear electron dispersion relation), the system eventually relaxes to a thermal state [101].

5.2 A SIMPLE CHARGE FRACTIONALIZATION MODEL

As a first attempt to study the problem of charge fractionalization in the $\nu = 2$ QH state we consider here a simple charge fractionalization model for the setup of Fig. (30). The two chiral edge channels co-propagate at different velocities u_1 and u_2. In the presence of a short range interaction u_{12} between them, a pulse of charge e injected into edge mode one at a first quantum point contact (QPC1) decomposes into a charge pulse and a neutral pulse as shown in Fig.(31). To see this, we make use of the low-energy description of the edge dynamics in terms of the chiral LL Hamiltonian density (if not otherwise stated, we adopt natural units $\hbar = k_B = 1$) :

$$\mathscr{H}_\eta = 2\pi \left\{ u_1 \rho_{1\eta}^2(x) + u_2 \rho_{2\eta}^2(x) + u_{12} \rho_{1\eta}(x) \rho_{2\eta}(x) \right\}, \tag{5.2.1}$$

where $\rho_{i\eta}(x)$ are density fields, "i" labels different edge modes and $\eta = R/L$ specifies the chirality; x is the space coordinate. The last term describes the density-density interaction of

the two modes, of strength u_{12}, which needs to satisfy a stability criterion $u_{12}^2 \leqslant u_1 u_2$[2]. The interacting Hamiltonian can be exactly diagonalized by means of a (canonical) Bogoliubov transformation M. For co-propagating states ($u_1 u_2 > 0$), M can be represented by the following rotation matrix in the density operator space:

$$M = \begin{pmatrix} \cos\theta & \sin\theta \\ -\sin\theta & \cos\theta \end{pmatrix} \tag{5.2.2}$$

This leads to a new Hamiltonian expressed in terms of the new (rotated) fields

$$\tilde{\mathscr{H}} = 2\pi \left\{ \tilde{u}_1 \tilde{\rho}_{1\eta}(x) + \tilde{u}_2 \tilde{\rho}_2(x) \right\}, \tag{5.2.3}$$

where the $\tilde{\rho}$ are related to the original ρ density fields by $\tilde{\rho}_i = \sum_j M_{ij}\rho_j$ and the new velocities depend on the old ones by :

$$\begin{aligned} \tilde{u}_1 &= u_1 \cos^2\theta + u_2 \sin^2\theta + \frac{1}{2} u_{12} \sin 2\theta \\ \tilde{u}_2 &= u_1 \sin^2\theta + u_2 \cos^2\theta - \frac{1}{2} u_{12} \sin 2\theta \end{aligned} \tag{5.2.4}$$

The mixing angle "θ" expresses the strength of the interaction through the relation $\tan 2\theta = u_{12}/(u_1 - u_2)$. After the charge and neutral pulses $(\tilde{\rho}_1, \tilde{\rho}_2)$ have separated due to their different velocities, the fractionalized charge can be obtained from undoing the Bogoliubov transformation using M^{-1}. In the charge pulse we find

$$\begin{pmatrix} \rho_{1,c} \\ \rho_{2,n} \end{pmatrix} = \begin{pmatrix} \cos\theta & -\sin\theta \\ \sin\theta & \cos\theta \end{pmatrix} \begin{pmatrix} \tilde{\rho}_1 \\ 0 \end{pmatrix} = \begin{pmatrix} \cos^2\theta\, \rho_1 + \cos\theta \sin\theta\, \rho_2 \\ \cos\theta \sin\theta\, \rho_1 + \sin^2\theta\, \rho_2 \end{pmatrix}. \tag{5.2.5}$$

Integrating the charge density over the space domain and using the relation between density fields and bosonic phase fields $\rho_{i\eta}(x) = \partial_x \phi_{i\eta}(x)/2\pi$, we find that in the charge pulse, a charge $e^* = e \sin 2\theta/2$ travels on mode two and $e_+ = e/2 + \sqrt{e^2/4 - (e^*)^2}$ on mode one[3]. Following same reasoning, we find that in the neutral pulse, there is a charge $-e^*$ on mode two and a charge $e_- = e/2 - \sqrt{e^2/4 - (e^*)^2}$ on mode one.

As a next step, we would like to use the above charge fractionalization model to derive an expression for the current noise at QPC2 due to quasi-particle tunneling. As a preliminary analysis we can use a simple semiclassical argument that we are now going to describe. As shown in Fig. (31), edge mode 2u contains both $\pm e^*$ charges that we will consider as well spatially separated. Moreover, we assume that tunneling at both QPCs is governed by Poisson statistics . Let us focus first on the e^* charge arriving at QPC2 and call the related impinging current I_{im}. Next we call I_3 the measured current at contact 3; note that this is an electron current since it is measured at the metallic contact. The impinging and the measured currents are simply related via the reflection probability as $I_3 = p\, I_{im}$. The two currents can

2 This follows from the physical requirement of positive energy.

3 To obtain the result in this form we have used standard trigonometric identities $\sin\theta\cos\theta = \sin 2\theta/2$ and $\cos^2\theta = (1 + \cos 2\theta)/2$

be generally expressed in terms of the average particle number passing through areference point in a time interval Δt as :

$$\begin{aligned} I_{im} &= e^* \frac{\langle N_{2u,e^*} \rangle}{\Delta t} \\ I_3 &= e \frac{\langle N_{2d,e} \rangle}{\Delta t}. \end{aligned} \tag{5.2.6}$$

Note that here $\langle O(t) \rangle$ means a time average of the observable. Using the relation between the measured and the impinging current we find

$$\langle N_{2d,e} \rangle = \left(p \frac{e^*}{e} \right) \langle N_{2u,e^*} \rangle. \tag{5.2.7}$$

This relation can be understood in terms of a renormalization of the probability $p \to p\, e^*/e$ for tunneling a e particle into the lower edge given an impinging e^* particle at QPC2. As a next step, we need to know the average number of particles having charge e^*. Consider again the schematic of Fig. (31), for every electron with charge e added to edge mode 1 a charge e^* is created at later time on edge mode 2. This means $\langle N_{2u,e^*} \rangle = \langle N_{1u,e} \rangle$, where the latter is the average number of electrons added to the first edge mode. Since the average number of electrons added to edge mode 1 after QPC1 is proportional to the transmitted current at QPC1, we find

$$I_{1u} = e \frac{\langle N_{1u,e} \rangle}{\Delta t} = a \frac{e^2}{h} V \Rightarrow \langle N_{1u,e} \rangle = a \frac{eV}{h} \Delta t. \tag{5.2.8}$$

Using the statistical definition of the low-frequency current noise together with Eq. (5.2.7) and (5.2.8) we can now find the fractionalization noise

$$\begin{aligned} S_{frac}(\omega \to 0) &= 2e^2 \frac{\langle N_{2d,e}^2 \rangle - \langle N_{2d,e} \rangle^2}{\Delta t} = 2e^2 \frac{\langle N_{2d,e} \rangle}{\Delta t} \\ &= 2p \frac{e}{\Delta t} e^* \langle N_{2u,e^*} \rangle = 2e^* a\, p \left(\frac{e^2}{h} \right) V \\ &= 2e^* a\, p\, I, \end{aligned} \tag{5.2.9}$$

where in the second equality of the first line we have used the assumption that the process is governed by Poisson statistics. We can repeat the same argument for the $-e^*$ charge pulse and find that also in this case the reflection probability at QPC2 is renormalized to $p\, e^*/e$ and gives a contribution to $S(\omega \to 0)$ exactly equal to Eq. (5.2.9). This means that the measured noise will be

$$S_{frac}(\omega \to 0) = 4e^* a\, p\, I. \tag{5.2.10}$$

The Fano factor is now easily evaluated taking the ratio between the Poissonian noise due to fractional charges and a reference noise of Poissonian, integer $\pm e$ charges equal to Eq. (5.2.10) with e^* replaced by e (in section 5.5.1 we will derive an expression for the reference noise in a more general way)

$$F = \frac{S_{frac}(\omega \to 0)}{S_{pois}(\omega \to 0)} = \frac{e^*}{e}. \tag{5.2.11}$$

Even though the above argument is appealing due to its simplicity, it is based on a semiclassical argument and effects due to Fermi statistics are not considered[4]. Neither are considered possible relaxation effects due to the initial non-equilibrium nature of the state and the strong inter-modes interaction. As we will show using our non-equilibrium model, relaxation (even though not towards an equilibrium state) alter the value of the Fano factor and therefore of the fractional charge measured at QPC2. In the next section we will discuss a scheme to drive the system out of equilibrium by turning the interactions in the system suddenly on after QPC1.

5.3 THERMAL QUANTUM QUENCH

The bosonized Hamiltonian (5.2.1) describing the electrons inside the Quantum Hall device contains a density-density interaction term. However, electrons inside the contacts are described in terms of free electrons at equilibrium at some chemical potential. Let us call the free Hamiltonian describing the electrons in the contacts $\mathscr{H}_0$. We need a "protocol" to switch on the interaction when the electrons enter the system, i.e.

$$\mathscr{H}_0 \xrightarrow{P} \mathscr{H} \tag{5.3.1}$$

where P is a unitary operator. For example, the familiar adiabatic protocol slowly turns on interactions in the system, lets the system interact and then it switch off the interactions at the end of the evolution. The success of this protocol is guaranteed by the Gell-Mann and Low Theorem [102]. Out of equilibrium this theorem is still valid, provided we choose as a time-path the Keldysh time-loop contour. Another possible protocol is the so called "quantum quench" [100]. Here the interactions are suddenly turned on in the system, leading to a full non-equilibrium situation. A class of these problems consists in instantaneously changing some parameters of the Hamiltonian of an isolated quantum system. Then, one has to study the time evolution of the ground state of the Hamiltonian before the quench under the influence of the Hamiltonian after the quench. In the context of the Tomonaga-Luttinger model, it has been shown [98, 99] that this protocol can be implemented in such a way that an exact solution of the full interacting problem is still possible. In the first step, P turns on the interaction at some time $t > 0$ by changing the coupling constant u_{12} from zero to a finite value and the velocity u to u_1 and u_2 for the outer and inner edge mode. The full interacting problem can now be diagonalized by means of a (canonical) Bogoliubov transformation M. For co-propagating states ($u_1 u_2 > 0$), M is given by Eq. (5.2.2). We start by expressing the edge state Hamiltonian density (5.2.2) in momentum space and use the mode decomposition of the density fields (2.1.16) to express everything in terms of bosonic ladder operators

$$H = \sum_{q>0} \left\{ q\, u_1\, b^\dagger_{1,q} b_{1,q} + q\, u_{2,q}\, b^\dagger_{2,q} b_{2,q} + \frac{q\, u_{12}}{2} \left(b^\dagger_{1,q} b_{2,q} + b_{1,q} b^\dagger_{2,q} \right) \right\}. \tag{5.3.2}$$

4 Quantum shot noise will be proportional to $a(1-a)$ due to Pauli blocking. See also the discussion in (B.3).

Performing the Bogoliubov transformation, we arrive at a new Hamiltonian expressed in terms of new (rotated) fields

$$\tilde{H} = \sum_{q>0} \left\{ q\tilde{u}_1 \beta^\dagger_{1,q}(t)\beta_{1,q}(t) + q\tilde{u}_{2,q}\beta^\dagger_{2,q}(t)\beta_{2,q}(t) \right\}, \tag{5.3.3}$$

where the βs are related to the original b operators by $\beta_{i,q} = \sum_j M_{ij} b_{j,q}$ and the relation between new and old velocities is the same as in Eq. (5.2.4). The mixing angle "θ" expresses the strength of the interaction through the relation $\tan 2\theta = u_{12}/(u_1 - u_2)$. At this point, the rotated operators evolve in the Heisenberg picture under the action of $\tilde{\mathscr{H}}$,

$$\beta_{iq}(t) = e^{-\imath q \tilde{u}_i t}\beta_{iq}(t=0). \tag{5.3.4}$$

Finally we need to undo the Bogoliubov transformation in order to express the $\beta_{iq}(t=0)$ in terms of the original operators. As a result of this chain of operations it is possible to obtain a relation between the bosonic operators at $t > 0$ and those at $t = 0$:

$$\begin{aligned} b_{1q}(t) &= u_q(t) b_{1q} + s_q(t) b_{2q} \\ b_{2q}(t) &= s_q(t) b_{1q} + v_q(t) b_{2q} \end{aligned} \tag{5.3.5}$$

where $b_{iq} \equiv b_{iq}(t=0)$. Now all the time dependence is encoded in the coefficients

$$\begin{aligned} u_q(t) &= \cos^2\theta e^{-\imath q\tilde{u}_1 t} + \sin^2\theta e^{-\imath q\tilde{u}_2 t} \\ v_q(t) &= \cos^2\theta e^{-\imath q\tilde{u}_2 t} + \sin^2\theta e^{-\imath q\tilde{u}_1 t} \\ s_q(t) &= \frac{\gamma_\theta}{2}\left(e^{-\imath q\tilde{u}_1 t} - e^{-\imath q\tilde{u}_2 t}\right), \end{aligned} \tag{5.3.6}$$

where $\gamma_\theta = \sin 2\theta$. Relations (5.3.5) and (5.3.6) allow us to compute any expectation values of operators in the grand canonical ensemble defined by $\mathscr{H}_0$.

5.3.1 Fermionic Propagator

As an application of the quantum quench model developed above, we can compute the equal time fermionic propagator in the absence of the QPC for the right moving inner edge mode 2 :

$$C_{\psi_2}(x) = \mathrm{Tr}\left\{ \hat{\rho}\psi_2^\dagger(x,t)\psi_2(0,t) \right\} \tag{5.3.7}$$

where $\hat{\rho} = Z^{-1}e^{-\beta\mathscr{H}_0}$ is the equilibrium density matrix of the electrons in the contacts (before interactions are turned on). Using the vertex representation of the femionic fields (2.1.37) at zero chemical potential [5]

$$C_{\psi_2}(x) = e^{[\phi_2(x,t),\phi_2(0,t)]/2}\mathrm{Tr}\left\{ \hat{\rho}e^{-\imath[\phi_2(x,t)-\phi_2(0,t)]} \right\}, \tag{5.3.8}$$

5 The above argument is trivially generalized to a finite chemical potential, that enters as a global phase factor in (5.3.8)

where we have used the Baker-Haussdorf formula. Using the mode expansion (2.1.16) for the phase fields and Eq. (5.3.5) in order to take into account interactions, we correctly find that since the Bogoliubov transformation is canonical, all the commutation relations are left unchanged. More explicitly :

$$\begin{aligned}
[\varphi_2^\dagger(x,t),\varphi_2(0,t)] &= \sum_{q>0}\frac{2\pi}{qL}e^{-q\alpha}e^{-\imath qx}[b_{2q}^\dagger(t),b_{2q}(t)] \\
&= \sum_{q>0}\frac{2\pi}{qL}e^{-q\alpha}e^{-\imath qx}\Big\{|s_q(t)|^2[b_{1q}^\dagger(t),b_{1q}(t)] \\
&+ |\nu_q(t)|^2[b_{2q}^\dagger(t),b_{2q}(t)]\Big\} \\
&= -\sum_{q>0}\frac{2\pi}{qL}e^{-q\alpha}e^{-\imath qx} = \log(1-e^{-\imath 2\pi(x+\imath\alpha)/L}).
\end{aligned} \tag{5.3.9}$$

where we have used $|s_q(t)|^2+|\nu_q(t)|^2 = 1$ and summed over discrete momentum $q = 2\pi n/L$ ($n \in \mathbb{Z}^+$). Summing Eq. (5.3.9) and its complex conjugate, we get in the continuum limit the standard expression :

$$[\phi_2(x,t),\phi_2(0,t)] = \log\left(\frac{\imath x+\alpha}{-\imath x+\alpha}\right) \tag{5.3.10}$$

We are then left with evaluating the trace of the vertex operators. Since in equilibrium the theory is Gaussian (see 2.2), we can use the standard formula :

$$\mathrm{Tr}\left\{\hat{\rho}e^{-\imath(\phi_2(x,t)-\phi_2(0,t)}\right\} = e^{-\frac{1}{2}\mathrm{Tr}\{\hat{\rho}[\phi_2(x,t)-\phi(0,t)]^2\}}. \tag{5.3.11}$$

The expectation value at the exponent can be computed using again (2.1.16) and (5.3.5) :

$$\begin{aligned}
-\frac{1}{2}\mathrm{Tr}\left\{\hat{\rho}\,[\phi_2(x,t)-\phi_2(0,t)]^2\right\} &= -\sum_{q>0}\frac{2\pi}{qL}e^{-q\alpha}(1-\cos qx) \\
&\times\left(|s_q(t)|^2(\,1+2n_1(\epsilon_q)\,)+|\nu_q(t)|^2(\,1+2n_2(\epsilon_q)\,)\right),
\end{aligned} \tag{5.3.12}$$

where $n_i(\epsilon_q)$ are bosonic distribution functions. Since the two edge modes are at equilibrium at zero temperature, they have the same bosonic distribution functions $n_1(\epsilon_q) = n_2(\epsilon_q)$ and so the interaction does not influence the propagator, and we are left with the non-interacting result. For example, at $T = 0$ we find the standard result (2.1.45)

$$C_{\psi_2}(x) = \frac{\imath}{2\pi}\frac{1}{(x+\imath\alpha)}. \tag{5.3.13}$$

Two comments are necessary here. First, we note that if we had to compute the equal space Green function instead of the equal time, even at equilibrium we would have found that the bare velocities of the two edge modes are renormalized to the ones defined in Eq. (5.2.4). In addition we would have found (at $T = 0$):

$$G_0^<(\tau) = \frac{1}{2\pi}\frac{1}{(-\imath\tilde{u}_1\tau+\alpha)^{\sin^2\theta}}\frac{1}{(-\imath\tilde{u}_2\tau+\alpha)^{\cos^2\theta}}, \tag{5.3.14}$$

where τ is the time variable. However, when computing the Fourier transform to energy space of the above (lesser) Green function we find :

$$G_0^<(\epsilon) = \frac{1}{\tilde{u}_1^{\sin^2\theta}\tilde{u}_2^{\cos^2\theta}}\theta(-\epsilon), \tag{5.3.15}$$

showing how interactions only affect the spectral function but not the electron distribution function. Furthermore, we note that choosing $n_1(\epsilon_q)$ and $n_2(\epsilon_q)$ in Eq. (5.3.12) to be equilibrium Bose distributions held at finite, but different temperatures, would have resulted in a "partial non-equilibrium" situation[6].

5.4 NON-EQUILIBRIUM BOSONIZATION

From Eq. (5.3.12) it is clear that as soon as edge modes 1 and 2 have different distributions, the interactions will affect the fermionic propagator. In this section, we will see how the first QPC in Fig. (15) will drive edge mode 1 out of equilibrium and therefore makes the propagator (5.3.7) interaction dependent. Let us focus our attention for the moment on edge mode 1 at the first QPC in the absence of interactions. The electrons coming out of contacts 1 and 2 have occupation numbers distributed according to an equilibrium Fermi distribution at chemical potential μ_1 and μ_2 respectively[7]. The QPC induces scattering between the top and bottom edges, partitioning in this way the current carrying states. In the scattering approach to transport in mesoscopic systems, incoming and outgoing electron states at the QPC are related by a scattering matrix $\hat{S}$ that generates a unitary evolution between $|in\rangle$ and $|out\rangle$ states. We take as a scattering matrix

$$\hat{S} = \begin{pmatrix} t & r \\ r & t \end{pmatrix} \tag{5.4.1}$$

where we have assumed the QPC to induce a symmetric potential barrier such that the quantum mechanical amplitudes for a state being transmitted (t) or reflected (r) is the same for the top and bottom edge. Moreover, the assumption that the scattering amplitudes are energy independent, and thus scattering is instantaneous, is equivalent to replacing a potential barrier having a finite width ($V(x)$) with one having $V(x) = V_0\delta(x)$. From the unitary condition $SS^\dagger = S^\dagger S = 1$ it follows :

$$\begin{aligned} |t|^2 + |r|^2 &= 1 \\ t^\star r + r^\star t &= 0. \end{aligned} \tag{5.4.2}$$

Defining $a = |t|^2$ as the transmission probability, the first condition of (5.4.2) simply expresses the conservation of probability $|r|^2 = 1 - a$ (and therefore charge conservation). In the sec-

6 Here by partial non-equilibrium we mean a situation where different subsystems are kept at different chemical potentials and/or temperatures, but each of them is defined by an equilibrium distribution

7 Even though in Fig. (30) $\mu_2 = 0$, in this section we derive a more general result valid for $\mu_2 \neq 0$. We will specialize to the $\mu_2 = 0$ case when computing the shot noise power for the actual setup depicted in Fig. (30).

ond quantization formalism we introduce creation and annihilation fermionic operators c_i, obeying canonical anti-commutation relation :

$$\{c_{i,k}, c^{\dagger}{}_{j,k'}\} = \delta_{i,j}\delta_{k,k'} \ , \ \{c_{i,k}, c_{j,k'}\} = \{c^{\dagger}_{i,k}, c^{\dagger}_{j,k'}\} = 0. \tag{5.4.3}$$

Then, according to (5.4.1) we have the following relation between incoming and outgoing states :

$$\begin{pmatrix} \tilde{c}_{1u,k} \\ \tilde{c}_{1d,k} \end{pmatrix} = \hat{S} \begin{pmatrix} c_{1u,k} \\ c_{2d,k} \end{pmatrix} \tag{5.4.4}$$

where the suffix 1u and 1d labels operators acting after the QPC respectively on the top and the bottom edge. The related particle number operator on the top edge is $\tilde{N}_{1u} = \tilde{c}^{\dagger}_{1u}\tilde{c}_{1u}$. Using (5.4.4) and its complex conjugate we find :

$$\tilde{N}_{1u,k} = a\, c^{\dagger}_{1u,k}c_{1u,k} + (1-a)\, c^{\dagger}_{1d,k}c_{1d,k} + t^{\star}r\, c^{\dagger}_{1u,k}c_{1d,k} + r^{\star}t\, c^{\dagger}_{1d,k}c_{1u,k}. \tag{5.4.5}$$

5.4.1 Steady State density matrix

According to the Landauer picture, biasing a mesoscopic system means that we let the particle number in the top and in the bottom edge fluctuates by injecting and absorbing charge carriers at the contacts. The contacts serve as electron reservoirs and are held at chemical potential μ_1 for the upper edge and at chemical potential μ_2 for the lower edge. Assuming ideal contacts, we can describe non-interacting electrons in the edge channels as being in a equilibrium state described by a grand-canonical density matrix :

$$\begin{aligned} \hat{\rho} &= Z^{-1} e^{\sum_i \lambda_i A_i} \\ Z &= \mathrm{Tr}\left\{ e^{\sum_i \lambda_i A_i} \right\}, \end{aligned} \tag{5.4.6}$$

where $\langle A_i \rangle$ is the complete set of constant of motions of the system. In the case of the Gibbs grand-canonical ensemble, these correspond to the average energy $E_i = \langle \hat{H}_i \rangle$ and the average particle number $\langle \hat{N}_i \rangle$. Without the QPC, the total density matrix of the system (assuming the two reservoirs to be independent) is given by the tensor product of the density matrices of the single subsystems : $\hat{\rho} = \hat{\rho}_1 \otimes \hat{\rho}_2$. We can see this explicitly as follows : the trace involving the total density matrix is taken over the joint Hilbert space $H = H_1 \oplus H_2$. If $|m_1\rangle \in H_1$ and $|m_2\rangle \in H_2$ are two orthonormal basis vectors in their respective Hilbert spaces, then a basis $|m\rangle \in H$ is given by $|m\rangle = |m_1\rangle \otimes |m_2\rangle \equiv |m_1, m_2\rangle$. Therefore the trace is a sum over $\{|m_1, m_2\rangle\}$. However, $\hat{H}_i$ and $\hat{N}_i$ only act on their respective subspaces, from which the factorization of the total density matrix follows.

Since total particle number is a conserved quantity, the QPC will not induce any change in the measured total current (for elastic or quasi elastic scattering at low energy), but it will induce excess noise (with respect to the pure thermal one). This means that there is no additional current flowing after the QPC and the conserved quantities are total energy

and total particle number; the elastic impurity just mixes the left and right movers and change (in case of reflection) the sign of their respective momentum (momentum is not individually conserved). Since this mixing will change the local chemical potential after the QPC, the particle number in each edge is not anymore individually conserved. All these considerations can be used to derive the density matrix following the maximum entropy approach [103], from which Eq. (5.4.6) has been obtained. To find the value of the Lagrange multiplier corresponding to the particle number operator $\hat{N}_i$ (i=1u,1d) we need to remind ourselves that λ_i is proportional to the (generalized) force needed to change the particle number in the system. This generalized force is given by the difference between the chemical potential μ_1 (or μ_2) and the local chemical potential after the QPC ($\tilde{\mu}$). The Gibbs entropy is therefore given by :

$$\begin{aligned} S &= -k_B \tilde{\rho}_1 \log \tilde{\rho}_1 - \lambda_1[E_T - Tr(\tilde{\rho}_1 H_T)] - \lambda_2[\langle N_{1u}\rangle - Tr(\tilde{\rho}_1 N_{1u})] - \lambda_3[\langle N_{2d}\rangle \\ &- Tr(\tilde{\rho}_1 N_{2d})] - \lambda_0[Tr\tilde{\rho}_1 - 1], \end{aligned} \tag{5.4.7}$$

where the first term is the statistical entropy, the second term enforces total energy conservation, the third and the forth one express particle number conservation in the individual channels, and the last term enforces the normalization of probability. By varying $\delta S/\delta\tilde{\rho}_1 = 0$ and identifying the Lagrange multipliers $\lambda_1 = -\beta$ ($\beta = 1/k_B T$), $\lambda_2 = \beta(\mu_1 - \tilde{\mu})$, $\lambda_3 = \beta(\mu_2 - \tilde{\mu})$ and $\lambda_0 = 1$ we find :

$$\tilde{\rho}_1 = \tilde{Z}^{-1} e^{-\beta(H_{1u}+H_{1d}-(\mu_1-\tilde{\mu})N_{1u}-(\mu_2-\tilde{\mu})N_{1d})}. \tag{5.4.8}$$

A convenient way to fix the value of $\tilde{\mu}$ is by demanding that in a stationary state, no additional net flow of particles should be present after the QPC[8]. Since we are interested in what happens on the top edge after the QPC, we impose that $\langle\delta\tilde{N}\rangle = 0$. This constraint fixes the value of the local chemical potential :

$$\tilde{\mu} = a\mu_1 + (1-a)\mu_2. \tag{5.4.9}$$

The final expression for the density matrix is then :

$$\tilde{\rho}_1 = Z_{1u}^{-1} e^{-\beta(\epsilon-(1-a)\Delta\mu)N_{1u}} Z_{1d}^{-1} e^{-\beta(\epsilon+a\Delta\mu)N_{1d}}. \tag{5.4.10}$$

The above density matrix, by construction, gives $\tilde{I} = 0$ for the current related to $\delta\tilde{N}$, so that the total current in the system is conserved. This can be explicitly seen by taking the trace of (5.4.5) with (5.4.10), that gives a "double step" distribution function (see Fig.32):

$$\begin{aligned} f_D(\epsilon) &= a\, f_{1u}(\epsilon) + (1-a)\, f_{1d}(\epsilon) \\ f_{1u}(\epsilon) &= 1/(e^{\beta(\epsilon-\tilde{\mu}_1)}+1) \\ f_{1d}(\epsilon) &= 1/(e^{\beta(\epsilon-\tilde{\mu}_2)}+1), \end{aligned} \tag{5.4.11}$$

where we have defined $\tilde{\mu}_1 = (1-a)\Delta\mu$ and $\tilde{\mu}_2 = -a\Delta\mu$.

8 Stated otherwise, we use as a normalization the equilibrium density matrix ρ_0.

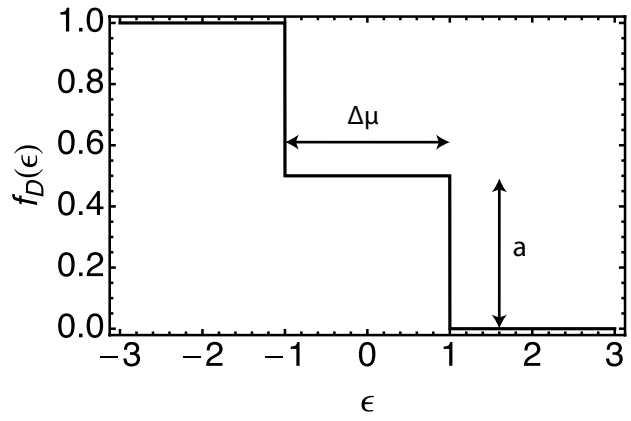

Figure 32: Fermionic distribution with double step singularities. The width of the step is set by the bias, while the height by the "transparency" a of the QPC.

5.4.2 Non-equilibium bosonic distribution

We are now able to compute the non-equilibrium bosonic distribution directly after QPC1, by simply taking $N(\epsilon_q) = \langle \tilde{b}_q^\dagger \tilde{b}_q \rangle$ [9]. After refermionizing the bosonic ladder operators using the identity (2.1.11) and the scattering matrix in order to connect incoming and outgoing states at QPC1, we are left with the evaluation of the following expectation values :

$$\begin{aligned} N(\epsilon_q) &= \frac{2\pi}{qL}\sum_{k,p=-\infty}^{\infty}\Big\{a^2\langle c^\dagger_{1u,k-q}c_{1u,k}c^\dagger_{1u,p+q}c_{1u,p}\rangle + (1-a)^2\langle c^\dagger_{1d,k-q}c_{1d,k}c^\dagger_{1d,p+q}c_{1d,k}\rangle \\ &+ a(1-a)\left(\langle c^\dagger_{1u,k-q}c_{1d,k}c^\dagger_{1d,p+q}c_{1u,p}\rangle + \langle c^\dagger_{1d,k-q}c_{1u,k}c^\dagger_{1u,p+q}c_{1d,p}\rangle\right)\Big\} \\ &= \frac{2\pi}{qL}\sum_{k=-\infty}^{\infty}\Big\{a^2 f_{1u}(\epsilon_k)(1-f_{1u}(\epsilon_k+\epsilon_q)) + (1-a)^2 f_{1d}(\epsilon_k)(1-f_{1d}(\epsilon_k+\epsilon_q)) \\ &+ a(1-a)\left[f_{1u}(\epsilon_k)(1-f_{1d}(\epsilon_k+\epsilon_q)) + f_{1d}(\epsilon_k)(1-f_{1u}(\epsilon_k+\epsilon_q))\right]\Big\}, \end{aligned} \tag{5.4.12}$$

where $f_{1u/d}(\epsilon_k)$ have been defined in (5.4.11). We see that the final expression resembles a noise term, due to the fact that the quantum channels are not anymore pure (thermodynamic) states. Moving to the continuum limit, we exchange the sum over electron momentum "k" with an integral and arrive at the final expression for the non-equilibrium distribution of the bosons after QPC1 :

$$N(\omega) = (a^2+(1-a)^2)n(\epsilon_q) + a(1-a)\left\{\left(1+\frac{\Delta\mu}{\epsilon_q}\right)n(\epsilon_q+\Delta\mu) + \left(1-\frac{\Delta\mu}{\epsilon_q}\right)n(\epsilon_q-\Delta\mu)\right\}, \tag{5.4.13}$$

This distribution is a sum of grand canonical bosonic distributions multiplied by combinations of the chemical potential difference and the transmission probability at QPC1. Everywhere in the above derivation we have considered all the contacts held at the same temperature. This distribution has been found using a Keldysh approach in [6] and we discuss

9 for notational simplicity we will equivalently use $\langle O \rangle \equiv \mathrm{Tr}(\hat{\rho} O)$

this more general derivation in appendix (B.2). In the $T \to 0$ limit, the non-equilibrium distribution reduces to :

$$N(\omega) = a(1-a)\left\{\left(\frac{\Delta\mu}{\epsilon_q} - 1\right)\theta(-\epsilon_q + \Delta\mu) - \left(\frac{\Delta\mu}{\epsilon_q} + 1\right)\theta(-\epsilon_q - \Delta\mu)\right\}. \tag{5.4.14}$$

5.4.3 Energy density conservation and effective temperature

As a check of the validity of Eq. (5.4.13) and (5.4.14), we verify that the energy density computed with the latter agrees with the one computed using the fermionic double step distribution (5.4.11). With no loss of generality, we compute here the $T \to 0$ limit of both distributions and take $\Delta\mu > 0$. In the fermionic case we find :

$$E_F = \int_{-\infty}^{\infty} \frac{d\epsilon_k}{\hbar u_1} \epsilon_k \left[f_D(\epsilon_k) - f_{0D}(\epsilon_k)\right] \xrightarrow{T\to 0} \frac{\Delta\mu^2}{2\hbar u_1} a(1-a), \tag{5.4.15}$$

where $f_{0D}(\epsilon_k)$ is the ground state Fermi distribution. Using the bosonic distribution (5.4.14) we find :

$$E_B = \int_0^{\infty} \frac{d\epsilon_q}{\hbar u_1} \epsilon_q N(\epsilon_q) \xrightarrow{T\to 0} \frac{\Delta\mu^2}{2\hbar u_1} a(1-a) \tag{5.4.16}$$

Finally, we can derive the effective temperature of the bosons after the QPC. In order to find the effective temperature, we consider a system of bosons at equilibrium and compute their energy density:

$$E_{B,eq} = \int_0^{\infty} \frac{d\epsilon_q}{\hbar u_1} \epsilon_q \, n(\epsilon_q) = \frac{(\pi k_B T)^2}{6\hbar u_1}, \tag{5.4.17}$$

where T_b is the "bosonic temperature" [10]. We can define the effective bosonic temperature by equating the latter expression and Eq. (5.4.16) :

$$T^* = \frac{\sqrt{3}}{\pi k_B} \Delta\mu \sqrt{a(1-a)}, \tag{5.4.18}$$

which depends on the chemical potential difference and the "shot noise prefactor" $a(1-a)$. In Fig. (33) we compare the zero temperature, non-equilibrium bosonic distribution (5.4.14) and an equilibrium one taken at the same effective temperature (5.4.18). We see that the two distributions, although having the same asymptotic behavior, differ for intermediate energy values. It is interesting to note that the discrepancy between the two distribution functions increases as the transmission coefficient is lowered.

5.4.4 Time evolution of the Fermi distribution function

In the previous sections we have derived the non-equilibrium distribution function of free bosons and compared it to an effective equilibrium distribution having the same energy density. As a next step, in this section we use the non-equilibrium bosonic distribution in order

10 The general expression for this type of integrals is : $F_n = \int_0^{\infty} dx \frac{x^n}{e^x - 1} = \Gamma(n+1)\xi(n+1)$, where $\Gamma(n)$ is the Euler gamma function and $\xi(n)$ is the Riemann zeta function.

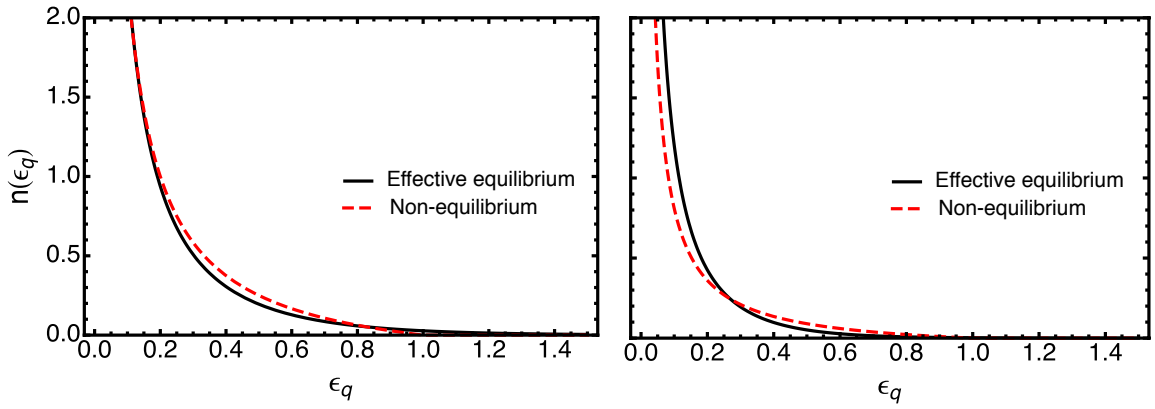

Figure 33: Bosonic distributions. Comparison between the non-equilibrium bosonic distribution Eq. (5.4.14) and an equilibrium distribution computed at the same effective temperature (5.4.18). (Left) Transparency $a = 0.5$. (Right) Transparency $a = 0.1$.

to compute the fermionic distribution function after a quantum quench. This section can be considered an extension of the original work of Iucci and Cazalilla [99], where they have investigated the evolution of the fermionic distribution function after a QQ, for a standard Luttinger liquid having an initial thermal distribution (i.e. before the QQ).

We start this analysis by employing a Gaussian approximation; even though this approximation is quantitatively incorrect (see 2.2), it gives nevertheless some useful informations on the relaxation dynamics of the system. In section 5.3.1, we have considered the equal time fermionic propagator $C_{\psi_2}(x)$ after a QQ. There, we found that due to the co-propagating nature of the two states, the QQ does not change the form of the propagator if the two edge modes are in equilibrium one with respect to the other. Here we consider instead a situation where edge mode one is described by the non-equilibrium distribution function of Eq. (5.4.14), while edge mode two is held at zero temperature. From Eq. (5.3.8) and (5.3.12) we have

$$C_{\psi_2}(x,t) \simeq \frac{\iota}{2\pi}\frac{1}{(x+\iota\alpha)}e^{-I(x,t)}. \tag{5.4.19}$$

The (time dependent) propagator factorizes into a non-interacting, time dependent part and a factor containing all the informations about non-equilibrium and interactions. The time dependent factor $I(x,t)$ can be explicitly found using equations (5.3.6), (5.3.12) and (5.4.14)

$$I(x,t) = \gamma_\theta^2 a(1-a)\int_0^Q \frac{dq}{q}\,(1-\cos(q\,x))\,(1-\cos(q\Delta\tilde{u}t))\left(\frac{Q}{q}-1\right). \tag{5.4.20}$$

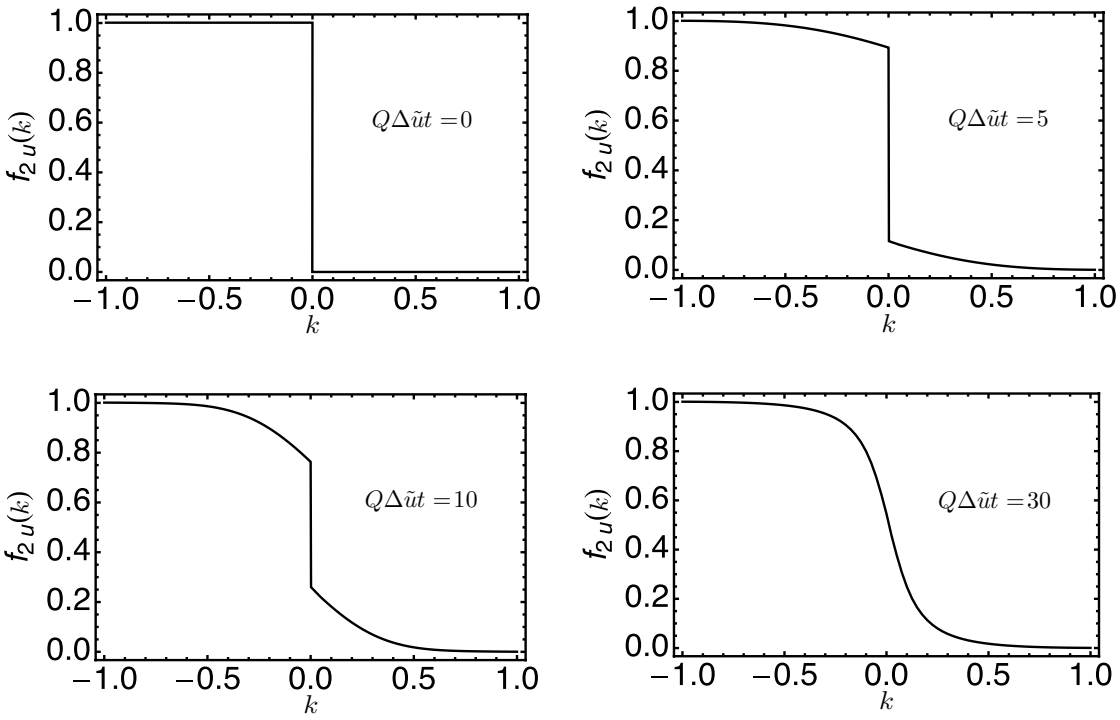

Figure 34: Time evolution of the distribution function after the QQ. The momentum distribution function develops from an initial step function into an effectively "thermal" distribution. The distribution function is here evaluated for $\theta = 0.45$ and $a = 1/2$.

Here we have defined $Q = eV/u_1$ ($eV > 0$) as the maximum wave vector set by the bias voltage and $\Delta\tilde{u} = \tilde{u}_1 - \tilde{u}_2$. The above integral can be solved exactly and gives

$$\begin{aligned} I(x,t) &= \frac{\gamma_\theta^2}{2} a(1-a)\Big\{ 2\cos(Q\,\Delta\tilde{u}\,t) + 2Ci[Q\,\Delta\tilde{u}\,t] - Ci[Q\,(\Delta\tilde{u}\,t - x)] \\ &- Ci[Q\,(\Delta\tilde{u}\,t + x)] + 2Q\,\Delta\tilde{u}\,t\,Si[Q\,\Delta\tilde{u}\,t] + Q\,(\tilde{u}_1\tau - \Delta\tilde{u}\,t)\,Si[Q\,(\Delta\tilde{u}t - x)] \\ &+ 2(Q\,x)\,Si[Q\,x] - Q(\Delta\tilde{u}\,t + x)\,Si[Q(\Delta\tilde{u}\,t + x)] + 2Ci[Q\,x] \\ &+ 4\cos(Q\,x)\,\sin^2[Q\,\Delta\tilde{u}\,t/2] - 2(1+\gamma_E) - 2\log\left(\frac{Q\,\Delta\tilde{u}\,t\,x}{((\Delta\tilde{u}\,t)^2 - x^2)^{1/2}}\right)\Big\}. \end{aligned} \tag{5.4.21}$$

In the above expression, $Ci(x)$ and $Si(x)$ are respectively the cosine and the sine integral, defined as [104]:

$$Ci(x) = -\int_x^\infty dy \frac{\cos(y)}{y} \tag{5.4.22}$$

$$Si(x) = \int_0^x dy \frac{\sin(y)}{y}. \tag{5.4.23}$$

$Si(x)$ is an entire function of its arguments with no branch cut discontinuities. $Ci(x)$ on the other hand has a branch cut discontinuity in the complex x plane, running from $-\infty$ to 0. In order to evaluate the momentum distribution function, we need to Fourier transform Eq. (5.4.26). In Fig. (34), we show the results of the numerical analysis of the time dependent,

momentum distribution function in mode u2. The distribution function develops from an initial single step Fermi distribution at $t = 0$ (i.e. before the interactions are switched on), to a final stationary non-equilibrium distribution in which the initial step singularity broadens due to interactions. Details concerning the numerical evaluation of the momentum distribution function can be found in (D.2). It is instructive to study Eq. (D.2.2) in the short and long time limit, where an analytical expression for the distribution function can be obtained.

Short time limit

We start considering the short time behavior of Eq. (D.2.2), which is defined by taking the two following limits :

$$\begin{aligned} Q\Delta\tilde{u}\cdot t &\ll 1 \\ Q\cdot x &\ll 1. \end{aligned} \tag{5.4.24}$$

In this limit, the time dependent part of $C_{\psi_2}(x,t)$ assumes the form of a Gaussian factor :

$$\begin{aligned} e^{-I(x,t)} &\simeq e^{-\frac{x^2}{2x_r^2(t)}} \\ x_r^{-1}(t) &= \gamma_\theta\sqrt{a(1-a)}\,\frac{\Delta\tilde{u}Q^2}{2\sqrt{6}}\,t. \end{aligned} \tag{5.4.25}$$

Here, $x_r(t)$ has dimension of length and therefore it can be interpreted as the relaxation length. From the statistical point of view, the above Gaussian factor means that, in the short time limit, the system has not had time yet to truly interact, therefore its subelements are still described by independent random variables. It is worth noting that this is a general result in stochastic dynamics [105]. In order to find the distribution function, we need to compute the Fourier Transform of

$$C_{\psi_2}(x,t) \simeq \frac{\iota}{2\pi}\frac{1}{(x+\iota\alpha)}e^{-\frac{x^2}{2x_r^2(t)}}. \tag{5.4.26}$$

The Fourier transform is most easily evaluated by using the dual convolution theorem (). In this way, we obtain the fermionic distribution shortly after QPC1

$$f_s(\epsilon_k,t) = \frac{1}{2}\left[1-\mathrm{Erf}\left(\frac{\epsilon_k}{\sqrt{2}k_B T_{\mathrm{eff}}(t)}\right)\right]. \tag{5.4.27}$$

Where Erf is the error function and we have defined the effective temperature of the fermions as :

$$T_{\mathrm{eff}}(t) = x_r^{-1}(t)\hbar\tilde{u}_2/k_B, \tag{5.4.28}$$

where $\epsilon_k = \hbar\tilde{u}_2 k$. The effective temperature above, expresses the temperature profile of edge mode two close to QPC1.

Long time limit

In the opposite limit

$$\begin{aligned} Q\Delta\tilde{u}\cdot t &\gg 1 \\ Q\cdot x &\gg 1. \end{aligned} \tag{5.4.29}$$

we find instead :

$$\begin{aligned} e^{-I(x)} &\simeq e^{-\eta\frac{\pi}{2}|Q\,x|}\,|Q\,x|^{\eta}\,e^{\eta(1+\gamma_E)} \\ \eta &= \gamma_\theta^2 a(1-a)/2, \end{aligned} \tag{5.4.30}$$

where γ_E is Euler's gamma. We can immediately note that the above expression is time independent. Also in this case we obtain a result qualitatively in agreement with the standard stochastic dynamics case. The factor $\exp(-|Q\,x|)$ is in fact related to the characteristic function of a Cauchy distribution, describing a process where relaxation has taken place. However, the sub-leading term $|Q\,x|^{\eta}$ is appearing,[11] giving rise to a quantitatively different behavior. In this limit, the equal time propagator reads

$$C_{\psi_2}(x) = \frac{1}{2\pi\alpha}\frac{e^{-\eta\frac{\pi}{2}|Q\,x|}\,|Q\,x|^{\eta}\,e^{\eta(1+\gamma_E)}}{(x+\imath\alpha)}. \tag{5.4.31}$$

Fourier transforming Eq. (5.4.31) we obtain the fermi distribution at long times

$$f_{2u,l}(\epsilon_k) = \frac{1}{2} + \frac{e^{\eta(1+\gamma_E)}}{2\pi}\,\epsilon_Q^{\eta}\,\Gamma(\eta)\,2\,\mathfrak{I}\left(\imath\epsilon_k + \frac{\pi\epsilon_Q\eta}{2}\right)^{-\eta}. \tag{5.4.32}$$

where $\epsilon_Q = \hbar Q\tilde{u}_2$ is the energy scale set by the bias, $\epsilon_k = \hbar k\tilde{u}_2$ and $\Gamma(\eta)$ is the gamma function. Even though the edge mode $2u$ relaxes to a fermionic distribution, this is distribution does not have the equilibrium form due to the integrability of the model. However, in contrast to the short time result, the fermionic distribution at long times does not depend on time anymore, signaling the existence of a steady state.

5.5 SHOT NOISE POWER AT QPC2

In this section, we evaluate the shot noise power at QPC2 (placed at some distance x_0 away from QPC1) using the non-equilibrium bosonization formalism. To be more specific, we consider the effect of QPC1 on the system non perturbatively in the tunneling amplitude t_1, while the effect of QPC2 will be considered perturbatively in the tunneling amplitude t_2. At lowest order in t_2, shot noise at QPC2 can be evaluated making use of the following formula [57]

$$\begin{aligned} S(\omega\to 0) &= 2\frac{e^2}{h}\frac{|t_2|^2}{2\pi}\int_\epsilon \left(G^<_{2u}(\epsilon)G^>_{2d}(\epsilon) + G^<_{2d}(\epsilon)G^>_{2u}(\epsilon)\right) \\ G^<_{2u}(\epsilon) &= \int_\tau e^{\imath\epsilon\,\tau}G^<_{2u}(\tau) \\ G^<_{2u}(\tau) &= \lim_{t\to\infty}\langle\psi^\dagger_{2u}(x_0,t+\tau)\psi_{2u}(x_0,t)\rangle, \end{aligned} \tag{5.5.1}$$

where e^2/h is the quantum of conductance. In our model, a peculiar feature of the shot noise at the second QPC is that there is no bias between the two edges. Scattering, however, occurs

11 We will se later that this term also appears in the Fisher-Hartwig conjecture used to evaluate the long time limit of Toeplitz determinants.

because of the different effective temperature between the two edges, so that the edge modes effectively carry only neutral excitations. We need to evaluate the "lesser" Green function $G^{<}_{2u}(\tau)$ at long times "t" using the bosonization formalism.

$$\begin{aligned} G^{<}_{2u}(\tau) &= \lim_{t\to\infty} \frac{1}{2\pi\alpha} \langle e^{-\imath\phi_{2u}(x_0,t+\tau)} e^{\imath\phi_{2u}(x_0,t)} \rangle \\ &= \lim_{t\to\infty} \frac{1}{2\pi\alpha} e^{[\phi_{2u}(x_0,t+\tau),\phi_{2u}(x_0,t)]/2} \langle e^{-\imath\{\phi_{2u}(x_0,t+\tau)-\phi_{2u}(x_0,t)\}} \rangle, \end{aligned} \tag{5.5.2}$$

where in the second line we used the Baker-Haussdorf formula. In this form, the lesser Green function is a product of an exponential of a commutator of bosonic fields and the expectation value of an exponential of the difference between bosonic fields. Since the commutator is a c-number, it can be taken out of the expectation value and for this reason it does not depend on the distribution function. In appendix (D.1), we derive the explicit expression for the commutator in terms of the zero temperature Green function $G^{<}_{0}(\tau)$. Equation (5.5.2) can be then written in the particularly useful form

$$\begin{aligned} G^{<}_{2u}(\tau) &= G^{<}_{0}(\tau) \langle e^{\sum_q \lambda^{\star}_{1u,q}(t,\tau) b^{\dagger}_{1u,q}} e^{-\sum_q \lambda_{1u,q}(t,\tau) b_{1u,q}} \rangle_1 \\ &\quad \langle\ e^{\sum_q \lambda^{\star}_{2u,q}(t,\tau) b^{\dagger}_{2u,q}} e^{-\sum_q \lambda_{2u,q}(t,\tau) b_{2u,q}} \rangle_2 . \\ G^{<}_{0}(\tau) &= \frac{1}{2\pi} \frac{1}{(-\imath\tilde{u}_1\tau+\alpha)^{\sin^2\theta}} \frac{1}{(-\imath\tilde{u}_2\tau+\alpha)^{\cos^2\theta}}. \end{aligned} \tag{5.5.3}$$

Here, $G^{<}_{0}(\tau)$ is the equilibrium Green function of edge mode 2 at long times in the presence of interactions. All the informations about non-equilibrium effects are contained in the average over bosonic coherent states in Eq. (5.5.3), where $\langle O \rangle_i$ means that the expectation value is taken with respect to the density matrix $\hat{\rho}_i$. The phase factors appearing at the exponents contains all the informations on the inter-mode interaction and are defined as :

$$\begin{aligned} \lambda_{1u,q}(t,\tau) &= \imath\sqrt{2\pi/qL}\, e^{\imath q x_0} e^{-q\alpha/2} [s_q(t+\tau) - s_q(t)] \\ \lambda_{2u,q}(t,\tau) &= \imath\sqrt{2\pi/qL}\, e^{\imath q x_0} e^{-q\alpha/2} [\nu_q(t+\tau) - \nu_q(t)] \end{aligned} \tag{5.5.4}$$

Since $\langle O \rangle_2$ is taken over an equilibrium ensemble, at $T = 0$ it is simply equal to unity. This means we are left evaluating $\langle O \rangle_1$ using the steady state, non equilibrium density matrix (5.4.10). In this section, we use non-equilibrium bosonization techniques in order to exactly evaluate Eq. (5.5.3) in the long time limit. As explained in chapter (2.2), a non-equilibrium distribution of the fermions results in a complicated bosonic density matrix [8]. As a result, when performing a cumulant expansion in order to evaluate the expectation value

$$\Delta_\tau(t) = \langle e^{\sum_q \lambda^{\star}_{1u,q}(t,\tau) b^{\dagger}_{1u,q}} e^{-\sum_q \lambda_{1u,q}(t,\tau) b_{1u,q}} \rangle_1, \tag{5.5.5}$$

terms beyond the Gaussian one fail to vanish and the entire infinite series should be considered. On the other hand, the above expectation value looks like the one involved in the problem of full counting statistics discussed in (2.2.2) and (B.3), the only difference being that in this case fermionic operators were involved. Instead of performing the mapping

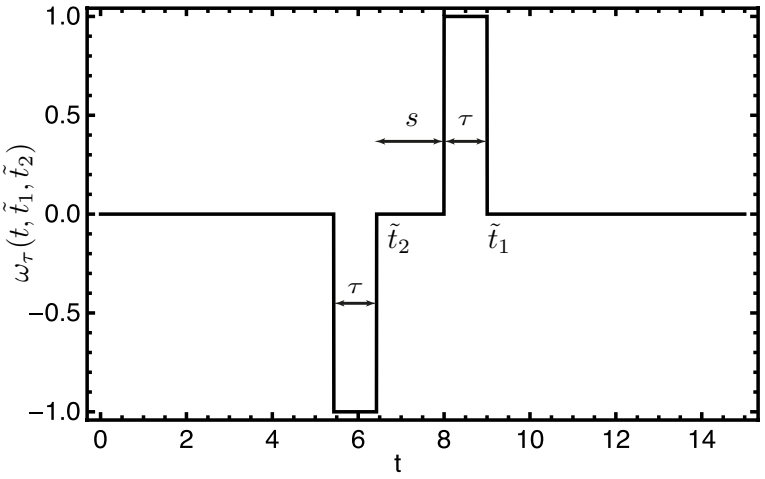

Figure 35: Window function. As a function of time, $\omega_\tau(t,\tilde{t}_1,\tilde{t}_2)$ represents two pulses of unit height with widths τ. The separation between the two pulses depends on their relative velocities $w = x_0(\tilde{u}_1^{-1} - \tilde{u}_2^{-1})$. According to Eq. (5.5.13), the two pulses can be interpreted as the $\pm e^\star$ quasiparticles of the charge fractionalization model.

$\hat{\rho}_F \to \hat{\rho}_B$, we note that it is convenient to refermionize the bosonic ladder operators using the bosonization identity

$$\begin{aligned} b^\dagger_{q,\eta} &= \imath\sqrt{\frac{2\pi}{Lq}}\sum_{k=-\infty}^{\infty} c^\dagger_{k+q,\eta}c_{k,\eta} \\ b_{q,\eta} &= -\imath\sqrt{\frac{2\pi}{Lq}}\sum_{k=-\infty}^{\infty} c^\dagger_{k-q,\eta}c_{k,\eta}. \end{aligned} \tag{5.5.6}$$

Since the bosonic operators in Eq. (5.5.5) refer to the system in the absence of interactions, the fermionic p-h operators in Eq. (5.5.6) also describe free excitations. This means that, after refermionization the expectation value in Eq. (5.5.5) can be evaluated using the free, non-equilibrium fermionic density matrix $\tilde{\rho}_1$ defined in Eq. (5.4.10). We find in this way

$$\Delta_\tau[t] = \mathrm{Tr}\left\{\hat{\rho}_1\, e^{\imath\sum_k\left(\sum_q\sqrt{\frac{2\pi}{Lq}}\lambda^\star_{1u,q}(t,\tau)\right)c^\dagger_{1u,k+q}c_{1u,k}} e^{\imath\sum_k\left(\sum_q\sqrt{\frac{2\pi}{Lq}}\lambda_{1u,q}(t,\tau)\right)c^\dagger_{1u,k-q}c_{1u,k}}\right\}, \tag{5.5.7}$$

that has the form of the correlator of full counting statistics. We can then use the trace formula (see B.3.1)

$$\mathrm{Tr}\left[e^{\hat{A}_1}e^{\hat{A}_2}\ldots e^{\hat{A}_i}\right] = \det\left[1 + e^{A_1}e^{A_2}\ldots e^{A_i}\right], \tag{5.5.8}$$

where the trace on the left is taken over operators defined in the 2^n-dimensional Fock space[12] while the determinant on the right is taken over operators defined in the n-dimensional

12 Here n is the dimension of the single-particle Hilbert space. The factor of 2 comes from the relation between the single-particle observable A and its Fock space representation in terms of a fermionic bilinear $\hat{A} = c^\dagger A c$.

single-particle Hilbert space. The trace formula allows us to express the expectation value of Eq. (5.5.7) in terms of a determinant of the Fredholm type (see Appendix (D.3) for additional details)

$$\bar{\Delta}_\tau[\delta(t)] = \frac{\det\left[1 + \left(e^{-\imath\hat{\delta}_\tau(t)} - 1\right)\hat{f}_D(\epsilon)\right]}{\det\left[1 + \left(e^{-\imath\hat{\delta}_\tau(t)} - 1\right)\hat{f}_0(\epsilon)\right]}, \tag{5.5.9}$$

where $f_D(\epsilon)$ is the zero temperature limit of the double step distribution function defined in Eq. (5.4.11). Here $\bar{\Delta}_\tau[\delta(t)]$ denotes the Fredholm determinant normalized to its zero temperature value and $\hat{f}_0(\epsilon)$ is the equilibrium, zero temperature Fermi distribution[13]. In the above expression we have defined the scattering phase

$$\hat{\delta}_\tau(t) = -\sum_{q>0}\sqrt{\frac{2\pi}{Lq}}(\lambda_{1q} + \lambda^\star_{1q}) = \delta\,\hat{\omega}_\tau(t, \tilde{t}_1, \tilde{t}_2), \tag{5.5.10}$$

where $\delta = \pi\gamma_\theta$ contains informations about the inter-edge interaction and $\hat{\omega}_\tau(t, \tilde{t}_1, \tilde{t}_2)$ is a "window function" [14]. In (D.3) we find the explicit for of the window function

$$\begin{aligned}\hat{\omega}_\tau(t, \tilde{t}_1, \tilde{t}_2) &= \theta(\tilde{t}_1 - t - \tau) - \theta(\tilde{t}_1 - t) + \theta(\tilde{t}_2 - t) - \theta(\tilde{t}_2 - t - \tau) \\ \tilde{t}_1 &= x_0/\tilde{u}_1 \\ \tilde{t}_2 &= x_0/\tilde{u}_2.\end{aligned} \tag{5.5.11}$$

In Fig. (35), $\omega_\tau(t, \tilde{t}_1, tildet_2)$ is plotted as a function of t. The window function represents two square pulses with unit height but opposite signs,of equal widths τ and whose separation in time is

$$w = \tilde{t}_1 - \tilde{t}_2 = x_0\left(\frac{1}{\tilde{u}_1} - \frac{1}{\tilde{u}_2}\right). \tag{5.5.12}$$

Since the scattering phase of a non-interacting system is equal to 2π, $\hat{\delta}_\tau(t)$ can be rewritten in the particularly useful form

$$\delta_\tau = 2\pi\left(\frac{e^\star}{e}\right)\hat{\omega}_\tau(t, \tilde{t}_1, \tilde{t}_2), \tag{5.5.13}$$

where we have used the definition of the fractional charge $e^\star = e\gamma_\theta/2$. In this form the scattering phase can be understood as describing two pulses with charges $\pm e^*$ passing by an observer at position x_0. For x_0 very small (i.e. close to QPC1), the window function is identically zero as the charge and neutral pulses in edge mode 2 have not yet separated in response to an electron which tunneled in into the first edge mode.

The main problem in evaluating the determinant defined in Eq. (5.5.9), is that the scattering phase and the distribution function are not simultaneously diagonalizable since energy and

13 As we explain in (D.3), we denote $\hat{f}(\epsilon)$ with a "hat" meaning that we consider it as the single-particle projector on the occupied states in energy space.

14 Here we follow the terminology used in the community and call $\hat{\omega}_\tau$ a "window function". However, as we explain in detail in appendix (D.3.1), $\hat{\omega}_\tau$ should be rather understood as a projector operator restricting the values of the determinant over some time window.

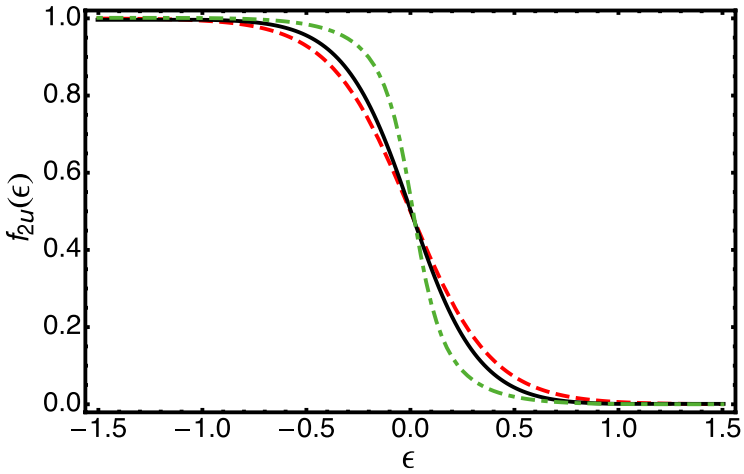

Figure 36: Steady state distribution of edge mode $(2u)$ **asymptotically far away from the QPC1.** (black full line) Nonequilibrium distribution obtained from Eqs. (5.5.3,5.5.5) by summing over all cumulants. (green dash-dotted line) distribution obtained by retaining only the Gaussian term. (red dashed line) fully equilibrated distribution at effective temperature $T^* = eV\sqrt{(3/2)a(1-a)}/\pi$ (see Eq.(5.4.18)). The mixing angle is $\theta = 0.47$, and the transmission probability of QPC1 is $a = 1/2$.

time are conjugate variables (see the discussion in B.3.2). However, since $\hat{\omega}_\tau$ is a projector operator, the determinant is different from zero only in the time windows of widths τ defining the two pulses depicted in Fig. (35). This means that the determinant only depends on the difference between two times and therefor it assumes a Toeplitz form (D.3.1). In addition, we find that for well separated pulses, the determinant formula (5.5.9) factorizes into a product of two single pulse determinants with identical scattering phase δ. As a consequence, the lesser Green function defined in Eq. (5.5.3) can be finally rewritten as

$$G^<_{2u}(\tau) = G^<_0(\tau)\,\bar{\Delta}^2_{\tau,s}(\delta), \tag{5.5.14}$$

where $\bar{\Delta}_{\tau,s}$ is a single pulse determinant. The above determinant can now be evaluated numerically by carefully defining the regularization scheme [8]; in appendix (D.3.1) we present an explicit evaluation of the above determinant formula using the theory of Toeplitz determinants.

Fourier transforming Eq. (5.5.14) into energy space, we can compute the distribution function at QPC2; as a consequence of interactions, the distribution function in edge mode two is broadened from the initial single step, Fermi distribution function. As a consequence of the broadening, the obtained distribution function resembles a thermal Fermi distribution; however, we would like to stress that such resemblance can be misleading since the distribution function in edge mode two, at long times, does not have the same functional form as a Fermi distribution, but rather describes a true non-equilibrium steady state. In Fig. (36) we compare the non-equilibrium distribution obtained by re-summing all higher order cumulants with one obtained by only retaining the Gaussian term in the cumulant expansion. The latter clearly deviates from the full one, making evident the necessity for including higher

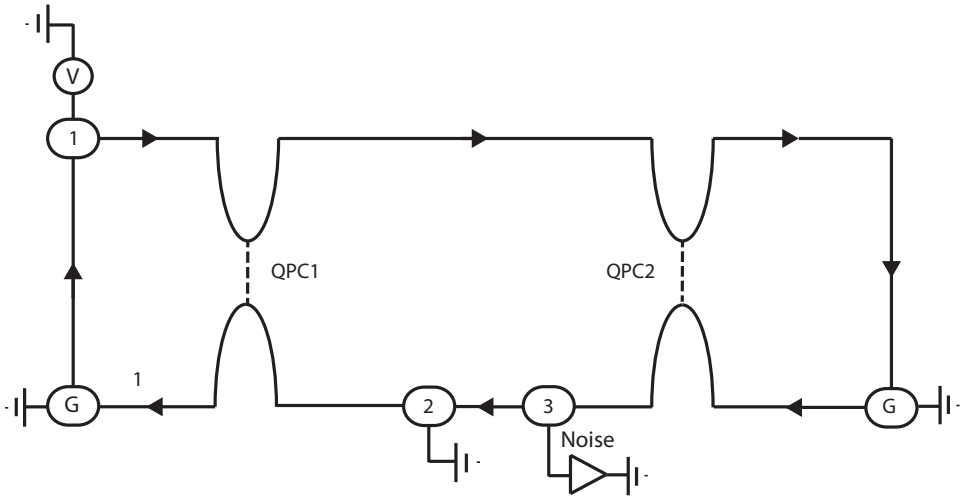

Figure 37: Setup considered for the evaluation of the reference noise. A quantum Hall bar at filling fraction $\nu = 1$ is pinched by two QPCs. Low frequency noise is measured at contact 3. All contacts are considered at zero temperature.

order terms. The non-equilibrium distribution also deviates from an equilibrium Fermi distribution with effective temperature

$$T^* = \frac{eV}{\pi}\sqrt{\frac{3}{2}a(1-a)}, \tag{5.5.15}$$

obtained by assuming that the two edge modes fully equilibrate and that each of them carries half the energy flux injected into the upper edge via QPC1, see Eq. (5.4.16) and (5.4.18).

5.5.1 Shot noise power and Fano factor

The Fano factor is generally defined as the ratio between the measured low frequency noise and a suitably chosen reference noise of an analogous non-interacting system (B.3.2). For example, in Eq. (5.2.11) of the simple charge factorization model, we compare the shot noise power of fractionalized charges tunneling at QPC2, with the Poissonian noise due to tunneling of non-interacting electrons. However, in defining a reference model for electron tunneling at QPC2 in edge mode two, we need to deal with an un-biased channel. It is worth stressing that in our model it is solely due to interactions and non-equilibrium effects that the edge mode becomes noisy, even though the edge mode is un-biased. This means that a naive choice of a non-interacting version of the setup depicted in Fig. (30) would not lead to a suitable reference noise. Before presenting the results for the shot noise power relative to Eq. (5.5.14), we first focus our attention on the definition of the reference model.

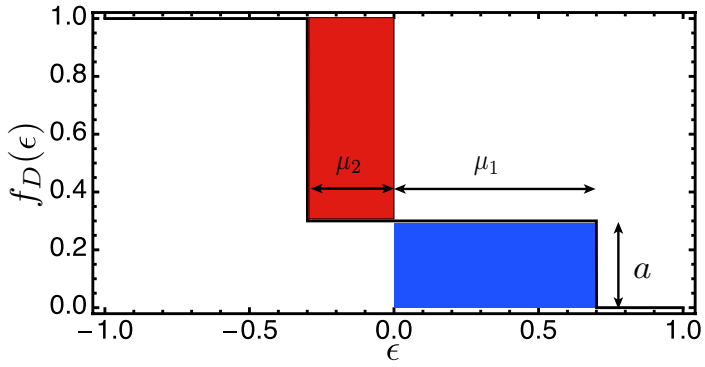

Figure 38: Double step distribution after QPC1. The red area describes a hole current I_h and the blue area a particle current $I_p = I_h = (e^2/h)\,V\,a(1-a)$. The reference noise at QPC2 is obtained as $S_{ref} = 2\,e\,p(I_p + I_h)$.

Reference model of non-interacting electrons

Since shot noise cannot be directly defined for an un-biased, non-interacting edge, we consider instead the setup of Fig. (37), where a single non-interacting edge mode is considered. In order to obtain a meaningful Fano factor, we evaluate the low frequency noise using as a distribution for the single edge mode after QPC1, the double step distribution of Eq. (5.4.11)[15], and a zero temperature distribution for the lower edge entering QPC2 :

$$\begin{aligned} f_D(\epsilon) &= a\,\theta(-\epsilon+\mu_1) + (1-a)\,\theta(-\epsilon) + \mu_2 \qquad (5.5.16)\\ f(\epsilon) &= \theta(-\epsilon), \end{aligned}$$

where $\mu_1 = (1-a)eV$ and $\mu_2 = -aeV$. Using the symmetry of the Fermi function $f(-\epsilon) = 1 - f(\epsilon)$ we can evaluate the low frequency noise

$$\begin{aligned} S_{ref}(\omega\to 0) &= 2\left(\frac{e^2}{h}\right) p \int_{-\infty}^{\infty} d\epsilon\,\{f_D(\epsilon)\theta(\epsilon) + \theta(-\epsilon) f_D(-\epsilon)\} \qquad (5.5.17)\\ &= 2\left(\frac{e^2}{h}\right) p \left\{\int_0^{\mu_1} d\epsilon\, a + \int_{\mu_2}^{0} d\epsilon\,(1-a)\right\}\\ &= 4\left(\frac{e^2}{h}\right) p\, a(1-a)eV = 2\,p\,e\,(I_h + I_p), \qquad (5.5.18) \end{aligned}$$

where p is the reflection probability at QPC2 and a is the transmission probability at QPC1. Note that the factor of 4 is due to the fact that both electrons and holes contribute to the low frequency noise. Since the double step distribution Eq. (5.5.16) is chosen in order to give a zero net current, the electron and the hole current have to be equal in magnitude. To make this more explicit, in the last line of Eq. (5.5.17) we have defined the hole and particle current $I_p = I_h = (e/h)\,V\,a(1-a)$. Finally, Fig. (38) gives an intuitive picture of the process described above.

15 In this way the edge mode after QPC1 will carry no net current.

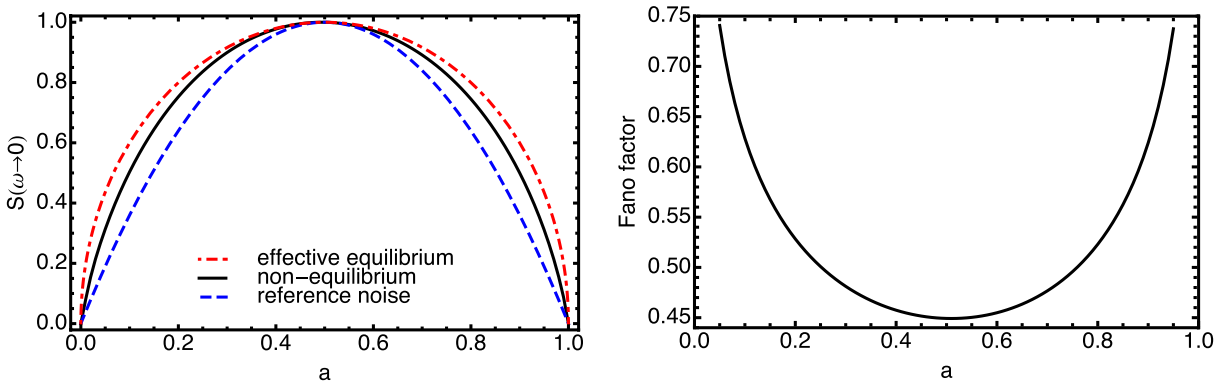

Figure 39: (Left) **Shot noise after QPC2** as a function of transparency a of QPC1, normalized to one at $a = 1/2$, for a mixing angle $\theta = 0.47$. Comparison of full non-equilibrium result (full black line), reference noise of noninteracting electrons (dashed blue line), and noise in a fully equilibrated thermal state (dash-dotted red line). (Right) **Fano factor as a function of transparency of QPC1** for the mixing angle $\theta = 0.47$. At $a = 1/2$ the Fano factor is $F = 0.45$.

Noise of a fully equilibrated edge mode

Consider now the noise due to a fully equilibrated edge mode at temperature T^* defined in Eq.(5.5.15). The low frequency noise at QPC2 due to an incoming upper edge mode characterized by a Fermi distribution $f_u(\epsilon)$ at temperature T^* and a lower edge mode characterized by a zero temperature Fermi distribution $f_d(\epsilon)$ is readily found to be

$$\begin{aligned} S_{th}(\omega \to 0) &= 2\left(\frac{e^2}{h}\right) p \int_{-\infty}^{\infty} d\epsilon \, \{f_u(\epsilon)\theta(\epsilon) + \theta(-\epsilon) f_u(-\epsilon)\} \\ &= 4\left(\frac{e^2}{h}\right) p \int_0^{\infty} d\epsilon \, \frac{1}{e^{\epsilon/T^*} + 1} \\ &= 4\left(\frac{e^2}{h}\right) p \, T^* \log 2. \end{aligned} \tag{5.5.19}$$

Discussion of the results

In Fig. (39), we display the dependence of low frequency noise computed from Eq. (5.5.1) on the transmission a of QPC1, normalizing the noise by its value at $a = 1/2$. One clearly sees that it deviates from both the standard free fermion dependence $a(1-a)$, and from the effective equilibrium result with $\sqrt{a(1-a)}$. Defining a Fano factor $F = S/S_{ref}$ as the ratio between the noise obtained from Eq. (5.5.1) and the reference noise obtained in Eq. (5.5.17) (see Fig. 39), we can make contact with the concept of fractional charges described in (5.2). For the simple charge fractionalization model we found

$$S_{fract}(\omega \to 0) = 4e^* \, p \, a \, I, \tag{5.5.20}$$

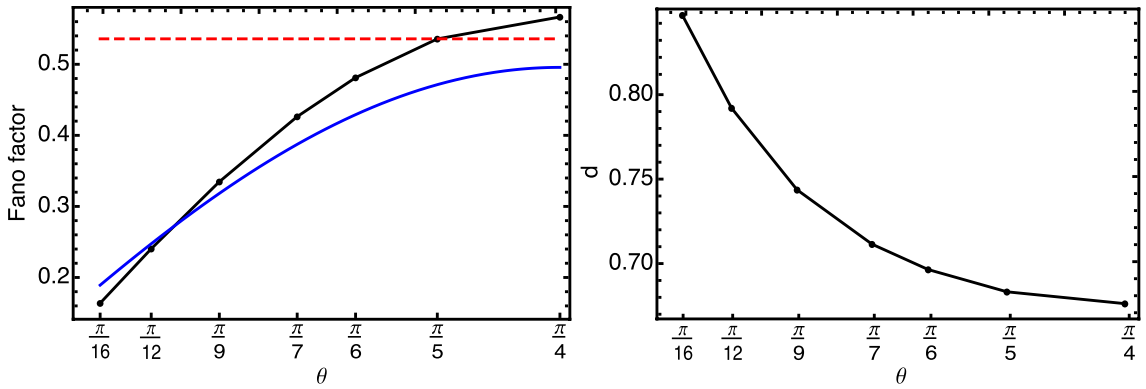

Figure 40: (Left) **Fano factor as a function of the mixing angle** for transmission $a = 1/2$ of QPC1. (red, dashed) Fully equilibrated edge, F is independent of interactions. (black, dotted) Full non-equilibrium situation. (blue, continuous) Reference model of a diluted system of fractional charges. (Right) **Fitting the non-equilibrium noise** by a function proportional to $[a(1-a)]^d$. The parameter d depends on the mixing angle θ. Black lines connecting the dots are a guide to the eye.

where the factor of 4 comes from the fact that both charges $\pm e^*$ contributes to the low frequency noise. In Fig. (40) the Fano factor is plotted as a function of the mixing angle for the specific transmission $a = 1/2$ of QPC1. For this value of a, there is a surprisingly good agreement between the value $F_{fract} = (1/2)\sin 2\theta$ of the simple fractionalization model and F of the full non-equilibrium noise, suggesting that the Fano factor can be interpreted as being due to formation of fractionalized charges in the $\nu = 2$ quantum Hall edge. However, the Fano factor obtained from the simple fractionalization model is independent from the transmission probabilities at the first and the second QPCs. Looking at Fig. (39) right, we see that $a = 1/2$ represents a minimum for the Fano factor obtained from our full non-equilibrium calculation, for any other value of a our result will deviate from the one expected from the simple fractionalization model.

Following previous discussions, we now look at the $eV\tau \gg 1$ regime of the noise power in the perturbative limit $a \ll 1$. We find that the shot noise power obtained from Eq. (5.5.1) and Eq. (5.5.14) depends in a singular way on a in the limit $a \ll 1$. To obtain the noise in this limit, the functional determinant can be approximated by its long time asymptotic (D.4)

$$\begin{aligned} \bar{\Delta}_\tau(\delta) &\simeq \exp(-|\tau|/(2\tau_\phi)), \\ \tau_\phi^{-1} &= -(eV/2\pi)\log[1-4a(1-a)\sin^2(\pi\gamma_\theta/2)]. \end{aligned} \tag{5.5.21}$$

It must be noted that only leading terms in the evaluation of the determinant have been kept. By comparing Eq. (5.5.21) with Eq. (5.4.30), we see that the two expressions differ by the sub leading term $|\tau\Delta\mu|^\eta$. Knowledge of $\bar{\Delta}_\tau(\delta)$ for large times allows to accurately calculate the distribution function of mode $(2u)$ for energies $\epsilon \ll eV$. However, for $a \ll 1$ the distribution function only deviates from a step function on the scale aeV, such that the long

time asymptotics allows an exact evaluation of the distribution function. Using Eq. (5.5.1) and taking the $a \ll 1$ limit, we find

$$S(\omega \to 0) \simeq eV \left(\frac{e^2}{h\pi^2}\right) 8p\, a \log(1/a) \sin^2(\pi\gamma_\theta/2). \tag{5.5.22}$$

As we can see, also in the full non-equilibrium case we find that the zero frequency noise power depends in a singular way on a. This non-analyticity explains the divergence in S with x_0 found in [106] when calculating S perturbatively in a.

A useful way to characterize the nonlinear dependence of experimentally measured shot noise on the transmission probability a of QPC1 is by fitting it to a function proportional to $[a(1-a)]^d$ [107]. For the reference noise of Eq. (5.5.17), d is trivially equal to unity. For "thermal" noise generated by the effective equilibrium temperature T^*, one finds $d = 0.5$. For the full equilibrium noise, we find that its dependence on a can be well fitted by the above power law, and that d varies from $d = 0.85$ for $\theta = \pi/16$ to $d = 0.68$ for $\theta = \pi/4$, see Fig. (40). In this way, from knowledge of d the mixing angle θ can be inferred, without making use of the Fano factor.

5.6 CONCLUSIONS

To conclude, we have studied charge fractionalization in a $\nu = 2$ QH edge state taking particular care of the non-equilibrium and interacting properties of the system. The setup shown in Fig. (30) is experimentally feasible and allows for detection of charge fractionalization through measurement of the low frequency quantum shot noise. The first QPC generates a unit charge pulse in edge mode 1 subject to a non-equilibrium distribution. As a consequence of the inter-edge interaction and the non-equilibrium configuration, two pulses carrying $\pm e^\star$ charges are also generated in the unbiased edge mode 2 according to the charge fractionalization model (5.2). However, the latter does not take into account the quantum statistical properties of the quasi-particles, that are indeed crucial when evaluating noise. In particular, it does not take into account possible relaxation processes that can modify the value of the observed noise. In order to take into account relaxation processes, we have shown that a quantitatively correct result can be obtained using the method of non-equilibrium bosonization. Nevertheless, the Gaussian result of section (5.4.4) gives us important (qualitatively correct) informations about the relaxation dynamics and allows for a nice analytical analysis. In section (5.5), we have numerically evaluated the non-equilibrium distribution function and we have shown that, even though it does not relax to a thermal state, for half transmission at QPC1 the distribution is close to a thermal distribution obtained in the assumption of full equilibration. Knowledge of the Green functions allows us to evaluate the shot noise at the second QPC. We compare the full non-equilibrium noise with the effective thermal noise and fit it to a function proportional to $[a(1-a)]^d$, Fig (39).

Defining a reference noise for a non-interacting neutral edge mode, we can extract the Fano factor and compare it to the one obtained from the simple fractionalization model and from the fully equilibrated edge. We find that at half transparency the Fano factor of the full non-equilibrium noise can be very close to the one predicted by the simple fractionalization model, Fig. (40). However, it is important to realize that the latter is independent of QPC1's transparency and the agreement is lost for different values of a.

A LANDAU-GINSBURG FIELD THEORY

In section (1.4) we have introduced the Chern-Simons field theory of the QHE. Even at the mean field level, peculiar properties of the FQH state such as fractional charges and statistics were understood on a intuitive level. However, the simple treatment of section (1.4) does not take into account the Coulomb interaction and the system, therefore it cannot give a correct account of the FQH effect. In this section we consider the Bosonic CS effective theory, including the hierarchical construction and the edge state theory. This appendix is mostly based on the lecture notes by Nayak [20] and the books by Wen and Zee [2, 22].

A.1 DUAL THEORY

In the Landau-Ginsburg-Chern-Simons theory, the interaction of particles with the external field is considered by the introduction of an external $U(1)$ gauge field A_μ. The coupling with the dynamical CS gauge field a_μ implements the flux-attachment procedure and gives rise to the correct Fermionic statistics (bosons+odd number of fluxes=fermions). Excitations over the mean field state are vortex-like and constitute the Laughlin quasi-particles. Since our aim is to write down an effective theory for those quasi-particles, we would like to treat them as the main object of the theory. Basically we are looking for a duality transformation that exchanges the roles of particles and vortices. We will work in natural units $\hbar = c = -e = 1$ and start by rewriting Eq. (1.4.3) in the bosonic form

$$\mathscr{L} = \imath\Phi^\dagger D_0\Phi - \frac{1}{2m}|D_i\Phi|^2 - \lambda(\Phi^\dagger\Phi - \bar{\rho})^2 + \frac{\epsilon^{\mu\nu\rho}}{4\pi(2k+1)}a_\mu\partial_\nu a_\rho, \tag{A.1.1}$$

where $i = (1,2) \equiv (x,y)$ are spatial coordinates and "$0 = t$" is the time one. The covariant derivative $D_\mu = \partial_\mu - \imath(A_\mu + a_\mu)$ takes care of the interaction between the matter and the gauge fields. Here, $\lambda = \lambda(x - x')$ is the Coulomb interaction strength and $\bar{\rho}$ is the average background density that constitutes the vacuum state of the theory. In its broken phase $\Phi(x) = \sqrt{\rho(x)}e^{\imath\theta(x)}$. Defining $D_0\theta = \partial_0\theta - A_0 - a_0$ and $D_i\theta = \partial_i\theta - A_i - a_i$ as the time and spatial components of the covariant derivative, we have:

$$\begin{aligned}\mathscr{L} &= -\rho D_0\theta - \frac{1}{2m}\left(\imath\rho D_i\theta - \frac{1}{2\sqrt{\rho}\partial_i\rho}\right)^2 - \frac{\imath}{2\sqrt{\rho}}\partial_0\rho - \lambda(\rho-\bar{\rho})^2 \\ &+ \frac{\epsilon^{\mu\nu\rho}}{4\pi(2k+1)}a_\mu\partial_\nu a_\rho = \mathscr{L}_M + \mathscr{L}_{CS}.\end{aligned} \tag{A.1.2}$$

Above we have denoted $\mathscr{L}_M$ the Lagrangian containing the matter fields and their interactions with the gauge fields, while $\mathscr{L}_{CS}$ contains the CS term alone. For the moment we

focus on deriving a low energy theory for $\mathscr{L}_M$ alone. In its superfluid phase $\langle\Phi\rangle \neq 0$, we can consider small fluctuations around the gapped modes $\rho = \bar{\rho} + \delta\rho$ and expand to second order with respect to $\delta\rho$ and the Goldstone boson θ

$$\mathscr{L}_M = -\bar{\rho}\, D_0\theta - \delta\rho\, D_0\theta + \frac{\bar{\rho}}{2m}(D_i\theta)^2 - \frac{1}{8m\bar{\rho}}(\partial_i\delta\rho)^2 - \lambda\,\delta\rho^2. \tag{A.1.3}$$

The first term is a total divergence and we can drop it. Since we are interested in the low energy theory for the phase field θ, we can safely integrate out the gapped modes

$$\mathscr{L}_M = \frac{\bar{\rho}}{2m}(D_i\theta)^2 - \frac{1}{2}D_0\theta\left(\frac{1}{\lambda - \frac{\partial_i^2}{8m\bar{\rho}}}\right)D_0\theta; \tag{A.1.4}$$

considering long wavelengths $(8m\bar{\rho})\lambda >> k^2$ (where k is the wave vector) and adding back the CS term we arrive at the following low energy effective Lagrangian

$$\mathscr{L}_{eff} = \frac{\chi}{2}(D_\mu\theta)^2 + \frac{\epsilon^{\mu\nu\rho}}{4\pi(2k+1)}a_\mu\partial_\nu a_\rho, \tag{A.1.5}$$

where we have defined $D_\mu = (D_0, uD_i)$[1], the compressibility $\chi = \lambda^{-1}$ and the fluid's velocity $u = \sqrt{\lambda\bar{\rho}/m}$ that we will take equal to unity hereafter. The first term of Eq. (A.1.5) describes a gauged superfluid with a linearly dispersing mode. Now remember that θ contains vortices, so we can break it into a smooth part and one containing the vortex $\theta = \theta_s + \theta_V$. The duality transformation to quasi-particle variables can be performed by introducing a source field ξ^μ in order to perform a "Gaussian transformation"[2]

$$\mathscr{L}_{eff} = -\frac{1}{2\chi}\xi_\mu^2 + \xi^\mu(\partial_\mu\theta_V + \partial_\mu\theta_s - A_\mu - a_\mu) + \frac{\epsilon^{\mu\nu\rho}}{4\pi(2k+1)}a_\mu\partial_\nu a_\rho. \tag{A.1.6}$$

Integrating out the smooth field configuration θ_s, determines a constraint on the system through the equation of motion for θ_s: $\partial_\mu\xi^\mu = 0$. Since we are in $2+1$ dimensions, the constraint can be solved by introducing a new gauge field such that $\xi^\mu = \epsilon^{\mu\nu\rho}\partial_\nu\alpha_\rho$. Using this constraint, we find that the quadratic term in Eq. (A.1.6) $\xi^\mu\xi_\mu = (1/2)\,f^{\mu\nu}f_{\mu\nu}$ is a Maxwell term for the gauge field α_μ[3] and arrive at

$$\mathscr{L}_{eff} = -\frac{1}{4\chi}f^{\mu\nu}f_{\mu\nu} + \epsilon^{\mu\nu\rho}\partial_\nu\alpha_\rho\partial_\mu\theta_V - \epsilon^{\mu\nu\rho}A_\mu\partial_\nu\alpha_\rho - \epsilon^{\mu\nu\rho}a_\mu\partial_\nu\alpha_\rho + \frac{\epsilon^{\mu\nu\rho}}{4\pi(2k+1)}a_\mu\partial_\nu a_\rho. \tag{A.1.7}$$

We are now able to extract some physics out of Eq. (A.1.7); in particular, we are looking for the vortex current. This can be derived by varying the effective Lagrangian with respect to α_ρ:

$$j_V^\mu = \epsilon^{\mu\nu\rho}\partial_\nu\partial_\rho\theta_V. \tag{A.1.8}$$

1 Here we use a Minkowski metric.

2 Here we mean the opposite operation with respect the Gaussian functional integral.

3 To derive this relation we have used the identity $\epsilon^{\mu\nu\rho}\epsilon_{\mu\lambda\gamma} = \delta_{\nu\lambda}\delta_{\rho\gamma} - \delta_{\nu\gamma}\delta_{\rho\lambda}$, where $\delta_{\mu\nu}$ is the Kronecker delta. Then we have used the relation between the field strength and the gauge field $f_{\mu\nu} = \partial_\mu\alpha_\nu - \partial_\nu\alpha_\mu$.

It is worth noting that for a smooth θ field, the above current would have been zero. However, since θ_V is not globally defined (it changes by 2π when we go around a vortex) $\partial_\nu\partial_\rho\theta_V \neq \partial_\rho\partial_\nu\theta_V$, and a vortex current is indeed observed. To make sure that j^μ_V is a vortex current, we can compute its related charge

$$Q_V = \int_\Sigma dx\, j^0_V = \oint_l dx\, \partial_x\theta_V = \theta_V(2\pi) - \theta_V(0) = 2\pi. \tag{A.1.9}$$

In a similar way, the electromagnetic current is derived by varying the effective Lagrangian with respect to the A_μ gauge field. In this case, we obtain

$$j^\mu = \epsilon^{\mu\nu\rho}\partial_\nu\alpha_\rho. \tag{A.1.10}$$

In the effective theory, the charge current is related to the dynamical field α_ρ; since this is a regular field configuration, we see that $\partial_\mu j^\mu = 0$ is indeed an identity that does not depend on the equation of motion (as opposed to the standard Noether's currents). We call j^μ a topological current. It is convenient to normalize Eq. (A.1.8) to 2π and introduce a complex scalar field Φ_V to create and annihilate the vortices. Note that Eq. (A.1.8) is the current related to Φ_V. The effective Lagrangian in its final dual form reads:

$$\begin{aligned}\mathscr{L}_{eff} &= -\frac{1}{4\chi}f^{\mu\nu}f_{\mu\nu} + \frac{1}{2}|(\partial_\mu - \imath\alpha_\mu)\Phi_V|^2 - V(\Phi_V) - \frac{\epsilon^{\mu\nu\rho}}{2\pi}A_\mu\partial_\nu\alpha_\rho - \frac{\epsilon^{\mu\nu\rho}}{2\pi}a_\mu\partial_\nu\alpha_\rho \\ &+ \frac{\epsilon^{\mu\nu\rho}}{4\pi(2k+1)}a_\mu\partial_\nu a_\rho.\end{aligned} \tag{A.1.11}$$

Above, the potential term $V(\Phi_V)$ describes the short distance vortex-vortex interaction[4]. In this final form, we have found a dual description of the initial problem in which the quasiparticles (i.e. the vortices) appear as the basic particles of the theory. The broken symmetry phase of the original theory corresponds to $\langle\Phi_V\rangle = 0$ in the dual theory, meaning that quasiparticles are gapped and we can integrate them out, renormalizing in this way the Maxwell term that can be successively dropped because irrelevant in the long-wavelength limit. Since the a_μ field appears quadratically, it can also be integrated out. In this way we obtain the final form of the Lagrangian ($q = 2k+1$):

$$\mathscr{L}_{eff} = \frac{q}{4\pi}\epsilon^{\mu\nu\rho}\alpha_\mu\partial_\nu\alpha_\rho + \alpha_\mu\left(j^\mu_V + \frac{1}{2\pi}\epsilon^{\mu\nu\rho}\partial_\nu A_\rho\right). \tag{A.1.12}$$

A.2 HALL CONDUCTANCE AND QUASIPARTICLE STATISTICS

In the previous section we have derived a dual Lagrangian in order to describe the low energy properties of the QH fluid. In order to explore the physical properties of the QH

4 Note that in principle, the form of the vortex-vortex potential is determined if we know the details of the original microscopic theory.

fluid we integrate out the α field (that appears quadratically) and obtain the following three terms:

$$\mathscr{L}_{eff} = \frac{\pi}{q} j^{\mu}_{V} \frac{1}{\epsilon_{\mu\nu\rho}\partial_{\nu}} j^{\rho}_{V} + \frac{1}{q} A_{\mu} j^{\mu}_{V} + \frac{1}{4\pi q} A_{\mu} \epsilon_{\mu\nu\rho} \partial^{\nu} A^{\rho}. \tag{A.2.1}$$

The above effective Lagrangian contains all the needed informations about the FQH fluid. The second term, coupling to the electromagnetic gauge field, specifies the charge of the vortices. Functionally differentiating with respect to A_0 we see that the excitations of the FHQ fluid carry fractional electric charge $e^* = (-e)/q$ (where we have reinstated the electron's charge). The third term describes the electromagnetic response of the system. If we consider its time component, we find $\delta n_e = (1/q)\delta B/\Phi_0$, and we can identify the filling fraction $\nu = 1/q$ in agreement with Eq. (1.3.4). The spatial component gives the Hall conductance $\sigma = \nu e^2/h$. Finally, the first term gives us information on the quasi-particle's statistics. To see this we write the current associated with the two quasi-particles as $j^{\mu}_{V} = j^{\mu}_{V,1} + j^{\mu}_{V,2}$, substitute it into the first term of Eq. (A.2.1), and consider only the action for the cross term:

$$S = \int dt d^2x \, j^{\mu}_{V,1} \frac{1}{\frac{1}{2\pi q}\epsilon_{\mu\nu\rho}\partial_{\nu}} j^{\nu}_{V,2} = \int dt d^2x \, j^{\mu}_{V,1} f_{\mu} \tag{A.2.2}$$

In the second term on the r.h. s., we have used the equation of motion for $j^{\mu}_{V,2} = 1/(2\pi q)\epsilon_{\mu\nu\rho}\partial_{\nu} f_{\mu}$. Basically, we image keeping the second particle fixed and move the first one around it in a loop. Substituting the quasi-particle density $j^{0}_{V,2} = \delta[\mathbf{x} - \mathbf{x}_2(t)]$ in the previous equation and integrating over the loop trajectory, we find the field generated by $j^{0}_{V,2}$: $f_j = 1/(qr_j)$. Using this result in Eq. (A.2.2), together with $j^{i}_{V,1} = \dot{\mathbf{x}}_1 \delta[\mathbf{x} - \mathbf{x}_1(t)]$, we arrive at:

$$S = \frac{1}{q} \int dt dr d\theta \, \frac{\dot{\mathbf{r}}_1}{\mathbf{r}} \delta[\mathbf{r} - \mathbf{r}_1(t)] = \frac{2\pi}{q}. \tag{A.2.3}$$

The statistical angle is given by half of the above result:

$$\theta = \frac{\pi}{q}. \tag{A.2.4}$$

Therefore, excitations in FQH states obeys fractional statistics.

A.3 HIERARCHY AND TOPOLOGICAL ORDER

In section (1.3.2) we have seen that new QH states can appear other than the ones in the principal Laughlin series. In Haldane's approach, the new states resulted from quasi-particles condensation on top of some other states. Let us see how this procedure is implemented in the effective theory. Consider again the effective dual Lagrangian (A.1.12); we can introduce a new $U(1)$ gauge field α^2_{μ} "on top" of the original one[5] . The CS coupling of the new term is taken as bosonic, and we have:

$$\mathscr{L}_{eff} = \frac{q}{4\pi} \epsilon^{\mu\nu\rho} \alpha^1_{\mu} \partial_{\nu} \alpha^1_{\rho} + \frac{1}{2\pi} \alpha^1_{\mu} \epsilon^{\mu\nu\rho} \partial_{\nu} A_{\rho} + \frac{2p_2}{4\pi} \epsilon^{\mu\nu\rho} \alpha^2_{\mu} \partial_{\nu} \alpha^2_{\rho} + \alpha^1_{\mu} j^{\mu}_{2}. \tag{A.3.1}$$

5 In our notation, the indices $1, 2..., n$ label the different n gauge fields. So, 1 stands for the parent gauge field, and 2 for the one "on top" of it.

By construction, α_μ^2 does not directly couple to A_μ but to the gauge field of the parent state. Using the definition of the vortex current

$$j_2^\mu = \frac{1}{2\pi}\epsilon^{\mu\nu\rho}\partial_\nu\alpha_\rho^2, \tag{A.3.2}$$

we can derive the new filling fraction from the equation of motion of the two α fields:

$$\begin{aligned} B + qb_1 + b_2 &= 0 \\ b_2 - \frac{1}{2p_2}b_1 &= 0, \end{aligned} \tag{A.3.3}$$

where we have defined the "magnetic fields" b_i associated with the CS gauge fields. Solving Eq (A.3.3) we obtain the Meissner effect

$$\left(q - \frac{1}{2p_2}\right) b_1 + B = 0. \tag{A.3.4}$$

Using that $b_1 = 2\pi\rho$, we finally obtain the expression for the filling fraction

$$\nu = \frac{1}{q - \frac{1}{2p_2}}. \tag{A.3.5}$$

This is Haldane's result, Eq. (1.3.8) for the quasi-electron. In order to obtain the hole, we simply change the sign of the charges. We can re-iterate the above procedure to find other states. Introducing the charge vectors $t^I = \delta_\tau^I$, we can rearrange Eq. (A.3.1) in the following compact form:

$$\mathscr{L}_{eff} = \frac{1}{4\pi}K_{IJ}\epsilon^{\mu\nu\rho}\alpha_\mu^I\partial_\nu\alpha_\rho^J + \frac{t_I}{2\pi}\alpha_\mu^I\epsilon^{\mu\nu\rho}\partial_\nu A_\rho + \alpha_\mu^I j_I^\mu, \tag{A.3.6}$$

where $I, J = 1, 2, ..., n$ label the different condensates. The above low energy Lagrangian density describes the most general Abelian QH state. For example, the previously considered first level of the hierarchy, is obtained by the K-matrix

$$\mathbf{K} = \begin{pmatrix} q & 1 \\ 1 & 2p_2 \end{pmatrix}. \tag{A.3.7}$$

Proceeding as we did in section (A.2), we can find the most general expression for the QH conductance, statistics and quasi-particle's charge of an Abelian QH state:

$$\begin{aligned} \sigma_H &= t^I t^J (K^{-1})_{IJ} \\ e_I^* &= t^J (K^{-1})_{IJ} \\ \theta_{IJ} &= \pi (K^{-1})_{IJ}. \end{aligned} \tag{A.3.8}$$

The K-matrix defines the universality class of the topological Abelian fluid [2]. In particular, the K-matrix also provides a way to partially define the topological order of the abelian FQH liquid. In this case, topological order is partially defined by ground-state degeneracy, a quantity that is robust against arbitrary perturbations, including disorder [108]. Even though the the CS Hamiltonian is identically zero, it possesses a non trivial ground-state, whose

degeneracy depends on the topology of space. On a Riemann surface of genus g, the ground-state degeneracy is $\det(\mathbf{K})^g$ [109].

If we now try to construct the Jain sequence, we will obtain a Lagrangian whose structure is identical to Eq. (A.3.6), but it is characterized by a different K-matrix and a different form of the charge vector: $\mathbf{t}^I = (1, 1, 1, ..., 1)$; Wen and Zee, showed that the two constructions are indeed equivalent and related by a change of basis [109]. The basis in which $t^I = (1, 0, 0, 0, ...0)$ is called the hierarchical basis, while the one in which $\mathbf{t}^I = (1, 1, 1, ..., 1)$ is called the symmetric basis. The two basis are related by $\mathbf{t}_h = \mathbf{W}^{-1}\mathbf{t}_s$, where $\mathbf{W} = \delta_{IJ} - \delta_{I+1,J}$ is the transformation matrix. Using this transformation, the relation between K-matrices in different basis is readily found to be: $\mathbf{K}^h = \mathbf{W}^T\mathbf{K}^s\mathbf{W}$.

A.4 EDGE STATES

In section (1.4.1) we have briefly discussed the effect of a local gauge transformation $\alpha'_\mu = \alpha_\mu + \partial_\mu\Lambda$ on the effective action (A.3.6), showing that the CS action changes by a boundary term

$$S' = S + \frac{q}{4\pi}\int_\Omega \epsilon^{\mu\nu\rho}\partial_\mu(\alpha_\nu\partial_\rho\Lambda). \tag{A.4.1}$$

For notational simplicity we consider here the principal Laughlin sequence. In section (1.5) we showed that, in order to have a total conserved current in a system with boundaries, dynamical gapless states exist at the edge of the system. Since current conservation is related to the invariance of the system with respect to local gauge transformations, it is reasonable to argue that the gauge anomaly of Eq. (A.4.1) should lead to the appearance of the edge states. In order to have a gauge invariant theory, we can impose as a boundary condition: $\alpha_0(x, y = 0, t) = 0$ (here we have chosen $y = 0$ as the position of the boundary). Under this choice, the CS action is now invariant with respect to all transformations that respect $\partial_0\Lambda = 0$ on the boundary. Any function $\Lambda : \Omega \to G$ satisfying $\Lambda(x, y = 0, t) = 1$ reflects the (local) gauge symmetry of the theory [3]. This choice of boundary conditions imposes a constraint on the dynamics of the system, that we are now going to study. Consider the CS term in Eq. (A.4.1) and its canonical momentum

$$\begin{aligned} \Pi_i &= \frac{\delta\mathscr{L}}{\delta\partial_0\alpha_i} = \frac{q}{4\pi}\epsilon^{ij}\alpha_j \\ \Pi_0 &= \frac{\delta\mathscr{L}}{\delta\partial_0\alpha_0} = 0. \end{aligned} \tag{A.4.2}$$

The zero value of the the temporal component of the canonical momentum is typical of gauge theories and mathematically it means that the associated Legendre map is not invertible[6]. As

6 The non invertibility of the Legendre map results in a non bijective map in phase space between the Lagrangian and the Hamiltonian representation. At the quantum level, this results in a redundant labeling of states in the Hilbert space; this redundancy is at the very heart of gauge theories. As a consequence of that, when quantizing the theory, constraint must be introduced either through the Dirac brackets formalism [37] or the Fadeev-Popov functional integral [22]

a consequence, α_0 is essentially arbitrary and plays the role of a (non dynamical) Lagrange multiplier. Let us get back to the edge problem; in order to study the dynamics at the edge we impose the previously found $\alpha_0 = 0$ constraint on the $\partial\Omega$ boundary of the system. To see explicitly the consequences of the α_0 constraint on the dynamic of the system, it is convenient to rewrite the action as follows:

$$S = \frac{q}{4\pi}\int_\Omega \left(2\epsilon^{ij}\alpha_0\partial_i\alpha_j + \epsilon^{ij}\alpha_i\partial_0\alpha_j\right). \tag{A.4.3}$$

Varying the above action with respect to the Lagrange multiplier α_0 results in the constraint $\epsilon^{ij}\partial_i\alpha_j = 0$, that is resolved by introducing a scalar field $\alpha_j = \partial_j\phi$. Substituting the constraint in the CS action we finally obtain:

$$S_{edge} = \frac{q}{4\pi}\int_{x,t}\partial_t\phi\partial_x\phi. \tag{A.4.4}$$

However, the above action does not describe propagating, one dimensional states. The problem here is that in our description there is no information about the dynamics of the edge. One way of introducing this information "by hand" is by noting that $a_0 + ua_1 = 0$, with u having the dimension of a velocity, is still a good boundary gauge fixing condition. In this way we find the correct chiral action. For a general quantum Hall state the edge action reads

$$S_{edge} = \int_{x,t}\left\{\frac{1}{4\pi}\left(K_{IJ}\partial_t\phi^I - U_{IJ}\partial_x\phi^I\right)\partial_x\phi^J + \frac{t_I}{2\pi}\epsilon^{\mu\nu}A_\mu\partial_\nu\phi^I\right\}. \tag{A.4.5}$$

Above, we have generalized the velocity u to the symmetric matrix U_{IJ}, whose off-diagonal elements describe a density-density interaction between different edge modes. It should be noted that the interaction strength depends both on the details of the edge confining potential and the electron-electron interaction, therefore it will be non-universal. The corresponding edge Hamiltonian (without the interaction with the external gauge field) is given by:

$$\mathscr{H}_{edge} = \frac{1}{4\pi}\int_x U_{IJ}\partial_x\phi^I\partial_x\phi^J. \tag{A.4.6}$$

From the above equation we also conclude that $\mathbf{U}$ must be a positive definite matrix. As for the K-matrix, positive eigenvalues will correspond to right-moving modes, while negative ones to left moving modes. We will prove this statement in the next section.

A.4.1 General diagonal form of the multi mode action

In this section we consider a general procedure for diagonalizing the edge state action (A.4.5). This section is rather abstract and the explicit form of the transformation will be illustrated in the main text for the various, specific cases. We want to transform the edge action of a generic, hierarchical QH state into a representation in which both $\mathbf{K}$ and the velocity matrix $\mathbf{U}$ are diagonal. This program can be accomplished in three steps [2, 80]:

We first diagonalize $\mathbf{K}$ performing an orthogonal transformation (i.e. a "rotation") of the fields

$$\phi_I = \sum_J (M_1)_{IJ} \tilde{\phi}_{1,J}. \tag{A.4.7}$$

Here, $\mathbf{M}_1$ is an orthogonal matrix $\mathbf{M}_1^T \mathbf{M}_1 = 1$ and $\tilde{\phi}_1$ is the new (rotated) field. When performing this transformation we also change

$$(\mathbf{K}, \mathbf{U}) \to (\mathbf{M}_1^T \mathbf{K} \mathbf{M}_1, \mathbf{M}_1^T \mathbf{U} \mathbf{M}_1^T) = (\mathbf{K}_1, \mathbf{U}_1). \tag{A.4.8}$$

Since the transformation diagonalizes the K-matrix, we have $(K_1)_{IJ} = \lambda_I \delta_{IJ}$, where λ_I are the eigenvalues of the K-matrix. In this way, the original action becomes

$$\tilde{S}_{edge,1} = \frac{1}{4\pi} \int_{x,t} \left(\lambda_I \delta_{IJ} \partial_t \tilde{\phi}_1^I - U_{1,IJ} \partial_x \tilde{\phi}_1^I \right) \partial_x \tilde{\phi}_1^J. \tag{A.4.9}$$

As a second step, it is convenient to rescale the fields as

$$\begin{aligned} \tilde{\phi}_{1,I} &= \sum_J (M_2)_{IJ} \tilde{\phi}_{2,J} \\ (M_2)_{IJ} &= \frac{\delta_{IJ}}{\sqrt{|\lambda_I|}}. \end{aligned} \tag{A.4.10}$$

The rescaled action now reads

$$\begin{aligned} \tilde{S}_{edge,2} &= \frac{1}{4\pi} \int_{x,t} \left(\eta_{IJ} \partial_t \tilde{\phi}_2^I - U_{2,IJ} \partial_x \tilde{\phi}_2^I \right) \partial_x \tilde{\phi}_2^J \\ \mathbf{U}_2 &= \mathbf{M}_2^T \mathbf{M}_1^T \mathbf{U} \mathbf{M}_1 \mathbf{M}_2 \\ \eta_{IJ} &= \frac{\lambda_I}{|\lambda_I|} \delta_{IJ} = \mathrm{sgn}(\lambda_I)\, \delta_{IJ}. \end{aligned} \tag{A.4.11}$$

The final step consists in finding a transformation that leaves η_{IJ} invariant but diagonalizes the velocity matrix $\mathbf{U}_2$

$$\tilde{\phi}_{2,I} = \sum_J (M_3)_{IJ} \tilde{\phi}_{3,J}. \tag{A.4.12}$$

As a consequence of this last transformation, we obtain $(M_3^T U_2 M_3)_{IJ} = \tilde{u}_i \delta_{IJ}$ and $(M_3^T \eta M_3)_{IJ} = \eta_{IJ}$. The final, diagonal, action reads

$$\tilde{S}_{edge,3} = \frac{1}{4\pi} \int_{x,t} \sum_I \left(\eta_I \partial_t \tilde{\phi}_3^I - \tilde{u}_I \partial_x \tilde{\phi}_3^I \right) \partial_x \tilde{\phi}_3^I, \tag{A.4.13}$$

where we have made explicit the sum over the edge modes and defined $\eta_I = \mathrm{sgn}(\lambda_I)$. As anticipated in the previous section, the sign of the eigenvalues of the K-matrix determines the direction of propagation of the edge modes, even in the interacting theory. The diagonal Hamiltonian reads

$$\mathscr{H}_{edge} = \pi \int_x \sum_I \tilde{u}_I \tilde{\rho}_{3,I}^2(x), \tag{A.4.14}$$

where the density fields now satisfy

$$\left[\tilde{\rho}_{3,I}(x), \tilde{\rho}_{3,J}(x') \right] = \eta_I \delta_{IJ} \frac{\imath}{2\pi} \partial_x \delta(x - x'). \tag{A.4.15}$$

A.4.2 Transport properties

Let us get back to the single edge mode action, for which $\mathbf{K} = q$. This action describes density waves propagating only in one direction. To see this explicitly we can derive the equation of motion for the ϕ-fields performing the variation $\phi \to \phi + \delta\phi$ and $\partial_\mu\phi \to \partial_\mu\phi + \partial_\mu\delta\phi$. In absence of external sources, the equation of motion reads

$$(\partial_t + u\partial_x)\,\rho(x) = 0, \tag{A.4.16}$$

where $\rho(x) = 1/(2\pi)\partial_x\phi$ is the density field. The equation above is the anticipated one-dimensional chiral wave equation. Next, we derive the transport properties of the edge states for a FQH system in the Laughlin series connected to electron reservoirs. We start considering the imaginary time action for a single mode

$$S_\pm = \frac{q}{4\pi}\int_{x,\tau} \partial_x\phi(x,\tau)(\pm\imath\partial_\tau + u\partial_x)\phi(x,\tau) + \frac{(-e)}{2\pi}\int_{x,\tau} \epsilon^{\mu\nu}A_\mu(x,\tau)\partial_\nu\phi(x,\tau), \tag{A.4.17}$$

where $\pm$ are respectively the right and left moving edge states, A_μ is the space-time component of the external gauge field ($\mu,\nu = \{0,1\} = \{\imath\tau, x\}$) and we have reinstated the electron's charge $-e$. Let us focus on one edge (say the $+$ one) for the moment, and compute the current response of the system due to the source term. The current can be derived as follows: first we perform a partial integration of the bosonic fields in Eq. (A.4.17) and then integrate them out to obtain an effective action in terms of the gauge fields

$$\begin{aligned} S_{eff}[A] &= -\frac{1}{2}\frac{e^2}{q2\pi}\int_{(x;\tau),(x';\tau')} \epsilon^{\mu\nu}\epsilon_{\rho\sigma}\partial_\nu A_\mu(x,\tau)\frac{1}{(\imath\partial_\tau + u\partial_x)\partial_x}\partial^\rho A^\sigma(x',\tau') \\ &= -\frac{1}{2}\frac{e^2}{q2\pi}\int_{(x;\tau),(x';\tau')} \Big\{\partial_\nu A_\mu(x,\tau)\frac{1}{(\imath\partial_\tau + u\partial_x)\partial_x}\partial^\mu A^\nu(x',\tau') \\ &- \partial_\nu A_\mu(x,\tau)\frac{1}{(\imath\partial_\tau + u\partial_x)\partial_x}\partial^\nu A^\mu(x',\tau')\Big\}, \end{aligned} \tag{A.4.18}$$

where in the second equality we have used the identity $\epsilon^{\mu\nu}\epsilon_{\rho\sigma} = (\delta_{\mu\rho}\delta_{\nu\sigma} - \delta_{\mu\sigma}\delta_{\nu\rho})$. The corresponding partition function can be written as

$$Z = \int \mathscr{D}A\, e^{-\frac{1}{2}\int A_\mu \Pi^{\mu\nu} A_\nu}. \tag{A.4.19}$$

Above, we have introduced the polarization tensor $\Pi^{\mu\nu}$. Since we are interested in computing the Landauer (non-local) conductance, we will consider the current response of the system to a density change due to the injection of electrons from the contacts into the edge [110], corresponding to the "transverse term" Π^{10} [7]. The induced charge current can be evaluated using linear response theory:

$$\left\langle J^1(x)\right\rangle = \int_{x'} \lim_{\omega\to 0}\Pi^{10}(x-x',\omega)A_0(x'). \tag{A.4.20}$$

7 The different response functions are related by the continuity equation [2].

When evaluating Eq. (A.4.18), it is important to take the limit $\omega \to 0$ before performing the integral. Physically, this correspons to a situation where a static electric field is applied over a finite part of the infinite wire. In linear response, the polarization tensor $\Pi^{\mu\nu}$ is defined in absence of the driving field, therefore if the system is translationally invariant (as it is in our case), this property is reflected in $\Pi^{\mu\nu}$, that will depend only on $x - x'$. Switching to Fourier space, we can now evaluate the polarization tensor:

$$\Pi^{10}(x - x', \omega_n) = \frac{-e^2}{q2\pi} \int_k \frac{e^{\imath k(x-x')}}{2\pi} \frac{\omega_n k}{k(\omega_n + \imath u k)} = \frac{-e^2}{q2\pi} e^{-\omega_n (x-x')/u} \frac{\omega_n}{u} \theta(x - x'). \quad \text{(A.4.21)}$$

Analytically continuing (A.4.21) to real frequencies ($\imath\omega_n \to \omega + \imath\epsilon$) and using Eq. (A.4.20), we arrive at:

$$\langle J^1(x) \rangle = \frac{e^2}{q2\pi} \int_{x'} \lim_{\omega \to 0} e^{\imath \frac{\omega}{u}(x-x')} \frac{\imath\omega}{u} \theta(x - x') A_0(x', \omega). \quad \text{(A.4.22)}$$

Taking the static limit $\omega \to 0$ we see that the integral gets most of its contribution when $x \ll x'$, that means from values deep down the "contact" where $A_0 = V_1$. Reinstating $\hbar$ and using $\nu = 1/q$, we obtain the quantized Hall conductance:

$$G = \nu \frac{e^2}{h}. \quad \text{(A.4.23)}$$

Similar procedure holds for the counter propagating edge, where the current is now proportional to $-V_2$. The net current is then given by $I = G(V_1 - V_2)$, where G is the quantized two terminal, non-local conductance.

B MORE ON BOSONIZATION

Bosonization has been proven an extremely useful framework to study strongly correlated systems in one spatial dimension. Although the underlying physical principle it is based on is intuitively simple (namely the impossibility of distinguishing fermions and bosons in one spatial dimension[1]), bosonization involves nevertheless many subtleties. In the first section we discuss some of these subtleties and give additional details to what has been already presented in the main text. In the second section we will have a closer look at non-equilibrium bosonization and highlight the differences with respect to the standard equilibrium approach. Finally in the third section we give an explicit derivation of the Levitov-Lesovik formula for the full counting statistics of mesoscopic quantum systems, using an approach originally introduced by Klich.

B.1 INSIGHT BOSONIZATION

In chapter (2.1.2) we have defined the bosonic ladder operators in terms of fermionic particle-hole (p-h) excitations

$$\begin{aligned} b^\dagger_{q,\eta} &= \imath\sqrt{\frac{1}{n_q}}\sum_{k=-\infty}^{\infty} c^\dagger_{k+q,\eta}c_{k,\eta} \\ b_{q,\eta} &= -\imath\sqrt{\frac{1}{n_q}}\sum_{k=-\infty}^{\infty} c^\dagger_{k-q,\eta}c_{k,\eta}. \end{aligned} \tag{B.1.1}$$

where $n_q \in \mathbb{Z}^+$ is the discrete momentum quantum number ($q = (2\pi/L)n_q$) of the excitations and $k = (2\pi/L)n_k$, $n_k \in \mathbb{Z}$ is the discrete fermionic quantum number. In order to be a meaningful transformation, Eq. (B.1.1) must reproduce the canonical bosonic commutation relations. While this task is easily accomplished for commutators of operators of the same kind (e.g. bb or $b^\dagger b^\dagger$), the commutator involving b and $b^\dagger$ turns out to be more tricky. In

1 Quantum statistics is defined by looking at how the phase of complex wave functions changes when two particles are moved one around the other. In one spatial dimension the very concept of "moving around" two particles is ill defined, so it cannot be used to distinguish between bosons and fermions. It is worth saying that the similarity does not end here. It turns out that quantum one dimensional systems can be understood in the context of conformal field theory (CFT). The key quantity defining the Virasoro algebra of the quantum CFT is the so called central charge c. One dimensional free fermions and bosons share the same central charge $c = 1$, suggesting that an equivalence between them exists [111].

what follows it is convenient to use the identity $[A, CD] = \{A, C\}D - C\{A, D\}$ connecting commutators and anti-commutators in order to obtain

$$\left[b_{q,\eta}, b^\dagger_{q',\eta'}\right] = \frac{1}{n_q}\sum_{k,k'}\left[c^\dagger_{k-q,\eta}c_{k,\eta}, c^\dagger_{k'+q',\eta'}c_{k',\eta'}\right] = \frac{1}{n_q}\sum_{k}\left(c^\dagger_{k+q'-q}c_k - c^\dagger_{k+q'}c_{k+q}\right). \tag{B.1.2}$$

Consider first the case $q \neq q'$; if we relabel $k \to k-q$ in the first term we correctly obtain the vanishing of the commutator. However, when $q = q'$ we obtain again the vanishing of the commutator when performing the above relabeling. This apparent paradox is due to the fact that, in the absence of a cutoff, the theory is not bounded from below. There are two ways of solving this problem, the first one consists in introducing normal ordered operators, while the second one consists in considering explicitly the physical cutoff of the theory[2] (2.1).

Normal ordering defines the action of an operator with respect to the ground state of the theory and is denoted by two columns, $:c^\dagger_k c_k: = c^\dagger_k c_k - \langle 0|c^\dagger_k c_k|0\rangle$. In our case we find for $q = q'$:

$$\left[b_{q,\eta}, b^\dagger_{q',\eta'}\right] = \frac{1}{n_q}\sum_{k}\left(:c^\dagger_k c_k: - :c^\dagger_{k+q}c_{k+q}: + \langle 0|c^\dagger_k c_k|0\rangle - \langle 0|c^\dagger_{k+q}c_{k+q}|0\rangle\right). \tag{B.1.3}$$

Since the normal ordered operators are now well defined objects, we can safely relabel $k+q \to k$. We are then left with the ground state expectations

$$\frac{1}{n_q}\sum_{k=-\infty}^{\infty}\left(\langle 0|c^\dagger_k c_k|0\rangle - \langle 0|c^\dagger_{k+q}c_{k+q}|0\rangle\right) = \frac{1}{n_q}\left(\sum_{n_k=-\infty}^{0} - \sum_{n_k=-\infty}^{-n_q}\right) = 1, \tag{B.1.4}$$

that is indeed the correct result.

In the second case we consider a bounded fermionic spectrum $k \in [-\Lambda, \Lambda]$. Since we are looking for an operator identity, Eq. (B.1.2) should be valid irrespectively of the specific cutoff we are considering. It is convenient to work again with the ground state, for $q = q'$ we find

$$\langle 0|\left[b_{q,\eta}, b^\dagger_{q',\eta'}\right]|0\rangle = \frac{1}{n_q}\sum_{k=-\Lambda}^{\Lambda}\langle 0|c^\dagger_k c_k - c^\dagger_{k+q}c_{k+q}|0\rangle = \frac{1}{n_q}\left(\sum_{n_k=-\Lambda}^{0} - \sum_{n_k=-\Lambda}^{-n_q}\right) = 1. \tag{B.1.5}$$

Since the Fermi sea is now bounded, when performing the change of variables $k+q \to k$ the correct result is obtained.

2 In chapter 2 we have been very careful in defining the energy and momentum cutoff of the low energy theory. However, when evaluating various propagators, we have exchanged the hard cutoff for a soft one and performed the integration over the entire spectrum of k and q. If we want to be consistent with this approach, we should work with normal ordered operators and a soft cutoff. However, it is instructive to consider the role of the hard cutoff in the evaluation of the commutators, and this is the main reason why we presented it here.

B.1.1 Vertex Representation of fermionic fields

The representation of fermionic fields in terms of a bosonic coherent state can be considered as the central bosonization identity. Here we consider a derivation of this relation using the operator formalism. Consider the mode decomposition of a fermionic field Eq. (2.1.8); if we choose to work with a left moving field we have

$$\psi(x) = \sqrt{\frac{2\pi}{L}} \sum_{k=-\infty}^{\infty} e^{-\imath k x} c_k, \tag{B.1.6}$$

the commutation relation of ψ with b_q is

$$[b_q, \psi(x)] = \sum_{k,k'} \sqrt{\frac{2\pi}{L n_q}} e^{-\imath k' x} \left[c^\dagger_{k-q} c_k, c_{k'}\right] = \alpha_q(x)\psi(x), \tag{B.1.7}$$

where $\alpha_q(x) = \imath e^{\imath q x}/\sqrt{n_q}$. If $|N\rangle_0$ is the bosonic many-particle ground state with $b_q|N\rangle_0 = 0$, then $[b_q, \psi(x)]\ |N\rangle_0 = b_q\psi(x)|N\rangle_0$. Using Eq. (B.1.7) we then have

$$b_q\psi(x)|N\rangle_0 = \alpha_q(x)\psi(x)|N\rangle_0, \tag{B.1.8}$$

that means $\psi(x)$ is an eigenstate of the bosonic ladder operator with eigenvalue $\alpha_q(x)$; this also means that $\psi(x)|N\rangle_0$ can be represented in the basis of bosonic coherent states. However, when adopting this interpretation a first problem arises : the ψ field is removing an electron from the many particle ground state, while b only destroys a p-h excitation. As explained in (2.1.2) this problem is solved by introducing the Klein factor $F_\eta = \chi_\eta e^{\imath\theta_\eta}$, χ_η is a Majorana fermionic field satisfying:

$$\{\chi_\eta, \chi_{\eta'}\} = 2\delta_{\eta,\eta'} \quad , \quad \chi_\eta^2 = 1 \tag{B.1.9}$$

and θ_η is the phase operator canonically conjugate to $\Delta N_\eta = N_\eta - N_{0,\eta}$

$$\left[\Delta N_\eta, \imath\theta_{\eta'}\right] = \delta_{\eta,\eta'}. \tag{B.1.10}$$

Using the Klein factor and Eq. (B.1.8), we arrive at

$$\psi(x)|N\rangle_0 = e^{-\sum_{q>0}\alpha_q(x)b_q} F\lambda|N\rangle_0 = e^{-\imath\varphi(x)} F\lambda|N\rangle_0. \tag{B.1.11}$$

The proportionality factor λ can be found to be proportional to the zero mode $\lambda = \sqrt{2\pi/L}e^{-\imath\pi\Delta N x/L}$[46]. Finally, by evaluating the action of ψ over a general many particle state $|N\rangle$ we arrive at the final expression (2.1.37).

B.1.2 Evaluation of expectation values

While in the last sections we have dealt with operator identities, here we will focus our attention on the evaluation of expectation values of vertex operators according to some given distribution function. We present two different proofs of Eq (2.1.42): the first one uses an operator approach and an equilibrium density matrix while the second one uses the Gaussian

property of the functional integral. Note that the Gaussian property of the functional integral is due to its equilibrium nature and, as we show in (2.2) and (B.2) below, it does not hold out of equilibrium. Nevertheless, when treating equilibrium problems, the functional integral approach is not only very general and useful to derive expectations of multiple vertex operators, but it also highlights some important physical properties of the electron gas. We start by reminding ourselves of the following standard formulas : if Z is a bosonic partition function, then

$$Z = \mathrm{Tr}\, e^{-\beta \sum_j \omega_j b_j^\dagger b_j} = \prod_j \sum_{\{m_j\}} \langle m_j | e^{-\beta \omega_j b_j^\dagger b_j} | m_j \rangle, \tag{B.1.12}$$

where $\beta = 1/K_B T$ and $|m_j\rangle$ are eigenstates of the free bosonic Hamiltonian $H_0 = \sum_j \omega_j b_j^\dagger b_j$ for every mode j. If we define $n_j = e^{-\beta\omega_j}$, then

$$Z = \prod_j \sum_{m_j=0}^{\infty} n^{m_j} = \prod_j \frac{1}{1-n_j}. \tag{B.1.13}$$

The expectation value of the number operator is readily found

$$\begin{aligned} \langle b^\dagger b \rangle &\equiv \mathrm{Tr}\left(\hat{\rho} b^\dagger b\right) = Z^{-1} \prod_j \sum_{\{m_j\}} \langle m_j | e^{-\beta\omega_j b_j^\dagger b_j} b_j^\dagger b_j | m_j \rangle = Z^{-1} \prod_j \sum_{m=1}^{\infty} n^{m_j} m_j \\ &= \prod_j \frac{1}{n_j^{-1} - 1} = \prod_j \frac{1}{e^{\beta\omega_j} - 1}. \end{aligned} \tag{B.1.14}$$

Using the Baker-Haussdorf formula $e^A e^B = e^{[A,B]/2} e^B e^A$ we can rewrite Eq. (2.1.38) as follows

$$C_\psi(x) = \frac{1}{2\pi\alpha} e^{[\phi(x),\phi(0)]/2} \mathrm{Tr}\left\{\hat{\rho}_B e^{-\imath[\phi(x)-\phi(0)]}\right\}. \tag{B.1.15}$$

The first term is a commutator and does not depend on the specific density matrix we use. In the above expression we have substituted the equilibrium fermionic density matrix with an equilibrium bosonic density matrix. Although this substitution is correct in equilibrium, it does not trivially hold out of equilibrium. Using Eq. (2.1.16) we can rewrite the difference of bosonic fields in the exponent as :

$$\begin{aligned} -\imath[\phi(x) - \phi(0)] &= \sum_{q>0} \sqrt{\frac{2\pi}{qL}} e^{-q\alpha/2} \left\{-\imath\left(e^{\imath q x} - 1\right) b_q - \imath\left(e^{-\imath q x} - 1\right) b_q^\dagger\right\} \\ &= \sum_{q>0} \lambda_q^*(x) b_q^\dagger - \sum_{q>0} \lambda_q(x) b_q \\ \lambda_q(x) &= \imath\sqrt{\frac{2\pi}{qL}} \left(e^{\imath q x} - 1\right) e^{-q\alpha/2}. \end{aligned} \tag{B.1.16}$$

The Trace can be evaluated as follows (here the index q and the summation over it is everywhere implied):

$$\begin{aligned}\mathrm{Tr}\left\{\hat{\rho}_B e^{-\imath(\phi(x)-\phi(0))}\right\} &= Z^{-1}\mathrm{Tr}\left\{e^{-\beta\omega b^\dagger b}e^{\lambda^* b^\dagger-\lambda b}\right\} \\ &= Z^{-1}\sum_{m=0}^{\infty}\langle m|e^{-\beta\omega b^\dagger b}e^{-\lambda\lambda^*[b,b^\dagger]/2}e^{\lambda^* b^\dagger}e^{-\lambda b}|m\rangle \\ &= Z^{-1}e^{-\lambda\lambda^*/2}\sum_{m=0}^{\infty}\sum_{l,l'=0}^{\infty}\langle m|e^{-\beta\omega b^\dagger b}\frac{(\lambda^*)^l(-\lambda)^{l'}}{l!\,l'!}(b^\dagger)^l(b)^{l'}|m\rangle.\end{aligned} \tag{B.1.17}$$

Here $|m\rangle$ are eigenstates of the harmonic oscillator satisfying $b|m\rangle = \sqrt{m}\,|m-1\rangle$ and $b^\dagger|m-1\rangle = \sqrt{m}\,|m-1\rangle$. The repeated action of b over $|m\rangle$ generates

$$b^{l'}|m\rangle = \sqrt{m}b^{l'-1}|m-1\rangle = \sqrt{m}\,\sqrt{m-1}\,\sqrt{m-2}\ldots\sqrt{m-l'-1}\,|m-l'\rangle \tag{B.1.18}$$

If $m \geqslant l'$, or 0 otherwise. When acting with $(b^\dagger)^l$ the trace will be zero unless the number of destruction and creation operators is the same i.e. $l = l'$.

$$\begin{aligned}(\text{B.1.17}) &= Z^{-1}e^{-\lambda\lambda^*/2}\sum_{m=l}^{\infty}\sum_{l,=0}^{\infty}n^m\frac{m!}{(m-l)!\,l!}\frac{(-\lambda^*\lambda)^l}{l!} \\ &= Z^{-1}e^{-\lambda\lambda^*/2}\sum_{l,=0}^{\infty}\frac{(-\lambda^*\lambda)^l}{l!}\sum_{m=l}^{\infty}n^m\begin{pmatrix} m \\ l\end{pmatrix} \\ &= Z^{-1}e^{-\lambda\lambda^*/2}\sum_{l,=0}^{\infty}\frac{(-\lambda^*\lambda)^l}{l!}\sum_{m=l}^{\infty}n^{m'+l}\begin{pmatrix} m'+l \\ l\end{pmatrix}\end{aligned} \tag{B.1.19}$$

where in the last line we have set $m' = m - l$. Now we can use some properties of the binomial coefficient, namely

$$\begin{pmatrix} m'+l \\ l\end{pmatrix} = \begin{pmatrix} m'+l \\ m'\end{pmatrix} \quad , \quad \sum_{m'=0}^{\infty}n^{m'}\begin{pmatrix} m'+l \\ m'\end{pmatrix} = \frac{1}{(1-n)^{l+1}}. \tag{B.1.20}$$

Using the above relations we find

$$(\text{B.1.19}) = Z^{-1}e^{-\lambda\lambda^*/2}\sum_{l,=0}^{\infty}\frac{(-\lambda^*\lambda\,n)^l}{l!(1-n)^{l+1}} = Z^{-1}e^{-\lambda\lambda^*/2}\sum_{l,=0}^{\infty}\frac{(-\lambda^*\lambda)^l}{l!(n^{-1}-1)^l}\frac{1}{(1-n)}. \tag{B.1.21}$$

Now we can use that $Z^{-1} = (1-n)$ and Eq. (B.1.14) to arrive at the final result

$$\mathrm{Tr}\left\{\hat{\rho}_B e^{-\imath(\phi(x)-\phi(0))}\right\} = e^{-\lambda\lambda^*/2}\sum_{l,=0}^{\infty}\frac{\langle b^\dagger b\rangle^l}{l!}(-\lambda^*\lambda)^l = e^{-\lambda\lambda^*/2}e^{-\lambda\lambda^*\langle b^\dagger b\rangle}, \tag{B.1.22}$$

that concludes the proof. Note that the main ingredients used in this proof are the equilibrium density matrix and the $|m\rangle$ as the eigenstates of the harmonic oscillator. Whenever the density matrix does not have an equilibrium form, the above formula is not valid as it is.

Let us consider now the functional integral approach. The Lagrangian density for a single edge mode is readily obtained from Eq. (A.4.5) taking $A_\mu = 0$, $K_{IJ} = m$ and $U_{IJ} = u$

$$\mathscr{L}_{0,\pm} = \frac{m}{4\pi}\partial_x\phi_\pm\left(\pm\partial_t\phi_\pm - u\partial_x\phi_\pm\right), \tag{B.1.23}$$

where $\pm$ labels right and left moving states. Note that as a consequence of the original fermionic chiral symmetry, the Lagrangian density (B.1.23) is invariant under $\phi \to \phi + \theta$, with θ an arbitrary constant. Physically this corresponds to the invariance of the original Fermionic system under a rigid displacement of the density field. Let us define a general vertex operator as[3] $V(q,x) \simeq e^{\imath q\phi(x)}$, where q is some pre-factor. Then we can use the functional integral representation of the expectation value of n vertex operators

$$\langle V(q_1,x_1)V(q_2,x_2)...V(q_n,x_n)\rangle_0 = Z^{-1}\int \mathscr{D}\phi e^{\imath S_0[\phi]}e^{\imath\sum_{j=1}^n q_j\phi(x_j)}, \tag{B.1.24}$$

where S_0 is the action correponding to the Lagrangian density $\mathscr{L}_0$ and Z is the partition function. If we now perform a rigid translation of the fields $\phi \to \phi + \theta$ we see that in order for the correlator to have the same symmetry of the action, the following condition must be satisfied:

$$\sum_{j=1}^n q_j = 0, \tag{B.1.25}$$

known as the charge-neutrality condition[4]. The idea now is that the vertex operator looks like a source term for the Gaussian integral. To make this explicit we define the source field

$$J(x) = \sum_{j=1}^n q_j\delta(x - x_j). \tag{B.1.26}$$

Using Gaussian integration we can obtain the desired result

$$\begin{aligned}\langle V(q_1,x_1)V(q_2,x_2)...V(q_n,x_n)\rangle_0 &= Z^{-1}\int \mathscr{D}\phi e^{\imath\int_x\left(\frac{-1}{2}\phi(x)G^{-1}(x)\phi(x)+J(x)\phi(x)\right)} \\ &= e^{\frac{1}{2}\int_{x,x'}J(x)G(x-x')J(x')} = e^{\frac{1}{2}\sum_{j,k=1}^n q_jq_kG(x_j-x_k)}.\end{aligned} \tag{B.1.27}$$

Where $G = 2\pi/[m(\partial_t - u\partial_x)]$. We can separate terms into $j = k$ and $j \neq k$ and obtain

$$\frac{1}{2}\sum_{j,k=1}^n q_jq_kG(x_j-x_k) = \frac{1}{2}\sum_{j=1}^n q_j^2G(0) + \sum_{j>k=1}^n q_jq_kG(x_j-x_k) = \sum_{j>k=1}^n q_jq_kG(x_j-x_k), \tag{B.1.28}$$

where in the last equality we have used the charge-neutrality condition.

3 Here we do not carry the normalization factor for notational simplicity.

4 The name comes from the fact that the expectation value of vertex operators has the same form of the partition function of the Coulomb gas, where q_js are the charges.

B.1.3 Finite temperature Green function

Here we consider the evaluation of the fermionic Green function at finite temperature making use of the bosonization approach. For simplicity we consider a non-interacting system, but the result can be trivially generalized to an interacting one. Consider the equal time propagator Eq. (B.1.15); using Eq. (B.1.22) and the results of section (2.1.4), this can be brought in the particularly useful form

$$C_\psi(x) = \frac{\imath}{2\pi}\frac{1}{x+\imath\alpha}e^{-\sum_q \lambda_q\lambda_q^* n(q)}, \tag{B.1.29}$$

where $n(q)$ is the equilibrium bosonic distribution. Using Eq. (B.3.8) the exponent can be conveniently manipulated as follows

$$\begin{aligned}\sum_{q>0}\lambda_q\lambda_q^* n(q) &= \sum_{q>0}\frac{2\pi}{qL}|e^{\imath qx}-1|^2 n(q)e^{-q\alpha} \\ &= \int_0^\infty \frac{dq}{q}(1-e^{\imath qx})e^{-q\alpha}n(q) + \int_0^\infty \frac{dq}{q}(1-e^{-\imath qx})e^{-q\alpha}n(q) \\ &= \int_0^\infty \frac{dq}{q}(1-e^{\imath qx})e^{-q\alpha}n(q) + \int_0^{-\infty} \frac{dq}{q}(1-e^{\imath qx})e^{q\alpha}n(-q).\end{aligned} \tag{B.1.30}$$

Using the symmetry of the bosonic distribution $n(-q) = -(1+n(q))$ we obtain

$$\begin{aligned}(\text{B.1.30}) &= P\int_0^\infty \frac{dq}{q}(1-e^{\imath qx})e^{-q\alpha}n(q) + P\int_0^\infty \frac{dq}{q}(1-e^{\imath qx})e^{q\alpha}(1+n(q)) \\ &\simeq P\int_{-\infty}^\infty \frac{dq}{q}(1-e^{\imath qx})e^{-q\alpha}n(q) + \sum_{q<0}\frac{2\pi}{qL}(1-e^{\imath qx})e^{-q\alpha} = I_1 + I_2.\end{aligned} \tag{B.1.31}$$

Note that in the last term of the last line we went back to a sum over discrete momenta. Consider first the I_1 integral containing the distribution function

$$I_1 = \int_{-\infty}^\infty \frac{dq}{q}\frac{1-e^{\imath qx}}{e^{\beta u q}-1}e^{-q\alpha}, \tag{B.1.32}$$

where β is the inverse temperature. This integral has poles at $q_n = \imath 2\pi n/\beta u$. For $n \neq 0$ all the poles are simple while for $n = 0$ there is a second order pole due to the contribution of the $1/q$ term. Upon analytic continuation $q_n \to z_n$ and using Jordan's lemma, the integral can be evaluated using the contour shown in Fig. (41).

$$\begin{aligned}I_1 &= \oint_\Gamma \frac{dz}{z}\frac{1-e^{\imath zx}e^{-z\alpha}}{e^{\beta u z}-1} = 2\pi\imath\sum_{n=1}^\infty \frac{1}{z_n}\frac{(1-e^{\imath z_n x})e^{-z_n\alpha}}{\beta u e^{\beta u z_n}} + \frac{\imath\pi}{\beta u}\left[\partial_{z_j}(1-e^{\imath z_j x})e^{-z_j\alpha}\right]_{z_j=0} \\ &= \sum_{n=1}^\infty \frac{\left(1-e^{-\left(\frac{2\pi}{\beta u}\right)nx}\right)e^{-\left(\frac{2\pi\imath}{\beta u}\right)n\alpha}}{n} + \frac{\pi x}{\beta u} = \log\frac{\left(1-e^{-\frac{2\pi}{\beta u}(x+\imath\alpha)}\right)}{\left(1-e^{-\frac{-2\pi\imath}{\beta u}\alpha}\right)} + \frac{\pi x}{\beta u} \\ &\simeq -\log\frac{\imath\pi\alpha/\beta u}{\sinh\left(\frac{\pi}{\beta u}(x+\imath\alpha)\right)}.\end{aligned} \tag{B.1.33}$$

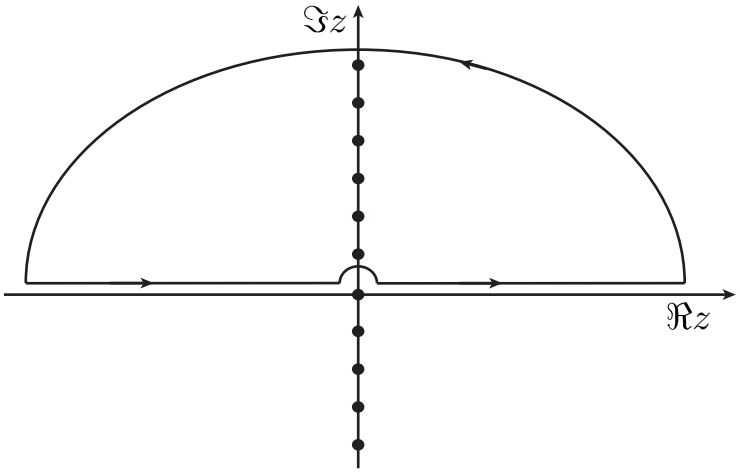

Figure 41: Integration contour for the finite temperature Green function. The integration contour is defined in the upper half plane in complex space. Simple poles are situated at $z_n = \imath 2\pi n/\beta u$ for $n \neq 0$. For $n = 0$ there is a second order pole due to the contribution of the $1/z_n$ term in the integral, corresponding to the small half circle around the origin.

In the last equality above we have considered the $\alpha \ll 1$ limit. Next we evaluate the I_2 term using $q = 2\pi n/L$

$$\begin{aligned} I_2 &= \sum_{n=-\infty}^{-1} \frac{1}{n} \left\{ e^{-\frac{2\pi\alpha}{L} n} - e^{\frac{2\pi}{L} n(\imath x - \alpha)} \right\} \\ &= \log\left(1 - e^{\frac{2\pi\alpha}{L}}\right) - \log\left(1 - e^{\frac{2\pi}{L}(-\imath x + \alpha)}\right) \\ &\simeq -\log \frac{-\imath x + \alpha}{\alpha}, \end{aligned} \tag{B.1.34}$$

where in the last line we have taken the $L \gg x$ limit. Using the results for I_1 and I_2 in Eq. (B.1.29) we finally find

$$C_\psi(x) = \frac{\imath}{2\pi} \frac{\pi T/u}{\sinh\left[\frac{\pi T}{u}(x + \imath\alpha)\right]}, \tag{B.1.35}$$

that is the known result for free fermions at finite temperature. Consider now the Fourier transform of the finite temperature Green function in the $\alpha \to 0$ limit

$$\lim_{\alpha\to 0} \int_{-\infty}^{\infty} dk\, e^{\imath kx} \frac{\imath}{2\pi} \frac{\pi T/u}{\sinh\left[\frac{\pi T}{u}(x + \imath\alpha)\right]} = \frac{1}{2}\left[1 - \tanh\left(\frac{\epsilon}{k_B T}\right)\right] = f(\epsilon), \tag{B.1.36}$$

where in the second equality we have reinstated $\hbar$ and k_B and used $\epsilon = \hbar u k$. The above Fourier transform correctly gives the finite temperature Fermi distribution function. When the system is interacting, Eq. (B.1.36) contains higher order poles when the Luttinger parameter is an integer number (that is the case of a FHQ state), or branch cuts in case it is a rational number. Taking the Fourier transform of the interacting propagator, we will obtain the exact distribution function of interacting fermions.

B.2 GOING OUT OF EQUILIBRIUM AND EVALUATING LOOPS

In section (2.2.1) we have derived a general formula for the loop expansion of the generating function of free, one dimensional fermions out of equilibrium. The $n = 1$ term cancels against the background (charge neutrality) while the $n = 2$ represents particle-hole fluctuations over the ground state. The $n = 2$ term corresponds to the bubble diagram of Fig. (8), where now the lines in the loop are of three different "species", advanced (a), retarded (r) and Keldysh (K). If we "cut" the external (wavy) lines we obtain the so called polarization operator. In Keldysh space this is given by (x here is a space-time point and all the Green functions are undressed, i.e. $G = G_0$)

$$\begin{aligned} \Pi^{r,a} &= \frac{-\imath}{2}\left\{G^{r,a}(x,x')G^{K}(x',x) + G^{a,r}(x,x')G^{K}(x,x')\right\} \\ \Pi^{K} &= \frac{-\imath}{2}\left\{G^{K}(x,x')G^{K}(x',x) + G^{r}(x,x')G^{a}(x,x') + G^{a}(x,x')G^{r}(x,x')\right\}. \end{aligned} \tag{B.2.1}$$

In order to evaluate the above expression it is convenient to move to energy momentum space; we denote the internal loop variables by ϵ and p, and the external ones by q and ω. Using the energy-momentum representation of the Green functions Eq. (2.2.7), we find for the advanced component of the polarization operator

$$\begin{aligned} \Pi^{a}(q,\omega) &= \frac{-\imath}{2}\int_{-\infty}^{\infty}\frac{d\epsilon\, dp}{(2\pi)^2}\left\{G^{r}(p,\epsilon)G^{K}(p+q,\epsilon+\omega) + G^{a}(p+q,\epsilon+\omega)G^{K}(p,\epsilon)\right\} \\ &= \frac{-\imath}{2}\int_{-\infty}^{\infty}\frac{d\epsilon\, dp}{(2\pi)^2}\Big\{\frac{1-2f(\epsilon+\omega)}{\epsilon-u\,p+\imath 0^{+}}\left[G^{r}(p+q,\epsilon+\omega) - G^{a}(p+q,\epsilon+\omega)\right] \\ &+ \frac{1-2f(\epsilon)}{\epsilon+\omega-u(p+q)-\imath 0^{+}}\left[G^{r}(p,\epsilon) - G^{a}(p,\epsilon)\right]\Big\} \\ &= \frac{1}{2\pi u}\int_{\epsilon}\frac{f(\epsilon+\omega)-f(\epsilon)}{-\omega+u\,q+\imath 0^{+}}. \end{aligned} \tag{B.2.2}$$

In order to move from the second to the third line we have used the identity

$$\left[G^{r}(p,\epsilon) - G^{a}(p,\epsilon)\right] = (-2\pi\imath)\delta(\epsilon - u\,p), \tag{B.2.3}$$

and integrated over the internal momentum. As shown in Fig. (42) the integral over energy depends only on the energy shift between the two distribution functions, therefore the polarization operator is temperature independent. Moreover, this result does not depend on the precise form of the distribution function. We can show this explicitly by performing the energy integral first with a thermal distribution function, and then with a double step distribution at zero temperature.

$$\begin{aligned} \int_{\epsilon}\left[f(\epsilon+\omega)-f(\epsilon)\right] &= \int_{-\infty}^{\infty}d\epsilon\left[\frac{1}{e^{\beta(\epsilon+\omega)}+1} - \frac{1}{e^{\beta(\epsilon)}+1}\right] \\ &= \int_{0}^{\infty}\frac{d\gamma}{\beta\,\gamma}\left[\frac{1}{\gamma\,\xi+1} - \frac{1}{\gamma+1}\right] = \frac{\beta\,\omega}{\beta}. \end{aligned} \tag{B.2.4}$$

To solve the above integral we have used the change of variables $\gamma = e^{\beta\,\epsilon}$ and $\xi = e^{\beta\,\omega}$. We can perform the same calculation using now the non-equilibrium distribution

$$f(\epsilon) = a\,\theta(-\epsilon+\mu_1) + (1-a)\,\theta(-\epsilon+\mu_2), \tag{B.2.5}$$

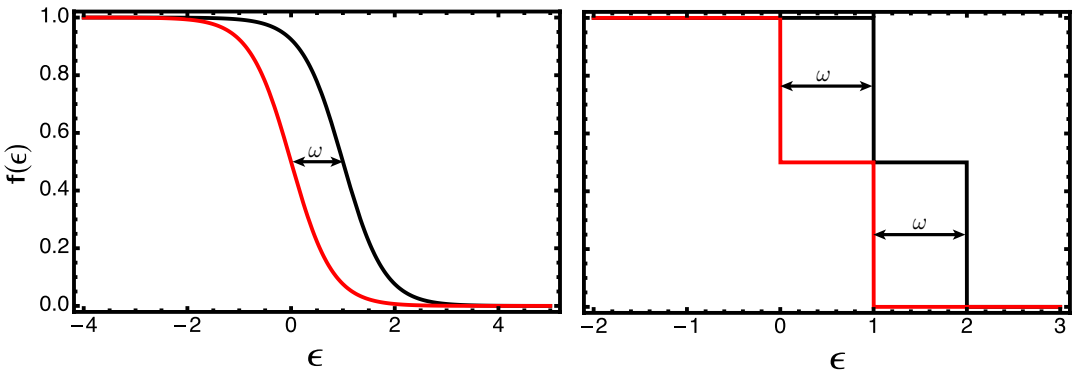

Figure 42: Fermi functions appearing in the retarded and advanced polarization operator. (left) Thermal Fermi distribution functions at temperature T shifted by an energy ω. (right) Non-equilibrium, double step Fermi distribution functions at zero temperature shifted by an energy ω. In both cases the integral in Eq. (B.2.2) involves only the area of width ω between the two curves.

and find

$$\begin{aligned}\int_\epsilon [f(\epsilon+\omega)-f(\epsilon)] &= \int_{-\infty}^{\infty} d\epsilon \Big\{ a\,[\theta(-\epsilon-\omega+\mu_1)-\theta(-\epsilon+\mu_1)] \\ &+ (1-a)\,[\theta(-\epsilon-\omega+\mu_2)-\theta(-\epsilon+\mu_2)] \Big\} \\ &= a\,(\omega-\mu_1+\mu_1)+(1-a)\,(\omega-\mu_2+\mu_2)=\omega.\end{aligned} \tag{B.2.6}$$

Finally we obtain for both the advanced and retarded component

$$\Pi^{a,r}(q,\omega) = \frac{1}{2\pi u}\frac{\omega}{uq-\omega\pm\imath 0^+}, \tag{B.2.7}$$

independent of temperature and non-equilibrium effects. The Keldysh component turns out to be more interesting since it contains all the informations about the non-equilibrium state. In energy-momentum space we have

$$\begin{aligned}\Pi^K\ (q,\omega) &= \frac{-\imath}{2}\int_{-\infty}^{\infty}\frac{d\epsilon dp}{(2\pi)^2}\Big\{G^K(\epsilon+\omega,p+q)G^K(\epsilon,p)+G^R(\epsilon+\omega,p+q)G^a(\epsilon,p) \\ &+ G^a(\epsilon-\omega,p-q)G^r(\epsilon,p)\Big\} \\ &= \frac{-\imath}{2}\int_{-\infty}^{\infty}\frac{d\epsilon dp}{(2\pi)^2}\Big\{[1-2f(\epsilon+\omega)]\,[1-2f(\epsilon)]\,(-2\pi\imath)^2\delta(\epsilon+\omega-u(p+q))\delta(\epsilon-uq) \\ &+ \frac{1}{\epsilon+\omega-u(p+q)+\imath 0^+}\frac{1}{\epsilon-up-\imath 0^+}+\frac{1}{\epsilon-\omega-u(p-q)-\imath 0^+}\frac{1}{\epsilon-up+\imath 0^+}\Big\}.\end{aligned} \tag{B.2.8}$$

The first integral can be solved using the property of the Dirac delta function

$$(-2\pi\imath)^2\int_{-\infty}^{\infty}\frac{dp}{2\pi}\delta(\epsilon+\omega-u(p+q))\delta(\epsilon-up)=\frac{-2\pi}{u}\delta(\omega-uq), \tag{B.2.9}$$

together with the symmetry property $\delta(-x)=\delta(x)$. The integrals involving a combination of retarded and advanced Green functions can be solved in the standard way using the residue

theorem and the fact that the Green function is a meromorphic function. Choosing to close the contour in the lower half plane we find

$$\int_{-\infty}^{\infty} \frac{dp}{2\pi} \frac{1}{\epsilon + \omega - u(p+q) + \imath 0^+} \frac{1}{\epsilon - up - \imath 0^+} = \frac{-\imath}{u} \frac{1}{-\omega + uq - \imath 0^+}. \tag{B.2.10}$$

We note that this term can be rewritten in terms of the retarded polarization Eq. (B.2.7). Using Eq. (B.2.9) and (B.2.10) in Eq. (B.2.8) we arrive at Eq. (2.2.11)

$$\begin{aligned} \Pi^K(\omega, q) &= [\Pi^r(\omega, q) - \Pi^a(\omega, q)]\, B(\omega), \\ B(\omega) &= \frac{1}{\omega} \int_\epsilon f(\epsilon)\{2 - f(\epsilon + \omega) - f(\epsilon - \omega)\}. \end{aligned} \tag{B.2.11}$$

Here $B(\omega)$ is a general bosonic distribution resulting from an initial fermionic distribution. If the fermions have an initial equilibrium distribution we find

$$\begin{aligned} B(\omega) &= \frac{1}{\omega} \int_{-\infty}^{\infty} \frac{d\epsilon}{e^{\beta\epsilon} + 1} \left\{ 2 - \frac{1}{e^{\beta(\epsilon+\omega)} + 1} - \frac{d\epsilon}{e^{\beta(\epsilon-\omega)} + 1} \right\} \\ &= \frac{1}{\omega} \left\{ \frac{\omega}{e^{\beta\omega} + 1} + \frac{\omega e^{\beta\omega}}{e^{\beta\omega} - 1} \right\} = 1 + 2n(\omega). \end{aligned} \tag{B.2.12}$$

The integral above has been evaluated using the usual change of variables $\gamma = e^{\beta\epsilon}$ and $\xi = e^{\beta\omega}$ and using a partial fraction decomposition

$$\begin{aligned} \int_{-\infty}^{\infty} d\epsilon \frac{1}{e^{\beta\epsilon} + 1} \frac{1}{e^{\beta(\epsilon+\omega)} + 1} &= \int_0^{\infty} \frac{d\gamma}{\beta\gamma} \frac{1}{1 - \xi} \left\{ \frac{1}{1 + \gamma} - \frac{1}{1 + \xi\gamma} \right\} \\ &= \frac{1}{\beta} \frac{\log \xi}{1 - \xi}. \end{aligned} \tag{B.2.13}$$

Now we consider a non-equilibrium situation and take as the initial non-equilibrium fermionic configuration the double step, zero temperature distribution

$$f(\epsilon) = a\, f(\epsilon - \mu_1) + (1 - a)\, f(\epsilon - \mu_2), \tag{B.2.14}$$

and compute Eq. (B.2.11)

$$\begin{aligned} B(\omega) &= \frac{1}{\omega} \int_{-\infty}^{\infty} d\epsilon \Big\{ a^2 f(\epsilon - \mu_1) f(-\epsilon - \omega + \mu_1) + (1 - a)^2 f(\epsilon - \mu_2) f(-\epsilon - \omega + \mu_1) \\ &+ a(1 - a)\left[f(\epsilon - \mu_1) f(-\epsilon - \omega + \mu_2) + f(\epsilon - \mu_2) f(-\epsilon - \omega + \mu_1) \right] \Big\}. \end{aligned} \tag{B.2.15}$$

Integrals here are similar to the one in (B.2.13) and we arrive at the final result

$$B(\omega) = (a^2 + (1 - a)^2) n(\omega) + a(1 - a) \left\{ \left(1 + \frac{\Delta\mu}{\omega} \right) n(\omega + \Delta\mu) + \left(1 - \frac{\Delta\mu}{\omega} \right) n(\omega - \Delta\mu) \right\}, \tag{B.2.16}$$

that is what we found in Eq. (5.4.13) using the operator approach.

B.2.1 Third order loops

The next step consists in looking at the behavior of the third-order correlator $\mathcal{S}_3$. It turns out that this task is most easily accomplished in the original basis of the Green functions (i.e. before the Keldysh rotation), the two representations being related by $\tilde{G}_0 = U^{-1}\hat{G}_0 U\sigma_3$, where the transformation matrix U has been defined in Eq. (2.2.4) and σ_3 is the third Pauli matrix. The third order correlator is given by

$$\mathcal{S}_3(x_1,x_2,x_3) = \langle T_K \rho(x_1)\rho(x_2)\rho(x_3)\rangle = \langle T_K \psi^\dagger(x_1)\psi(x_1)\psi^\dagger(x_2)\psi(x_2)\psi^\dagger(x_3)\psi(x_3)\rangle, \quad \text{(B.2.17)}$$

We can define the above correlator on the time-loop contour by introducing a Keldysh index $\sigma_i = \pm$ specifying on which branch the fermionic fields are defined. Using Wick's theorem we find

$$\begin{aligned} -\imath\mathcal{S}_3(x_1,x_2,x_3) &= G^{\sigma_1\sigma_2}(x_1,x_2)G^{\sigma_2\sigma_3}(x_2,x_3)G^{\sigma_3\sigma_1}(x_3,x_1) \\ &+ G^{\sigma_1\sigma_3}(x_1,x_3)G^{\sigma_3\sigma_2}(x_3,x_2)G^{\sigma_2\sigma_1}(x_2,x_1) \end{aligned} \quad \text{(B.2.18)}$$

Let us first choose $\sigma_1 = \sigma_2 = +$ and $\sigma_3 = -$. Moving to energy momentum space and using the following definitions for the Green functions

$$G^{+-}(\epsilon,p) = 2\pi\imath\,\delta(\epsilon - up)\,f(\epsilon) \quad \text{(B.2.19)}$$

$$G^{-+}(\epsilon,p) = -2\pi\imath\,\delta(\epsilon - up)\,(1-f(\epsilon)) \quad \text{(B.2.20)}$$

$$G^{++}(\epsilon,p) = -2\pi\imath\,\delta(\epsilon - up)\,(1-2f(\epsilon)), \quad \text{(B.2.21)}$$

we find

$$\begin{aligned} -\imath\ \mathcal{S}_3 &= (2\pi)^3\int_{-\infty}^{\infty}\frac{d\epsilon\,dp}{(2\pi^2)}\Big\{[1-2f(\epsilon+\omega_1)]\,\delta(\epsilon+\omega_1-u(p+q_1))f(\epsilon+\omega_1+\omega_2) \\ &\times\ \delta(\epsilon+\omega_1+\omega_2-u(p+q_1+q_2))\,[1-f(\epsilon)]\,\delta(\epsilon-up) \\ &+\ f(\epsilon+\omega_1+\omega_2)\delta(\epsilon+\omega_1+\omega_2-u(p+q_1+q_2))\,[1-f(\epsilon)]\,\delta(\epsilon-up) \\ &\times\ [1-2f(\epsilon+\omega_2)]\,\delta(\epsilon+\omega_2-u(p+q_2))\Big\} \\ &= \frac{4\pi}{u}\delta(\xi_1)\delta(\xi_2)\int_{-\infty}^{\infty}d\epsilon\,f(\epsilon+\omega_1+\omega_2)\,[1-f(\epsilon)]\,[1-f(\epsilon+\omega_2)-f(\epsilon+\omega_2)]\,. \end{aligned} \quad \text{(B.2.22)}$$

In the above expression we have defined $\xi_i = \omega_i - uq_i$. The above term is represented by the two diagrams in Fig. (12). For the sake of simplicity consider now the zero temperature equilibrium situation, then the above integral over the internal energy is identically zero since none of the constraints imposed by the theta functions can be simultaneously satisfied. The same result is true at finite temperature, even though more lengthy to obtain. Out of equilibrium however, the above term is different from zero. These considerations can be extended to higher order loops and prove the initial statement that non-equilibrium effects result in a non-Gaussian theory.

B.3 FULL COUNTING STATISTICS AND KLICH'S TRACE FORMULA

In this section we provide a complete derivation of the Levitov-Lesovik formula of electron full counting statistics. In the original derivation [112] the authors imagined a spin "galvanometer" embedded into a mesoscopic device. When tracing out the spin degrees of freedom, an effective parameter called the counting field appears in the description of the electronic part of the Hamiltonian. The counting field provides then a conceptual device for counting the number of electrons transmitted at a scatterer (being this the contact itself or an impurity). Here we will not follow the original derivation but instead the one proposed by Klich [113]. This derivation will prove particularly useful when considering the problem of non-equilibrium bosonization.

The starting point is the definition of the characteristic function we gave in Eq. (2.2.19); this can be rewritten in the following form

$$\Delta(\bar{\lambda},\tau)=\sum_{\bar{\alpha},\bar{\beta}} P[\bar{\alpha}(t=0),\bar{\beta}(t=\tau)]e^{\imath\frac{q}{2}\sum_i \lambda_i(\beta_i-\alpha_i)}, \tag{B.3.1}$$

where $\bar{\alpha}=(\alpha_1,\alpha_2,...,\alpha_n)$ and $\bar{\beta}=(\beta_1,\beta_2,...,\beta_n)$ label states in Fock space in the occupation number representation. Since we are working with fermions $\alpha_i=\beta_i=0,1$. Here $\bar{\lambda}=(\lambda_1,\lambda_2,...,\lambda_n)$ are the counting "fields", one for each state, q is the charge of the carriers and the factor of $1/2$ has been introduced for normalization reasons. Here, $(\beta_i-\alpha_i)=m$ is the number of electrons being transferred at the scatterer (the number of successes) and $P[\bar{\alpha}(t=0),\bar{\beta}(t=\tau)]$ is the probability that an electron initially in a state α_i is measured at time τ in a final state β_i. States at time $t=0$ and $t=\tau$ are related by a unitary evolution operator U such that $|\beta(t=\tau)\rangle=U(\tau,0)|\beta(t=0)\rangle$. In the interaction picture, the evolution operator reads

$$U(\tau,0)=e^{-\frac{\imath}{\hbar}\int_0^\tau dt\, H_I(t)}, \tag{B.3.2}$$

where $H_I(t)$ is a time dependent perturbation of the Hamiltonian. The transition probability is given by the modulus squared of the transition amplitude times the initial density matrix ρ_α, so Eq. (B.3.1) can be rewritten as follows

$$\begin{aligned}\Delta(\bar{\lambda},\tau) &= \sum_{\bar{\alpha},\bar{\beta}}|\langle\bar{\beta}(\tau)|\bar{\alpha}(0)\rangle|^2\rho_\alpha e^{\imath\frac{q}{2}\sum_i\lambda_i(\beta_i-\alpha_i)}=\sum_{\bar{\alpha},\bar{\beta}}|\langle\bar{\beta}|U^\dagger|\bar{\alpha}\rangle|^2\rho_\alpha e^{\imath\frac{q}{2}\sum_i\lambda_i(\beta_i-\alpha_i)}\\ &= \sum_{\bar{\alpha},\bar{\beta}}\langle\bar{\alpha}|\hat{\rho}|\bar{\alpha}\rangle\langle\bar{\alpha}|U^\dagger(0,\tau)e^{\imath\frac{q}{2}\sum_i\hat{\lambda}_i c_i^\dagger c_i}|\bar{\beta}\rangle\langle\bar{\beta}|U(\tau,0)e^{-\imath\frac{q}{2}\sum_i\hat{\lambda}_i c_i^\dagger c_i}|\bar{\alpha}\rangle\\ &= \mathrm{Tr}\left(\hat{\rho}U^\dagger e^{\imath\frac{q}{2}\sum_i\hat{\lambda}_i c_i^\dagger c_i}Ue^{-\imath\frac{q}{2}\sum_i\hat{\lambda}_i c_i^\dagger c_i}\right).\end{aligned} \tag{B.3.3}$$

The density matrix $\hat{\rho}$ is by definition diagonal in the α_i, with $\{\alpha_i\}$ an initial eigenstate of the Hamiltonian. Here we denote with $\hat{\lambda}$ the single particle operator whose eigenvalue is λ_i when acting on the single particle Hilbert space. Standard fermionic ladder operators $c^\dagger$, c have

been introduced. It is now convenient to define the one particle operator $\Gamma(\lambda) = \sum_i \hat{\lambda} c_i^\dagger c_i$ and perform a change of basis $c_i^\dagger = \sum_k c_k^\dagger \langle k|i\rangle$ to obtain

$$\Gamma(\lambda) = \sum_{k,j} \langle k|\hat{\lambda}|j\rangle c_k^\dagger c_j, \tag{B.3.4}$$

where now $\langle k|\hat{\lambda}|j\rangle$ is the Fock space version of the single particle operator $\hat{\lambda}$. First we use the above representation in Eq. (B.3.3), then we expand the exponentials involving the one particle operators, consider the action of the evolution operator term by term and then sum the series again. Since the evolution operator is a unitary operator, i.e. $U^\dagger U = 1$, Eq. (B.3.3) can be rewritten in the particularly useful form

$$\Delta(\bar{\lambda}, \tau) = \mathrm{Tr}\left(\hat{\rho} e^{\imath \frac{q}{2} U^\dagger \Gamma(\hat{\lambda}) U} e^{-\imath \frac{q}{2} \Gamma(\hat{\lambda})}\right). \tag{B.3.5}$$

B.3.1 Trace Formula

In order to evaluate Eq. (B.3.5), we give here a proof of Klich's trace formula. The starting point is the following form of the Baker-Haussdorf formula :

$$e^{\Gamma(A)} e^{\Gamma(B)} = e^{\Gamma(C)}, \tag{B.3.6}$$

with A, B, C matrices. We start by proving that if $C = [A, B]$, then $\Gamma(C) = [\Gamma(A), \Gamma(B)]$:

$$\begin{aligned}
[\Gamma(A), \Gamma(B)] &= \left[\sum_{i,j} \langle i|A|j\rangle c_i^\dagger c_j, \sum_{k,l} \langle k|B|l\rangle c_k^\dagger c_l\right] = \sum_{i,j,k,l} \langle i|A|j\rangle \langle k|B|l\rangle \left[c_i^\dagger c_j, c_k^\dagger c_l\right] \\
&= \sum_{i,j,k,l} \langle i|A|j\rangle \langle k|B|l\rangle \left(c_i^\dagger c_j \delta_{jk} - c_k^\dagger c_j \delta_{il}\right) = \sum_{i,l} \langle i|AB|l\rangle c_i^\dagger c_l - \sum_{k,j} \langle k|BA|j\rangle c_k^\dagger c_j \\
&= \sum_{i,l} \langle i|[A, B]|l\rangle c_i^\dagger c_l = \Gamma\left([A, B]\right),
\end{aligned} \tag{B.3.7}$$

where we have used Eq. (B.3.4) to represent the matrix elements of A and B. In what follows we will work within a finite dimensional Hilbert space, generalization to the infinite dimensional case can be found in [114]. Any matrix C can be brought in Jordan normal form, that is $C = \mathrm{diag}(\mu_1, \mu_2, ..., \mu_n) + K$, where K is an upper triangular matrix and μ_i are eigenvalues of C. Then

$$\begin{aligned}
\mathrm{Tr}\left(e^{\Gamma(C)}\right) &= \mathrm{Tr}\left(e^{\Gamma(\mathrm{diag}(\mu_1,\mu_2,...,\mu_n)+K)}\right) = \mathrm{Tr}\left(e^{\sum_i \mu_i c_i^\dagger c_i}\right) = \prod_i \left(\mathrm{Tr} \sum_{n=0}^{\infty} \frac{\mu_i^n}{n!} \left(c_i^\dagger c_i\right)^n\right) \\
&= \prod_i \left(1 + \mu_i \mathrm{Tr}\left\{c_i^\dagger c_i\right\} + \frac{\mu_i^2}{2} \mathrm{Tr}\left\{c_i^\dagger c_i\right\}^2 + ...\right) \\
&= \prod_i \left(1 + \left(1 + \mu_i + \frac{\mu_i^2}{2} + ... - 1\right) \mathrm{Tr}\left\{c_i^\dagger c_i\right\}\right) \\
&= \prod_i \left(1 + \left(e^C - 1\right) \mathrm{Tr}\left\{c_i^\dagger c_i\right\}\right) = \det\left(1 + \left(e^A e^B - 1\right) \mathrm{Tr}\left\{c_i^\dagger c_i\right\}\right)
\end{aligned} \tag{B.3.8}$$

where 1 is the identity matrix and we have used $\left(c_i^\dagger c_i\right)^2 = c_i^\dagger c_i$. We can now apply the trace formula to Eq. (B.3.5) to finally obtain

$$\begin{aligned}\Delta(\bar{\lambda},\tau) &= \mathrm{Tr}\left[\frac{e^{-\beta\Gamma(\mathscr{H}_0)}}{Z_0} e^{\imath\frac{q}{2}U^\dagger\Gamma(\bar{\lambda})U} e^{-\imath\frac{q}{2}\Gamma(\bar{\lambda})}\right] \\ &= \det\left[1+\left(U^\dagger e^{\imath q\lambda/2} U\, e^{-\imath q\lambda/2}-1\right)\mathrm{Tr}\left\{\frac{e^{-\beta\mathscr{H}_{0,i}}}{Z_{0,i}} c_i^\dagger c_i\right\}\right] \\ &= \det\left[1+\left(U^\dagger e^{\imath q\lambda/2} U e^{-\imath q\lambda/2}-1\right)F(\epsilon)\right].\end{aligned} \tag{B.3.9}$$

The determinant is evaluated with respect to the index i (the number of channels in Landauer terminology) and the trace is with respect the density matrix. The trace of the number operator with respect the density matrix gives the distribution function in channel i, that we generically represent as the diagonal matrix of Fermi distributions $F(\epsilon)$. The matrix elements of the counting field are defined as $e^{\imath q\lambda} = (e^{\imath q\lambda})_{ij}\delta_{ij}$ where δ_{ij} is the kronecker delta function and $\lambda_{kl} = -\lambda_{lk}$. Equation (B.3.9) is the most general form of the characteristic function of full counting statistics expressed in terms of a determinant of Fredholm type. The determinant formula derived above is an exact expression that in principle can be evaluated numerically once the evolution operator and the distribution function are known [115, 116]. In the next section we will consider a particularly useful approximation of the above determinant formula that allows for an insightful analytical result.

B.3.2 Long time limit and the Levitov-Lesovik formula

Consider now the specific situation of a mesoscopic system in which the right-/left-moving channels are coupled by a point scatterer, Fig. (14). If the scattering time is much smaller than the entire time over which the system evolves, we can consider the scattering amplitudes as energy-independent[5], that means we can replace the time dependent perturbation $H_I(t)$ with a time independent scattering matrix S [112]. Since the setup of Fig. (14) contains only two channels, the matrix space will be two dimensional. In this case the scattering matrix and the distribution functions of the two channels are defined as

$$S = \begin{pmatrix} r & t \\ t & r \end{pmatrix} \quad F(\epsilon) = \begin{pmatrix} f_1(\epsilon) & 0 \\ 0 & f_2(\epsilon) \end{pmatrix}. \tag{B.3.10}$$

Far away from the scatterer the states $|\alpha_i\rangle$ are energy eigenstates $|\alpha_i\rangle = e^{\imath\epsilon_i t}|\alpha_i\rangle_A$, where $|\rangle_A$ denotes an asymptotic (or scattering) state. We can power expand the U operator in Eq. (B.3.9) to first order in the perturbation and evaluate its matrix elements

$$\begin{aligned}\langle\beta_j|U|\alpha_i\rangle &\simeq -\imath\int_0^\tau dt\,\langle\beta_j|S|\alpha_i\rangle = -\imath\,{}_A\langle\beta_j|S|\alpha_i\rangle_A\int_0^\tau dt e^{\imath(\epsilon_i-\epsilon_j)t} \\ &= {}_A\langle\beta_j|S|\alpha_i\rangle_A\frac{(1-e^{\imath\epsilon_{ij}\tau})}{\epsilon_{ij}},\end{aligned} \tag{B.3.11}$$

5 Note that this is equivalent to say that the scattering is instantaneous.

where $\epsilon_{ij} = \epsilon_i - \epsilon_j$. Similarly, we find

$$\langle \alpha_i | U^\dagger | \beta_j \rangle \simeq {}_A\langle \alpha_i | S^\dagger | \beta_j \rangle_A \frac{(1 - e^{-\imath \epsilon_{ij} \tau})}{\epsilon_{ij}}. \tag{B.3.12}$$

The product of Eq. (B.3.11) and (B.3.12) contains the oscillatory factor $4 \sin^2(\epsilon_{ij}\tau/2)/\epsilon_{ij}^2$. In the long time limit only states satisfying $\epsilon_{ij} \sim 2\pi/\tau$ give a non-zero contribution. This statement can also be read as a time-energy uncertainty relation $\delta\tau\,\delta\epsilon \sim \hbar$. The long time limit can be exactly evaluated using

$$\lim_{d\to\infty} \frac{1}{\pi} \frac{\sin^2(w\,d)}{w^2 d} = \delta(w). \tag{B.3.13}$$

In order to use the scattering states representation in Eq. (B.3.9), it is convenient to take the logarithm of both sides of this expression

$$\begin{aligned} \lim_{\tau\to\infty} \log \Delta(\lambda, \tau) &= \lim_{\tau\to\infty} \log \det \left[\hat{1} + \left(U^\dagger e^{\imath q \lambda/2} U e^{-\imath q\lambda/2} - 1 \right) F(\epsilon) \right] \\ &= \lim_{\tau\to\infty} \sum_{n=1}^{\infty} \frac{(-1)^{n+1}}{n} \mathrm{Tr} \left\{ \left[\left(U^\dagger e^{\imath q\lambda/2} U e^{-\imath q\lambda/2} - U^\dagger U \right) F(\epsilon) \right]^n \right\}, \end{aligned} \tag{B.3.14}$$

where we have used $U^\dagger U = 1$ and the trace is over energy and matrix space. Using now Eq. (B.3.11), (B.3.12) and taking the long time limit we find

$$\log \Delta_L(\bar{\lambda}, \tau) = \frac{\tau}{2\pi} \int d\epsilon \log \det \left[\left(S^\dagger e^{\imath q\lambda/2} S e^{-\imath q\lambda/2} - \hat{1} \right) F(\epsilon) \right], \tag{B.3.15}$$

where Δ_L denotes the long time expression of the characteristic function and the determinant is only taken in the two dimensional matrix space. The product of S-matrices gives

$$W = S^\dagger e^{\imath q\lambda/2} S e^{-\imath q\lambda/2} = \begin{pmatrix} |r|^2 + |t|^2 e^{-\imath q\lambda} & r^* t e^{\imath q\lambda} + t^* r \\ r^* t e^{-\imath q\lambda} + t^* r & |r|^2 + |t|^2 e^{\imath q\lambda} \end{pmatrix}. \tag{B.3.16}$$

The determinant can be evaluated now explicitly :

$$\begin{aligned} \log \Delta_L(\lambda, \tau) &= \frac{\tau}{2\pi} \int d\epsilon \log \Big[(1 - f_1)(1 - f_2) + \left(|r|^2 + |t|^2 e^{\imath q\lambda} \right) f_2 (1 - f_1) \\ &+ \left(|r|^2 + |t|^2 e^{-\imath q\lambda} \right) f_1 (1 - f_2) + f_1\, f_2 \det W \Big] \\ &= \frac{\tau}{2\pi} \int d\epsilon \log \left[1 + a(e^{\imath q\lambda} - 1) f_2 (1 - f_1) + a(e^{-\imath q\lambda} - 1) f_1 (1 - f_2) \right]. \end{aligned} \tag{B.3.17}$$

It is interesting to note that in the long time limit the characteristic function depends only on the time difference and its matrix representation is therefore of the Toeplitz type. Let us consider the easier case of a system at zero temperature and choose $\epsilon_{1,2} = \epsilon \pm qV/2$ respectively for the two distribution functions f_1 and f_2, where $qV > 0$ is the bias voltage. In the limit $qV\tau \gg 1$ the Toeplitz determinant can be evaluated analytically[6] to obtain

$$\log \Delta_L(\lambda, \tau) = \frac{\tau\, qV}{\hbar} \log \left[1 + a(e^{\imath q\lambda} - 1) \right]. \tag{B.3.18}$$

6 More generally, since at zero temperature the Fermi function is replaced by a step function, the logarithm in Eq.(B.3.18) contains step-like singularities. According to the Fisher-Hartwig conjecture, these singularities give rise to sub-leading terms coming from summation over the different branches of the logarithm [117, 118]. However, in the $qV\tau \gg 1$ limit, the contribution of the sub-leading terms can be neglected.

The dimensionless pre-factor in the above equation can be identified with the number of trials $N(\tau) = \tau\, qV/h$. Making this identification we can write Eq. (B.3.18) in the more appealing from

$$\Delta_L(\lambda, \tau) = (1 - a + a\, e^{\imath q \lambda})^{N(\tau)}, \tag{B.3.19}$$

that has exactly the form of the characteristic function of a Bernoulli process, as found in section 2.2.2. According to Eq. (2.2.20) and (2.2.21), we can now obtain all the moments of the current by differentiating with respect to λ. In this way we correctly find for the current and the zero frequency quantum noise

$$\begin{aligned} \langle I \rangle &= \frac{\langle m \rangle}{\tau} = a \frac{q^2}{h} V \\ S(\omega \to 0) &= 2 \frac{\langle (m - \langle m \rangle)^2 \rangle}{\tau} = 2q \langle I \rangle (1 - a), \end{aligned} \tag{B.3.20}$$

where m is the number of electrons that have been transferred from one side of the sample to the other. Note that the $1 - a$ factor in the noise formula is due to Pauli blocking and that Poissonian noise is recovered only in the $a \ll 1$ limit. As a consequence of Pauli blocking, electron tunneling events are not independent random processes since they need to satisfy an additional constraint imposed by the exclusion principle. We can measure the deviation from the Poissonian behavior by introducing the Fano factor

$$F = \frac{S(\omega \to 0)}{S_{pois}(\omega \to 0)} = 1 - a. \tag{B.3.21}$$

The Fano factor provides a measure of the degrees of correlation of the tunneling events, providing in this way a useful way to characterize the interactions in the system by means of noise measurement.

C DETAILS ON NON-EQUILIBRIUM SPECTROSCOPY

In this appendix we provide additional details concerning the non-equilibrium spectroscopy of chiral and non-chiral Luttinger liquids. In the first section we present a detailed derivation of the tunneling current to leading order in the tunneling amplitudes η_1 and η_2. Then, we evaluate the tunneling current for the $\nu = 1/3$ QH state. Most of this subsection is dedicated to the exact evaluation of the integrals appearing in the expression for the tunneling current at finite temperature. Finally, we consider the zero temperature limit of our finite temperature result and show that it correctly reproduces the tunneling current evaluated directly at zero temperature. In the second section, we analyze the tunneling current for the standard Luttinger liquid in the limit of small energy loss. Finally, in the third section we consider a perturbative expansion of the chiral Luttinger liquid result for small interaction strenght. In this case we find that a perturbative treatment fails to reproduce the energy relaxation result; we argue that this feature is related to the topological stability of the QH fluid.

C.1 TUNNELING CURRENT AT THE PROBE

In section (3.2) the model system for tunneling spectroscopy has been defined. In this appendix we will give a detailed evaluation of the tunneling current at the probe. We are interested in evaluating the tunneling current at the second QD ($H_T = H_{T1} + H_{T2}$)

$$\langle I(t_1)\rangle = \langle T_K\{\hat{I}(t_1)e^{-i\int_{C_K} dt\, H_T(t)}\}\rangle_0 \tag{C.1.1}$$

to leading order in the tunneling amplitudes η_1 and η_2. To this purpose it is convenient to define the operator [66]

$$O_i^{\pm}(t) = \frac{1}{\sqrt{2\pi\alpha}} e^{\mp \imath\phi(t,x_i)/\nu}\psi_i^{\pm}(t,x_i), \tag{C.1.2}$$

where $x_1 = 0$ and $x_2 = L$ defines the injection and the extraction points, $i = 1,2$ labels the QD operator and we have introduced the notation $\psi^+ = \psi$ and $\psi^- = \psi^\dagger$. Using Eq. (C.1.2), we can re-write the current (3.2.4) and the tunneling operators (3.2.3) in the following compact form :

$$I(t) = \imath e_0\eta_2 \sum_{s_1=\pm} s_1 e^{\imath s_1 E_2 t} O_2^{s_1}(t) \tag{C.1.3}$$

$$\begin{aligned} H_{T1}(t) &= \eta_1 \sum_{s_3=\pm} e^{\imath s_3 E_1 t} O_1^{s_3}(t) \\ H_{T2}(t) &= \eta_2 \sum_{s_2=\pm} e^{\imath s_2 E_2 t} O_2^{s_2}(t), \end{aligned} \tag{C.1.4}$$

where we have introduced the index $s_i = \pm$. In the perturbative expansion of Eq. (C.1.1) the zeroth order term is zero since the expectation value $\langle O_2^{s_1}(t_1)\rangle_0 = 0$. The first order term is given by

$$\begin{aligned}\langle J_1(t_1)\rangle &= -\imath\left\langle T_K\left\{I(t_1)\int_{C_K} dt_2\, H_T(t_2)\right\}\right\rangle_0 \\ &= e_0|\eta_2|^2\sum_{s_1,s_2=\pm} s_1\int_{C_K} dt_2\, e^{\imath E_2(s_1t_1+s_2t_2)}\left\langle T_K O_2^{s_1}(t_1)O_2^{s_2}(t_2)\right\rangle_0,\end{aligned} \tag{C.1.5}$$

where the term $\langle O_2(t_1)O_1(t_2)\rangle_0 = 0$. In order to evaluate the expectation values of bosonic exponents we use the "charge neutrality" condition of the bosonic exponents $s_1 + s_2 = 0$ (B.1.25). Next, we perform the mapping of the fields over the time-loop contour

$$\begin{aligned} t_k &\to \sigma_k t_k \\ \int_{C_K} dt_k &\to \sum_{\{\sigma_K\}}\sigma_k\int_{-\infty}^{\infty} dt_k,\end{aligned} \tag{C.1.6}$$

where $\sigma_k = \pm$ specifies over which side of the contour the fields are evaluated, and k labels the time variable.

$$\begin{aligned}\langle J_1(0)\rangle &= e_0|\eta_2|^2\sum_{\{\sigma_k\}}\sigma_2\int_{-\infty}^{\infty} dt_2\Big\{e^{\imath E_2 t_{12}}\left\langle T_K O_2^+(\sigma_1t_1)O_2^-(\sigma_2t_2)\right\rangle_0 \\ &- e^{-\imath E_2 t_{12}}\left\langle T_K O_2^-(\sigma_1t_1)O_2^+(\sigma_2t_2)\right\rangle_0\Big\}.\end{aligned} \tag{C.1.7}$$

Next we perform the permutation $\sigma_1 t_1 \to \sigma_2 t_2$ in the second integral, we arrive at the useful form

$$\langle J_1(0)\rangle = e_0|\eta_2|^2\sum_{\{\sigma_k\}}(\sigma_2-\sigma_1)\int_{-\infty}^{\infty} dt_2 e^{\imath E_2 t_{12}}\left\langle T_K O_2^+(\sigma_1t_1)O_2^-(\sigma_2t_2)\right\rangle_0 \tag{C.1.8}$$

At this point it is convenient to move to imaginary time in order to evaluate the correlators in terms of the finite temperature Green function found in section (B.1.3). We first perform a Wick rotation to imaginary time $t_i \to -\imath\tau_i$ [52], then we use the expression for the finite temperature Green function

$$G_{1/\nu}(\tau_{ij}) = \frac{1}{2\pi\alpha}\frac{(\pi T\alpha/u)^{1/\nu}}{[\sin\pi T(\alpha/u+\sigma_{ij}\tau_{ij})]^{1/\nu}}, \tag{C.1.9}$$

where $\tau_{ij} = \tau_i - \tau_j$.

$$\begin{aligned}\left\langle T_K O_2^+(\sigma_1t_1)O_2^-(\sigma_2t_2)\right\rangle_0 &= \left\langle T_\tau e^{-\imath\phi(\tau 1,L)}e^{\imath\phi(\tau_2,L)}\right\rangle_0\left\langle T_\tau\psi_2(\tau_1,L)\psi_2^\dagger(\tau_2,L)\right\rangle_0 \\ &= \theta(\tau_{12})G_{1/\nu}(\tau_12).\end{aligned} \tag{C.1.10}$$

The above result has been found by expanding the time ordered product of the ψ_2 fields and imposing the constraint on the dot's occupancy: $\langle\psi_2^\dagger\psi_2\rangle = 0$. After mapping back to real time

we arrive at the final expression for the current (here we set $t_1 = 0$ since the measurement time is arbitrary)

$$\langle J_1(0)\rangle = e_0|\eta_2|^2 2\int dt_2 e^{-\imath E_2 t_2}\left(\imath G^{>}_{1/\nu}(-t_2) - \imath G^{<}_{1/\nu}(-t_2)\right), \tag{C.1.11}$$

Where the lesser/greater Green functions (now in real time) are defined as

$$\imath G^{\gtrless}_{\beta}(t) = \pm\frac{1}{2\pi\alpha}\frac{(\pi T\alpha/u)^{\beta}}{[\sin\pi T(\alpha/u \pm it)]^{\beta}}. \tag{C.1.12}$$

In order to solve the integral in Eq. (C.1.11) it is convenient to define the new time variable $\mu = \pi T t_2 + \imath\pi/2$. Since the shift of $\imath\pi/2$ in the time variable does not cross any singularity, it does not change the analytical properties of the integral. Using $\sin(\theta + \pi/2) = \cos(\theta)$ and $E_2 > 0$ we find

$$\langle J_1(0)\rangle = -e_0|\eta_2|^2\frac{2^{1/\nu}\alpha^{1/\nu-1}2(\pi T)^{1/\nu-1}}{\pi u^{1/\nu}}e^{-\frac{E_2}{2T}}\int_{-\infty}^{\infty}d\mu\frac{e^{-\imath\frac{E_2}{\pi T}\mu}}{\cosh(\mu)^{1/\nu}}. \tag{C.1.13}$$

The integral can be conveniently solved by rewriting the cosine term as a sum of complex exponentials and then defining a new variable $\gamma = e^{\mu}$

$$\begin{aligned}\langle J_1(0)\rangle &= -e_0|\eta_2|^2\frac{2^{1/\nu}2(\alpha\pi T)^{1/\nu-1}}{\pi u^{1/\nu}}e^{-\frac{E_2}{2T}}\int_0^{\infty}d\gamma\frac{\gamma^{-1-\imath\frac{E_2}{\pi T}+1/\nu}}{(1+\gamma^2)^{2/\nu}} \\ &= -e_0|\eta_2|^2\frac{(2\alpha\pi T)^{1/\nu-1}}{2\pi u^{1/\nu}}\quad e^{-\frac{E_2}{2T}}\quad\frac{\Gamma[\frac{1}{2\nu}-\imath\frac{E_2}{4\pi T}]\Gamma[\frac{1}{2\nu}+\imath\frac{E_2}{4\pi T}]}{\Gamma[1/\nu]}.\end{aligned} \tag{C.1.14}$$

In the second line we have used the following results ([104] pag. 325, n. 11)

$$\int_0^{\infty}d\gamma\frac{\gamma^{g-1}}{(1+\gamma^2)^{\eta}} = \frac{1}{2}B\left[\frac{g}{2}, \eta - \frac{g}{2}\right] \quad , \quad B[x,y] = \frac{\Gamma[x]\Gamma[y]}{\Gamma[x+y]}, \tag{C.1.15}$$

where $B[x,y]$ is the beta function and $\Gamma[x]$ is the gamma function. The first order term describes the tunneling current at the second QD due to thermally excited electrons. However, at temperatures small compared to the energy of the injected electrons, this term can be neglected because exponentially suppressed.

We now proceed evaluating the next non-zero term in the perturbative expansion. Following a similar procedure, we arrive at

$$\begin{aligned}\langle I(t_1)\rangle &\simeq -e_0\frac{|\eta_1|^2|\eta_2|^2}{2}\sum_{\{s_k\}}s_1\int_{C_K}d^3t e^{\imath E_2(s_1t_1+s_2t_2)+\imath E_1(s_3t_3+s_4t_4)} \\ &\times \left\langle T_K O_2^{s_1}(t_1)O_2^{s_2}(t_2)O_1^{s_3}(t_3)O_1^{s_4}(t_4)\right\rangle_0.\end{aligned} \tag{C.1.16}$$

To derive the above expression we have interchanged dummy time variables and combined in this way the three non-zero terms coming from the perturbative expansion. Now we can perform a mapping to Keldysh space using Eq. (C.1.6) and use the "charge neutrality" condition (B.1.25). In this way, we obtain the additional constraints $s_1 + s_2 = 0$ and $s_3 + s_4 =$

0. Due to these constraints, we are left with only two independent combinations of operators in the correlator, coming from the sum over $\{s_k\} = \{s_1, s_2, s_3, s_4\}$, namely

$$\{+,-,-,+\}\,,\{-,+,+,-\} \tag{C.1.17}$$

$$\begin{aligned}\langle I(t_1)\rangle &\simeq -e_0\frac{|\eta_1|^2|\eta_2|^2}{2}\sum_{\{\sigma_k\}}\sigma_2\sigma_3\sigma_4\int d^3t e^{\imath E_2 t_{12}+\imath E_1 t_{34}}\langle T_K[O_2^+(\sigma_1 t_1) \\ &\times O_2^-(\sigma_2 t_2)O_1^-(\sigma_3 t_3)O_1^+(\sigma_4 t_4)] - \left[O_2^-(\sigma_1 t_1)O_2^+(\sigma_2 t_2)O_1^+(\sigma_3 t_3)O_1^-(\sigma_4 t_4)\right]\rangle_0.\end{aligned} \tag{C.1.18}$$

Due to time translational invariance, the three integrals over time can be shifted to any three of the times t_2, t_3 and t_4. Performing the permutations $\sigma_1 t_1 \to \sigma_2 t_2$ and $\sigma_3 t_3 \to \sigma_4 t_4$ we arrive at the final form

$$\begin{aligned}\langle I(t_1)\rangle &\simeq e_0\frac{|\eta_1|^2|\eta_2|^2}{2}\sum_{\{\sigma_k\}}(\sigma_2-\sigma_1)\sigma_3\sigma_4\int d^3t e^{\imath E_2 t_{12}+\imath E_1 t_{34}}\Theta(\{\sigma_k,t_k\}) \\ \Theta(\{\sigma_k,t_k\}) &= \left\langle T_K\, O_2^+(\sigma_1 t_1)O_2^-(\sigma_2 t_2)O_1^-(\sigma_3 t_3)O_1^+(\sigma_4 t_4)\right\rangle_0.\end{aligned} \tag{C.1.19}$$

Moving to imaginary time, the Θ correlator can be evaluated using Wick's theorem and Eq. (C.1.9)

$$\begin{aligned}\Theta(\{\sigma_k,\tau_k\}) &= \langle T_\tau \psi_2(\sigma_1\tau_1,L)\psi_2^\dagger(\sigma_2\tau_2,L)\rangle_0\langle T_\tau\psi_1^\dagger(\sigma_3\tau_3,0)\psi_1(\sigma_4\tau_4,0)\rangle_0 \\ &\times \frac{1}{(2\pi\alpha)^2}\langle T_\tau e^{-\imath\phi(\sigma_1\tau_1,L)/\nu}e^{\imath\phi(\sigma_2\tau_2,L)/\nu}e^{\imath\phi(\sigma_3\tau_3,0)/\nu}e^{-\imath\phi(\sigma_4\tau_4,0)/\nu}\rangle_0 \\ &= \frac{1}{(2\pi\alpha)^4}\frac{\theta(\tau_{12})\theta(\tau_{34})(\pi T\alpha/u)^{2/\nu}}{[\sin\pi T(\alpha/u+\sigma_{12}\tau_{12})]^{1/\nu}[\sin\pi T(\alpha/u+\sigma_{34}\tau_{34})]^{1/\nu}} \\ &\times \left\{\frac{\sin\pi T[\alpha/u+\sigma_{13}(\tau_{13}-\imath L)]\sin\pi T[\alpha/u+\sigma_{24}(\tau_{24}-\imath L)]}{\sin\pi T[\alpha/u+\sigma_{23}(\tau_{23}-\imath L)]\sin\pi T[\alpha/u+\sigma_{14}(\tau_{14}-\imath L)]}\right\}^{1/\nu}.\end{aligned} \tag{C.1.20}$$

The operator $\sigma_{ij} = \mathrm{sgn}(\tau_i - \tau_j)$ specifies the ordering of the Green functions in imaginary time. When mapping back to real time, the ordering of the Green functions is determined by the ordering on the Keldysh contour and $\sigma_{ij} = \pm$ depends on whether $\sigma_i t_i$ comes earlier or later than $\sigma_j t_j$ on the time loop contour. This means that σ_{ij} not only depends on the sign of the time difference $w_{ij} = \mathrm{sgn}(t_i - t_j)$, but also on the sign of the branch of the Keldysh contour. We can express this relation in compact form as

$$\sigma_{ij} = \frac{1}{2}[(\sigma_i - \sigma_j) + w_{ij}(\sigma_i + \sigma_j)] \tag{C.1.21}$$

In the large L limit, most of the contribution to the integral comes from regions $t_{1,2} \simeq t_{3,4} + L$ [66] and we can fix the time-contour operators as $\sigma_{13} = \sigma_{23} = \sigma_3$ and $\sigma_{14} = \sigma_{24} = \sigma_4$. In this approximation, the current can be rewritten as

$$\begin{aligned}\langle I(t_1)\rangle &\simeq \frac{-e_0|\eta_1|^2|\eta_2|^2}{2}\sum_{\{\sigma_k\}}(\sigma_2-\sigma_1)\sigma_3\sigma_4\int d^3t e^{\imath E_2 t_{12}+\imath E_1 t_{34}}\theta(t_{12})\theta(t_{34}) \\ &\times G_{1/\nu}^{\sigma_{12}}(t_{12})G_{1/\nu}^{\sigma_{34}}(t_{34})\Pi_{1/\nu}^{\sigma_3\sigma_4}(\{t_k\},L),\end{aligned} \tag{C.1.22}$$

where we have defined the real time Green functions

$$G_{\beta}^{\sigma_{ij}}(t_{ij}) = \frac{1}{2\pi\alpha}\frac{(\pi T\alpha/u)^{\beta}}{[\sin\pi T(\alpha/u + \sigma_{ij}\imath t_{ij})]^{\beta}}, \tag{C.1.23}$$

and the Π-matrix is given by

$$\Pi_{1/\nu}^{\sigma_3\sigma_4}(\{t_k\}, L) = \left\{\frac{\sin\pi T[\alpha/u + \sigma_3\imath(t_{13} - L)]\sin\pi T[\alpha/u + \sigma_4\imath(t_{24} - L)]}{\sin\pi T[\alpha/u + \sigma_3\imath(t_{23} - L)]\sin\pi T[\alpha/u + \sigma_4\imath(t_{14} - L)]}\right\}^{1/\nu}. \tag{C.1.24}$$

As we can see from Eq. (C.1.22), the current is different from zero only if $\sigma_1 \neq \sigma_2$, i.e. only if the current is purely "quantum", in the terminology introduced in chapter (2.2). Moreover, the condition on the occupancy of the dots, expressed by the two theta functions, imposes an additional constraint on the ordering of the Green functions on the time-loop contour. We find that due to the restriction on the occupancy of the quantum dots, only $G_{1/\nu}^{+-}(t_{12})$ and $G_{1/\nu}^{-+}(t_{34})$ are different from zero. Imposing these constraints we find that only three terms are left in the evaluation of the sum over $\{\sigma_k\} = \{\sigma_1, \sigma_2, \sigma_3, \sigma_4\}$:

$$\{+,-,+,+\}\,,\{+,-,-,-\}\,,\{+,-,-,+\}, \tag{C.1.25}$$

and the tunneling current assumes the form

$$\begin{aligned}\langle I(t_1)\rangle \;&\simeq\; e_0|\eta_1|^2|\eta_2|^2\int d^3t e^{\imath E_2 t_{12} + \imath E_1 t_{34}}\theta(t_{12})\theta(t_{34})G_{1/\nu}^{+-}(t_{12})G_{1/\nu}^{-+}(t_{34}) \\ &\times\; \left\{\frac{1}{2}(\Pi_{1/\nu}^{++} + \Pi_{1/\nu}^{--}) + \frac{s_{34}}{2}(\Pi_{1/\nu}^{++} - \Pi_{1/\nu}^{--}) - \Pi_{1/\nu}^{-+}\right\}.\end{aligned} \tag{C.1.26}$$

In deriving the above expression we have used the explicit expression of the time ordered $(++)$ and anti-time ordered $(--)$ Green functions

$$\begin{aligned}G^{++}(t_{ij}) &= \frac{1}{2}(1 + s_{ij})G^{+-}(t_{ij}) + \frac{1}{2}(1 - s_{ij})G^{-+}(t_{ij}) \\ G^{--}(t_{ij}) &= \frac{1}{2}(1 - s_{ij})G^{+-}(t_{ij}) + \frac{1}{2}(1 + s_{ij})G^{-+}(t_{ij}),\end{aligned} \tag{C.1.27}$$

and used as a representation of the Heaviside step function $\theta(i-j) = (1 + s_{ij})/2$, being $s_{ij} = \mathrm{sgn}(i-j)$. It turns out that not all of the terms in Eq. (C.1.26) are independent [66] and we can actually find a simplified expression for the tunneling current. To see this explicitly we consider the integral involving the second term

$$T_2 \propto \int d^3t e^{\imath E_2 t_{12} + \imath E_1 t_{34}} G_{1/\nu}^{+-}(t_{12})G_{1/\nu}^{-+}(t_{34})(\Pi_{1/\nu}^{++} - \Pi_{1/\nu}^{--}) \tag{C.1.28}$$

and move to the average time difference variable $t_0 = (t_1 + t_2 - t_3 - t_4)/2$. This time variable can be interpreted as the time it takes electrons to propagate from the injection to the extraction dot. We also set $l_1 = t_{12}$ and $l_2 = t_{34}$ and as usual $l_{ij} = l_i - l_j$. In the new variables the Π-matrix reads

$$\Pi_{1/\nu}^{\pm\pm} = \left\{\frac{\sin\pi T[\alpha/u \pm \imath(t_0 + l_{12}/2 - L)]\sin\pi T[\alpha/u \pm \imath(t_0 + l_{21}/2 - L)]}{\sin\pi T[\alpha/u \pm \imath(t_0 - (l_1 + l_2)/2 - L)]\sin\pi T[\alpha/u \pm \imath(t_0 + (l_1 + l_2)/2 - L)]}\right\}^{1/\nu}. \tag{C.1.29}$$

We can simplify even further this expression using the identity $\sin\theta\sin\varphi = [\cos(\theta-\varphi) - \cos(\theta+\varphi)]/2$ and introducing the index $m = \pm$ to obtain

$$\begin{aligned} T_2 \;\propto\; & -\int dl_1 \int dl_2 e^{\imath E_2 l_1 + \imath E_1 l_2} G^{+-}_{1/\nu}(l_1) G^{-+}_{1/\nu}(l_2) \\ & \times \sum_{m=\pm} \int dt_0\, m \left\{ \frac{A - \cos(\alpha/u + 2m\imath(t_0 - L))}{a - \cos(\alpha/u + 2m\imath(t_0 - L))} \right\}^{1/\nu}, \end{aligned} \tag{C.1.30}$$

where $A = \cos m l_{12}$ and $a = \cos m(l_1 + l_2)$ are constants with respect to t_0. The integral over t_0 can be computed by means of the Residue theorem. There are two $1/\nu$th order poles $z_\pm = (2\imath L m + \imath\alpha/u \pm \arccos a)/(2m)$. If $1/\nu$ is an integer value (as it is in our case), these contributions cancel each other and the integral over t_0 is identically zero. Therefore, we obtain as an additional condition for Eq. (C.1.26): $\Pi^{++}_{1/\nu} = \Pi^{--}_{1/\nu}$. Setting $t_1 = 0$ we obtain the final expression Eq. (3.2.13)

$$\begin{aligned} \langle I(0)\rangle \;=\; & e_0 |\eta_1|^2 |\eta_2|^2 \int_{-\infty}^{\infty} dt_2 dt_3 dt_4 e^{-iE_2 t_2 + iE_1 t_{34}} \\ & \times \left(iG^{<}_{1/\nu}(-t_2) \right) \left(iG^{>}_{1/\nu}(t_{34}) \right) \left\{ \Pi^{<>}_{1/\nu} - \Pi^{<<}_{1/\nu} \right\}, \end{aligned} \tag{C.1.31}$$

where we have renamed the Green functions as $G^{+-} = G^{<}$ and $G^{-+} = G^{>}$ and the Π matrices in the long distance limit are defined as

$$\Pi^{\rho\sigma}_{\beta} = \frac{G^{\rho}_{\beta}(t_{23}) G^{\sigma}_{\beta}(-t_4)}{G^{\rho}_{\beta}(-t_3) G^{\sigma}_{\beta}(t_{24})}, \tag{C.1.32}$$

C.1.1 Evaluation of the tunneling current for the $\nu = 1/3$ QH state

In this section we specialize to the QH state at filling fraction $\nu = 1/3$ and evaluate exactly Eq. (C.1.31). First of all we note that shifting variables $t_3 + L \to t_3$ and $t_4 + L \to t_4$, the L-dependence completely drops out of the expression for the current. Physically this is due to the fact that in the large L limit the system, far away from the dots, is translationally invariant. In addition, we can scale the temperature dependence into the time variables $\pi T t_i \to t_i$. Consider the difference between Π-matrices

$$\begin{aligned} \Pi^{<>}_3 - \Pi^{<<}_3 \;&=\; \left(\frac{\sin(\alpha/u + \imath t_3)\sin(\alpha/u + \imath t_{24})}{\sin(\alpha/u - \imath t_{23})\sin(\alpha/u - \imath t_4)} \right)^3 - \left(\frac{\sin(\alpha/u + \imath t_3)\sin(\alpha/u - \imath t_{24})}{\sin(\alpha/u - \imath t_{23})\sin(\alpha/u + \imath t_4)} \right)^3 \\ &\simeq\; -\frac{\sin^3(\imath t_3)\sin^3(\imath t_{24})}{\sin^3(\alpha/u - \imath t_{23})} \left\{ \frac{1}{\sin^3(\alpha/u - \imath t_4)} + \frac{1}{\sin^3(\alpha/u + \imath t_4)} \right\}, \end{aligned} \tag{C.1.33}$$

where in the second line we have sent α to zero in the numerator. The term in curly brackets is a representation of the second order derivative of the Dirac delta function

$$\left\{ \frac{1}{\sin^3(\alpha/u + \imath t_4)} + \frac{1}{\sin^3(\alpha/u - \imath t_4)} \right\} = -\pi\delta''(t_4). \tag{C.1.34}$$

We can rearrange Eq. (C.1.31) as follows

$$\begin{aligned}\langle I(0)\rangle &= -e_0\frac{|\eta_1|^2|\eta_2|^2\pi^2\alpha^4T^3}{4u^6}\int dt_2\,dt_3\,e^{-iX_2t_2/\pi+iX_1t_3/\pi}\frac{\sin^3(\imath t_3)}{\sin^3(\alpha/u+\imath t_2)\sin^3(\alpha/u-\imath t_{23})}\\ &\times \int dt_4 e^{-\imath X_1 t_4/\pi}\frac{\sin^3(\imath t_{24})}{\sin^3(\alpha/u+\imath t_{34})}\delta''(t_4),\end{aligned} \tag{C.1.35}$$

where we have defined $X_i = E_i/T$. The integral over t_4 can be solved using the property of the Dirac delta function

$$\int_t f(t)\delta''(t) = f''(t)\Big|_{t=0}. \tag{C.1.36}$$

Using the above property we obtain

$$\begin{aligned}\langle I(0)\rangle &= -e_0\frac{|\eta_1|^2|\eta_2|^2\pi^2\alpha^4T^3}{4u^6}\int_{t_2,t_3}\frac{e^{-iX_2t_2/\pi+iX_1t_3/\pi}}{\imath\sinh^3(t_{23}+\imath\alpha/u)}\Big(\frac{X_1^2}{\pi^2}+6\imath\frac{X_1}{\pi}\coth(t_2-\imath\alpha/u)\\ &- 6\imath\frac{X_1}{\pi}\coth(t_3-\imath\alpha/u)-6\coth^2(t_2-\imath\alpha/u)-12\coth^2(t_3-\imath\alpha/u)\Big)\\ &+ 18\coth(t_2-\imath\alpha/u)\coth(t_3-\imath\alpha/u)\\ &= -e_0\frac{|\eta_1|^2|\eta_2|^2\pi^2\alpha^4T^3}{4u^6}\left(I_1+I_2-I_3-I_4-I_5+I_6\right).\end{aligned}$$

In what follows we are going to discuss how to evaluate the different terms in the above integral. We start considering a detailed evaluation of the first term. We first note that the time dependence in the integral can be disentagled by performing a shift of the time variable $t_2 \to t_2 + t_3$

$$I_1 = -\imath\left(\frac{X_1}{\pi}\right)^2\int_{t_3}e^{\imath(\Delta X/\pi)t_3}\int_{t_2}\frac{e^{-\imath X_2t_2/\pi}}{\sinh^3(t_2+\imath\alpha/u)}. \tag{C.1.37}$$

The integral over t_3 gives $2\pi\delta(\Delta X/\pi)$, where we have defined $\Delta X = X_1 - X_2$. As in the evaluation of Eq. (C.1.13), it is now convenient to perform a shift in the time variable $t_2 \to t_2 + \imath\pi/2$ to move the poles of the integrals over the imaginary axes

$$\begin{aligned}I_1 &= \left(\frac{X_1}{\pi}\right)^2 2\pi^2\delta(\Delta X)e^{X_2/2}\int_{-\infty}^{\infty}dt_2\frac{e^{-\imath X_2t_2/\pi}}{\cosh^3(t_2)}\\ &= \left(\frac{X_1}{\pi}\right)^2\pi^2\delta(\Delta X)e^{X_2/2}2^4\int_0^{\infty}d\gamma\frac{\gamma^{-\imath X_2/\pi+2}}{(\gamma^2+1)^3},\end{aligned} \tag{C.1.38}$$

where in the second line we moved to the new variable $\gamma = e^{t_2}$. Under an analytic continuation, we can evaluate the integral on the "keyhole" contour shown in Fig. (43), where a branch cut from zero to infinity is present. We first discuss the key-hole integral for a more general situation and then specialize to the case of Eq. (C.1.38). The contour is made of four pieces $\Gamma = \Gamma_R \bigcup \Gamma_r \bigcup \Gamma_1 \bigcup \Gamma_2$

$$\oint_\Gamma\frac{z^{\mp\imath m+2}}{(z^2+1)^l} = \lim_{R\to\infty}\int_{\Gamma_R}\frac{z^{\mp\imath m+2}}{(z^2+1)^l}+\lim_{r\to0}\int_{\Gamma_r}\frac{z^{\mp\imath m+2}}{(z^2+1)^l}+(1-e^{\pm2\pi m})\int_0^{\infty}d\gamma\frac{\gamma^{\mp\imath m+2}}{(\gamma^2+1)^l}, \tag{C.1.39}$$

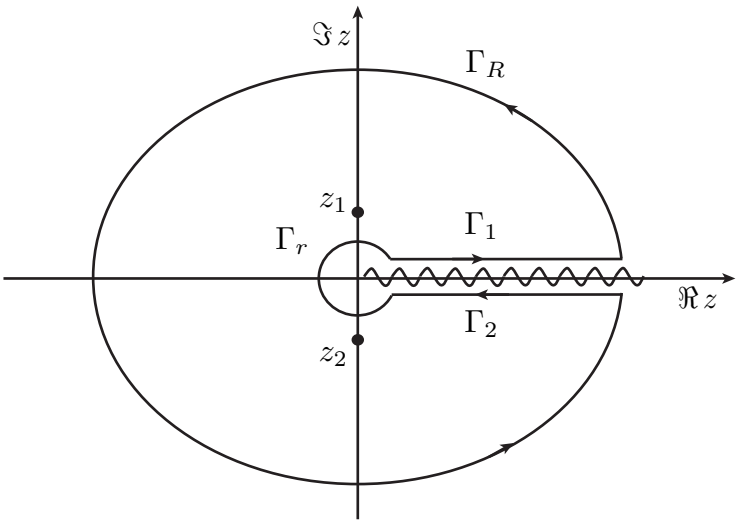

Figure 43: The "keyhole" contour. The domain $\gamma \in [0, \infty]$ is deformed over the complex Γ contour after an analytical continuation. The wiggled line represents the branch cut. For the specific case of Eq. (C.1.39), there are two third order poles at $z_1 = e^{\imath\pi/2}$ and $z_2 = e^{\imath 3\pi/2}$.

where z is a complex variable, l is a positive integer and m a positive real number. We first show that the integral over Γ_r vanishes in the limit of $r \to 0$. In order to do that we move to polar coordinates $z = re^{\imath\theta}$

$$\begin{aligned} \lim_{r\to 0} \left| \imath r^3 \int_0^{2\pi} d\theta e^{2\imath\theta} \frac{e^{\mp\imath m(\log r + \imath\theta)}}{(r^2 e^{2\imath\theta} + 1)^l} \right| &\leqslant \lim_{r\to 0} r^3 \int_0^{2\pi} d\theta \frac{|e^{\mp\imath m \log r}||e^{\pm m\theta}|}{|r^2 e^{\imath 2\theta} + 1|^l} \\ &\leqslant \pm \frac{(e^{\pm 2\pi m} - 1)}{m} \lim_{r\to 0} \frac{r^3}{(1-r^2)^l} \to 0. \end{aligned} \tag{C.1.40}$$

In the same way we, can show that also the integral over Γ_R goes to zero when $R \to \infty$. In this way we find the relation

$$\int_0^\infty d\gamma \frac{\gamma^{\mp\imath m+2}}{(\gamma^2+1)^l} = \frac{1}{(1 - e^{\pm 2\pi m})} \oint_\Gamma \frac{z^{\mp\imath m+2}}{(z^2+1)^l}. \tag{C.1.41}$$

Using the above relation in Eq. (C.1.38), we see that the integral has two third order poles at $z_1 = e^{\imath\pi/2}$ and $z_2 = e^{\imath 3\pi/2}$; using the residue theorem we find

$$\begin{aligned} I_1 &= (X_1)^2 \delta(\Delta X) 2^4 \frac{e^{X_2/2}}{1 - e^{2X_2}} 2\pi\imath \sum_{z=z_1,z_2} \text{Res} \frac{z^{-\imath X_2/\pi+2}}{(z^2+1)^3} \\ &= \frac{X_1^2 \pi e^{X_1/2}}{\cosh(X_1/2)} \left(1 + \left(\frac{X_1}{\pi}\right)^2\right) \delta(\Delta X). \end{aligned} \tag{C.1.42}$$

In the last line we have used the property of the delta function in order to exchange X_2 for X_1.

The method described above can also be used to compute the remaining integrals. Consider the I_2 integral, proportional to $\coth(t_2 - \imath\alpha/u)$

$$\begin{aligned} I_2 &= 6\imath\frac{X_1}{\pi}\int_{t_2,t_3}\frac{e^{-\imath X_2 t_2/\pi+\imath X_1 t_3/\pi}}{\imath\sinh^3(t_{23}+\imath\alpha/u)}\coth(t_2-\imath\alpha/u) \\ &= -6\frac{X_1}{\pi}\int_{t_3}\frac{e^{\imath X_1 t_3/\pi}}{\sinh^3(t_3-\imath\alpha/u)}\int_{t_2}e^{\imath\Delta X t_2/\pi}\coth(t_2-\imath\alpha/u) \\ &= \frac{3\pi X_1 e^{\Delta X/2}e^{X_1/2}}{\cosh(X_1/2)\sinh(\Delta X/2)}\left(1+\left(\frac{X_1}{\pi}\right)^2\right). \end{aligned} \tag{C.1.43}$$

The solution of the I_3, I_4 and I_5 integrals follows from the one above.

Finally, we need to compute the "mixed" term, involving the product $\coth(t_2 - \imath\alpha/u)$ $\coth(t_3 - \imath\alpha/u)$. Unfortunately, shifting one of the two time will not lead to any simplification here. It is convenient to perform first a shift of both times $t_2 = t_2 + \imath\pi/2$ and $t_3 = t_3 + \imath\pi/2$.

$$\begin{aligned} I_6 &= -18\imath e^{\Delta X/2}\int_{t_2,t_3}\frac{e^{-\imath X_2 t_2/\pi+\imath X_1 t_3/\pi}}{\sinh^3(t_{23}+\imath\alpha/u)}\tanh(t_2)\tanh(t_3) \\ &= 18\imath e^{\Delta X/2}\int_{t_3}\frac{e^{\imath X_1 t_3/\pi}}{\sinh^3(t_3-\imath\alpha/u)}\int_{t_2}e^{\imath\Delta X/\pi t_2}\tanh(t_2)\tanh(t_2+t_3) \end{aligned} \tag{C.1.44}$$

In the second line we have shifted the time variable by $t_3 = t_3 + t_2$. Defining $\gamma_i = e^{t_i}$, we can evaluate the γ_2 integral over the key-hole contour. There are now four simple poles at $z_2 = (e^{\imath\pi/2}, e^{\imath 3\pi/2}, e^{\imath\pi/2}z_3^{-1}, e^{\imath 3\pi/2}z_3^{-1})$. Using the residue theorem we find

$$\begin{aligned} I_6 &= 18\imath e^{\Delta X/2}\int_0^\infty d\gamma_3\frac{\gamma_3^{\imath X_1/\pi+2}\,2^3}{\left(\gamma_3^2-1-\imath\alpha/u\right)^3}\left(\frac{\imath\pi}{\sinh(\Delta X/2)}\frac{\gamma_3^2+1}{\left(\gamma_3^2-1-\imath\alpha/u\right)}\left(1-\gamma_3^{-\imath\Delta X/\pi}\right)\right) \\ &= \frac{-18\pi e^{\Delta X/2}2^3}{\sinh(\Delta X/2)}\left\{\int_0^\infty d\gamma_3\frac{\gamma_3^{\imath X_1/\pi+2}(\gamma_3^2+1)}{\left(\gamma_3^2-1-\imath\alpha/u\right)^4}-\int_0^\infty d\gamma_3\frac{\gamma_3^{\imath X_2/\pi+2}(\gamma_3^2+1)}{\left(\gamma_3^2-1-\imath\alpha/u\right)^4}\right\} \\ &= \frac{-3\pi e^{\Delta X/2}}{\sinh(\Delta X/2)}\left\{\frac{e^{X_1/2}}{\cosh(X_1/2)}X_1\left(1+\left(\frac{X_1}{\pi}\right)^2\right)-\frac{e^{X_2/2}}{\cosh(X_2/2)}X_2\left(1+\left(\frac{X_2}{\pi}\right)^2\right)\right\}. \end{aligned} \tag{C.1.45}$$

It is interesting to see how the original integral factorizes into the two terms in the curly brackets, each of them depending only on one of the two bias voltages. Adding all terms together we finally find:

$$\begin{aligned}
\langle I(0)\rangle &= -e_0\frac{|\eta_1|^2|\eta_2|^2\pi^3\alpha^4(K_BT)^3}{4u^6\hbar^7}\Big\{\frac{X_1^2e^{X_1/2}}{\cosh(X_1/2)}\left(1+\left(\frac{X_1}{\pi}\right)^2\right)\delta(\Delta X) \qquad \text{(C.1.46)}\\
&+ \frac{3e^{\Delta X/2}e^{X_1/2}}{\sinh\Delta X/2\cosh X_1/2}\left(1+\left(\frac{X_1}{\pi}\right)^2\right)(\Delta X - X_1 + X_1)\\
&+ \frac{3e^{\Delta X/2}e^{X_2/2}}{\sinh\Delta X/2\cosh X_2/2}\left(1+\left(\frac{X_2}{\pi}\right)^2\right)(2\Delta X - X_1 + X_2)\Big\}\\
&= -e_0\frac{\pi^3|\eta_1|^2|\eta_2|^2\alpha^4(k_BT)^3}{4u^6\hbar^7}\Bigg\{\frac{X_1^2e^{\frac{X_1}{2}}}{\cosh(X_1/2)}\left(1+\frac{X_1^2}{\pi^2}\right)\delta(\Delta X)\\
&+ \frac{3\Delta Xe^{\Delta X/2}}{\sinh(\Delta X/2)}\sum_{i=1}^{2}\frac{e^{X_i/2}}{\cosh(X_i/2)}\left(1+\frac{X_i^2}{\pi^2}\right)\Bigg\},
\end{aligned}$$

that is Eq. (3.2.19).

C.1.2 Zero temperature limit

In order to evaluate the finite temperature tunneling current, we had to perform different analytic continuations and "rotation" of singular points in complex space. In order to check the validity of the result we can compare it with its zero temperature value. First, we remind ourselves of the connection between the finite and the zero temperature Green function :

$$\frac{(\pi T)^\beta}{[\sinh\pi T(t-\imath\alpha]^\beta} \to \frac{1}{(t-\imath\alpha)^\beta}. \qquad \text{(C.1.47)}$$

A simple way to obtain the above relation is to power expand the sinh for small T[1]. Consider the low temperature expression of integral (C.1.43)

$$\begin{aligned}
T^3I_2 &\to 6T^3\frac{X_1}{\pi}\int_{t_2,t_3}\frac{e^{-\imath X_2t_2/\pi+\imath X_1t_3/\pi}}{(t_{23}+\imath\alpha/u)^3}\frac{1}{(t_2-\imath\alpha/u)} \qquad \text{(C.1.48)}\\
&= -6T^3\frac{X_1}{\pi}\int_{t_3}\frac{e^{\imath X_1t_3/\pi}}{(t_3-\imath\alpha/u)^3}\int_{t_2}\frac{e^{\imath\Delta Xt_2/\pi}}{(t_2-\imath\alpha/u)}\\
&= 12\frac{E_1^3}{\pi}\theta(\Delta E).
\end{aligned}$$

1 It is interesting to note that we can obtain the finite temperature Green function from the zero temperature one, by means of a conformal mapping in imaginary time from the complex plane with coordinates $z = \imath ut$ to the cylinder with coordinates $\omega = \imath u\tau$, via the conformal transformation $\imath ut \to e^{2\pi\imath T\tau}$. Here $0 \leqslant \tau \leqslant 1/T$ is the radius of the cylinder.

On the other hand we can directly take the $X_1, X_2 >> 1$ limit of the finite temperature result of Eq. (C.1.43)

$$\begin{aligned} T^3 I_2 &= \frac{3\pi X_1 T^3 e^{\Delta X/2} e^{X_1/2}}{\cosh(X_1/2)\sinh(\Delta X/2)}\left(1+\left(\frac{X_1}{\pi}\right)^2\right) \\ &= \frac{12\pi X_1 T^3 e^{\Delta X/2} e^{X_1/2}}{(e^{X_1/2}+e^{-X_1/2})(e^{\Delta X/2}-e^{-\Delta X/2})}\left(1+\left(\frac{X_1}{\pi}\right)^2\right) \\ &\xrightarrow[X_1,X_2\gg 1]{} 12\frac{E_1^3}{\pi}\theta(\Delta E), \end{aligned} \tag{C.1.49}$$

in agreement with the previous result. Adding contributions from the different terms, the zero temperature tunneling current reads

$$\langle I(0)\rangle = -e_0 \frac{\pi|\eta_1|^2|\eta_2|^2\alpha^4}{4u^6\hbar^7}\left(E_1^4\delta(\Delta E)+6\theta(\Delta E)(E_1^2+E_2^2)\Delta E\right). \tag{C.1.50}$$

C.2 STANDARD LUTTINGER LIQUID : SMALL ENERGY LOSS APROXIMATION

In this section we analyze the tunneling current for a standard LuL. The tunneling current can be derived following the steps of the previous section, starting from the following Hamiltonian

$$H_{LL} = \frac{u}{4\pi g}\int dx\left\{(\partial_x\phi_R(x))^2+(\partial_x\phi_L(x))^2\right\}, \tag{C.2.1}$$

where $g<1$ is the LuL parameter and the chiral boson operators satisfy $[\phi_R(x),\phi_R(x')] = -[\phi_L(x),\phi_L(x')] = i\pi g\,\mathrm{sgn}(x-x')$. The tunneling Hamiltonian is identical to equation (3.2.3), where the electron operator is now given by $\psi(x)=\psi_R(x)+\psi_L(x)$, and

$$\psi_{R,L}(x) = \exp[i(g_\pm\phi_R(x)+g_\mp\phi_L(x))]/\sqrt{2\pi\alpha} \tag{C.2.2}$$

$$g_\pm = (g^{-1}\pm 1)/2 \tag{C.2.3}$$

$$g = \sqrt{\frac{u+(g_4-g_2)/2\pi}{u+(g_4+g_2)/2\pi}}. \tag{C.2.4}$$

The final expression for the tunneling current at QPC2 is

$$\begin{aligned} \langle I(0)\rangle &= e_0|\eta_1|^2|\eta_2|^2\int d^3t e^{-iE_2t_2+iE_1t_{34}}[iG^<_{2\gamma+1}(-t_2)][iG^>_{2\gamma+1}(t_{34})] \\ &\times \{\Pi^{<>}_{1+\gamma}-\Pi^{<<}_{1+\gamma}+\Pi^{<>}_{\gamma}-\Pi^{<<}_{\gamma}+2\Pi^{<>}_{\gamma'}-2\Pi^{<<}_{\gamma'}\}, \end{aligned} \tag{C.2.5}$$

where $\gamma = g_-^2 g$ and $\gamma' = (g_-^2+g_-)g$. Next we set $\hbar = u = 1$ and define the energy loss $\Delta E = E_1 - E_2$. Our goal is to derive the leading contribution to the current for $\Delta E \ll E_1$ at zero temperature. The main steps in this analysis consist in

- Setting $E_1 = 1/\alpha$, i.e. we take the energy of the injected electrons to be of the order of the high energy cut-off scale.

- Shifting the time variable $t_3 = t_3 + t_2$.
- Rescaling α inside the time variable $t_i = t_i/\alpha$ and then define $\tilde{\alpha} = \alpha\Delta E$.

After these operations Eq. (C.2.5) can be explicitly written as

$$\begin{aligned}\langle I\rangle &= \frac{e_0|\eta_1|^2|\eta_2|^2}{(2\pi\alpha)^2}\alpha^3\int d^3t \frac{e^{i\tilde{\alpha}t_2+it_{34}}}{(1+\imath t_2)^{2\gamma+1}(1+\imath t_{34}+\imath t_2)^{2\gamma+1}}\Big\{\frac{(1+\imath t_3+\imath t_2)^{\gamma+1}}{(1+\imath t_3)^{\gamma+1}}\\ &\times \left(\frac{(1-\imath t_{24})^{\gamma+1}}{(1+\imath t_4)^{\gamma+1}}-\frac{(1+\imath t_{24})^{\gamma+1}}{(1-\imath t_4)^{\gamma+1}}\right)+\frac{(1+\imath t_3+\imath t_2)^{\gamma}}{(1+\imath t_3)^{\gamma}}\left(\frac{(1-\imath t_{24})^{\gamma}}{(1+\imath t_4)^{\gamma}}-\frac{(1+\imath t_{24})^{\gamma}}{(1-\imath t_4)^{\gamma}}\right)\\ &+ 2\frac{(1+\imath t_3+\imath t_2)^{\gamma'}}{(1+\imath t_3)^{\gamma'}}\left(\frac{(1-\imath t_{24})^{\gamma'}}{(1+\imath t_4)^{\gamma'}}-\frac{(1+\imath t_{24})^{\gamma'}}{(1-\imath t_4)^{\gamma'}}\right)\Big\}. \end{aligned} \tag{C.2.6}$$

For $\tilde{\alpha} \ll 1$ the integral over t_2 gets most of the contribution from $t_2 \gg 1$. This means $t_2 \gg t_3, t_4$ and we can drop t_3, t_4 with respect to t_2 to obtain

$$\begin{aligned}\langle I\rangle &= \frac{e_0|\eta_1|^2|\eta_2|^2}{(2\pi\alpha)^2}\alpha^3\int d^3t \frac{e^{i\tilde{\alpha}t_2+it_{34}}}{(1+\imath t_2)^{2(2\gamma+1)}}\Big\{\frac{(1+\imath t_2)^{\gamma+1}}{(1+\imath t_3)^{\gamma+1}}\left(\frac{(1-\imath t_2)^{\gamma+1}}{(1+\imath t_4)^{\gamma+1}}-\frac{(1+\imath t_2)^{\gamma+1}}{(1-\imath t_4)^{\gamma+1}}\right)\\ &+ \frac{(1+\imath t_2)^{\gamma}}{(1+\imath t_3)^{\gamma}}\left(\frac{(1-\imath t_2)^{\gamma}}{(1+\imath t_4)^{\gamma}}-\frac{(1+\imath t_2)^{\gamma}}{(1-\imath t_4)^{\gamma}}\right)+2\frac{(1+\imath t_2)^{\gamma'}}{(1+\imath t_3)^{\gamma'}}\left(\frac{(1-\imath t_2)^{\gamma'}}{(1+\imath t_4)^{\gamma'}}-\frac{(1+\imath t_2)^{\gamma'}}{(1-\imath t_4)^{\gamma'}}\right)\Big\}. \end{aligned} \tag{C.2.7}$$

Now the integral can be solved using standard methods and we obtain

$$I = \frac{e_0|\eta_1|^2|\eta_2|^2}{(2\pi\alpha)^2e^2}\alpha^3(2\pi)^3\theta(\tilde{\alpha})\left\{\frac{\tilde{\alpha}^{2\gamma-1}e^{-\tilde{\alpha}}}{\Gamma^2(\gamma+1)\Gamma(2\gamma)}+\frac{\tilde{\alpha}^{2\gamma+1}e^{-\tilde{\alpha}}}{\Gamma^2(\gamma)\Gamma(2(\gamma+1))}+\frac{\tilde{\alpha}^{4\gamma-2\gamma'+2}e^{-\tilde{\alpha}}}{\Gamma^2(\gamma')\Gamma(4\gamma-2\gamma'+2)}\right\}. \tag{C.2.8}$$

The last two terms in the above formula, are sub-leading with respect to the first one and we can drop them for our purpose. Reinstating $\hbar$, u and writing everything in terms of ΔE we finally arrive at Eq. (3.3.6)

$$I \simeq -\frac{2\pi e_0}{\hbar}\frac{|\eta_1|^2|\eta_2|^2\theta(\Delta E)}{u^2\hbar^2E_1\Gamma^2(1+\gamma)}\left(\frac{\alpha E_1}{u\hbar}\right)^{4\gamma}\left[\frac{(\Delta E/E_1)^{2\gamma-1}}{\Gamma(2\gamma)}\right]. \tag{C.2.9}$$

Above, we have also used $e^{-\tilde{\alpha}} \simeq 1$.

C.3 PERTURBATIVE EXPANSION OF THE CLUL

In this section we consider the problem of injecting and extracting high energy electrons from the resonant levels of two coupled quantum dots weakly coupled to a CLuL in the limit of small electron-electron interaction strength. Since the CLuL describes the edges of a FQH state, this small interaction analysis is not physically justified. Therefore, the present section should be seen more as a formal exercise than representing a real physical situation.

The starting point is the expression for the tunneling current Eq. (3.2.13)

$$\langle I(t_1)\rangle = e_0|\eta_1|^2|\eta_2|^2\int_{-\infty}^{\infty} d^3t e^{\imath E_2 t_{12}+\imath E_1 t_{34}}\left(\imath G^{<}_{1/\nu}(-t_2)\right)\left(\imath G^{>}_{1/\nu}(t_{34})\right)\left\{\Pi^{<>}_{1/\nu}-\Pi^{<<}_{1/\nu}\right\}, \tag{C.3.1}$$

where $t_{ij}=t_i-t_j$. The Π-matrices and the Green functions are defined at zero temperature as :

$$\Pi^{\rho\sigma}_{\beta}=\frac{G^{\rho}_{\beta}(-t_3)G^{\sigma}_{\beta}(t_{24})}{G^{\rho}_{\beta}(t_{23})G^{\sigma}_{\beta}(-t_4)} \quad , \quad G^{\pm}_{1/\nu}(t_{ij})=\frac{\alpha^{1/(1-\eta)-1}}{[(\alpha\pm it_{ij})]^{1/(1-\eta)}}. \tag{C.3.2}$$

The repulsive interaction strength is governed by $g=\nu$, that appears as an exponent in the Green functions and it determines the order of their poles (correponding in the bulk to the zeros of the Laughlin wave-function). Here we will try to solve Eq. (C.3.1) in the case of a weakly interacting Luttinger liquid, i.e. we expand the interaction parameter $g=\nu$ close to the non-interacting value $g=1-\eta$. Since now on, η will play the role of the small parameter. At zero temperature the Green function, up to first order in η, is readily found to be

$$G^{\pm}_{1/\nu}(t_{ij})=\frac{\alpha^{1/(1-\eta)-1}}{[(\alpha\pm it_{ij})]^{1/(1-\eta)}}=\frac{1}{(\alpha\pm it_{ij})}\left[1-\eta\log\left(1\pm i\frac{t_{ij}}{\alpha}\right)+O(\eta^2)\right]. \tag{C.3.3}$$

Now we can use the above expansion in (C.3.1), keeping only linear terms in η:

$$\begin{aligned}\langle\hat{I}(t_1)\rangle \;\simeq\; & -e_0|\eta_1|^2|\eta_2|^2\int_{-\infty}^{\infty} d^3t e^{i(E_2t_{12}+E_1t_{34})}\frac{(1-\eta\log(1-it_{12}/\alpha))}{(\alpha-it_{12})}\\
\times\; & \frac{(1-\eta\log(1-it_{34}/\alpha))}{(\alpha+it_{34})}\Big\{\Pi_1^{--}\Big[(1-\eta\log(1-it_{23}/\alpha)-\eta\log(1-it_{14}/\alpha)\\
+\; & \eta\log(1-it_{13}/\alpha)+\eta\log(1-it_{24}/\alpha))\Big]-\Pi_1^{-+}\Big[1-\eta\log(1-it_{23}/\alpha)\\
-\; & \eta\log(1+it_{14}/\alpha)+\eta\log(1-it_{13}/\alpha)-\eta\log(1-it_{24}/\alpha)\Big]\Big\}.\end{aligned} \tag{C.3.4}$$

At this point we can proceed using the following partial fraction decomposition:

$$\frac{\Pi_1^{--}}{(\alpha-it_{12})(\alpha+it_{34})}=\frac{1}{(\alpha-it_{12})(\alpha+it_{34})}-\frac{1}{(\alpha-it_{14})(\alpha-it_{23})} \tag{C.3.5}$$

$$\frac{\Pi_1^{-+}}{(\alpha-it_{12})(\alpha+it_{34})}=\frac{1}{(\alpha-it_{12})(\alpha+it_{34})}+\frac{1}{(\alpha+it_{14})(\alpha-it_{23})} \tag{C.3.6}$$

The first terms on the right hand side of the above expressions represents "non-propagating" solutions and do not contribute to the tunneling current, as it will be shown later on. Due

to time translational invariance we can set $t_1 = 0$. Using (C.3.5) in (C.3.3), and keeping only terms linear in η, we arrive at

$$\begin{aligned}
\langle \hat{I} \rangle \simeq & -e_0|\eta_1|^2|\eta_2|^2 \Big\{ \int_{-\infty}^{\infty} d^3t \frac{e^{i(E_1 t_{34} - E_2 t_2)}}{(\alpha - it_{23})} \left[\frac{1}{(\alpha + it_4)} + \frac{1}{(\alpha - it_4)} \right] \\
& (\quad 1 + \eta(\log(1 - it_{23}/\alpha) - \eta \log(1 + it_3/\alpha) + \eta \log(1 + it_2/\alpha) + \eta \log(1 + it_{34}/\alpha)) \\
& + \int_{-\infty}^{\infty} d^3t \frac{e^{i(E_1 t_{34} - E_2 t_2)}}{(\alpha - it_{23})(\alpha + it_4)} \eta \left[\log(1 + it_4/\alpha) - \log(1 - it_{24}/\alpha) \right] \\
& + \int_{-\infty}^{\infty} d^3t \frac{e^{i(E_1 t_{34} - E_2 t_2)}}{(\alpha - it_{23})(\alpha - it_4)} \eta \left[\log(1 - it_4/\alpha) - \log(1 + it_{24}/\alpha) \right] \\
& + \int_{-\infty}^{\infty} d^3t \frac{e^{i(E_1 t_{34} - E_2 t_2)}}{(\alpha + it_2)(\alpha + it_{34})} \eta \left[\log(\frac{1 + it_4/\alpha}{1 - it_4/\alpha}) - \log(\frac{1 - it_{24}/\alpha}{1 + it_{24}/\alpha}) \right] \Big\}.
\end{aligned} \tag{C.3.7}$$

As anticipated, we start noting that the last integral in (C.3.7), corresponding to the "non-propagating" term, is zero. The total current is basically given by:

$$\langle \hat{I} \rangle \simeq -e_0|\eta_1|^2|\eta_2|^2 \Big\{ I_1 + I_2 + I_3 \Big\}, \tag{C.3.8}$$

where the integrals have been named following the order in Eq. (C.3.7). Let us start with I_1 : we notice that the term in parenthesis gives a $2\pi\delta(t_4)$ contribution, while the remaining terms are:

$$\begin{aligned}
I_1 &= 2\pi \int_{-\infty}^{\infty} dt_2 dt_3 \frac{e^{i(E_1 t_{34} - E_2 t_2)}}{(\alpha - it_{23})} (1 + \eta(\log(1 - it_{23}/\alpha) + \eta \log(1 + it_2/\alpha)) \\
&= 2\pi \Big\{ (2\pi)^2 \delta(\Delta E) + 2\pi\eta\delta(\Delta E) \int_{-\infty}^{\infty} dt_2 \frac{e^{i(E_1 t_{34} - E_2 t_2)}}{(\alpha + it_3)} \log(1 + it_3/\alpha) \\
&+ 2\pi\eta e^{-E_1\alpha} \int_{-\infty}^{\infty} dt_2 e^{i\Delta E t_2} \log(1 + it_2/\alpha) \Big\} \\
&= (2\pi)^2 \left[2\pi\delta(\Delta E) \left(1 + \eta \frac{J_1}{2\pi} \right) + \eta e^{-E_1\alpha} J_2 \right].
\end{aligned} \tag{C.3.9}$$

Here J_1 and J_2 are the two integrals to evaluate. The I_1 term is equal to

$$\begin{aligned}
I_2 &= \eta \int_{-\infty}^{\infty} dt_2 dt_3 dt_4 \frac{e^{i(E_1 t_{34} - E_2 t_2)}}{(\alpha - it_{23})(\alpha + it_4)} \left[\log(1 + it_4/\alpha) - \log(1 - it_{24}/\alpha) \right] \\
&= \eta \int_{-\infty}^{\infty} dt_2 dt_4 \frac{e^{-i(E_1 t_4 - \Delta E t_2)}}{(\alpha + it_4)} \left[\log(1 + it_4/\alpha) - \log(1 - it_{24}/\alpha) \right] \int_{-\infty}^{\infty} dt_3 \frac{e^{iE_1 t_3}}{(\alpha + it_3)} \\
&= \eta 2\pi e^{-E_1\alpha} \Big\{ 2\pi\delta(\Delta E) \int_{-\infty}^{\infty} dt_4 \frac{e^{-i(E_1 t_4)}}{(\alpha + it_4)} \log(1 + it_4/\alpha) \\
&- \int_{-\infty}^{\infty} dt_2 e^{i(\Delta E t_2)} \log(1 - it_2/\alpha) \int_{-\infty}^{\infty} dt_4 \frac{e^{-iE_2 t_4}}{(\alpha + it_4)} \Big\} \\
&= \eta (2\pi)^2 e^{-E_1\alpha} \delta(\Delta E) J_4.
\end{aligned} \tag{C.3.10}$$

Above, we have used the fact that being $E_2 > 0$, the last integral in the last line is zero since it presents poles on the "wrong" side of the imaginary axes. The last "I" integral to compute is similar to (C.3.10), therefore following previous considerations we find

$$\begin{aligned} I_3 &= \eta 2\pi e^{-E_1\alpha}\Big\{2\pi\delta(\Delta E)\int_{-\infty}^{\infty} dt_4 \frac{e^{-i(E_1 t_4)}}{(\alpha - it_4)}\log(1 - it_4/\alpha) \\ &- \int_{-\infty}^{\infty} dt_2 e^{i(\Delta E t_2)}\log(1 + it_2/\alpha)\int_{-\infty}^{\infty} dt_4 \frac{e^{-iE_2 t_4}}{(\alpha - it_4)}\Big\} \\ &= \eta(2\pi)^2 e^{-E_1\alpha}\left[\delta(\Delta E)J_6 - e^{-E_2\alpha}J_2\right]. \end{aligned} \tag{C.3.11}$$

Using what we found so far in Eq. (C.3.8) we finally have :

$$\langle\hat{I}\rangle \simeq -(2\pi)^2 e_0|\eta_1|^2|\eta_2|^2\Big\{2\pi\delta(\Delta E)\left[1 + \frac{\eta}{2\pi}(J_1 + J_4 + J_6)\right] + \eta e^{-E_1\alpha}J_2(1 - e^{-E_2\alpha})\Big\}. \tag{C.3.12}$$

The Integral terms proportional to $\delta(\Delta E)$ only contribute to the renormalization of the elastic peak. The energy relaxation is then due to the term proportional to J_2, where

$$J_2 \simeq -2\pi\left[\alpha + \alpha^2\Delta E\right]. \tag{C.3.13}$$

To leading orders in α, the relaxation term is zero. This is not surprising if we consider that in a FQH state the parameter $1/\nu$ reflects the topological order of the bulk system and is itself a topological quantum number who, by definition, cannot be continuously varied.

D DETAILS ON SHOT NOISE AND NON-EQUILIBRIUM BOSONIZATION

In this appendix we present additional details concerning the evaluation of expectation values of exponents of bosonic fields out of equilibrium. In the first section we show how to evaluate thermal expectation values of bosonic fields after a quantum quench. In the second section we show how, in the Gaussian approximation, it is possible to study the time evolution of the distribution function and the low frequency noise power after a quantum quench. In the third section we describe how to evaluate the reference and the thermal noise introduced in the main text. In the forth section we give additional details on the derivation of the determinant formula Eq. (5.5.5) and its reduction to Toeplitz form. Thereafter we show how to implement a regularization scheme and numerically evaluate the determinant of the Toeplitz matrix. In this section we also provide a finite scaling analysis of the numerical results presented in the main text. Finally, in the fifth section we study the low-frequency noise in the weak transmission limit at the first QPC ($a \ll 1$) and show how the $a \log(1/a)$ dependence can be analytically obtained employing a lowest order approximation of the Toeplitz determinant.

D.1 EXPECTATION VALUES OF BOSONIC FIELDS AFTER A QUANTUM QUENCH

Consider the (lesser) Green function in the upper 2u edge mode after QPC1 and after the interaction has been turned on using the quantum quench protocol (see section 5.3) :

$$G^{<}_{2u}(\tau) = \langle \psi^{\dagger}_{2u}(t+\tau, x_0)\psi_{2u}(t, x_0)\rangle, \tag{D.1.1}$$

where the ψs are fermionic fields in the original basis after the quantum quench and x_0 is the position where the local Green function is evaluated. Using Eq. (2.1.40) we can rewrite the fermionic fields in the associated bosonic representation as

$$G^{<}_{2u}(\tau) = \frac{1}{2\pi\alpha} e^{[\phi_{2u}(x_0,t+\tau),\phi_{2u}(x_0,t)]/2} \langle e^{-\imath\{\phi_{2u}(x_0,t+\tau)-\phi_{2u}(x_0,t)\}}\rangle. \tag{D.1.2}$$

Hereafter we drop the suffix "u" since we will only consider operators defined on the upper edge. Using the mode decomposition of the bosonic fields Eq. (2.1.16) and the transforma-

tions between bosonic ladder operators before and after the quantum quench Eq. (5.3.5) and (5.3.6), we find :

$$\begin{aligned}\phi_2(x_0,t) &= \sum_{q>0}\left(\frac{2\pi}{qL}\right)^{1/2} e^{\imath q x_0} e^{-q\alpha/2}\Big(s_q(t)b_{1q}+v_q(t)b_{2q}\\ &+ s_q^*(t)b_{1q}^\dagger + v_q^*(t)b_{2q}^\dagger\Big).\end{aligned} \tag{D.1.3}$$

Here $t>0$ is the time at which the system is in the quenched state and τ should be interpreted as the tunneling time at the second QPC. Using the above expression we can write the difference between bosonic fields in Eq. (D.1.2) as :

$$\begin{aligned}-\imath(\phi_2(x_0,t+\tau)-\phi_2(x_0,t)) &= \sum_{q>0}\left(-\lambda_{1q}(t,\tau)b_{1q}+\lambda_{1q}^*(t,\tau)b_{1q}^\dagger\right)\\ &- \sum_{q>0}\left(-\lambda_{2q}(t,\tau)b_{2q}+\lambda_{2q}^*(t,\tau)b_{2q}^\dagger\right)\end{aligned} \tag{D.1.4}$$

where we have defined the coefficients

$$\begin{aligned}\lambda_{1q}(t,\tau) &= \imath\,(2\pi/qL)^{1/2}e^{\imath q x_0}e^{-q\alpha/2}\left(s_q(t+\tau)-s_q(t)\right)\\ \lambda_{2q}(t,\tau) &= \imath\,(2\pi/qL)^{1/2}e^{\imath q x_0}e^{-q\alpha/2}\left(v_q(t+\tau)-v_q(t)\right).\end{aligned} \tag{D.1.5}$$

Using again the Baker-Haussdorf formula and the fact that b_{1q} and b_{2q} are independently distributed at $t=0$ (i.e. before the quantum quench), we can disentangle the exponents in the expectation value and write

$$\begin{aligned}G_2^<(\tau) &= G_0^<(\tau)\langle e^{\sum_q \lambda_{1q}^* b_{1q}^\dagger}e^{-\sum_q\lambda_{1q}b_{1q}}\rangle_1\,\langle e^{\sum_q\lambda_{2q}^*b_{2q}^\dagger}e^{-\sum_q\lambda_{2q}b_{2q}}\rangle_2.\\ G_0^<(\tau) &= \frac{1}{2\pi\alpha}e^{[\phi_2(x_0,t+\tau),\phi_2(x_0,t)]/2}e^{-\sum_q|\lambda_{1q}|^2[b_{1q},b_{1q}^\dagger]/2}e^{-\sum_q|\lambda_{2q}|^2[b_{2q},b_{2q}^\dagger]/2}\end{aligned} \tag{D.1.6}$$

The commutator of the bosonic ϕ fields can be evaluated by making use of the mode decomposition in terms of bosonic ladder operators :

$$\begin{aligned}[\phi_2(x_0,t+\tau),\phi_2(x_0,t)] &= -\sum_{q>0}\left(\frac{2\pi}{qL}\right)e^{-q\alpha}\Big\{s_q^\star(t+\tau)s_q(t)-s_q(t+\tau)s_q^\star(t)\\ &+ v_q^\star(t+\tau)v_q(t)-v_q(t+\tau)v_q^\star(t)\Big\}\\ &= (2\imath)P\int_0^\infty\frac{dq}{q}\left\{\left(\frac{\gamma_\theta^2}{4}+\sin^4\theta\right)\sin(q\,\tilde{u}_1\,\tau)+\left(\frac{\gamma_\theta^2}{4}+\cos^4\theta\right)\sin(q\,\tilde{u}_2\tau)\right\}\\ &= \left(\frac{\gamma_\theta^2}{4}+\sin^4\theta\right)\log\left(\frac{\alpha+\imath\,\tilde{u}_1\,\tau}{\alpha-\imath\,\tilde{u}_1\,\tau}\right)+\left(\frac{\gamma_\theta^2}{4}+\cos^4\theta\right)\log\left(\frac{\alpha+\imath\,\tilde{u}_2\,\tau}{\alpha-\imath\,\tilde{u}_2\,\tau}\right),\end{aligned} \tag{D.1.7}$$

where in the equality we have moved to the continuum by exchanging the sum over momenta for a principal value integral. The remaining two commutators involving bosonic ladder operators in Eq. (D.1.6) can be evaluated following a similar procedure:

$$\begin{aligned}
&- \sum_{q>0} \left(|\lambda_{1q}|^2 \left[b_{1q}, b_{1q}^\dagger \right] + |\lambda_{2q}|^2 \left[b_{2q}, b_{2q}^\dagger \right] \right) = - \sum_{q>0} \left(\frac{2\pi}{qL} \right) e^{-q\alpha} \Big\{ |s_q(t+\tau)|^2 + |s_q(t)|^2 \\
&- \left(s_q^\star(t+\tau) s_q(t) + s_q(t+\tau) s_q^\star(t) \right) + |\nu_q(t+\tau)|^2 + |\nu_q(t)|^2 \qquad \text{(D.1.8)} \\
&- \left(\nu_q^\star(t+\tau) \nu_q(t) + \nu_q(t+\tau) \nu_q^\star(t) \right) \Big\} \\
&= -P \int_0^\infty \left(\frac{2\pi}{qL} \right) e^{-q\alpha} \Big\{ \frac{-\gamma_\theta^2}{2} \left[\cos(q\,\tilde{u}_1\,\tau) + \cos(q\,\tilde{u}_2\,\tau) \right] + 2\cos^4\theta \left[1 - \cos(q\,\tilde{u}_2\,\tau) \right] \\
&+ 2\sin^4\theta \left[1 - \cos(q\,\tilde{u}_1\,\tau) \right] \Big\} \\
&= -\left(\frac{\gamma_\theta^2}{4} + \sin^4\theta \right) \log\left(\frac{\tilde{u}_1^2\tau^2 + \alpha^2}{\alpha^2} \right) - \left(\frac{\gamma_\theta^2}{4} + \cos^4\theta \right) \log\left(\frac{\tilde{u}_2^2\tau^2 + \alpha^2}{\alpha^2} \right).
\end{aligned}$$

Noticing that $\gamma_\theta^2 + \sin^4\theta = \sin^2\theta$, $\gamma_\theta^2 + \cos^4\theta = \cos^2\theta$ and summing Eq. (D.1.7), (D.1.8) we finally obtain

$$\begin{aligned}
G_0^<(\tau) &= \frac{1}{2\pi\alpha} \exp\Big\{ \frac{1}{2}\sin^2\theta \left[\log\left(\frac{\alpha + \imath\,\tilde{u}_1\,\tau}{\alpha - \imath\,\tilde{u}_1\,\tau} \right) - \log\left(\frac{\alpha^2 + \tilde{u}_1^2\tau^2}{\alpha^2} \right) \right] \\
&+ \frac{1}{2}\cos^2\theta \left[\log\left(\frac{\alpha + \imath\,\tilde{u}_2\,\tau}{\alpha - \imath\,\tilde{u}_2\,\tau} \right) - \log\left(\frac{\alpha^2 + \tilde{u}_2^2\tau^2}{\alpha^2} \right) \right] \Big\} \\
&= \frac{1}{2\pi} \frac{1}{(-\imath\,\tilde{u}_1\,\tau + \alpha)^{\sin^2\theta}} \frac{1}{(-\imath\,\tilde{u}_2\,\tau + \alpha)^{\cos^2\theta}}.
\end{aligned}$$

D.2 GAUSSIAN APPROXIMATION AND TIME EVOLUTION

Even though the Gaussian approximation cannot give the correct result (see B.1), it nevertheless provides a qualitative insights into the system's relaxation dynamics. The time dependent fermionic propagator, at the Gaussian level, is given by

$$C_{\psi_2}(x,t) \simeq \frac{\imath}{2\pi} \frac{1}{(x + \imath\alpha)} e^{-I(x,t)} = g(x) h(x,t), \qquad \text{(D.2.1)}$$

where all informations regarding interactions and non-equilibrium effects are contained in the exponent

$$\begin{aligned}
I(x,t) &= \frac{\gamma_\theta^2}{2} a(1-a) \Big\{ 2\cos(Q\,\Delta\tilde{u}\,t) + 2\mathrm{Ci}[Q\,\Delta\tilde{u}\,t] - \mathrm{Ci}[Q\,(\Delta\tilde{u}\,t - x)] \qquad \text{(D.2.2)} \\
&- \mathrm{Ci}[Q\,(\Delta\tilde{u}\,t + x)] + 2Q\,\Delta\tilde{u}\,t\,\mathrm{Si}[Q\,\Delta\tilde{u}\,t] + Q\,(\tilde{u}_1\tau - \Delta\tilde{u}\,t)\,\mathrm{Si}[Q\,(\Delta\tilde{u}t - x)] \\
&+ 2(Q\,x)\,\mathrm{Si}[Q\,x] - Q(\Delta\tilde{u}\,t + x)\,\mathrm{Si}[Q(\Delta\tilde{u}\,t + x)] + 2\mathrm{Ci}[Q\,x] \\
&+ 4\cos(Q\,x)\,\sin^2[Q\,\Delta\tilde{u}\,t/2] - 2(1 + \gamma_E) - 2\log\left(\frac{Q\,\Delta\tilde{u}\,t\,x}{((\Delta\tilde{u}\,t)^2 - x^2)^{1/2}} \right) \Big\}.
\end{aligned}$$

$\mathrm{Si}(x)$ is an entire function of its arguments with no branch cut discontinuities. $\mathrm{Ci}(x)$ on the other hand has a branch cut discontinuity in the complex x plane, running from $-\infty$ to 0.

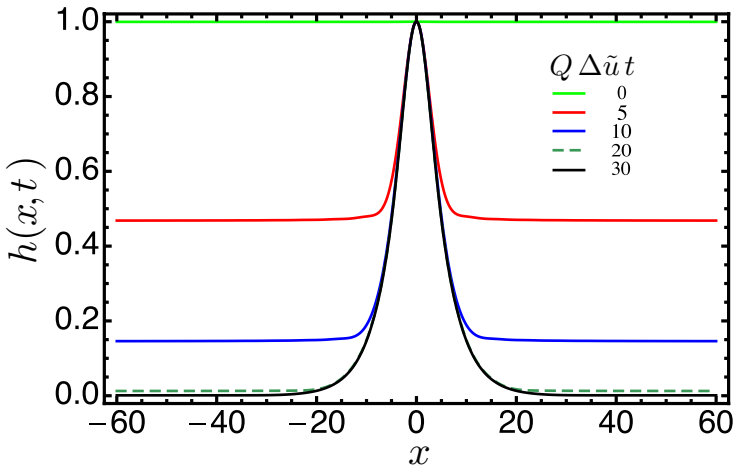

Figure 44: Time evolution of the pulse signal. The function $h(x,t)$ is plotted as a function of x. The different curves in the plot correspond to different values of the dimensionless parameter $Q\,\Delta\tilde{u}t$. The function $h(x,t)$ has been evaluated for $\theta = 0.47$ and a=1/2.

In Fig. (44) we show the time evolution of $h(x,t)$; this term varies from a constant value (1), corresponding to the non-interacting system at $t = 0$, to a stationary value describing a pulse signal of width x. In order to evaluate the momentum distribution function, we need to Fourier transform Eq. (D.2.1). This evaluation is greatly simplified with the help of the so called "dual convolution" theorem.

Dual convolution theorem. *If* $f(x) = g(x)\,h(x)$, *where g(x) and h(x) satisfy the Dini criterion on convergence of Fourier series, then the Fourier transform of* $f(x)$ *ca be obtained as*

$$\hat{f}(k) = \frac{1}{2\pi}\int_{-\infty}^{\infty} dq\,\hat{g}(k-q)\,\hat{h}(q) \tag{D.2.3}$$

$$\hat{g}(q-k) = \int_{-\infty}^{\infty} dx e^{\imath(k-q)x} g(x) \tag{D.2.4}$$

$$\hat{h}(q) = \int_{-\infty}^{\infty} dx e^{\imath q x} h(x) \tag{D.2.5}$$

The Fourier transform of $g(x)$ can be easily evaluated analytically and it gives $\hat{g}(k-q) = \theta(q-k)$ in the $\alpha \to 0$ limit. The convolution between the step function and the pulse-like function $h(x,t)$ can be evaluated numerically with a simple Mathematica code (D.2.1). The convolution is most easily (and more rapidly) performed moving to discrete time. To obtain a faithful digital representation of the original continuous function we use the Nyquist–Shannon sampling theorem [119, 120] that states that a band limited function $f(t)$, with $t \in [-b,b]$ is faithfully discretized by choosing a sampling rate (or discretization pace) $s > 1/(2b)$. This choice of s avoids phenomena such as aliasing when performing any operations on the discretized function and it guarantees a high precision numerical result. Unfortunately, the theorem only gives a lower bound for the value of s, and the actual value should be found using some test function. Once $h(x,t)$ has been discretized, it is possible to

perform a discrete Fourier transform of it to momentum space, that we call $\hat{h}(x,t)$. From the dual convolution theorem, we have

$$\begin{aligned} f_{2u}(k,t) &= \frac{1}{2\pi}\int_{-\infty}^{\infty} dq\, \theta(q-k)\hat{g}(q,t) \\ &= \frac{1}{2\pi}\int_{k}^{\infty} dq\, \hat{g}(q,t) \\ &\simeq s'\sum_{q=k}^{L}\hat{g}(q,t). \end{aligned} \tag{D.2.6}$$

In the last line we have switched the integral over continuous momentum to a discrete sum. The optimal sampling frequency (that is proportional to the reciprocal of the discretization step) is $s' = 6.3/2b$ and it has been found using some appropriate test function. $L = max[\hat{g}]$ is the maximum dimension of the array $\hat{g}$. In this final form, the convolution can be computed in a very efficient way using the Mathematica function "Total" and its parallelization; further details are given in the next paragraph.

D.2.1 Mathematica code for the Gaussian approximation

Here we present the Mathematica code developed for the evaluation of the distribution functions of Fig.(34). In the code we use the following convention for the functions :

- $bn[x,t,\Delta\mu,a,\theta] = h(x,t)$,
- $f_{2u}(k) = convtime$.

```
(* Initialization *)

b = 6*21; (*extremum of the data chunk. It is defined by the  value for which
the real space function is zero. *)

pace = 6.3/(2*b); (* Defines the sampling frequency of bn *)

tpace = 0.5; (* time discretization pace*)

n = IntegerPart[(2*b)/pace] (* number of elements in the array *)

mom = Table[m, {m, -b, b, pace}] ;(* Creates an array whose entries
are the discrete values of the energy *)

time = Table[ ti, {ti, 0.01, 150.01, 0.5}]; (* Creates an array whose entries
are the time slices at which the function bn is evaluated*)
```

```
L = Length[mom];  (* Gives the length of the momentum array*)

Lt = Length[time] ; (* Gives the length of the time array*)
zero = n/2 + 1; (* Gives the position of the zeroth element*)

(* Sampling of bn and evaluation of the distribution function *)

ft = Parallelize[ Table[ bn[x, t, 1, 1/2, 0.47], {t, 0.01, 150.01, 0.5},
{x, -b, b, pace}]]; (*Initialize the function to be sampled.
"ft" is a matrix with entries the time interval x, t, the bias voltage,
the transmission probability and the mixing angle respectively *)

ftl = RotateLeft[ ft, {0, n/2}];
(* "RotateLeft" moves the x=0 term in the first element of the array *)

ftT = Table[ Flatten[Chop[RotateRight[Fourier[ftl[[i]],
FourierParameters -> {0, 1}], n/2]]], {i, 1, Lt}];
(*Perform the FFT on the datas and put the array's elements
back  in normal order  *)

convtime = Table[Table[(pace/(Sqrt[2 \[Pi]]))* Total[ftT[[i, j ;; L]]],
{j, 1, L}], {i, 1, Lt}];
(*Performs the convolution with the step function. It returns the momentum
distribution function *)

M[Q] = IntegerPart[Q/ pace)];
(* Boundary of the integration domain. It depends on the bias voltage *)

(* Evaluation of the low frequency noise at different times *)

i = 1;

Noiset = Array[z, {300}];

For[k = 1, k < 301, k += 1,

 Noiset[[i]] = (pace*Total[ Table[(convtime[[k, j]]),
 {j, zero + 1, zero + M[1]}]] +
 pace*Total[Table[((convtime[[k, zero - M[1]]]
 - convtime[[k, j]])), {j,zero - M[1], zero}]]);
```

```
i++;
 ];
```

D.3 EXACT EVALUATION IN THE LONG TIME LIMIT

We start this section deriving the determinant formula Eq. (5.5.5) of non-equilibrium bosonization. Next we show that the evaluation of the determinant is simplified by a reduction of the associated matrix to Toeplitz form. Following [8] we will bring the determinant in a form suitable for being evaluated numerically. Finally we will show the numerical procedure used to evaluate the low frequency noise power and present a finite scaling analysis of the results.

Our starting point is the correlator of bosonic exponentials in Eq. (D.1.9)

$$\Delta_\tau[t] = \langle e^{\sum_q \lambda^\star_{1u,q}(t,\tau) b^\dagger_{1u,q}} e^{-\sum_q \lambda_{1u,q}(t,\tau) b_{1u,q}} \rangle_1, \tag{D.3.1}$$

where the subscript 1 means that the expectation value is taken with respect to the density matrix of the first edge mode. The phase factor $\lambda_{1u,q}(t,\tau)$ contains information on the inter-mode interaction and is defined in Eq. (5.5.4) as

$$\lambda_{1u,q}(t,\tau) = \imath\,(2\pi/qL)^{1/2} e^{\imath q x_0 - q\alpha/2}(s_q(t+\tau) - s_q(t)). \tag{D.3.2}$$

At this point we note that since the b operators are defined before the quantum quench, and therefore in the absence of interactions, we can re-express them in terms of free fermionic operators using the bosonization identity :

$$\begin{aligned} b^\dagger_{q,\eta} &= \imath\sqrt{\frac{2\pi}{Lq}} \sum_{k=-\infty}^{\infty} c^\dagger_{k+q,\eta} c_{k,\eta} \\ b_{q,\eta} &= -\imath\sqrt{\frac{2\pi}{Lq}} \sum_{k=-\infty}^{\infty} c^\dagger_{k-q,\eta} c_{k,\eta}. \end{aligned} \tag{D.3.3}$$

In this way we can can use the (non interacting) fermionic density matrix after QPC1

$$\hat\rho_1 = \frac{e^{-\beta \hat H_1}}{\mathrm{Tr}\left\{e^{-\beta \hat H_1}\right\}} \tag{D.3.4}$$

to evaluate the expectation value in Eq. (D.3.1) :

$$\Delta_\tau[t] = \mathrm{Tr}\left\{\hat\rho_1\, e^{\imath \sum_k \left(\sum_q \sqrt{\frac{2\pi}{Lq}} \lambda^\star_{1u,q}(t,\tau)\right) c^\dagger_{1u,k+q} c_{1u,k}} e^{\imath \sum_k \left(\sum_q \sqrt{\frac{2\pi}{Lq}} \lambda_{1u,q}(t,\tau)\right) c^\dagger_{1u,k-q} c_{1u,k}}\right\}. \tag{D.3.5}$$

In the present form Δ_τ can be interpreted in terms of the correlator of full counting statistics described in (B.3). We can then use the trace formula

$$\mathrm{Tr}\left[e^{\hat A_1}\, e^{\hat A_2} ... e^{\hat A_i}\right] = \det\left[1 + e^{A_1}\, e^{A_2} ... e^{A_i}\right], \tag{D.3.6}$$

where the trace on the left hand side is taken over operators defined in the 2^n-dimensional Fock space while the determinant on the right hand side is taken over operators defined in the n-dimensional single-particle Hilbert space. Using the trace formula we find

$$\begin{aligned}\Delta_\tau[\delta(t)] &= \frac{\det\left[1+e^{-\beta\,\epsilon_1}e^{\sum_q\sqrt{\frac{2\pi}{Lq}}\lambda^\star_{1u,q}(t,\tau)}e^{\sum_q\sqrt{\frac{2\pi}{Lq}}\lambda_{1u,q}(t,\tau)}\right]}{\det\left[1+e^{-\beta\,\epsilon_1}\right]} \\ &= \det\left[1+\left(e^{\imath\sum_q\sqrt{\frac{2\pi}{Lq}}(\lambda_{1q}+\lambda^\star_{1q})}-1\right)\hat{f}_D(\epsilon)\right],\end{aligned} \tag{D.3.7}$$

where we have used the fact that the distribution function in edge mode 1 is a double step Fermi function. Here we denote $\hat{f}_D(\epsilon)$ with a "hat" meaning that we consider it as the single-particle projector on the occupied states in energy space. The scattering phase can now be evaluated

$$\begin{aligned}\imath &\sum_{q>0}\sqrt{\frac{2\pi}{Lq}}(\lambda_{1q}+\lambda^\star_{1q}) = -\imath\gamma_\theta\sum_{q>0}\frac{2\pi}{qL}\Big(\sin q[x_0-\tilde{u}_1(t+\tau)] \\ &- \sin q[x_0-\tilde{u}_1\,t]-\sin q[x_0-\tilde{u}_2(t+\tau)]+\sin q[x_0-\tilde{u}_2\,t]\Big) \\ &= -\imath\gamma_\theta\frac{\pi}{2}\Big(\mathrm{sgn}[x_0-\tilde{u}_1(t+\tau)]-\mathrm{sgn}[x_0-\tilde{u}_1\,t] \\ &- \mathrm{sgn}[x_0-\tilde{u}_2(t+\tau)]+\mathrm{sgn}[x_0-\tilde{u}_2\,t]\Big).\end{aligned} \tag{D.3.8}$$

In order to evaluate the above expression, we have as usual exchanged the sum over q for a principal value integral. Finally, using the identity $\mathrm{sgn}(x) = 2\theta(x)-1$ we can define the time dependent scattering phase operator as

$$\begin{aligned}\hat{\delta}_\tau(t) &= \delta\,\hat{\omega}_\tau(t,x_0) \\ \hat{\omega}_\tau(t,x_0) &= \theta(x_0-\tilde{u}_1(t+\tau))-\theta(x_0-\tilde{u}_1\,t)+\theta(x_0-\tilde{u}_2 t) \\ &- \theta(x_0-\tilde{u}_2(t+\tau)),\end{aligned} \tag{D.3.9}$$

Where we have defined the time independent part of the scattering phase $\delta = \pi\gamma_\theta$ and the "window operator" $\hat{\omega}_\tau(t,x_0)$. It is convenient to scale out the velocities from the window function as follows

$$\begin{aligned}\hat{\omega}_\tau(t,\tilde{t}_1,\tilde{t}_2) &= \theta(\tilde{t}_1-t-\tau)-\theta(\tilde{t}_1-t)+\theta(\tilde{t}_2-t)-\theta(\tilde{t}_2-t-\tau) \\ \tilde{t}_1 &= x_0/\tilde{u}_1 \\ \tilde{t}_2 &= x_0/\tilde{u}_2.\end{aligned} \tag{D.3.10}$$

Using these relations, we can finally write Eq. (D.3.1) as

$$\Delta_\tau[\delta(t)] = \det\left[1+\left(e^{-\imath\hat{\delta}_\tau(t)}-1\right)\hat{f}_D(\epsilon)\right]. \tag{D.3.11}$$

In order to make the connection to the full counting statistics meaningful, δ should be understood as the "counting parameter", and $\hat{\omega}_\tau$ as a single-particle projector on the edge

mode in real time[1]. As in the problem of full counting statistics, time and energy in the Fredholm determinant should be understood as conjugate variables. In Fig. (35) we plot $\hat{\omega}_\tau$ for $\tau \ll x_0(\tilde{u}_1^{-1} - \tilde{u}_2^{-1})$, where there are two well separated unit square pulses of opposite signs. Making use of the definition of $\gamma_\theta = \sin 2\theta$, we can rewrite the scattering phase as $\delta_\tau = 2\pi(e^*/e)\omega_\tau(t, \tilde{t}_1, \tilde{t}_2)$, where 2π is the phase associated with a non-interacting particle. In this form we can interpret the two pulses in terms of the $\pm e^*$ charges arriving at QPC2 respectively at time $\tilde{t}_1$ and $\tilde{t}_2$. Note that in this limit the two pulses are orthogonal to each others. When the above condition over τ is not fulfilled, the widths of the two pulses is larger than their mutual separation and they partially overlap. However, this limit is not usually physically realized. Finally, note that if $\tilde{t}_1$ and $\tilde{t}_2$ are close to zero, that means we look at the system in a close neighbourhood of the first QPC, there are no pulses at all in the second edge mode. Physically this is due to the fact that in our model a charge e electron is tunneled in the first edge mode and it fractionalizes on both edge modes only after a finite time away form QPC1, see Fig. (31).

D.3.1 Reduction to Toeplitz form and numerical evaluation of shot noise power

The main problem in evaluating the determinant defined in Eq. (D.3.11) is that $\bar{\delta}_\tau(t)$ and $\hat{f}_D(\epsilon)$ are not in general simultaneously diagonalizable. However, being $\hat{\omega}_\tau$ a projector, we can use the identity $e^{-\imath\delta\hat{\omega}_\tau} = 1 + \hat{\omega}_\tau(e^{-\imath\delta} - 1)$ to write the Fredholm determinant as :

$$\Delta_\tau[\delta] = \det\left[1 + \hat{\omega}_\tau(t, \tilde{t}_1)\left(e^{-\imath\delta} - 1\right)\hat{f}_D(\epsilon) + \hat{\omega}_\tau(t, \tilde{t}_2)\left(e^{\imath\delta} - 1\right)\hat{f}_D(\epsilon)\right]. \tag{D.3.12}$$

Where

$$\hat{\omega}_\tau(t, \tilde{t}_i) \quad = \quad \begin{cases} 1 & t \in [\tilde{t}_i, \tau], i = 1, 2 \\ 0 & otherwise. \end{cases} \tag{D.3.13}$$

Note that the last term in Eq. (D.3.12) contains a positive scattering phase. However, as we will show later, the determinant is symmetric with respect to the $\pm\imath\delta$ phase. In the above expression t_i can also be set to zero since the pulse is solitonic and doesn't change its shape in time. In other words, t_i just corresponds to a time shift with no effect on the evaluation of the determinant. The above relation also states that the determinant is different from "1" only in an interval of width τ. This means that the determinant only depends on the difference between two times (t_i and $t_i + \tau$) and therefore it can be recast in Toeplitz form. Since the determinant does not depend explicitly on t anymore, we have adopted the new notation $\Delta_\tau[\delta(t)] \to \Delta_\tau[\delta]$. Before showing that the determinant can be recast in Toeplitz form, we see that by exponentiating both sides of Eq. (D.3.12) we can write the determinant as

$$\Delta_\tau[\delta] \simeq \Delta_{\tau,s}[-\delta]\Delta_{\tau,s}[\delta], \tag{D.3.14}$$

where $\Delta_{\tau,s}[\mp\delta]$ involves respectively the negative and the positive phase term in Eq.(D.3.12) and the suffix s means that it involves only a single pulse. However, the determinant has

1 Note that this property follows from the property of the Heaviside step function $\theta(x)^2 = \theta(x)$.

the following symmetry $\Delta_\tau[-\delta] = \Delta_{-\tau}[\delta]$ [6] and the two terms in Eq. (D.3.14) are therefore equivalent. We still have to deal with two projectors: one in real time and the other in energy space. In order to make the Toeplitz form of the determinant explicit we need to Fourier transform it such that everything is defined in real time. First we note that due to the property $\hat{\omega}_\tau^2 = \hat{\omega}_\tau$, we can write

$$\begin{aligned} \Delta_{\tau,s}[\delta] &= \det[1 + \hat{\omega}_\tau(t,0)(e^{-\imath\delta} - 1)\hat{\omega}_\tau(t,0)\hat{f}_D(\epsilon)] \\ &= \det[g(\epsilon)]. \end{aligned} \tag{D.3.15}$$

Expectation values of bosonic coherent states have an ultraviolet singularity, physically coming from the linearization of the original electron dispersion relation. In order to regularize $g(\epsilon)$ we restrict the energy variable $\epsilon \in [-\Lambda, \Lambda]$ (2.1). The next step consist in discretizing time by introducing an elementary time step $\Delta t = \pi/\Lambda$[2], such that $t_j = j\,\Delta t$. The matrix elements are given by Fourier transforming $g(\epsilon)$ and using the fact that due to the time projector, the Fourier transform can only depend on time differences

$$T_{jk} = \frac{1}{2\pi}\int d\epsilon\, e^{\imath\,\epsilon\,(t_j - t_k)} g(\epsilon). \tag{D.3.16}$$

Since the matrix T_{jk} only depends on the difference $j - k$ it is of the Toeplitz type. In order to bring Eq. (D.3.15) in the canonical Toeplitz form [118] we need to define $g(\epsilon)$ on the unit circle $z = e^{\imath\varphi}$, parametrized by the angle $\varphi \in [-\pi, \pi]$. From the above definition it follows that $\varphi = \pi\epsilon/\Lambda$. However, when performing this identification directly on $g(\epsilon)$, the Fermi function presents a non-physical jump at $\varphi = \pm\pi$ that would give rise to an additional contribution of the Fermi-edge type. This problem can be avoided by redefining $g(\epsilon)$ with an additional phase factor [3] :

$$g(\epsilon) = e^{-\imath\frac{\epsilon\delta}{2\Lambda}}\left(1 + (e^{-\imath\delta} - 1)f_D(\epsilon)\right). \tag{D.3.17}$$

In the theory of Toeplitz matrices, $g(\varphi)$ is known as the symbol of the Toeplitz matrix[4]. In our case of a double step[5] Fermi distribution, the symbol of the Toeplitz matrix presents jump singularities corresponding to the Fermi edges[6]

$$g(\varphi) = e^{-\frac{\imath\delta}{2\pi}\varphi}\begin{cases} 1 & (1-a)\,eV/\Lambda < \varphi < \pi \\ 1 + a(e^{-\imath\delta} - 1) & -eV\,a\,\pi/\Lambda < \varphi < (1-a)\,eV\,\pi/\Lambda \\ e^{-\imath\delta} & -\pi < \varphi < -eV\,a\,\pi/\Lambda. \end{cases} \tag{D.3.18}$$

2 This is coming from the energy time "uncertainty" $\Delta\epsilon\,\Delta t \sim 2\pi$, in units of $\hbar = 1$. See also the discussion in (B.3.2).

3 This additional contribution is essentially due to the hard cut-off we chose in energy space. For example in Eq. (D.3.20) without the additional phase factor we would get 1 at $\varphi = \pi$ and $e^{-\imath\delta}$ at $\varphi = -\pi$. This additional jump in $g_0(\varphi)$ can be eliminated by introducing the additional phase factor.

4 In the mathematical literature the symbol of the Toeplitz matrix is often referred to as $g(e^{\imath\varphi})$.

5 The above analysis is valid for a general multi-step distribution.

6 These are also known as Fisher-Hartwig singularities.

The corresponding Toeplitz matrix for the double step distribution is found using Eq. (D.3.16). Note that the dimension of the NxN matrix depends on the discretization step as $N = \tau/\Delta t$, that means $\pi/\Lambda = \tau/N$. Using this identity we find

$$\begin{aligned}(T_D)_{jk} &= \frac{\Lambda}{2\pi^2}\int_{-\pi}^{\pi} d\varphi\, e^{\imath\varphi(j-k)} g(\varphi) \\ &= \frac{\Lambda}{2\pi^2\,\imath\gamma_{jk}}\Big(e^{\imath\pi\gamma_{jk}} - e^{-\imath(\pi\gamma_{jk}+\delta)} + e^{\imath(1-a)(eV\tau/N)\gamma_{jk}}(e^{-\imath\delta}-1)a \\ &+ e^{-\imath\pi a(eV\tau/N)\gamma_{jk}}(e^{-\imath\delta}-1)(1-a)\Big),\end{aligned} \tag{D.3.19}$$

where we have defined $\gamma_{jk} = j - k - \delta/2\pi$. It turns out that the determinant formula (D.3.7) does not give a properly normalized result for the Toeplitz determinant. This is due to the fact that in deriving the determinant formula, the expectation value of the Fermionic operators was not taken with respect to the ground state[7]. This problem can be solved by introducing the normalized determinant $\bar{\Delta}_{\tau,s}$, defined as the ratio between $\Delta_{\tau,s}[\delta]$ and its zero temperature value. The zero temperature determinant can be evaluated following same reasoning as before; the symbol of the determinant is given by

$$g_0(\varphi) = e^{-\frac{\imath\delta}{2\pi}\varphi}\begin{cases}1 & 0 < \varphi < \pi \\ e^{-\imath\delta} & -\pi < \varphi < 0,\end{cases} \tag{D.3.20}$$

and the corresponding Toeplitz matrix by

$$(T_0)_{jk} = \frac{\Lambda}{2\pi^2\,\imath\gamma_{jk}}\Big((e^{-\imath\delta}-1) + e^{\imath\pi\gamma_{jk}} - e^{-\imath(\pi\gamma_{jk}+\delta)}\Big). \tag{D.3.21}$$

To conclude, we found that Eq. (D.3.7) can be rewritten in the discretized form ($N = \tau/\Delta t$)

$$\bar{\Delta}_{N,s}[\delta] = \frac{\det[\hat{T}_D]}{\det[\hat{T}_0]}. \tag{D.3.22}$$

To obtain the low frequency noise power, we need to evaluate first the Fourier transform of $G^<_{2u}(\tau) = G^<_0(\tau)\,\bar{\Delta}^2_{\tau,s}(\delta)$ and then use the noise Formula. The discretized determinant of Eq. (D.3.22) can be evaluated using the standard Mathematica function. Our strategy consists again in using the dual convolution theorem to disentangle the evaluation of the Fourier transform of G_0 and $\bar{\Delta}^2_{\tau,s}$. We start by evaluating the Fourier transform of $G^<_0(\tau)$ as a convolution of the two zero temperature Green functions of the two different edge modes

$$\begin{aligned}I_1(\xi) &= \int d\tau \frac{e^{-\imath\xi\tau}}{(-\imath\,\tilde{u}_1\,\tau+\alpha)^{\sin^2\theta}} = \frac{2\pi\,\xi^{\sin^2\theta-1}}{\Gamma\left(\sin^2\theta\right)\tilde{u}_1^{\sin^2\theta}} e^{-\alpha\xi/\tilde{u}_1}\theta(-\xi) \\ I_2(\xi) &= \int d\tau \frac{e^{-\imath\xi\tau}}{(-\imath\,\tilde{u}_2\,\tau+\alpha)^{\cos^2\theta}} = \frac{2\pi\,\xi^{\cos^2\theta-1}}{\Gamma\left(\cos^2\theta\right)\tilde{u}_2^{\cos^2\theta}} e^{-\alpha\xi/\tilde{u}_2}\theta(-\xi).\end{aligned} \tag{D.3.23}$$

7 Note that in the derivation of the full counting statistics this problem was not present. In that case we always obtain particle number fluctuations between two excited states, resulting in terms proportional to $f_1(\epsilon)(1-f_2(\epsilon))$. See also (B.3.2).

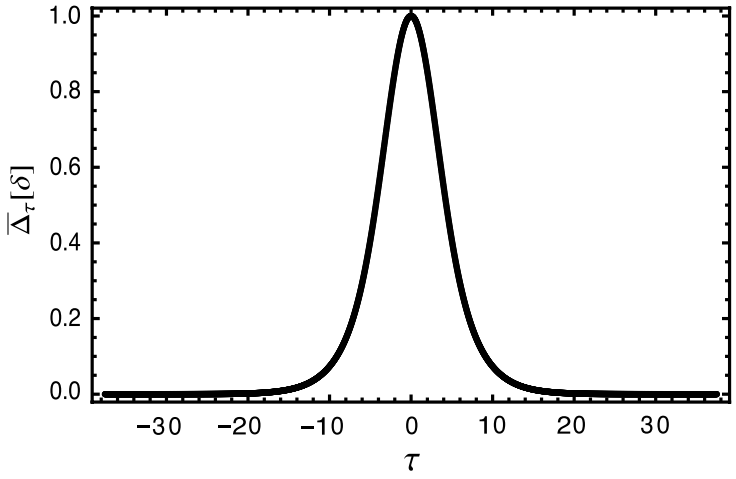

Figure 45: Numerical evaluation of the normalized Fredholm determinant. Here we plot Eq. (D.3.22) for $\theta = 0.47$, $a = 1/2$ and $eV = 1$. Choosing N=200 the above plot contains 25606 points, that make it indistinguishable from a continuous plot.

Note that, if we want to take the $\alpha \to 0$ limit after the convolution, we need to use a properly symmetrized combination :

$$\begin{aligned}
\tilde{h}(\epsilon) &= \frac{1}{(2\pi)^2}\left\{\frac{1}{2}\int_\xi I_1(\xi)I_2(\epsilon-\xi) + \frac{1}{2}\int_\xi I_1(\epsilon-\xi)I_2(\xi)\right\} \qquad \text{(D.3.24)}\\
&= \frac{\theta(-\epsilon)}{2\,\tilde{u}_1^{\sin^2\theta}\tilde{u}_2^{\cos^2\theta}}\Big\{e^{-\alpha\epsilon/(\tilde{u}_2)}\,{}_pF_q\left(\sin^2,1,-\alpha\epsilon(\tilde{u}_1^{-1}-\tilde{u}_2^{-1})\right)\\
&+ e^{-\alpha\epsilon/\tilde{u}_1}\,{}_pF_q\left(\cos^2\theta,1,-\alpha\epsilon(\tilde{u}_1^{-1}-\tilde{u}_2^{-1})\right)\Big\}\\
&\xrightarrow{\alpha\to 0} \frac{\theta(-\epsilon)}{\tilde{u}_1^{\sin^2\theta}\tilde{u}_2^{\cos^2\theta}}.
\end{aligned}$$

The function ${}_pF_q(a;b;z)$ is the generalized Hypergeometric function [104]. Note that since the integrand is analytic, we could have taken the $\alpha \to 0$ limit before the convolution, in this case the symmetrization is not needed and (D.3.24) is recovered.

Next, we discuss the evaluation of the determinant $\bar{\Delta}^2_{\tau,s}$. In Fig. (45) the determinant is plotted as a function of τ for a specific value of the mixing angle θ and the transmission parameter a at QPC1. Again, the determinant describes a well defined, band limited signal that can be analyzed using the methods explained in section (D.2). We find good convergence of the result for a matrix size of $N = 200$ when the resulting non-equilibrium distribution function is correctly symmetrized around $1/2$. However, we may wonder how the Fano factor computed from this procedure depends on the matrix size N and in particular how much the computed value deviates from the one corresponding to continuous time. Remember that $N \propto 1/\Delta t$, so the continuous limit $\Delta t \to 0$ corresponds to $N \to \infty$. This problem is equivalent to the problem of finite size scaling in critical phenomena [121]. We consider the computed

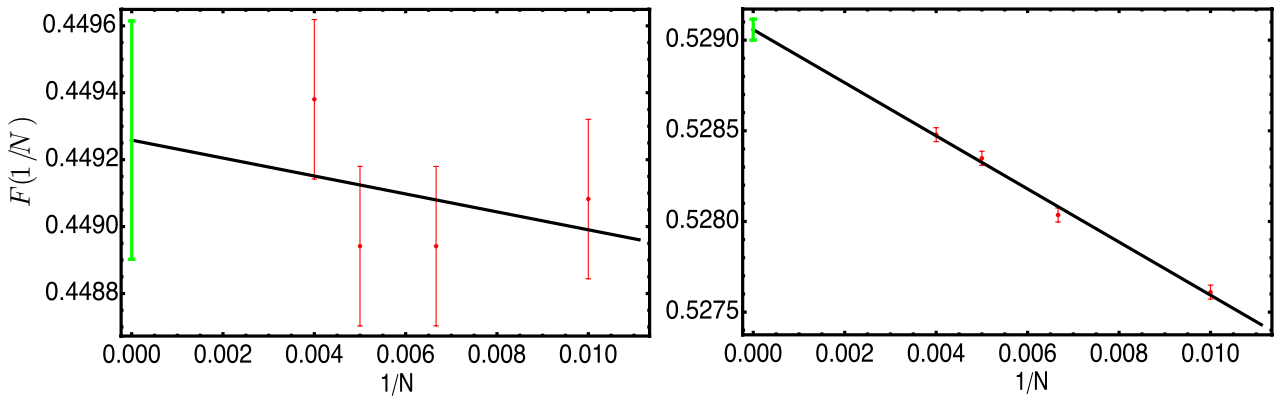

Figure 46: Finite size scaling of the Fano factor. Fano factor evaluated at $a = 1/2$ (left) and $a = 0.2$ (right) as a function of inverse matrix size. The green point corresponds to the extrapolated value in the $N \to \infty$ limit.

Fano factor as a function of $1/N$; in the continuum time limit $F(1/N) \to F(0)$, while for a finite size system the Fano factor scale as a power law in $1/N$

$$F(1/N) = F(0)\,(1/N)^{a}\,. \tag{D.3.25}$$

In Fig. (46) we plot the logarithm of the above expression for different matrix sizes. The value of $F(0)$ and a is found by a linear fit of the datas. Errors on the extrapolated quantities are computed by standard error analysis.

D.3.2 Mathematica code for the full non-equilibrium noise

```
(*Initialization*)
del = Pi Sin[2 0.47];

g[j_, k_] = (j - k) - del/(2 Pi);

f[j_, k_, U_, a_, x_, N_] = (Exp[I Pi g[j, k]] - Exp[-I Pi g[j, k]] Exp[-I del ]
    +Exp[I (1 - a) U x/N g[j, k] ] a (Exp[-I del ] - 1)
    +Exp[-I a U x/N g[j, k]] (1 - a) ( Exp[-I del] - 1))/(2 Pi I g[j, k] );
(*Toeplitz Matrix from the double step distribution*)

f0[j_, k_] = (Exp[I Pi g[j, k]] - Exp[-I Pi g[j, k]] Exp[-I del]] +
              Exp[-I del] - 1)/(2 Pi I g[j, k] );
(* Zero temperature Toeplitz Matrix *)

p = 1/2;
Noisea = Array[z, 21];(*Array to store the noise value at different QPC1
```

```
transparency*)

N = 200;
i = 1;
transp = Table[y, {y, 0., 1., 0.05}];
pace = N[ Pi/N]; (*Sampling frequency*)
elem = IntegerPart[(2*N)/pace]; (*Number of elements in the array*)
zero = elem/2 + 1; (*Position of the zero*)
M[U_] = IntegerPart[U/(pace)]; (*Boundary of the integration domain.
It depends on  the bias voltage*)

stmp=OpenWrite["noisea50_pi/4.dat",FormatType->OutputForm];
(*save the value of Noisea in real time*)

For[a = 0., a < 1.05, a += 0.05, (*Loop over a*)

  Print[a];

  Clear[T, T0, convd, DelL, DelLF, Del, x, Div];

  T[x_] = Parallelize[Table[ N[f[j, k, 1, a, x, N]], {j, 0, N - 1},
  {k, 0, N - 1}]];
  (*Evaluation of the matrix "f" *)
  T0 = Parallelize[Table[ N[f0[j, k]], {j, 0, N - 1}, {k, 0, N - 1}]];
   (*Evaluation of the matrix "f0"*)

  m = 1;

  Clear[Del];
  Del = Array[z, elem + 1];
  time = Table[y, {y, -n, n, pace}];

  Div = Det[T0]; (*Evaluation of the zero temperature determinant*)

  (*Evaluation of the determinant for the double step distribution*)

  For[x = -N, x < n, x += pace,

   Del[[m]] = (Det[T[[x]]/Div) (Det[T[[x]]/Div);
   m++;
   ];
```

```
   (*Evaluation of the distribution function*)

   DelL = RotateLeft[Del, elem/2];
   DelLF = Flatten[Chop[RotateRight[Fourier[DelL,
                FourierParameters -> {0, 1}], elem/2]]];

   convd = Chop[Table[(pace/(Sqrt[2 Pi ]))* Total[ DelLF[ [ j ;;
                Length[Del]]]]], 
                {j, 1, Length[\[CapitalDelta]]}]];

   (*Noise Evaluation *)

  Noisea[[i]] = 2 p (1 - p) (pace*Total[ Table[(convd[[j]]),
  {j, zero + 1, zero + M[1]}]]
  + pace*Total[Table[((convd[[zero - M[1]]] - convd[[j]])),
   {j, zero - M[1], zero}]]);

  Write[stmp,a,"  ",Noisea[[i]]];
  i++;

  ];
Clear[a, p, T, T0, DelL, DelLF, N]
Close[stmp]
```

D.4 WEAK TRANSMISSION LIMIT AND LOWEST ORDER APPROXIMATION OF TOEPLITZ DETERMINANTS

Consider the normalized Toeplitz determinant

$$\bar{\Delta}_{\tau,s}(\delta) = \frac{\det\left[1 + (e^{-\imath\delta} - 1) f_D(\epsilon)\right]}{\det\left[1 + (e^{-\imath\delta} - 1)\theta(-\epsilon)\right]}, \tag{D.4.1}$$

where the scattering phase $\delta = \pi\gamma_\theta$ depends on the inter-edge interaction and the non-equilibrium fermionic distribution has a double step form :

$$f_D(\epsilon) = a\,\theta(-\epsilon + \mu_1) + (1 - a)\,\theta(-\epsilon + \mu_2), \tag{D.4.2}$$

with $\mu_1 = eV(1-a)$ and $\mu_2 = -eVa$. For $\tau eV \gg 1$ we can find a leading order approximation to the functional determinant as follows :

$$\begin{aligned}
\log \bar{\Delta}_{\tau,s}(\delta) &= \mathrm{Tr}\log\left\{1+(e^{-\imath\delta}-1)f_D(\epsilon)\right\} - \mathrm{Tr}\log\left\{1+(e^{-\imath\delta}-1)\theta(-\epsilon)\right\} \qquad \text{(D.4.3)}\\
&= \frac{|\tau|}{2\pi}\int_{-\infty}^{\infty} d\epsilon \left\{\log\left[1+(e^{-\imath\delta}-1)f_D(\epsilon)\right] - \log\left[1+(e^{-\imath\delta}-1)\theta(-\epsilon)\right]\right\}\\
&= \frac{|\tau|}{2\pi}\left\{\int_{-eVa}^{eV(1-a)} d\epsilon \log\left[1+(e^{-\imath\delta}-1)a\right] + \int_{-\infty}^{-eVa} d\epsilon\,[-\imath\delta] - \int_{-\infty}^{0} d\epsilon\,[-\imath\delta]\right\}\\
&= \frac{|\tau|}{2\pi}\left\{\log\left[1-a+ae^{-\imath\delta}\right] + \imath a\,\delta\right\}. \qquad \text{(D.4.4)}
\end{aligned}$$

In the above expression, the trace is taken over discrete energy and time. In the continuum limit we can move to an integral over energy and one over time, restricted to a time range τ (see previous discussion). Here we see how the zero temperature normalization is essential to cancel the infinite contribution coming from the background. Since we are interested only in the decaying behavior of the determinant, we consider here only its real part, making use of the polar representation of a complex number : $\log(z) = \log(|z|e^{\imath\phi}) = \log|z| + \imath\phi$.

$$\begin{aligned}
\Re\log\bar{\Delta}_\tau(\delta) &= \frac{|\tau|}{2\pi}\Re\log\left[1-a+ae^{-\imath\delta}\right] \qquad \text{(D.4.5)}\\
&= \frac{|\tau|}{2\pi}\log\sqrt{(1-a+a\cos\delta)^2+a^2\sin^2\delta}\\
&= \frac{|\tau|}{2\pi}\frac{1}{2}\log\left[1-4a(1-a)\sin^2\frac{\delta}{2}\right].
\end{aligned}$$

Using Eq. (D.4.5) we find the dephasing rate defined in Eq. (5.5.21)

$$\begin{aligned}
\bar{\Delta}_\tau(\delta) &\simeq \exp(-|\tau|/(2\tau_\phi)), \qquad \text{(D.4.6)}\\
\tau_\phi^{-1} &= -(eV/2\pi)\log[1-4a(1-a)\sin^2(\pi\gamma_\theta/2)].
\end{aligned}$$

The next step consist in evaluating $G^<_{2u}(\tau) = G^<_0(\tau)\,\bar{\Delta}^2_\tau(\delta)$, Eq. (5.5.3) :

$$G^<_{2u}(\tau) = \frac{1}{2\pi}\frac{e^{-\frac{|\tau|}{\tau_\phi}}}{(-\imath\tilde{u}_1\tau+\alpha)^{\sin^2\theta}(-\imath\tilde{u}_2\tau+\alpha)^{\cos^2\theta}}, \qquad \text{(D.4.7)}$$

by making use of the dual convolution theorem (D.3.24). The Fourier transform of the decaying kernel is

$$\hat{h}(\xi) = \int d\xi\, e^{-\imath\xi\tau}e^{-|\tau|/\tau_\phi^{-1}} = \frac{2\tau_\phi^{-1}}{\xi^2+(\tau_\phi^{-1})^2}. \qquad \text{(D.4.8)}$$

We find that to leading order in $eV\tau$ Eq. (D.4.8) describes the broadening of the energy distribution in terms of a Lorentzian. By performing the last convolution we finally find

$$\begin{aligned}
G^<_{2u}(\epsilon) &= \frac{1}{\tilde{u}_1^{\gamma_\theta^2/2}\tilde{u}_2^{1-\gamma_\theta^2/2}}\int d\xi\theta(-\xi+\epsilon)\frac{2\tau_\phi^{-1}}{\xi^2+(\tau_\phi^{-1})^2} \qquad \text{(D.4.9)}\\
&= \frac{1}{\tilde{u}_1^{\sin^2\theta}\tilde{u}_2^{\cos^2\theta}}f_{2u}(\epsilon),
\end{aligned}$$

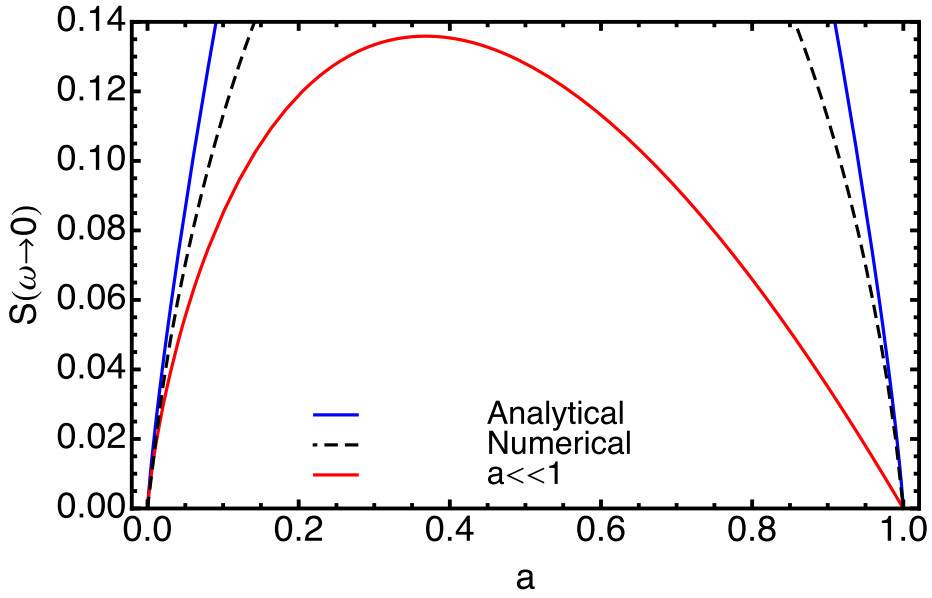

Figure 47: Low frequency noise in different regimes. (Blue) noise evaluated from the leading order approximation to the functional determinant. (Black dashed) numerically exact evaluation. (Red) weak transmission limit as computed from the leading order approximation of the functional determinant.

where the steady state distribution is given by

$$f_{2u}(\epsilon) = \frac{1}{2} - \frac{1}{\pi}\arctan\left(\frac{\epsilon}{\hbar\tau_\phi^{-1}}\right). \tag{D.4.10}$$

We note that the above distribution function has the symmetry $\hat{f}_{2u}(-\epsilon) = 1 - \hat{f}_{2u}(\epsilon)$, typical of a Fermi distribution. Using this and Eq. (5.5.1) we can finally find the noise:

$$\begin{aligned} S(\omega\to 0) &= 2\left(\frac{e^2}{h}\right) p\int_{-eV}^{eV} d\epsilon\left\{\hat{f}_{2u}(\epsilon)\theta(\epsilon) + \theta(-\epsilon)\hat{f}_{2u}(-\epsilon)\right\} = 4\left(\frac{e^2}{h}\right) p\int_0^{eV} d\epsilon \hat{f}_{2u}(\epsilon) \\ &= 4\left(\frac{e^2}{h}\right) p\frac{eV}{2\pi}\left\{\pi - 2\arctan\left(\frac{eV}{\tau_\phi^{-1}}\right) + \tau_\phi^{-1}\log\left[1+\left(\frac{eV}{\tau_\phi^{-1}}\right)^2\right]\right\}. \end{aligned} \tag{D.4.11}$$

Expanding the above result for $a \ll 1$ we find to leading order in a :

$$S(\omega\to 0) = 8\left(\frac{e^2}{h}\right) eV\sin^2\left(\frac{\delta}{2}\right)\frac{p}{\pi^2} a\log\left(\frac{1}{a}\right), \tag{D.4.12}$$

that is Eq. (5.4.31). We see that zero frequency noise power depends in a singular way on a in the limit $a \ll 1$, therefore invalidating a perturbative approach to the problem. If Fig. (47) we compare the analytical result of Eq. (D.4.11) with the noise obtained from the numerical evaluation of the Toeplitz determinant and the $a \ll 1$ expansion of Eq. (D.4.12).

BIBLIOGRAPHY

[1] M. J. Duff. "The world in eleven dimensions: a tribute to Oskar Klein". In: *eprint arXiv:hep-th/0111237* (2001) (cit. on p. i).

[2] X.G. Wen. *Quantum field Theory of Many-Body Systems*. Oxford University Press, 2008 (cit. on pp. i, 2, 5, 9, 16, 58, 107, 111, 113, 115).

[3] C. Nayak et al. "Non-Abelian anyons and topological quantum computation". In: *Rev. Mod. Phys.* 80 (2008), pp. 1083–1159 (cit. on pp. i, 2, 112).

[4] M. Rigol, V. Dunjko, and M. Olshanii. "Thermalization and its mechanism for generic isolated quantum systems". In: *Nature* 452 (2008), p. 854 (cit. on pp. ii, 80).

[5] A. Polkovnikov et al. "Colloqium: Nonequilibrium dynamics of closed interacting quantum systems". In: *Rev. Mod. Phys.* 83 (2011), pp. 863–883 (cit. on p. ii).

[6] D. B. Gutman, Y. Gefen, and A.D. Mirlin. "Bosonization of one-dimensional fermions out of equilibrium". In: *Phys. Rev. B* 81 (2010), p. 085436 (cit. on pp. ii, 19, 32, 36, 39, 81, 90, 160).

[7] D. B. Gutman, Yuval Gefen, and A.D. Mirlin. "Non-equilibrium 1D many-body problems and asymptotic properties of Toeplitz determinants". In: *J. Phys. A:Math. Theor.* 44 (2011), p. 165003 (cit. on pp. ii, 19, 81).

[8] I.V. Protopopov, D.B. Gutman, and A.D. Mirlin. "Many-particle correlations in non-equilibrium Luttinger liquid". In: *J. Stat. Mech.* (2011), P11001 (cit. on pp. ii, 19, 81, 96, 99, 157).

[9] I.V. Protopopov, D.B. Gutman, and A.D. Mirlin. "Luttinger liquids with multiple Fermi edges: Generalized Fisher-Hartwig conjecture and numerical analysis of Toeplitz determinants". In: *arxiv:1203.6418v1* (2012) (cit. on pp. ii, 19, 81).

[10] S. Takei, M. Milletarí, and B. Rosenow. "Nonequilibrium electron spectroscopy of Luttinger liquids". In: *Phys. Rev. B (R)* 82 (2010), p. 041306 (cit. on pp. iii, iv).

[11] M. Milletarí and B. Rosenow. "Shot Noise Signatures of Charge Fractionalization in the $\nu = 2$ Quantum Hall edge". In: *eprint arXiv:1207.1719* (7/2012) (cit. on pp. iii, iv).

[12] stillyellow. *Lineland* (cit. on p. v).

[13] L. Pantieri and T. Gordini. *L'arte di scrivere con LaTeX*. URL: http://www.lorenzopantieri.net/LaTeX_files/ArteLaTeX.pdf (cit. on p. v).

[14] E.H. Hall. "On a New Action of the Magnet on Electric Currents". In: *American Journal of Mathematics* 2 (1879), pp. 287–292 (cit. on p. 1).

[15] K. Von Klitzing, G.Dorda, and M.Pepper. "New method for high-accuracy determination of the fine-structure constant based on quantized Hall resistance". In: *Phys. Rev. Lett.* 45.6 (1980), p. 494 (cit. on p. 1).

[16] K. Von Klitzing. "25 Years of Quantum Hall Effect (QHE) A Personal View on the Discovery, Physics and Applications of this Quantum Effect". In: *Seminaire Poincare* 2 (2004), pp. 1–26 (cit. on p. 2).

[17] Q. Niu, D.J. Thouless, and Y.S. Wu. "Quantized Hall conductance as a topological invariant". In: *Phys. Rev. B* 31.6 (1985), p. 3372 (cit. on p. 2).

[18] D.C. Tsui, H.L. Stormer, and A.C. Gossard. "Two-Dimensional Magnetotransport in the Extreme Quantum Limit". In: *Phys. Rev. Lett.* 48.22 (1982), pp. 1559–1562 (cit. on p. 2).

[19] E. Fradkin. *Field Theories of Condensed Matter Systems*. the advanced Book Program. Addison-Wesley, 1991 (cit. on pp. 2, 5, 20, 25).

[20] C. Nayak. *Quantum Condensed Matter Physics - Lecture Notes*. 2004. URL: http://www.physics.ucla.edu/~nayak/many_body.pdf (cit. on pp. 2, 57, 107).

[21] D. Yoshioka. *The Quantum Hall Effect*. Vol. 133. Solid-State Sciences. Springer-Verlag, 1998 (cit. on p. 2).

[22] A. Zee. *Quantum Field Theory in a Nutshell*. 2nd. Princeton University Press, 2010 (cit. on pp. 2, 13, 107, 112).

[23] Alexander Atland and Ben Simons. *Condensed Matter Field Theory*. second. Cambridge University Press, 2010 (cit. on pp. 2, 7, 63).

[24] J.D. Bjorken and S.D. Drell. *Relativistic Quantum Mechanics*. New York: McGraw-Hill, 1964 (cit. on p. 4).

[25] C.J. Joachain and B.H. Brandsen. *Physics of Atoms and Molecules*. Ed. by Longman House. Burnt Mill, Arlow, Essex (UK): Longman Scientific Technical, 1983 (cit. on p. 4).

[26] E. Abrahams et al. "Scaling Theory of Localization: Absence of Quantum Diffusion in Two Dimensions". In: *Phys. Rev. Lett.* 42.10 (1979), pp. 673–676 (cit. on p. 6).

[27] A.M.M. Pruisken. "On localization in the theory of the quantized hall effect: A two-dimensional realization of the θ-vacuum". In: *Nuclear Physics B* 235.2 (1984), pp. 277–298 (cit. on p. 7).

[28] R.B. Laughlin. "Quantized Hall conductivity in two dimensions". In: *Phys. Rev. B* 23.10 (1981), pp. 5632–5633 (cit. on p. 7).

[29] B. I. Halperin. "Quantized Hall conductance, current-carrying edge states, and the existence of extended states in a two-dimensional disordered potential". In: *Phys. Rev. B* 25.4 (1982), pp. 2185–2190 (cit. on pp. 7, 15).

[30] R.B. Laughlin. "Anomalous Quantum Hall Effect: An Incompressible Quantum Fluid with Fractionally Charged Excitations". In: *Phys. Rev. Lett.* 50.18 (1983), p. 1395 (cit. on p. 9).

[31] F.Wilczek. "Magnetic Flux, Angular Momentum, and Statistics". In: *Phys. Rev. Lett.* 48.17 (1982), pp. 1144–1146 (cit. on p. 10).

[32] F.D.M. Haldane. "Fractional Quantization of the Hall Effect : A Hierarchy of Incompressible Quantum Fluid States". In: *Phys. Rev. Lett.* 51.7 (1983), p. 605 (cit. on p. 10).

[33] J.K. Jain. "Composite-Fermion Approach for the Fractional Quantum Hall Effect". In: *Phys. Rev. Lett.* 63.2 (1989), p. 199 (cit. on pp. 10, 11).

[34] B.I. Halperin. "Statistics of Quasipartciles and the Hierarchy if Fractional Quantized Hall States". In: *Phys. Rev. Lett.* 52.18 (1984), p. 1583 (cit. on p. 10).

[35] S.C. Zhang, T.H. Hansson, and S. Kivelson. "Effective-Field-Theory Model for the Fractional Quantum Hall Effect". In: *Phys. Rev. Lett.* 62.1 (1989), pp. 82–85 (cit. on p. 12).

[36] J.C. Baez and J.P. Munian. *Gauge Fields, Knots and Gravity*. Ed. by L. Kauffman. Vol. 4. K and E Series on knots and everything. World Scientific, 1994 (cit. on pp. 13, 27).

[37] P.A.M. Dirac. *Lectures on Quantum Mechanics*. Belfer Graduate School of Science, Yeshiva University. New York: Dover Pubblications INC., 1964 (cit. on pp. 13, 112).

[38] X.G. Wen. "Chiral Luttinger liquid and the edge excitations in the fractional quantum Hall states". In: *Phys.Rev. B* 41 (1990), pp. 12838–12844 (cit. on p. 15).

[39] X.G. Wen. "Electrodynamical properties of gapless edge excitations in the fractional quantum Hall states". In: *Phys. Rev. Lett.* 64 (1990), pp. 2206–2209 (cit. on p. 15).

[40] F.P. Milliken, C.P. Umbach, and R.A. Webb. "Indications of a Luttinger liquid in the fractional quantum Hall regime". In: *Solid State Comm.* 97 (1996), pp. 309–313 (cit. on p. 15).

[41] A.M. Chang, L. N. Pfeiffer, and K. W. West. "Observation of chiral Luttinger behaviour in electron tunneling into fractional quantum Hall edges". In: *Phys. Rev. Lett.* 77 (1996), pp. 2538–2541 (cit. on p. 15).

[42] M.Grayson et al. "Resonant tunneling into a biased fractional quantum Hall edge". In: *Phys. Rev. Lett.* 86 (2001), pp. 2645–2648 (cit. on p. 15).

[43] S. Bieri and J. Fr$'$ohlich. "Physical principles underlying the quantum Hall effect". In: *C.R. Physique* 12 (2011), pp. 332–346 (cit. on pp. 15, 16).

[44] D.C. Mattis and E.H. Lieb. "Exact solution of a many fermion system and its associated boson field". In: *J.Math.Phys.* 6 (1965), pp. 304–312 (cit. on p. 20).

[45] F.D.M. Haldane. "'Luttinger liquid theory' of one-dimensional quantum fluids. I. Properties of the Luttinger model and their extension to the general 1D interacting spinless Fermi gas". In: *J. Phys. C: Solid State Phys.* 14.19 (1980), p. 2585 (cit. on pp. 20, 23).

[46] J. Von Delft and H. Schoeller. "Bosonization for beginners, refermionization for expert". In: *Ann. Phys. (Leipzig)* 7 (1998), p. 225 (cit. on pp. 20, 119).

[47] M. Stone, ed. *Bosonization*. World Scientific, 1994 (cit. on pp. 20, 25).

[48] A.O.Gogolin, A.A. Nersesyan, and A.M. Tsvelik. *Bosonization and Strongly Correlated Systems*. Cambridge University Press, 1998 (cit. on pp. 20, 27).

[49] F. Bastianelli and P. van Nieuwenhuizen. *Path Integrals and Anomalies in Curved Space*. Cambridge University Press, 2006 (cit. on p. 22).

[50] T. Giamarchi. *Quantum Physics in One Dimension*. Vol. 1. Oxford University Press, 2003 (cit. on pp. 23, 25, 52).

[51] M.Fabrizio and A.O.Gogolin. "Interacting one-dimensional electron gas with open boundaries". In: *Phys. Rev. B* 51.24 (1995), pp. 17827–17841 (cit. on p. 23).

[52] A. Kamenev and A. Levchenko. "Keldysh technique and non-linear sigma-model: basic principles and applications". In: *Advances in Physics* 58 (2009), p. 197 (cit. on pp. 33, 36, 77, 136).

[53] I. E. Dzyaloshinskii and A. I. Larkin. "Correlation functions for a one-dimensional Fermi system with long-range interaction (Tomonaga model)". In: *Sov. Phys. JETP* 38.1 (1973), p. 202 (cit. on p. 35).

[54] T.Bohr. "Lectures on the Luttinger Model". Nordita preprint 81/4 (unpublished). 1981 (cit. on p. 35).

[55] I.V. Yurkevish. "Bosonization as the Hubbard Stratonovich Transformation". In: ed. by I. V. Lerner et al. StronglyCorre- lated fermions and bosons in Low-Dimensional Disordered Systems 69. Kluwer Academic Publishers, 1986 (cit. on p. 35).

[56] T. Martin. "Noise in mesoscopic physics". In: *Nanophysics : Coherence and Transport*. Ed. by H. Bouchiat et al. Vol. LXXXI. Les Houches. Elsevier B.V., 2005, pp. 283–359 (cit. on pp. 36, 56).

[57] L.S. Levitov. *The Quantum Theory of Noise*. Ed. by Yu V Nazarov. Quantum Noise in Mesoscopic Systems. cond-mat/0210284v1: Kluwer, 2003 (cit. on pp. 37, 95).

[58] L.S. Levitov and G.B. Lesovik. "Charge distribution in quantum shot noise". In: *JETP Lett.* 58.3 (1993), pp. 225–230 (cit. on p. 39).

[59] Antonio Fasano and Stefano Marmi. *Analytical Mechanics : An Introduction*. Oxford Graduate Texts. Oxford University Press, 2006 (cit. on p. 41).

[60] Y.F. Chen et al. "Nonequilibrium tunneling spectroscopy in carbon nanotubes". In: *Phys. Rev. Lett.* 2009 (102), p. 036804 (cit. on p. 41).

[61] D. B. Gutman, Yuval Gefen, and A.D. Mirlin. "Tunneling spectroscopy of Luttinger liquid structures far from equilibrium". In: *Phys. Rev. B* 80 (2009), p. 045106 (cit. on p. 41).

[62] D.A. Bagrets, I.V. Gornyi, and D.G. Polyakov. "Nonequilibrium kinetics of a disordered Luttinger liquid". In: *Phys. Rev. B* 80 (2009), p. 113403 (cit. on p. 41).

[63] M. Khodas et al. "Fermi-Luttinger liquid: Spectral function of interacting one-dimensional fermions". In: *Phys. Rev. B* 76 (2007), p. 155402 (cit. on p. 41).

[64] E.V. Deviatov et al. "Energy Transport by Neutral Collective Excitations at the Quantum Hall Edge". In: *Phys. Rev. Lett.* 106.25 (2011), p. 256802 (cit. on p. 41).

[65] J. Rammer and H. Smith. "Quantum field-theoretical methods in transport theory of metals". In: *Rev.Mod.Phys.* 58 (1986), pp. 323–359 (cit. on p. 44).

[66] C.L. Kane and M.P.A. Fisher. "Shot noise and the transmission of dilute Laughlin quasiparticles". In: *Phys. Rev. B* 67 (2003), p. 045307 (cit. on pp. 44, 45, 135, 138, 139).

[67] C. de C. Chamon and X.G. Wen. "Resonant Tunneling in the Fractional Quantum Hall Regime". In: *Phys. Rev. Lett.* 70 (1993), pp. 2605–2608 (cit. on p. 47).

[68] X.G. Wen. *An Introduction to Topological Order*. URL: http://dao.mit.edu/~wen/topartS3.pdf (cit. on p. 53).

[69] C.L. Kane and M.P.A. Fisher. "Nonequilibrium Noise and Fractional Charge in the Quantum Hall Effect". In: *Phys. Rev. Lett.* 72.5 (1993), p. 724 (cit. on p. 56).

[70] P. Fendley, A. W. W. Ludwig, and H. Saleur. "Exact Nonequilibrium dc Shot Noise in Luttinger Liquids and Fractional Quantum Hall Devices". In: *Phys. Rev. Lett.* 75.11 (1995), p. 2196 (cit. on p. 56).

[71] R. de Picciotto et al. "Direct observation of a fractional charge". In: *Nature* 389 (1997), p. 162 (cit. on p. 56).

[72] A. Bid et al. "Shot Noise and Charge at 2/3 Composite Fractional Quantum Hall State". In: *Phys. Rev. Lett.* 103 (2009), p. 236802 (cit. on pp. 56, 57).

[73] P. Fendley, A. W. W. Ludwig, and H. Saleur. "Exact nonequilibrium transport through point contacts in quantum wires and fractional quantum Hall devices". In: *Phys. Rev. B* 52.12 (1995), p. 8934 (cit. on p. 57).

[74] S. Roddaro et al. "Interedge Strong-to-Weak Scattering Evolution at a Constriction in the Fractional Quantum Hall Regime". In: *Phys. Rev. Lett.* 93.4 (2004), p. 046801 (cit. on p. 57).

[75] B. Rosenow and B. I. Halperin. "Signatures of neutral quantum Hall modes in transport through low-density constrictions". In: *Phys. Rev. B* 81 (2010), p. 165313 (cit. on pp. 57, 64).

[76] D.B. Chklovskii and B.I. Halperin. "Consequences of a possible adiabatic transition between $\nu = 1/3$ and $\nu = 1$ quantum Hall states". In: *Phys. Rev. B* 57.7 (1996), p. 3781 (cit. on p. 57).

[77] X.G. Wen. "Impurity effects on chiral one-dimensional electron systems". In: *Phys. Rev. B* 50.8 (1994), p. 5420 (cit. on pp. 57, 67).

[78] K.E. Nagaev. "Influence of electron-electron scattering on shot noise in diffusive contacts". In: *Phys. Rev. B* 52.7 (1995), pp. 4740–4743 (cit. on pp. 57, 76).

[79] C.L. Kane, M.P.A. Fisher, and J. Polchinski. "Randomness at the Edge: Theory of Quantum Hall Transport at Filling $\nu = 2/3$". In: *Phys. Rev. Lett.* 72.26 (1994), p. 4129 (cit. on pp. 57, 60–62).

[80] C.L. Kane and M.P.A. Fisher. "Impurity scattering and transport of fractional quantum Hall edge states". In: *Phys. Rev. B* 51 (1994), p. 13449 (cit. on pp. 57, 59, 62, 113).

[81] C.L. Kane and M.P.A. Fisher. "Contacts and edge-state equilibration in the fractional quantum Hall effect". In: *Phys. Rev. B* 52.24 (1995), p. 17393 (cit. on p. 57).

[82] U. Klass et al. "Imaging of the dissipation in quantum-Hall-effect experiments". In: *Z. Phys. B* 82 (1991), pp. 351–354 (cit. on p. 62).

[83] T. Ise, H. Akera, and H. Suzuura. "Electron Temperature Distribution and Hot Spots in Quantum Hall Systems". In: *JPJS* 74.1 (2005), pp. 259–262 (cit. on p. 62).

[84] J. Weis and K. Von Klitzing. "Metrology and microscopic picture of the integer quantum Hall effect". In: *Phil. Trans. R. Soc. A* 369 (2011), pp. 3954–3974 (cit. on p. 62).

[85] S. Datta. *Electronic Transport in Mesoscopic Systems*. Ed. by H.Ahmed, M. Pepper, and A. Broers. Vol. 3. Cambridge srudies in semiconductor physics and microelectronic engineering. Cambridge, UK: Cambridge University Press, 2002 (cit. on p. 62).

[86] C.L. Kane and M.P.A. Fisher. "Quantized thermal transoprt in the fractional quantum Hall effect". In: *Phys. Rev. B* 55.23 (1996), p. 15 832 (cit. on pp. 62, 63, 73, 77).

[87] A. Cappelli, M. Huerta, and G.R. Zemba. "Thermal transport in chiral conformal theories and hierarchical quantum Hall states". In: *Nuclear Physics B* 636 (2002), pp. 568–582 (cit. on p. 63).

[88] A. Furusaki et al. *Electromagnetic and thermal responses in topological matter: topological terms, quantum anomalies and D-branes*. 2012 (cit. on p. 63).

[89] S. Wang, X.L. Qi, and S.C. Zhang. "Topological field theory and thermal response of interacting topological superconductors". In: *Phys. Rev. B* 84 (2011), p. 014527 (cit. on p. 63).

[90] M. Stone. "Gravitational anomalies and thermal Hall effect in topological insulators". In: *Phys. Rev. B* 85 (2012), p. 184503 (cit. on p. 63).

[91] Line junction in a quantum Hall system with two filling fractions. "D. Sen and A. Agarwal". In: *Phys.Rev. B* 78 (2008), p. 085430 (cit. on pp. 64, 67).

[92] C.L. Kane and M.P.A. Fisher. "Line junctions in the quantum Hall effect". In: *Phys. Rev. B* 56.23 (1996), p. 15231 (cit. on pp. 64–66).

[93] J.E.Moore and F.D.M. Haldane. "Edge excitations of the $\nu = 2/3$ spin-singlet quantum Hall state". In: *Phys. Rev. B* 55.12 (1996), pp. 7818–7823 (cit. on p. 80).

[94] H. le Sueur et al. "Energy Relaxation in the Integer Quantum Hall Regime". In: *Phys. Rev. Lett.* 105 (2010), p. 056803 (cit. on p. 80).

[95] P. Degiovanni et al. "Plasmon scattering approach to energy exchange and high-frequency noise in $\nu = 2$ quantum Hall edge channels". In: *Phys. Rev. B* 81(R) (2010), p. 121302 (cit. on p. 80).

[96] D.L. Kovrizhin and J.T. Chalker. "Equilibration of integer quantum Hall edge states". In: *Phys. Rev. B* (84), p. 085105 (cit. on p. 80).

[97] I.P. Levkivskyi and E.V Sukhorukov. "Energy Relaxation at Quantum Hall Edge". In: *Phys. Rev. B* 85 (2012), p. 075309 (cit. on p. 80).

[98] M.A. Cazalilla. "Effect of Suddenly Turning on Interactions in the Luttinger Model". In: *Phys. Rev. Lett.* 97 (2006), p. 156403 (cit. on pp. 81, 84).

[99] A.Iucci and M.A. Cazalilla. "Quantum quench dynamics of the Luttinger Model". In: *Phys. Rev. A* 80 (2009), p. 063619 (cit. on pp. 81, 84, 92).

[100] S. Sotiriadis, P. Calabrese, and J. Cardy. "Quantum Quench from a Thermal initial state". In: *EPL* 87 (2009), p. 20002 (cit. on pp. 81, 84).

[101] T. Karzig et al. "Relaxation and edge reconstruction in integer quantum Hall systems". In: *cond-mat* (2012), arxiv:1206.0261 (cit. on p. 81).

[102] A. L. Fetter and J. D. Walecka. *Quantum Theory of Many-Particle Systems*. 7th. Dover Pubblications INC., 2003 (cit. on p. 84).

[103] M. Le Bellac, F. Mortessagne, and G.G. Batrouni. *Equilibrium and Non-equilibrium Statistical Thermodynamics*. Cambridge University Press, 2004 (cit. on p. 89).

[104] I.S. Gradshteyn and I.M. Ryzhik. *Table of Integrals, Series and Products*. Ed. by A. Jeffrey and D. Zwillinger. seventh. Elsevier Academic Press, 2007 (cit. on pp. 93, 137, 162).

[105] R.Kubo, M. Toda, and N. Hashitsume. *Statistical Physics*. Vol. 2. Springer-Verlag (cit. on p. 94).

[106] I. Neder. "Fractionalization noise in edge channels of integer quantum Hall states." In: *Phys. Rev. Lett.* 108 (2012), p. 12838 (cit. on p. 104).

[107] M.Heiblum. private communication (cit. on p. 104).

[108] X.G. Wen and Q. Niu. "Ground-state degeneracy of the fractional quantum Hall states in the presence of a random potential and on high-genus Riemann surfaces". In: *Phys. Rev. B* 41.13 (1989), pp. 9377–9397 (cit. on p. 111).

[109] X.G. Wen and A. Zee. "Classification of Abelian quantum Hall states and matrix formulation of topological fluids". In: *Phys. Rev. B* 46 (1992), pp. 2290–2301 (cit. on p. 112).

[110] D. L. Maslov. "Fundamental aspects of electron correlations and quantum transport in one-dimensional systems". In: *LXXXI Les Houches Summer School "Nanoscopic Quantum Transport"*. 2004, p. 108 (cit. on p. 115).

[111] G.Mussardo. *Statistical Field Theory. An Introduction to Exactly Solved Models in Statistical Physics*. first. Oxford Graduate Texts. Oxford University Press, 2010 (cit. on p. 117).

[112] L.S. Levitov, H. Lee, and G.B. Lesovik. "Electron counting statistics and coherent states of electric currents". In: *J.Math.Phys.* 37.10 (1996), pp. 4845–4866 (cit. on pp. 129, 131).

[113] I. Klich. *Full Counting Statistics : An elementray derivation of Levitov's formula*. Ed. by Yu V Nazarov. Quantum Noise in Mesoscopic Systems. cond-mat/0209642v1: Kluwer, 2003 (cit. on p. 129).

[114] J.E.Avron et al. "Fredholm Determinants and the Statistics of Charge Transport". In: *Commun. Math. Phys.* 280 (2007), pp. 807–829 (cit. on p. 130).

[115] K. Sch´onhammer. "Full Counting Statistics for noninteractong fermions: Exact results and the Levitov-Lesovik formula". In: *Phys. Rev. B* 75 (2007), p. 205329 (cit. on p. 131).

[116] K. Sch´onhammer. "Full Counting Statistics for noninteractong fermions: exact finite-temperature results and generalized long-time approximation". In: *J. Phys.: Condens. Matter* 21 (2009), p. 495306 (cit. on p. 131).

[117] A.G. Abanov, D.A. Ivanov, and Y Qian. "Quantum Fluctuations of one-dimensional free fermions and Fisher-Hartwig Formula for Toeplitz determinants". In: *J. Phys. A:Math. Theor.* 44 (), p. 485001 (cit. on p. 132).

[118] P. DEIFT, A. ITS, and I. KRASOVSKY. "Asymptotics of Toeplitz, Hankel, Aand Toeplitz+Hankel determinants With Fisher-Hartwig singularities". In: *Ann. of Math.* 174 (2011), pp. 1243–1299 (cit. on pp. 132, 160).

[119] C.E. Shannon. "Communication in the presence of noise". In: *Proc. Institute of Radio Engineers* 37.1 (1949), pp. 10–21 (cit. on p. 154).

[120] H. Nyquist. "Certain topics in telegraph transmission theory". In: *Trans. AIEE* 47 (1928), pp. 617–644 (cit. on p. 154).

[121] J. Cardy, ed. *Finite-Size Scaling*. Vol. 2. Current Physics. Elsevier Science Publishing, 1988 (cit. on p. 162).